# REINFORCED FOUNDATION BEDS : SOIL - REINFORCEMENT INTERACTION ANALYSES

*A Thesis Submitted*
*In Partial Fulfilment of the Requirements*
*for the Degree of*

**DOCTOR OF PHILOSOPHY**

*By*

**N. KUMAR PITCHUMANI**

*to the*

DEPARTMENT OF CIVIL ENGINEERING

INDIAN INSTITUTE OF TECHNOLOGY KANPUR

JUNE, 1992

# CERTIFICATE

It is certified that the work contained in the thesis entitled, "Reinforced Foundation Beds : Soil - Reinforcement Interaction Analyses" by *N. Kumar Pitchumani*, has been carried out under my supervision and that this work has not been submitted elsewhere for a degree.

M. R. Madhav

Dr. M. R. Madhav

Dept. of Civil Engineering

I.I.T., Kanpur

June, 1992

# ABSTRACT

Man has always been associated with soil. The responsibility of designing foundations for structures has forced the Geotechnical Engineer to study the suitability of the soil in taking the load from the super-structure. Often it becomes imperative to improve the soil properties to prevent its failure under the load. Reinforcing the ground with inclusions in the form of steel, bamboo, nails, fibres etc., helps in increasing the load carrying capacity of the soil. The last decade has seen the advent of geosynthetics in the form of geotextiles, geomembranes, geogrids, geocells, etc., and their varied applications. Geo-synthetics are used to design steep slopes and retaining walls, and for improving the performance of the soil-foundation systems. The need for designing the reinforced soil rationally has kindled research activity in this field.

While a large number of model test results have been reported, only few analytical models are available to study the performance of reinforced foundation beds. Most of the analytical studies deal with the increase in the bearing capacity of the system whereas very few of them deal with the reduction of foundation settlements due to reinforcement embedded in the soil. Further, the interaction between the soil and the reinforcement, has not been studied fully or rationally in many of the analyses. In the present work, an attempt has been made to analyse the soil-strip reinforcement interaction in order to compute the interfacial stresses and eventually, the settlement reduction of

the surface, using the elastic continuum approach. The membrane effect of the reinforcement, however has not been considered.

The mechanisms that contribute to a reduction in the surface settlements may be enumerated as follows. The applied surface load causes the soil below it to move downward and outward. The reinforcement, placed at some depth below this load, experiences vertical deformation as well as axial extension. Depending on its vertical and horizontal stiffnesses, the reinforcement resists the soil displacements and consequently, normal and shear stresses are mobilised at the interface. These stresses, in turn push the soil up thus bringing about a surface heave which eventually is the reduction in the surface settlements. In the thesis, the rigidity of the strip reinforcement in the horizontal (Chapter 3) and vertical (Chapter 4) directions is initially considered separately. Following the analyses for rigid strips, the same is extended (Chapter 5) to extensible and flexible ones. For high values of the respective stiffnesses the results compare well with those obtained for rigid strips. The combined effect of the horizontal and vertical rigidity of the strips is then considered and allowance made for possible slip along the strip-soil interface. Axi-symmetric problems for rigid and extensible sheets are studied and reported in Chapter 6.

The investigation is carried out for a strip reinforcement placed at a given depth, centrally below an uniformly loaded rectangular area. The Boussinesq's equation for displacements within a soil mass due to a point force on the surface is

numerically integrated over the loaded area to calculate the horizontal and vertical displacements of points along the length of the strip. The reinforcing strip resists these displacements. Shear and normal stresses are mobilised at the soil-strip interface. In chapter 3, the horizontal displacements of these points due to the shear stresses are computed by integrating numerically the Mindlin's solution for horizontal displacements due to a horizontal force within an elastic continuum over the area of the reinforcing strip. Satisfying the compatibility of displacements at the points, a set of simultaneous equations are obtained, the solution of which yields shear stresses mobilised along the strip. For a rigid (inextensible) strip the net horizontal displacements are zero whereas they are equal to the elongations of points along the strip for an extensible one. For the vertical displacements of the points along the strip (Chapter 4) due to normal stresses on it, Mindlin's solution for vertical displacements due to a vertical force within an elastic continuum is integrated over the area of the strip. The compatibility condition for a rigid strip is that the net vertical displacements of points in the soil adjacent to the strip are equal to the rigid body translation of the strip. For a flexible strip the soil displacements are equal to the flexural deformations of the strip. For the case where the rigidity of the strip in the horizontal and vertical directions are considered simultaneously (Chapter 5), the effects of the vertical stresses on horizontal displacements and vice versa, are also included. Slip along the strip is incorporated by limiting the shear stresses mobilised to the frictional resistances available at the interface due to the

normal stresses including the overburden stresses at that depth. The reduction of settlement of points on the surface due to the shear stresses along and the normal stresses on the strip, are computed by integrating Mindlin's equation for vertical displacements due to horizontal and vertical forces respectively, over the area of the strip. A similar analysis is presented (Chapter 6) for an axi-symmetric case. In the case of strip reinforcements, pairs of strips are also considered and the applicability of the principle of superposition examined.

A parametric study brings out the effects of the aspect ratio of the loaded area, length, depth and the distance of the strip from the centre, and the Poisson's ratio of the soil for strip reinforcements, on the stresses mobilised at the interface and the reduction of settlements of points along the surface. The effects of the radius of the extent of reinforcement and depth of its placement for the axi-symmetric case, on the quantities mentioned are also studied. The predicted reduction in surface settlements are compared with those from selected test results available in literature.

The elastic continuum approach is thus used to model the complex problems of reinforced foundation beds. The analysis quantifies the reduction in foundation settlements due to strip and circular sheet reinforcements. An effective method to predict the reduction in surface settlement due to strip and circular type reinforements placed beneath a loaded area is developed.

## ACKNOWLEDGMENT

I express my heartfelt gratitude to Prof. M. R. Madhav for excellent guidance and constant motivation. I am grateful to him for having introduced me to the area of soil-reinforcement. I am thankful to my faculty members, Dr. Basudhar, Dr. N.S.V.K. Rao, Dr. Yudhbir, and Dr. S. Chandra for having given me suggestions regarding my thesis work.

I once again thank Dr. Madhav for his extremely quick manuscript corrections which were carried out through postal correspondence (EMS) after his departure to Japan. I am specially grateful to department here and the Saga University in helping us carry out the "Postal Corrections". Indirectly I am indebted to the postal department of India and Japan.

I am grateful to Venugopala Rao, DNS, Chandan Ghosh, and K. Srinivasan for the discussions I had during the course of my work. Their ideas and suggestions have been very helpful.

I am thankful to my friends, Harish, Sabhahit, Srinivasan, Raman and Seetharaman who helped me in getting my thesis typed. I express my gratitude to Anand, Kalyanaraman, DNS, Venu, Deshpande, Murali, Galagali and Taha in shaping out the thesis to the final form.

I am thankful to my innumerable friends, to mention a few;

ckr, gsv, selva, jg, Narayanan, Seetharam, Manjoor, Subramanian, Siva, Kasi, Govind and Sampath for their lively company. I am also grateful to the Tamil gang, Kannada gang, Ghati gang, Telugu gang, the Navy group, the SPIC-MACAY group and the Counselling Service group for the enjoyable company.

A special thanks to Raghavan, Sudha and their parents for their homely treatment and delicious food. I am grateful to the families of Dr. Sathyamurthy, Dr. Madhav, Dr. Raghavendra, Dr. Ramaseshan, Dr. Radhakrishnan, Sri Sadagopan, Sri Narasimhan Dr. Venkobachar, Dr. Ramesh, Dr. Sundararajan, Sri Venugopala Rao, Sri (Dr.) Manoravi and Sri Thyagarajan for making me feel at home in an otherwise mundane social atmosphere.

A very special thanks to the enjoyable, hilarious and exuberent company of my little friends, Anju, Aruna, Teju, Putti, Sruthi, Ravi, Harini, Rahul, Arun, Mala, Sowmya and Shivani.

TABLE OF CONTENTS

# LIST OF FIGURES

# LIST OF TABLES

# NOTATION

$a$ : Radius of Circular Reinforcement

$B_f$ : Half-Width of Loaded Area

$B_r$ : Half-Width of Strip Reinforcement

$c$ : Depth at which Force acts (Mindlin Problem)

$dA$ : Elemental Area

$dl$ : Length of Element

$dr$ : Length of Element

$d\theta$ : Elemental Angle

$E_m I_m$ : Flexural Rigidity of Circular Reinforcement

$E_r I_r$ : Flexural Rigidity of Strip Reinforcement

$E_s$ : Young's Modulus of Soil

$F_x$ : Force Component in x-direction

$F_y$ : Force Component in y-direction

$G_s$ : Shear Modulus of Soil

$I_{ij}^f$ : Influence on Displacement of node i due to Surface Loading on Element j

$I_{ij}^r$ : Influence on Displacement of node i due to Stress on Element j along Reinforcement

$I_{sc}$ : Settlement Reduction Coefficient at the Centre of the Loaded Area

$I_z$ : Influence Coefficient for Vertical Surface Displacements due to Point Force at Depth

$[I_b]$ : Finite Difference Coefficient Matrix

$[I_\sigma]$ : Moment Coefficient Matrix

$K_B$ : Flexibility Ratio

$\alpha_{ij}$ : Angle made by the line joining the nodes i and j with x-axis

$\gamma$ : Unit Weight of Soil

$\delta_o$ : Rigid Body Displacement of Reinforcement

$\Delta\theta$ : Elemental Angle

$\nu_s$ : Poisson's Ratio of Soil

$\nu_m$ : Poisson's Ratio of Circular Reinforcement

$\rho_E$ : Elongation of Reinforcement

$\rho_x^f$ : Horizontal Displacement due to Surface Load

$\rho_x^r$ : Horizontal Displacement due to Stresses

$\rho_{x\tau}^r$ : Horizontal Displacement due to Shear Stresses

$\rho_{x\sigma}^r$ : Horizontal Displacement due to Normal Stresses

$\rho_z^f$ : Vertical Displacement due to Surface Load

$\rho_z^r$ : Vertical Displacement due to Stresses

$\rho_{z\tau}^r$ : Vertical Displacement due to Shear Stresses

$\rho_{z\sigma}^r$ : Vertical Displacement due to Normal Stresses

$\sigma$ : Normal Stresses Mobilised at the Soil-Reinforcement Interface

$\tau$ : Shear Stresses Mobilised at the Soil-Reinforcement Interface

$[\ ]$ : Denotes Matrix

$\{\ \}$ : Denotes Column Vector

$[\ ]$ : Denotes Row Vector

$K_\gamma$ : Elongation Ratio

$L_f$ : Half-Length of Loaded Area

$L_r$ : Half-Length of Strip Reinforcement

$n_f$ : Number of Sub-Elements along Radius of Loaded Area

$n_B$ : Number of Sub-Elements along Width of Loaded Area

$n_L$ : Number of Sub-Elements along Tangential Direction of Loaded Area

N : Number of Elements along Reinforcement

O : Origin of the Co-ordinate System

P : Point Load on Surface

q : Intensity of Loading on Surface

Q : Point Load at Depth

r : Radial Distance along Reinforcement

$r_f$ : Radial Distance along Surface

R : Radius of Reinforcement

SRC : Settlement Reduction Coefficient

$S_Y$ : Distance of Strip from x-axis

$S_{Y1}$ : Distance of Strip 1 from x-axis

$S_{Y2}$ : Distance of Strip 2 from x-axis

$S_{yD}$ : Spacing Difference Between Multiple Strips

$t_r$ : Thickness of Strip Reinforcement

$t_m$ : Thickness of Circular Reinforcement

T : Tension in Reinforcement

$U_o$ : Depth of Placement of Reinforcement

$U_1$ : Depth of Placement of Strip 2

w : Flexural Deflection of Strip Reinforcement

x : Distance Along Surface

# CHAPTER 1

# INTRODUCTION

From time immemorial, man has been associated with soil. Any civil engineering structure, whether a compound wall or a multistorey building has to be founded in or on the surface of the earth. Foundations have to be designed with a proper understanding of the soil characteristics. There are situations wherein the soil is extremely weak or soft to take any load. Design of foundations on soft soils involves heavy expenditure as this requires large foundation dimensions. Embankments on soft soils call for flatter slopes, thus occupying large areas which may not be available. Many a times it may be required to construct steep slopes for highways. Further, unpaved roads on soft soils require a thick course of aggregate spread over a large area so that the wheel loads are distributed over a wide area. This again would result in an uneconomic design.

The increased cost of these conventional designs and numerous environmental constraints greatly encourage the in-situ improvements of weak subsoils. Environmental constraints include the depletion of supply of sites with good foundation conditions due to rapid urbanisation. Under such circumstances it becomes imperative to enhance certain soil properties, thus resulting in a significant improvement in the bearing capacity of the soil. To achieve this, various ground improvement techniques are in vogue which may be listed as follows,

1. Dynamic Compaction, wherein the soil is compacted and allowed to consolidate by repeated dropping of a heavy weight on the surface of the soil
2. Installation of sand drains to expedite the consolidation process
3. Use of lime piles to increase the shear strength of the soil and reduce its compressibility
4. Use of stone columns/Granular piles
5. Chemical stabilization
6. Thermal stabilization
7. Consolidation by preloading
8. Heating and freezing
9. Soil Reinforcement

Soil Reinforcement is one of the latest and fast growing techniques of ground improvement. Although the systematic study of reinforced soil did not start until very recently, the practice of building houses and roads on fibre-reinforced soil and constructing earth walls with different types of reinforcing inclusions is an age old art. Use of rope fibres and bamboo strips to strengthen rural base roads has not been uncommon. There still is a practice of using rectangular grids of bamboo strips as the central core around which mud walls are built in rural areas.

It was not very late when the potential of soil reinforcement was realised. The infrastructure for systematic study of reinforced soil was only lacking until Vidal (Jones, 1985) gave

the geotechnical community a basis for a rational approach to reinforced soil design. Research in this area started picking up momentum and as a consequence, various types of reinforcing methods and forms have emerged. The major structural effects of reinforcing inclusions can be tension, compression, bending and shearing. Broadly, reinforcements can be classified into three types, viz., vertical, inclined, and horizontal reinforcements.

Reinforcement techniques such as stone columns and micropiles can be categorised as vertical reinforcements. A stone column is a vertical column of highly compacted sand, gravel and aggregates. It acts as a 'granular pile' and its role is to increase the resistance and stiffness of the foundation soil. The merit of a stone column is its ability to adjust to the applied load and thereby redistribute the load where stress concentration occurs. Unlike piles, the mechanism of interaction is that of a restrained expansion in the surrounding soft soil. The inherent advantage is that there is no collapse because an overloaded stone column automatically gets relieved of the stresses as it deforms.

A micropile is made of a bar or a tube of a few centimeters diameter surrounded by grout all along its length. Micropiles help in increasing the factor of safety of a slope against sliding and transmit the shear force from a possible sliding mass to the stable soil. Inclined reinforcements are used to stabilise slopes and embankments. Soil-nailing, a recent technique for stabilising slopes is an example of the same. This method is based on the principle of reinforcing soils by means of tension carrying bars

(so called 'nails'). Soil-nailing is being used at present to stabilise natural slopes, cuts and excavations in granular soils with some cohesion, stiff clays and soft rocks.

Horizontal reinforcements in the form of strips and sheets are routinely used in almost all soil-reinforcement projects. Sheet reinforcement used in highway construction helps in reducing the thickness of the required subgrade. Strips are also used to reinforce embankments and retaining walls. Strips, as well as sheets are used under footings to increase the bearing capacity of the soil-foundation system and to bring about a reduction in foundation settlements. The advent of Geosynthetics has resulted in their extensive application to soil reinforcement. Geosynthetics in the form of geotextiles, geomembranes, geogrids, geomats, etc. have found varied applications in geotechnical engineering. Geosynthetics used in pavement design help in redistributing the wheel loads over a larger area and hence the thickness required for the subgrade is reduced.

The basic mechanisms of reinforced soil can be explained as follows. When a sample of cohesionless soil is loaded vertically, it experiences lateral strain. However, if horizontal reinforcing elements are placed within the soil mass, the reinforcements will prevent lateral strain because of friction between the reinforcing elements and the soil, and the behaviour will be as if a lateral restraining force or load had been imposed on the element. Thus it is evident that the reinforced soil concept is essentially based on the mobilisation of the interfacial shearing resistance

(so called 'nails'). Soil-nailing is being used at present to stabilise natural slopes, cuts and excavations in granular soils with some cohesion, stiff clays and soft rocks.

Horizontal reinforcements in the form of strips and sheets are routinely used in almost all soil-reinforcement projects. Sheet reinforcement used in highway construction helps in reducing the thickness of the required subgrade. Strips are also used to reinforce embankments and retaining walls. Strips, as well as sheets are used under footings to increase the bearing capacity of the soil-foundation system and to bring about a reduction in foundation settlements. The advent of Geosynthetics has resulted in their extensive application to soil reinforcement. Geosynthetics in the form of geotextiles, geomembranes, geogrids, geomats, etc. have found varied applications in geotechnical engineering. Geosynthetics used in pavement design help in redistributing the wheel loads over a larger area and hence the thickness required for the subgrade is reduced.

The basic mechanisms of reinforced soil can be explained as follows. When a sample of cohesionless soil is loaded vertically, it experiences lateral strain. However, if horizontal reinforcing elements are placed within the soil mass, the reinforcements will prevent lateral strain because of friction between the reinforcing elements and the soil, and the behaviour will be as if a lateral restraining force or load had been imposed on the element. Thus it is evident that the reinforced soil concept is essentially based on the mobilisation of the interfacial shearing resistance

between the soil and the reinforcement which in turn restrains the lateral deformation of the soil. Beneath a footing the reinforcement checks the lateral displacement of the soil by introducing lateral confinement. Further, the footing load also causes vertical movement of the soil. If the soil is reinforced with strips with some flexural stiffness, these strips will resist the vertical deformations because of the mobilisation of the interfacial normal stresses between the soil and the reinforcing strip. These stresses, in effect push the soil mass above upward. In the earlier case, the shear stresses at the interface push the soil upward. It can hence be concluded that shear and normal stresses are mobilised at the soil-reinforcement interface as a consequence of its rigidity in the axial and vertical directions which in turn result in the reduction of surface settlements.

The present work aims at computing the stresses mobilised along the soil-reinforcement interface and hence to predict the settlement reduction of points along the surface. Strip reinforcements are considered below rectangular loaded areas and circular reinforcements below circular loaded areas. The elastic continuum approach is resorted to model the reinforced foundation system. The following chapter reviews the literature available on reinforced foundations.

Chapter 3 deals with the rigidity of strip reinforcement in the horizontal direction. The strip is considered to be inextensible. The horizontal displacements of points along the soil-strip interface due to the surface load are calculated using

Boussinesq's equation (Poulos and Davis, 1975) for radial displacements at any point within an elastic half-space due to a point load on the surface. The strip being inextensible counteracts these displacements and hence shear stresses are mobilised at the strip-soil interface. The displacements of the points along the strip due to these stresses are evaluated using Mindlin's equation (Poulos and Davis, 1975) for horizontal displacements due to horizontal force within an elastic continuum. The shear stresses are computed by equating the net horizontal displacements of the points along the strip to zero. The settlement reduction of points along the surface due to these stresses are calculated using Mindlin's equation for vertical displacements due a horizontal force within the elastic continuum.

The rigidity of the strip in the vertical direction (inflexible strip) is considered in chapter 4. In this chapter the vertical displacements of points at the soil-strip interface are evaluated using Boussinesq's equation for vertical displacements. The strip being inflexible experiences a uniform rigid body translation and as a result normal stresses are mobilised at the interface. These stresses are the difference of the normal stresses acting on the top and bottom faces of the strip. The vertical displacements due to these stresses are computed using Mindlin's equation for vertical displacements due to a vertical force at depth. The compatibility of displacements at the interface yields equations for the normal stresses and the rigid body displacement which are solved for the same. The settlement reduction of points on the surface due to these stresses are then

Following the analyses for rigid strips, the same is extended (Chapter 5) to extensible and flexible ones. For an extensible strip the net horizontal soil displacements are equated to the elongation of the points along the strip. For a flexible one the net vertical soil displacements equal the flexural deformations of the points along the strip. The shear stresses (for extensible strips) and normal stresses (for the flexible one) are computed from the equations obtained on satisfying the displacement compatibility and force equilibrium. The coupled effect for the horizontal and vertical rigidity of rigid strips is also considered and allowance made for possible slip along the strip-soil interface. In the case of slip, the shear stresses are restricted to the strength available at the interface.

Using the elastic continuum theory, an analysis for predicting the reduction in surface settlements due to the presence of a circular reinforcement at depth is presented in chapter 6. The problem considered is axi-symmetric in nature. The effects of the radius of the reinforcement, and depth of its placement on the shear and normal stresses mobilised along the reinforcement-soil interface and the subsequent reduction in surface settlements are studied. The horizontal and vertical rigidity of the reinforcement sheet are considered separately. Subsequently, the extensibility of the sheet is also accounted for.

# CHAPTER 2
# LITERATURE REVIEW

## 2.1 Introduction

Improving the soil properties by reinforcing it has been in vogue from early times and in particular from the time Vidal introduced this concept to Geotechnical Engineering. Research in this area to study the mechanisms of reinforced soil has been progressing with great momentum over the last few years. Innumerable model tests using various forms of reinforcing materials have been conducted to have an insight into the reinforcing mechanisms of these materials. Some analytical approaches have been presented based on limit equilibrium methods and earth pressure theories. Finite element analysis has helped in quantifying the increase in the bearing capacity of reinforced foundation beds. Very few models based on elastic theories are available in literature. The present chapter gives a broad insight into the state-of-the-art of reinforced foundation beds, the various methods of analysis available and the mechanisms proposed by various authors. Since the present study uses the elastic continuum theory, the next paragraph gives a short description of the elastic solutions available.

Boussinesq has given equations for calculating the stresses and displacements of a point within an elastic half-space due to a point load acting on the surface. Stresses within the elastic continuum for various types of surface loading are available

(Poulos and Davis, 1975; Teferra and Schultze, 1988). Mindlin has given equations for the stresses and displacements of points within an elastic half-space due a point force acting either vertically or horizontally within the continuum. The soil in both these cases (Boussinesq or Mindlin problems) is assumed to be linearly elastic, homogeneous, isotropic, and semi-infinite.

This chapter deals with the available literature on reinforced foundation beds. The various aspects considered are the theoretical approaches, and model and field test results.

## 2.2 Theoretical Solutions

### 2.2.1 Analytical Solutions

Binquet and Lee (1975a) were the pioneers in carrying out an analytical study on the bearing capacity of reinforced soil beds. Using the Boussinesq's stress distribution they have calculated the shear stress distribution on the plane of reinforcement and hence the maximum tensile stress in the reinforcement. They have also defined the locus of the maximum shear stresses with depth. The distance, $x_o$, along the length of the reinforcement where the shear stress is maximum, is a function of the depth of reinforcement and the soil properties. They have suggested values of maximum shear stress as $0.3q_o$ at a depth of 0.25B and around $0.1q_o$ at a depth of 2B, where $q_o$ is the intensity of the applied loading and B, the width of the footing. The normal force on the reinforcement due to the loading is obtained by integrating the vertical stress over the area of the reinforcement. The authors

have considered three failure mechanisms, viz., pull-out and tension failure of the reinforcements and shear failure of the soil above the reinforcement. They assume that the tension in the reinforcement is inversely proportional to the number of reinforcing layers. Based on this assumption they have given expressions for the tension as a function of the shear stresses and normal stresses at that depth, and the BCR, defined as the ratio of the average contact pressures for the reinforced and unreinforced soil.

Giroud and Noiray (1981) have made an analysis of the unpaved road behaviour with and without geotextile as reinforcement. They have considered the effect of geotextile in increasing the bearing capacity of the soil. This method is based on the consideration of the 'tension membrane' effect for the case of plane strain reinforced unpaved road deforming under the action of a single application of dual wheel load. Assuming an allowable rut depth, load spread angle, suitable geometric configuration and firm anchorage of the reinforcement, the strain in the reinforcement is calculated. On knowing the strain, the tension in the reinforcement is easily computed. The authors have given design charts for the reduction in road base thickness, due to reinforcement effect of geosynthetic for various traffic intensities.

Ingold and Miller (1982) have proposed a theory for bearing capacity of footings on reinforced clay which is based on an equivalent undrained strength of reinforced clay. Number of

layers of reinforcement spaced at a distance, S, are considered. The vertical stress at any depth is calculated using a 2(v):1(h) stress distribution. Considering the force equilibrium of an element of soil spliced between two layers of reinforcement they arrive at an expression for the equivalent undrained shear strength as

$$C_u' = C_u\left[1 + \alpha(B + D/2)/(2S(2 + \pi))\right] \qquad (2.1)$$

where $C_u$ is the undrained shear strength, $\alpha$ is the adhesion factor, D is the depth to the bottom most layer of reinforcements and B is the width of the footing. The proposed theory has been verified by conducting model footing tests on clay reinforced with geogrids under plane strain conditions. The test results show close agreement with the predicted response for S/B, ranging from 0.4 to 0.8. It is observed that BCR increases significantly with the increase in the number of reinforcing layers and decreases with increase in the depth ratio, d/B, d being the depth to the top layer of reinforcement.

Based on their test results and the observed failure modes for the reinforced ground, Huang and Tatsuoka (1988) have presented an analysis to predict the increase in the bearing capacity of reinforced ground. The failure modes observed have been described in the section dealing with model tests. They have obtained expressions for the BCR based on the failure of the block mentioned with respect to the failure modes. The predicted values of BCR match well with the test results. The results indicate an

increase in BCR with increase in length of strips and the number of layers upto 3. The authors have defined a term called the Covering Ratio (CR) which is the ratio of the width of a strip (W) to the sum of the width (W) and the horizontal spacing (S) between two strips. Their results indicate that for CR>0.9 failure occurs according to mode 1. As CR increases the BCR also increases.

Madhav and Ghosh (1988) have presented two and three parameter models to quantify the effect of tension in the membrane on settlements. They have also presented solutions for embankment and axi-symmetric loadings. Their results indicate that in a two parameter model, greater values of tension in the membrane reduce the settlements below the centre of the embankment. It is further seen that, in a three parameter model the maximum settlement reduces and settlements tend to become uniform with increasing tensile force in the membrane. Further, an increase in the stiffness of the fill reduces the maximum settlement.

Sridharan et. al. (1988) have presented a method of analysis for a reinforced sand mattress on soft soil. In their analysis they assume that the total load carried by the reinforced system is composed of two components, one carried by the unreinforced soil and the other by the reinforcement due to frictional interaction. The load taken by the reinforcement is a function of the normal force acting over it due to the applied loading and the overburden pressure. The total load is expressed as

$$P = P_s + P_r \qquad (2.2)$$

where $P_s$ is the load taken by the unreinforced soil and $P_r$ is the load taken by the reinforcement. $P_r$ is considered proportional to the BCR, the area of the reinforcement, the normal force and the interfacial friction angle. To examine the validity of their analysis, the authors carried out model footing tests. Saw dust was used to model soft soil. Their test results indicated that there was practically no increase in the load carrying capacity of saw dust due to the placement of reinforcement since the interfacial friction angle was very low. Provision of a sand mattress over the geotextile increased the bearing capacity considerably. There was good agreement between their predictions and test results. One of their results also shows that the geotextile performs more as a separator than as a reinforcement if provided at the interface. This result seems true because they had used a locally available woven geotextile. The performance of a geotextile largely depends on its stiffness and it so turned out that the fabric they used was well suited for separation than for reinforcement. Further, an inclusion in any form at the interface improves the performance of the soil-foundation system and as a result an increase in the load carrying capacity of the reinforced system was observed.

Madhav and Poorooshasb (1989) have proposed a model consisting of Pasternak shear layers, Winkler springs and newly proposed rough membrane to represent the mechanical response of a granular fill-geosynthetic-soft soil system. Satisfying the force equilibrium, coupled differential equations for displacement of soil and tension in the fabric are arrived at. These equations

are solved numerically and iteratively. Their results show that the settlements of the soil decrease and tend to become uniform with increasing rigidity of the shear layer. As anticipated, the tension is maximum at the centre of the fabric and reduces with increasing distance. The results based on the coefficients of friction on the top and bottom of the fabric indicate that it is advisable to place the geosynthetic within the granular fill rather than laying it directly on soft ground. The influence of the geofabric in reducing settlements increases with the load intensity. The results obtained from this model compare well with reality.

Houlsby and Jewell (1990) have presented an analysis for reinforced unpaved roads in which tension-membrane effect is not considered since it is insignificant at small rut depths. In this analysis, the loaded area is treated as axi-symmetric. It is assumed that below the circular footing active pressures are developed as the fill tends to spread out laterally. Passive conditions are generated outside the footing. Based on these assumptions the minimum average shear stress at the fill-clay interface is calculated. The presence of a reinforcement at this interface prevents the subgrade from taking this inward stresses upto the limit load. The authors comment that although there is an increase in the bearing capacity for reinforced road as compared to an unreinforced one, the increase is not simply by a constant factor as suggested by other authors. An important feature of this analysis is that the reinforcement, unlike in previous design methods is perceived to carry the outward shear

stresses which would otherwise be transmitted to the subgrade. These stresses automatically put the reinforcement into tension. This model seems quite appropriate and simpler as emphasis is not placed on the role of the reinforcement acting as a curved tension membrane. They have presented design charts which demonstrate that for certain combination of parameters, enhancement of bearing capacity can be achieved by the use of reinforcement. The required reinforcement force can also be determined from the charts.

Sellmeijer (1990) has presented a model for the behaviour of a soil-geotextile-aggregate system, based on combined membrane action and lateral restraint. The aggregate behaviour is modelled by elasto-plastic shear theory, the geotextile by membrane action and lateral restraint, and the subsoil by its bearing capacity. The vertical and horizontal equilibrium and the compatibity of displacements for both the aggregate and geotextile are satisfied. Consequently, differential equations are derived for the geotextile deflection and tension. The novelty of this model is that the lateral restraint and membrane action of the geotextile, the concept of mobilised friction and the bearing capacity of the subsoil, are used.

### 2.2.2 Finite Element Models

Brown and Poulos (1981) have demonstrated how a finite element model of reinforced earth can be used to investigate the increase in bearing capacity and stiffness of a foundation due to placement of reinforcement in the soil. The model examines the effect of reinforcement on the load-settlement behaviour of a

strip foundation. The analysis considers the various components of the reinforced soil structure separately and incorporates an elasto-plastic soil model obeying Mohr-Coulomb failure criterion. The reinforcement strip is treated as elastic with zero flexural stiffness transmitting axial forces only. The model accounts for slip at the reinforcement-soil interface governed by a Mohr-Coulomb criterion. Two cases, a footing on a homogeneous foundation, and a footing on a foundation incorporating a cavity or a pocket of extremely soft material are studied. The results of the finite element study show similar patterns of behaviour to the laboratory model test results. The reduction in the bearing capacity of the unreinforced footing due to the presence of cavity from the finite element analysis agrees well with experimental observation. The analysis shows that the quantity of reinforcement required to produce a significant increase in the bearing capacity is high, and since the limit state of the reinforcement-soil bond is reached at an early stage, the reinforcement-soil interface slip (rather than the stiffness of the reinforcement) is the governing factor. The analysis brings out that the provision of the reinforcement helps in spreading the load, thereby causing mobilisation of soil resistance over wider area and at shallow depth.

Andrawes et. al. (1982) have presented a finite element analysis to predict the load-settlement behaviour of soil-geotextile systems. The variational approach is used to obtain the stiffness matrix for the soil elements. The geotextile is represented by linear elements which have no bending stiffness.

The soil-geotextile interaction is assumed to be only frictional and simulated by spring elements of zero length connecting the nodes of soil elements to those of geotextile element. Results obtained from this analysis are compared with those obtained from laboratory model tests which consisted of a geotextile reinforced sand layer loaded to failure by a strip footing. The measured and predicted data for the load-settlement curve show that for the case where the geotextile was placed at a depth equal to half the width of the footing (0.5B) the difference in these values are within 10% upto peak footing load. For the case where the geotextile is placed at a depth equal to the width of the footing (1.0B) the difference is again within 10% but only upto 85% of the peak load. Beyond this, the predicted behaviour rapidly diverges and grossly overestimates the bearing capacity of the footing. The model is able to predict the behaviour upto 85% of the peak load but fails beyond this load. This is because the model is inappropriate as local failure in the soil occurs which the authors say could not be accommodated in the finite element procedure.

In order to verify the results of their model tests, Love et. al. (1987) formulated a finite element program. This program was able to handle large diplacements and strains induced in the actual model. The subgrade was modelled as an elastic-perfectly plastic material with the maximum shear stress equal to $C_u$. The fill material was modelled as an elastic frictional material obeying Matsuoka yield criterion. The reinforcement was treated as perfectly rough, so that any failure would occur in soil elements adjacent to the reinforcement rather than at the

interface. Yielding of the reinforcement was not considered, as it was not observed in the model test, and compressive stress was not allowed in the reinforcement. The results of this analysis compare well with those obtained from model tests for reinforced and unreinforced cases. The authors have commented that this model may be used with some confidence to perform accurate predictions for full-scale structures. They have assumed that no compressive stresses are developed in the reinforcement but such a condition is possible for reinforcements placed very close to the footing. Further, as pointed out by Binquet and Lee (1975a) strips at shallow depths fail due to breakage which the authors could have included if this model is to be used for predictions for full-scale structures.

Burd and Houlsby (1989) have presented a finite element model capable of computing the behaviour of a reinforced unpaved road deforming in plane strain. The calculations are based on the use of a Von Mises plasticity model for the clay subgrade and a model based on the Matsuoka yield function for the granular fill. The reinforcement is modelled using elastic membrane elements. The formulation is based on a large strain, large displacement approach. The finite element model is used to back-analyse laboratory scale model tests in which a footing is jacked monotonically into a model reinforced unpaved road. There is good agreement in the load-displacement curve for reinforced and unreinforced systems between the model test results and finite element results. The authors say that the finite element model may be used to obtain values for parameters that are necessary for

a full understanding of the behaviour of reinforced unpaved road but are difficult to measure in physical tests. The authors give plots of two such parameters, viz. strain in the reinforcement and normal stresses acting on the reinforcement. They conclude that the finite element model is useful in estimating values of those parameters that are difficult to measure through model tests.

Burd and Brocklehurst (1990) have reported a small displacement finite element parametric study on unpaved roads subjected to single monotonic loading. The load is applied by a rigid, rough footing of width, 2B, placed on the surface of the fill. An elastic-perfectly plastic model is used to model the clay subgrade and an elastic-perfectly frictional model is used for the fill. The reinforcement is modelled as a perfectly elastic material with an infinite yield stress in tension and zero yield stress in compression. It is also assumed that no slip occurs at the soil-reinforcement interface. It is seen that the variations in reinforcement stiffness have a significant effect on the magnitude of shear stresses on the upper and lower surfaces of the reinforcement and on the tension developed in the reinforcement. The authors conclude that for static loading excessively stiff reinforcements are not very beneficial since large shear stresses are developed, which they say, do not contribute to an improvement in static bearing capacity of the road. Further, these large stresses induce large values of reinforcement forces. There appear to be some reservations with this model since it considers only small displacements. Reinforcements may be subjected to compression at shallow depths. Further, higher shear stresses help

of a line element with no bending stiffness. They carried out a series of analysis in which the reinforcement characteristics were linear and the elastic modulus, J (defined as the force/unit width/unit strain), varied widely (J=0, 150, 1500, 15000KN/m). Their results show that the reinforcement helps in reducing deformations if it is sufficiently stiff and strong. Shear stresses are mobilised along the interface which eventually induce tension in the reinforcement. The effect of the reinforcemnt is limited either by its yield or by slip at the interface.

## 2.3 Laboratory Model Tests

A large number of model tests are available in literature which aim at studying the behaviour of reinforced soil and understanding the mechanisms involved. Since the material available is exhaustive only a few test results have been cited here.

Binquet and Lee (1975b) investigated the mechanisms and potential benefits of using reinforced earth slabs to improve the bearing capacity of granular soil. They conducted model tests with strip footings on reinforced foundations for three conditions: (1) Homogeneous deep sand; (2) sand above an extensive layer of very soft material; and (3) sand above a finite size pocket of very soft material. The reinforcing material consisted of 13mm wide strips of household aluminium foil. Tests were conducted for a Linear Density Ratio (LDR) defined as the total width of the strips per unit width of the footing of 0.425. Three series of tests were conducted and results of these tests showed that the load-settlement and the ultimate bearing capacities of

the footing can be improved by a factor of about 2-4 times above the same load-settlement or bearing capacity of an unreinforced soil under identical conditions. Results were obtained to study the effects of the depth of the top layer of reinforcement and number of layers of reinforcement. It was observed that the bearing capacity continued to improve with increasing number of layers upto six to eight, beyond which there was little additional improvement. It was also seen that the optimum location of the top strip was at a depth of 1.33B, B being the width of the footing and with further increase in this depth the BCR value decreased.

Akinmusuru and Akinbolade (1981) have presented results of laboratory model tests with square footings on a deep homogeneous sand bed reinforced with flat strips of the rope fibre material. The parameters they studied were the horizontal spacing of the strips, vertical spacings between horizontal layers of reinforcement, number of layers, and depth below the footing of the first layer, on the bearing capacity of the footing. The fibre strips were 10mm wide and thick. The strips of length 1m were placed in both directions one over the other. The loads were applied in small increments and the load-displacement curve to failure for each experiment was obtained. The bearing capacity ratio (BCR) was defined with the difference that it was restricted to only the ultimate failure condition. The study of the effects of the various parameters on the BCR revealed the following conclusions.

1. The BCR decreased with increase in the horizontal and the vertical spacings of the strips.

2. There were three types of failure depending on the vertical spacing of the strips which were in agreement with the modes of failure identified by Binquet and Lee.
3. The maximum BCR was observed for the depth of the first layer equal to 0.5B, B being the width of the footing.
4. For number of layers, N, increasing upto three, there was a sharp increase in bearing capacity but with further increase in N no appreciable improvement was observed.

The results from the tests conducted by these researchers are in agreement with results reported in literature.

Fragaszy and Lawton (1984) conducted a series of laboratory model studies to determine the influence of soil density and reinforcing strip length on the load-settlement behaviour of reinforced sand. The strips were placed in such a way that the linear density ratio (LDR) defined by Binquet and Lee (1975) was 47% which was slightly higher than the values of the latter. Tests were conducted on unreinforced and reinforced sands and the effects of strip length and soil density on the bearing capacity ratio (BCR) were studied. Their results showed that when BCR was calculated at a settlement equal to 10% of the footing width, the BCR was independent of soil density. When calculated at a settlement of 4% of the footing width, the percentage increase in bearing capacity appeared to be less for loose sands than for dense sands. Failure of rectangular footings on dense reinforced sand occured at a larger settlement than for an identical footing on unreinforced sand at the same density. As the strip length increased from three to seven times the footing width, the BCR

increased rapidly. Additional strip length did not appear to affect significantly the bearing capacity.

The authors compared their results using Binquet and Lee's (1975a) theoretical analysis of reinforced earth slabs. Their results agreed well with the prediction of Binquet and Lee (1975a) that the bottom layer of reinforcement breaks first. The authors comment that the equations developed by Binquet and Lee are very sensitive to the value of friction angle at failure.

Guido et.al. (1985) conducted laboratory model tests to study the bearing capacity of shallow foundations reinforced with geotextiles. Their experimental set-up included square sheets of geotextile placed concentrically under a square footing. Their results show that at smaller deformations, the full benefits of the presence of the geotextile are not exhibited. They comment that for the settlement to footing width ratio greater than 0.017, the fabric deforms sufficiently to mobilise its tensile stress, thereby increasing the load carrying capacity. For a given value of the depth of the top reinforcement, the BCR increses with decreasing values of the vertical spacing of the reinforcements and increases steadily with increase in number of layers from 0 to 3. There is little improvement in the BCR with further increase in the number of layers of reinforcement. Guido et. al. (1986) have made a comparative study on the behaviour of the reinforced earth slabs using geogrids and geotextiles as reinforcements

Love et. al. (1987) conducted small-scale model tests to study the effectiveness of geogrid reinforcement, placed at the base of a layer of granualar fill on the surface of soft clay. To make the modelling as realistic as possible, the various components were scaled by a factor four. The reinforcement used was a version of Tensar SS geogrid. In the tests, monotonic loading was applied by a rigid footing, under plane strain conditions, to the surface of reinforced and unreinforced systems using a range of fill thicknesses and subgrade strengths. Deformations of the subgrade and of the geogrid were measured from photographs. One set of tests was performed using a double footing. The results of the model studies indicated that the geogrid reinforcement tends to reduce the shear stress transmitted to the surface of the clay subgrade. The authors also comment that the failure mechanisms in the clay are mobilised at small deformations of the fill, and therefore large deformations are not necessary for the benefits of reinforcement to be felt. At large deformations, where these are permissible, additional benefit is obtained from the membrane action of the reinforcement.

Setty and Rao (1987) conducted model tests by reinforcing locally available lateritic soil with synthetic fibres. The reinforced soil contained discontinuous, discrete, and randomly oriented fibres with an aspect ratio of about 25. It was observed that there was some reduction in the angle of internal friction and a substantial increase in the value of cohesion due to the presence of fibre reinforcement. There was an overall improvement in the CBR values as well as the tensile strength of the soils.

The expansion ratio of the soil sample decreased. The authors infer that fibre reinforced soil can be effectively used in the lower layers of pavement to improve its tensile resistance and in the subgrades of rural roads where surface cracking becomes a big hurdle.

Miura et.al. (1988) conducted model and field tests of reinforced pavement by polymer grids on very soft ground. Field tests were performed on a 300m long test road with six sections of different types of pavement. Cyclic load tests were carried out on reinforced and unreinforced model test pavements. The model and field test results showed that polymer grid placed at the interface of the subbase and the subgrade suppresses the settlement under repeated loading. From the field data obtained after one and three months of construction it was observed that the modulus of subgrade reaction was smaller than that of conventional pavement. It is reasoned that this might be partly due to the overestimation of the grid function and partly from insufficient compaction of base owing to the action of the polymer grid. The results from a finite element analysis indicated that the polymer grid is not effective in suppressing the surface settlement of the pavement. The authors suggest that interlocking effect in polymer grids is an important function which is not accounted for in the analysis and that while using polymer grids as reinforcing material for pavements, care should be taken while compacting so that no gap is left between the grids and the underneath layers.

Dembicki and Alenowicz (1988) conducted model tests on two-layer subsoil consisting of a layer of sand fill underlain by soft soil. They have investigated the influence of a geotextile inclusion on bearing capacity of the system. In order to simulate a truck axle under plane strain conditions, the surface of the two-layer system was subjected to static loading applied by two steel plates. The model tests also aimed at observing the failure mechanism of reinforced and unreinforced systems. The geotextile used was needlepunched nonwoven. From the load-settlement curves for the unreinforced and reinforced systems it was observed that at small plate penetration values there was little difference between both the systems. On the other hand, at large displacements of the plates, influence of the geotextile on measured pressure was significant. They have compared the indicated load-carrying capacity due to inclusion of a geotextile with the reduction in pressure on the weak subsoil due to the fabric calculated from the analysis given by Giroud and Noiray (1981). The results show that the calculated reduction of pressure differs from the increase in the load-carrying capacity indicated in the tests. The authors attribute this difference to the fact that tests consider the changes in failure mechanisms as well as tensile force induced in the geotextile, while the calculated values show reduction connected only with the latter effect.

Huang and Tatsuoka (1988) performed a series of model tests to investigate the reinforcing mechanisms for strip reinforced foundation beds. Strips made of phosphor bronze were placed beneath a strip footing. The tests were aimed at studying the

reinforcing effect of short strips having the same length as the footing, the effects of length of reinforcement, number of reinforcing layers and the density of reinforcing strips. Tests were also conducted on deep footings. The researchers have given figures for the strain fields for the cases of unreinforced and reinforced grounds. It was seen that the ground reinforced with short strips behaved very similar to the deep footing with depth of the footing ($D_f$) equal to the total depth of reinforcing layers ($D_r$). This trend indicated that the failure was progressive and the compressive strength of the active zone beneath the footing controls the bearing capacity of the ground. The authors call such an effect as 'the deep footing effect'. Based on the test results they suggest two modes of failure. The first mode is observed for densely reinforced conditions wherein the shear bands starting from the edges of the footing extend downward to the depth, $D_r$, then form a wedge beneath the reinforced zone. The second mode is observed for lightly reinforced conditions wherein the shear bands start from the footing edges and form a wedge within the reinforced zone. In this case, the bearing capacity of the reinforced ground is controlled by the strength of the block immediately beneath the footing.

Model tests were conducted by various researchers (Sreekantiah, 1988; Shankariah and Narahari, 1988; and Sargunan and Hussain, 1988) on square and strip footings on sand beds reinforced with different types of reinforcements like aluminium foil, G.I., and bamboo strips. Their experimental investigations revealed that the bearing capacity of the foundation increases due

to the introduction of reinforcement. There is no appreciable increase in the BCR for depths of placement of reinforcements beyond 1.4B, B being the width of the footing. With the increase in the number of layers of reinforcement, the BCR increases.

To study the effect of a geotextile placed at the interface of a granular fill and a weak clay layer, Das (1989) performed a number of model tests on strip and square foundations. He has studied the effects of the height of the granular fill to width of the footing ratio (H/B), the depth of embedment of footing ($D_f$) and the width of geotextile ($B_G$) on the ultimate bearing capacity of the foundation. The length of the geotextile was equal to the length of the foundation. The test results indicate that the ultimate bearing capacity increases to a maximum at H/B=0.75 and decreases to a constant value at H/B=2 for $D_f/B=0.5$. The author has indicated that the ultimate bearing capacity for a given H/B ratio can be expressed as

$$q_{u(H/B)} = q_{u(H/B=0)} + \Delta q_{u(S)} + \Delta q_{u(G)} \qquad (2.3)$$

or

$$BCR = 1 + \Delta(BCR)_S + \Delta(BCR)_G \qquad (2.4)$$

where $q_{u(H/B)}$=ultimate bearing capacity with geotextile interface; $\Delta q_{u(S)}$=net increase of ultimate bearing capacity due to the sand layer of height, H, only; $\Delta q_{u(G)}$=net increase of the ultimate bearing capacity due to the inclusion of geotextile; and BCR is the bearing capacity ratio. Using the test results the variations of $\Delta(BCR)_S$ and $\Delta(BCR)_G$ were computed from the equations which indicated that the beneficial effect of the geotextile reaches a maximum value at H/B=0.75. The geotextile has practically no

effect for H/B>1.5 for strip foundations and for H/B>1 for square foundations. The computed results also indicated that without the inclusion of the geotextile, the BCR increases upto a maximum of about 2.8 at H/B=1.6, while the BCR increases to about 3 at H/B=0.75, for a strip foundation if a geotextile is placed at the sand-clay interface. The corresponding values for a square foundation are 1.75 at H/B=1 without a geotextile and 1.9 at H/B=0.5 with a geotextile at the interface. Also, the most economical width of the geotextile for a strip and a square footing are 4B and 3B respectively

Shimizu and Inui (1990) carried out model tests on soft soil reinforced with geotextile cell wall. A six-sided cell of geotextile wall frame was buried in the subsurface of the soft ground and vertical loads were applied at the centre of the cell. The loading tests were carried out to find the necessary conditions for realizing the increase in the bearing capacity. Furthermore, in order to investigate why and how the bearing capacity increases, X-ray photographs were taken of the displacements of small lead pieces embedded in the model. The load-settlement behaviour showed that installation of the cell increases the bearing capacity of the ground. The critical value of the height to width ratio of the cell, is about 1.5 for which the bearing capacity is maximum. The stiffness of the geotextile affects the bearing capacity too. Furthermore, it was observed that if the horizontal tensile strength is not high enough to resist the expansion caused by the ground deformation, the cell would be ruptured. The X-ray photographs showed that at

relatively small settlement, the movements of the particles is restricted by the cell wall.

In order to study the behaviour of reinforced soil beds with reinforcements within the size of the footing, Sridharan et. al. (1991) conducted model plate load tests. They used two types of reinforcements, viz., mild steel grids and aluminium strips and conducted tests with varying number of layers. To compare the behaviour of this foundation system they conducted tests on unreinforced sand bed with embedded footings with the depth of embedment equal to the depth to the bottom most layer of reinforcement. The test results indicated that for stiff and sufficiently closely spaced ($S_v$<B/4) reinforcements, the increase in load bearing capacity was equal to that of embedding the footing to a depth equal to that of the bottom most layer of reinforcement with the maximum depth of embedment being equal to B. B is the width of the footing and $S_v$, the vertical spacing between the strips. These results are similar to the results obtained by Huang and Tatsuoka (1988). They have given an expression for the bearing capacity ratio (BCR) by modifying the expression given by Binquet and Lee (1975) to account for the embedment effect as

$$BCR = (P_s + k\Delta P_s + P_r)/P_s \qquad (2.5)$$

where $\Delta P_s$ is the increase in load carrying capacity due to the embeddment of the footing and $k=(EA)_{material}/(EA)_{steel}$ with a minimum value of $(EA)_{steel}$ equal to 60,000 kg per cm width of the

footing. $P_s$ and $P_r$ are the load carrying capacities of the soil and the reinforcement respectively.

## 2.4 Field Tests

Jones and Dawson (1990) have studied the performance of reinforced granular foundations on soft clay in situ to exploit this system for foundations for structures. Footings were constructed in a 3.5m×2.5m×1.5m trenches. The reinforcement consisted of welded mesh with PVC coated galvanised high tensile wire. The footings were loaded and their performance monitered with a range of instruments. From the load-settlement curves it was evident that the total settlement was within tolerable limits even under high loads. The authors comment that reinforced granular soil is a promising technique for lightly loaded foundations.

Lindh and Ericksson (1990) performed field tests on two stretches of pavement by incorporating a 100mm layer of sand in the pavement mixed with short plastic fibres. The performance of the pavement was studied for over a year and it was observed that no rutting took place. It was also seen that there was no difference in the stiffness of the layer of stretches with and without reinforcement. The authors comment that the performance will be observed for further three years. They conclude that sand reinforced with short fibres is an interesting method to create cohesion in non-cohesive soils. This method also brings about an improvement in the strength of the soil.

The state-of-art of reinforced soil indicates that lot of work has been in progress to understand the mechanisms of reinforced soil and to predict the increase in the bearing capacitiy of reinforced soil. Inumerable model tests have been performed using various types of reinforcing materials to improve the performance of footings on soft soil. Attempts have been made to put forth theories to predict the behaviour of soils reinforced with strip and sheet form of reinforcements. Few theories are available, most of which either deal with the limit equilibrium techniques or are based on the Finite Element approaches. Further, most of them aim at predicting the increase in the bearing capacity of reinforced soil. Many a times and especially for pavements, settlement governs the design criteria. It hence becomes very essential that the reduction in surface settlements due to reinforcement is known. From the review of the literature it is evident that not much effort has been made to devise theories to predict the reduction in surface settlements due to reinforcements. The present study aims at predicting the settlement reduction of the surface due to strip and sheet form (axi-symmetric) of reinforcements placed beneath rectangular and circular (for the axi-symmetric case only) loaded areas. The elastic continuum theory is resorted to. The tension-membrane action of the reinforcements has however, not been considred.

# CHAPTER 3

# SOIL-RIGID STRIP REINFORCEMENT INTERACTION - SHEAR STRESSES

## 3.1 Introduction

As mentioned in chapter 1, the surface loading causes the points to move downward and outward. The points along the reinforcing strip placed at depth tend to move vertically and horizontally, away from the centre. The strip, in this chapter is considered to be rigid (inextensible in its axial direction). As a result, the horizontal movements of the points along the strip are prevented by the shear stresses mobilised at the interface. The displacements of the points along the strip, due to the surface loading are calculated using the Boussinesq's equation for horizontal displacements of points within an elastic continuum due to a point force on the surface. The horizontal displacements of points along the strip-soil interface due to the mobilised shear stresses are computed using Mindlin's equation for horizontal displacements of points within an elastic continuum due to a horizontal force within the continuum. The compatibility of displacements at the nodes is satisfied by equating the net displacements to zero. This results in a set of simultaneous equations, the solution of which yields the desired shear stresses mobilised at the interface. These stresses, by restricting lateral displacements tend to push the soil above, resulting in the heave of the surface which, in effect is the settlement reduction of the points on the surface.

## 3.2 Single Strip

### 3.2.1 Problem Definition

The problem consists of a rectangular area of size, $2L_f \times 2B_f$, transmitting a uniform load of intensity, q, on the surface of a semi-infinite continuum (Fig. 3.1). A rigid reinforcing strip of size, $2L_r \times 2B_r$, is placed centrally within the soil and below the loaded area at a depth, $U_o$. The width of the strip is relatively small and its thickness, $t_r$, negligible.

Since the width of the strip is assumed to be relatively small, the shear stress developed are assumed to be constant over the width and to vary only along its length. In this chapter only shear interactions are considered. Hence it is assumed that the displacements of the strip in the vertical direction (i.e, with respect to the normal stresses) have no effect on the shear stresses mobilised along the interface. The elastic continuum approach is used to obtain these shear stresses by carrying out an interaction analysis. These stresses, acting inward on the soil, cause the soil above the reinforcement to move upward. This results in the upward displacement of the points along the surface, the origin showing the maxmium displacement. Hence, the net settlement of the surface is reduced due to reinforcing action of the strip.

### 3.2.2 Analysis

Since the analysis is based on the elastic continuum approach, the soil is assumed to be homogeneous, isotropic and

linearly elastic. Firstly, the horizontal displacements along the soil-reinforcement interface due to the applied load are calculated. This is done by using Boussinesq's solution for horizontal displacements at any point within an elastic half-space due to a point load acting on the surface of the elastic half-space. The Boussinesq's problem is as shown in Fig. 3.2. The displacement of point A, as shown in Fig. 3.2, along the radial direction due to load, P, is given by

$$\rho_r = \frac{P(1+\nu_s)}{2\pi E_s R}\left[\frac{rz}{R^2} - \frac{(1-2\nu_s)r}{(R+z)}\right] \qquad (3.1)$$

where r and z are the radial distance and depth of point A, with respect to the load P, $R=\sqrt{r^2+z^2}$, $E_s$ and $\nu_s$ are the modulus of deformation and Poisson's ratio of the medium.

Eq. 3.1 is integrated over the loaded area to obtain the horizontal displacement at point A, (Fig. 3.2), within the half-space due to the uniform load of intensity, q, with appropriate modifications for the direction. That is, the radial displacement, $\Delta\rho_r$, at A due to load intensity, q, on an elemental area $\Delta A$ is

$$\Delta\rho_r = \frac{q\Delta A(1+\nu_s)}{2\pi E_s R}\left[\frac{rz}{R^2} - \frac{(1-2\nu_s)r}{(R+z)}\right] \qquad (3.2)$$

The lateral displacement, $\Delta\rho_x$, along the x-direction is

$$\Delta\rho_x = \Delta\rho_r \cos\alpha \qquad (3.3)$$

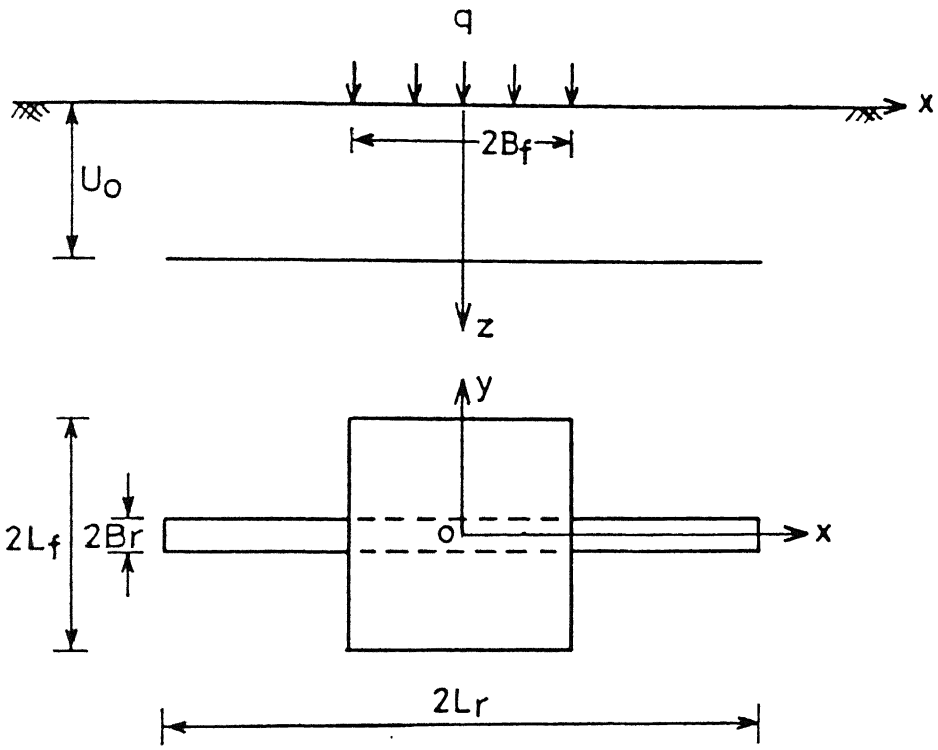


Fig. 3.1 Definition Sketch — Single Strip

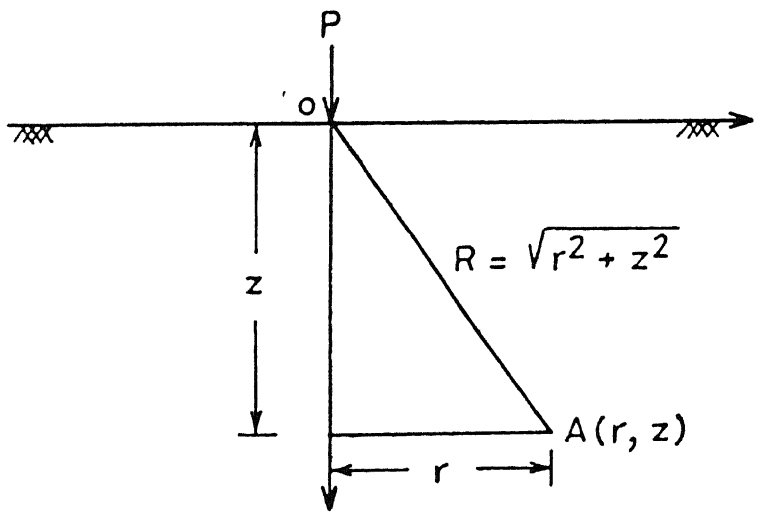


Fig. 3.2 Boussinesq Problem

where $\alpha$ is the angle between the radial line from the elemental area to point A and the x-axis. The total lateral displacement, $\rho_x$, of point A is

$$\rho_x = \int_A \Delta\rho_x = \int_A \Delta\rho_r \, \mathrm{Cos}\alpha \qquad (3.4)$$

The horizontal displacement, $\rho_x$, along the reinforcing strip due to the uniform loading, q, is then evaluated as

$$\rho_x^f = \int_{-B_f}^{B_f} \int_{-L_f}^{L_f} \frac{q(1+\nu_s)}{2\pi E_s R} \left[ \frac{rz}{R^2} - \frac{(1-2\nu_s)r}{(R+z)} \right] \mathrm{Cos}\alpha \, dA \qquad (3.5)$$

In practice, it is found convenient to carry out the integration of Eq. 3.5. numerically. For this purpose the width of the loaded area is sub-divided into $n_B$ sub-elements and length into $n_L$ sub-elements. Due to symmetry only half the length of the strip is considered. This half-length is divided into N elements and over each element the shear stress is assumed to be constant. The horizontal displacement, $\rho_{xij}^f$, of the centre of the $i^{th}$ element (Fig. 3.3), due to loading, q, on an elemental area, $\Delta A$, of element j, on the surface is

$$\rho_{xij}^f = \frac{q(1+\nu_s)}{2\pi E_s R} \left[ \frac{rU_o}{R^2} - \frac{(1-2\nu_s)r}{(R+U_o)} \right] \mathrm{Cos}\alpha_{ij} \, \Delta A \qquad (3.6)$$

where $r=\sqrt{x^2 + y^2}$ and $R=\sqrt{r^2 + U_o^2}$, $U_o$ being the depth to the reinforcing strip.

The horizontal displacement, $\rho^f_{xi}$, of the node i, due to the rectangular surface load is obtained by integrating Eq. 3.6 over the entire rectangular area numerically, as

$$\rho^f_{xi} = \sum_{i_f=1}^{n_B} \sum_{j_f=1}^{n_L} \frac{q(1+\nu_s)}{2\pi E_s R} \left[ \frac{rU_o}{R^2} - \frac{(1-2\nu_s)r}{(R+U_o)} \right] \text{Cos}\alpha \; dA \qquad (3.7)$$

Non-dimensionalising all length parameters with half-width of the loaded area, $B_f$, Eq. 3.7 is expressed as

$$\rho^f_{xi} = \frac{B_f}{E_s} I^f_i \, q \qquad (3.8)$$

where $I^f_i$ is a dimensionless influence coefficient that depends on the aspect ratio of the loaded area, $L_f/B_f$, the depth of placement of the strip, $U_o/B_f$, the Poisson's ratio, $\nu_s$, of the soil and the location of the node i. The horizontal displacements of all the nodes along the half-length of the reinforcing strip are obtained by evaluating Eq. 3.8 for all the nodes, 1 to N. The vector of the displacements for all the nodes is expressed as

$$\left\{ \rho^f_x \right\} = \frac{B_f}{E_s} \left\{ I^f \right\} q \qquad (3.9)$$

where the vectors $\left\{ \rho^f_x \right\}$ and $\left\{ I^f \right\}$ are of size N.

The horizontal displacements due to the surface loading are counteracted by the shear stresses mobilised along the soil-reinforcement interface. In order to obtain these shear

stresses, the horizontal displacements due to these stresses are to be computed. It is achieved by using Mindlin's solution for horizontal displacements due to a horizontal force acting beneath the surface of a semi-infinite medium.

The horizontal displacement of a point, A(x,y,z), due to a horizontal force, Q (Fig. 3.4), acting at a depth, c, within a semi-infinite elastic continuum is

$$\rho_x = \frac{Q\,(1+\nu_s)x}{8\pi E_s(1-\nu_s)}\left[\,F\,\right] \qquad (3.10)$$

where $F = \dfrac{(3-4\nu_s)}{R_1} + \dfrac{1}{R_2} + \dfrac{x^2}{R_1^3} + \dfrac{(3-4\nu_s)x^2}{R_2^3} + \dfrac{2cz}{R_2^3}\left(1 - \dfrac{3x^2}{R_2^2}\right) +$

$$\frac{4(1-\nu_s)(1-2\nu_s)}{(R_2+z+c)}\left(1 - \frac{x^2}{R_2^2(R_2+z+c)}\right)$$

$$R_1 = \sqrt{x^2+ y^2+ (z-c)^2}$$

$$R_2 = \sqrt{x^2+ y^2+ (z+c)^2}$$

and x, y, z are the co-ordinates of point A (Fig. 3.4). The lateral displacement of any point along the strip due to shear stress, $\tau$, on an elemental area, dA, is

$$d\rho_x = \frac{\tau dA(1+\nu_s)x}{8\pi E_s(1-\nu_s)}\left[\,F\,\right] \qquad (3.11)$$

In order to obtain the lateral displacement, $\rho_x^r$, of points along the reinforcement due to the mobilised shear stresses,

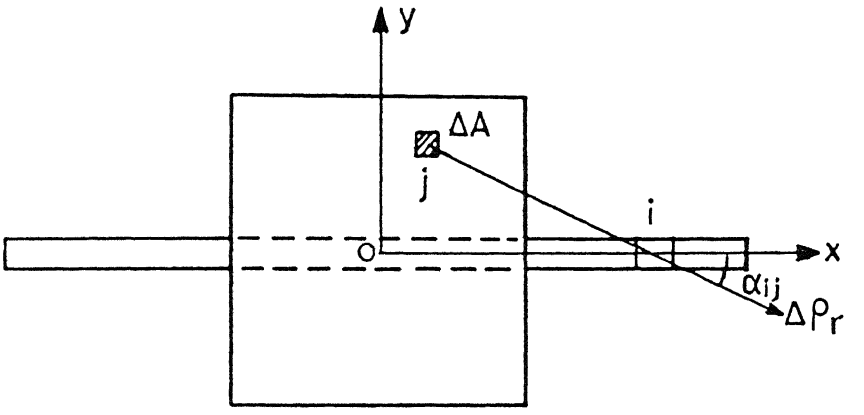


Fig. 3.3 Radial Displacement along Strip due to Surface Load

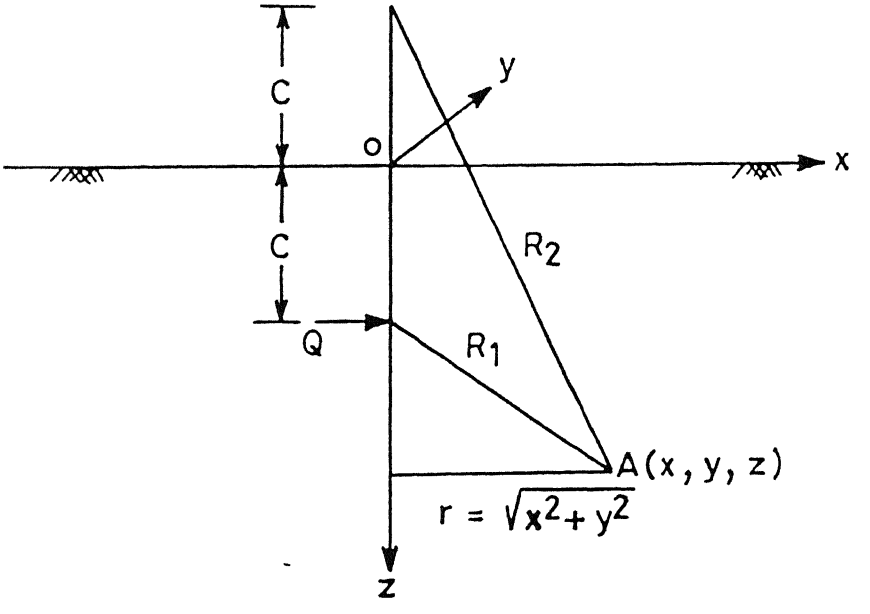


Fig. 3.4 Mindlin Problem

reinforcing strip. Only half the length of the strip is considered due to symmetry and this length is discretized into N elements. The lateral displacement, $\rho^{r}_{xij}$, of node i due to shear stress, $\tau_j$, acting on element j (Fig. 3.5) is

$$\rho^{r}_{xij} = \int_{dA} \frac{(1+\nu_s)\ x}{B\pi E_s (1-\nu_s)} \left[ F \right] \tau_j \, dA \qquad (3.12)$$

where x and y are the horizontal distances of node i with respect to the elemental area, dA, of the $j^{th}$ element. The other parameters are as mentioned in Eq. 3.10 with $c = U_o = z$.

Eq. 3.12 is also integrated numerically to obtain the influence of shear stress, $\tau_j$, on the horizontal displacement of node i. Non-dimensionalising all length parameters with $B_f$, Eq. 3.12 is written as

$$\rho^{r_1}_{xij} = \frac{B_f}{E_s} I^{r_1}_{ij} \tau_j \qquad (3.13)$$

where $I^{r_1}_{ij}$ is a dimensionless coefficient that depends on the length, $L_r/B_f$, and the depth of placement of the strip, $U_o/B_f$, the Poisson's ratio, $\nu_s$, of the soil and the location of the node i and element, j. For every element j, there exists an image j', (Fig. 3.5), shear stress on which is of the same magnitude but acting in a direction opposite to the one acting on element, j. The influence of the stresses acting on element j', on the lateral displacement of node i, is written as

$$\rho^{r_2}_{xij} = \frac{B_f}{E_s} I^{r_2}_{ij} \tau_j \qquad (3.14)$$

where $I^{r_2}_{ij}$ is the influence coefficient for the influence on the displacement at node, i due to the shear stress on element j'. $I^{r_2}_{ij}$ is obtained from Eq. 3.12 wherein x and y are the distances of node i, with respect to the elemental area, dA, of the $j^{th}$ element. It is to be noted that the horizontal displacement, $\rho^{r_2}_{xij}$, will be in the opposite direction with respect to the displacement, $\rho^{r_1}_{xij}$.

Combining Eqs. 3.13 and 3.14, i.e., combining the influences of the shear stresses on the $j^{th}$ element and of its mirror image, the lateral displacement of node, i is

$$\rho^{r}_{xij} = \frac{B_f}{E_s} \left( I^{r_1}_{ij} - I^{r_2}_{ij} \right) \tau_j \qquad (3.15)$$

To obtain the displacement at node, i due to the shear stresses on all the elements along the full length of the strip, Eq. 3.15 is integrated numerically over the N elements along the half-length of the strip as

$$\rho^{r}_{xi} = \sum_{j=1}^{N} \frac{B_f}{E_s} \left( I^{r_1}_{ij} - I^{r_2}_{ij} \right) \tau_j \qquad (3.16)$$

The horizontal displacements of the centre of all the elements along the half length of the strip is

$$\left\{ \rho_x^r \right\} = \frac{B_f}{E_s} \sum_{j=1}^{N} \left[ I_{ij}^{r_1} - I_{ij}^{r_2} \right] \left\{ \tau \right\} \qquad (3.17)$$

Expressing Eq. 3.17 in matrix form, the vector of horizontal displacements, $\left\{ \rho_x^r \right\}$, is written as

$$\left\{ \rho_x^r \right\} = \frac{B_f}{E_s} \left[ I^r \right] \left\{ \tau \right\} \qquad (3.18)$$

where vectors, $\left\{ \rho_x^r \right\}$ and $\left\{ \tau \right\}$ are of size N, $\left[ I^r \right]$ is a square matrix of size N. An interesting property of this matrix is that $I_{ij}^r = I_{ji}^r$.

At this juncture, the lateral displacements of the centres of all the elements along the strip due to the applied surface loading (Eq. 3.9) and those due to the mobilised shear stresses (Eq. 3.18) are known. The net soil displacement of node i, is the difference of the displacements due to the surface load and the interaction stresses, i.e.,

$$\rho_{xi}^{net} = \rho_{xi}^{f} - \rho_{xi}^{r} \qquad (3.19)$$

The net soil displacements should be compatible with the displacements of the reinforcing strip. The solution of the shear stresses is obtained by satisfying the compatibility of displacements at the soil-reinforcement interface. For a rigid (inextensible) strip the net lateral displacements are zero, i.e,

$$\left\{ \rho_x^f \right\} - \left\{ \rho_x^r \right\} = \left\{ 0 \right\} \qquad (3.20)$$

Combining Eqs. 3.9, 3.18 and 3.20 one obtains

$$\frac{B_f}{E_s} \left\{ I^f \right\} q - \frac{B_f}{E_s} \left[ I^r \right] \left\{ \tau \right\} = \left\{ 0 \right\} \qquad (3.21)$$

or

$$\left[ I^r \right] \left\{ \tau/q \right\} = \left\{ I^f \right\} \qquad (3.22)$$

Eq. 3.22 gives N equations for $\tau/q$, the normalised shear stresses. It is solved by the Gauss elimination technique for the shear stresses on all elemental areas.

These shear stresses are developed at the interface of the soil and strip. The thickness of the strip being negligibly small, it can be assumed that the stresses above and below the strip are equal to half the calculated values. The stresses mobilised in the soil in turn develop tension in the reinforcing strip. The tension is evaluated as under (Fig. 3.6)

$$\Delta T_i = \tau_i \Delta A = \tau_i \, 2B_r \, dl \qquad (3.23)$$

where $\Delta T_i$ is the elemental tension on the element i, and dl is the length of element i. The total tension at the centre of element i is

$$T_i = \frac{1}{2} \tau_i \, \Delta A + \sum^{N} \tau_j \, \Delta A \qquad (3.24)$$

$$T_i = \frac{1}{2} \tau_i \, \Delta A + \sum^{N} \tau_j \, \Delta A \qquad (3.24)$$

The tension at the centre of the strip, i.e., at x=0 is

$$T_{x=o} = \frac{1}{2}\tau_i \Delta A + T_1 = \sum_{j=1}^{N} \tau_j \Delta A_j \qquad (3.25)$$

where $\Delta A_j$ is the area of element j. The tension at $x=L_r$ i.e., at the edge of the strip is zero.

The primary aim of this analysis is to estimate the reduction in settlement of the surface due to the presence of a reinforcing strip inclusion within the soil. As mentioned earlier, the shear stresses mobilised help in causing an upward displacement of the soil at the surface as depicted in Fig. 3.7. The shear stresses cause the soil above it to move upward and inward. As a result, the centre or the origin, 'O', experiences a maximum upward displacement. The surface displacement profile is as shown in Fig. 3.7. Once, this profile is evaluated the problem is solved completely.

In order to arrive at this profile, Mindlin's solution for vertical displacement at any point within an elastic half-space due to a horizontal force within the half-space is used. Referring to Fig. 3.4, the vertical displacement of point A due to a horizontal load, Q, is given by

$$\rho_z = \frac{Q\,(1+\nu_s)x}{8\pi E_s(1-\nu_s)}\left[\frac{z-c}{R_1^3} + \frac{(3-4\nu_s)(z-c)}{R_2^3} + \frac{6cz(z+c)}{R_2^5} + \frac{4(1-\nu_s)(1-2\nu_s)}{R_2(R_2+z+c)}\right] \qquad (3.26)$$

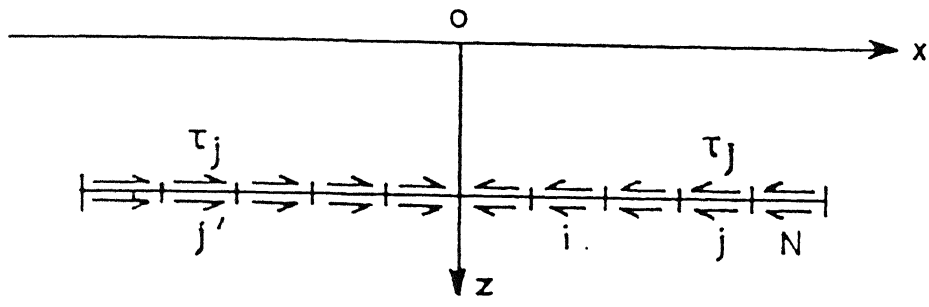


Fig. 3.5 Shear Stresses in Soil

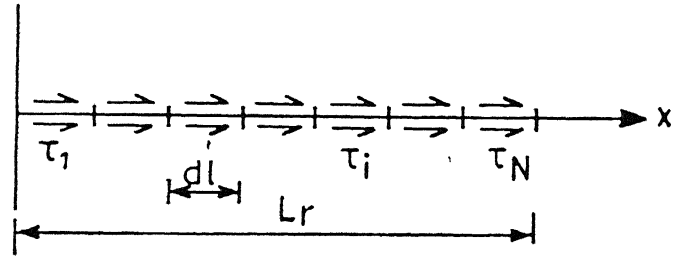


Fig. 3.6 Stresses on the Strip

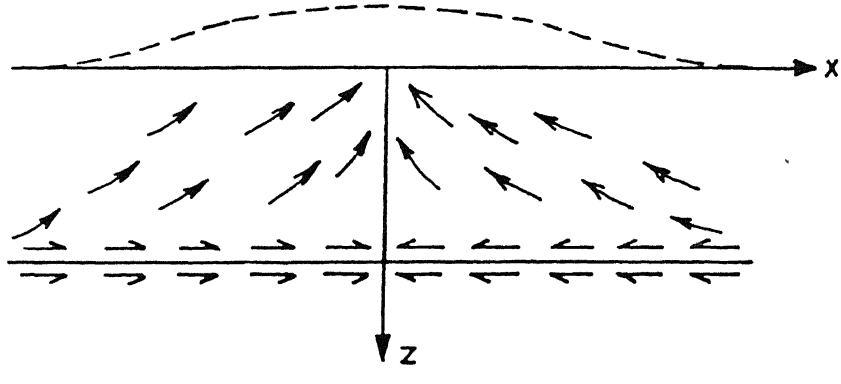


Fig. 3.7 Settlement Reduction of Surface

the shear modulus of soil ($G_s=E_s/2(1+\nu_s)$). Non-dimensionalising length parameters with $B_f$, Eq. 3.29 is rewritten as

$$\rho^{r_1}_{zkj} = \frac{B_f}{G_s} I^{r_1}_{skj} \tau_j \qquad (3.30)$$

where $\rho^{r_1}_{zkj}$ is the vertical displacement of point k, due to shear stress on element j. Displacement at point k, due to shear stress on the image element j′, on the left half of the strip is

$$\rho^{r_2}_{zkj} = \frac{B_f}{G_s} I^{r_2}_{skj} \tau_j \qquad (3.31)$$

where $I^{r_1}_{skj}$ and $I^{r_2}_{skj}$ are dimensionless displacement coefficients for the influence of shear stresses on the elements j and j′ on the displacements of node k, and are functions of the ratios, $L_r/B_f$, $U_o/B_f$, $\nu_s$ and the location of the respective elements. Combining Eq. 3.30 and 3.31, the vertical displacement at node k, on the surface is

$$\rho_{zkj} = \frac{B_f}{G_s} \left( I^{r_1}_{skj} + I^{r_2}_{skj} \right) \tau_j \qquad (3.32)$$

The displacement of node, k due to shear stresses on all the elements along the strip is

$$\rho_{zk} = \sum_{j=1}^{N} \frac{B_f}{G_s} \left( I^{r_1}_{skj} + I^{r_2}_{skj} \right) \tau_j \qquad (3.33)$$

Expressing Eq. 3.33 in matrix form as

$$\left\{ \rho_z \right\} = \frac{B_f}{G_s} \left[ I_s^r \right] \left\{ \tau \right\} \qquad (3.34)$$

The width of the loaded area is divided into $N_f$ points where $\rho_z$ is evaluated. The vector, $\left\{ \rho_z \right\}$, is of size $N_f$, vector, $\left\{ \tau \right\}$, of size N and the matrix $\left[ I_s^r \right]$ is of size $N_f \times N$.

Eq. 3.34 is rewritten as

$$\left\{ \rho_z \right\} = \frac{B_f}{G_s} \left\{ I_s \right\} q \qquad (3.35)$$

The elements of this vector are termed as Settlement Reduction Coefficients (SRC). SRC at any node k, on the surface is

$$SRC_k = I_{sk} = \frac{\rho_{zk}}{B_f} \frac{G_s}{q} \qquad (3.36)$$

where $\rho_{zk}$ is the vertical upward displacement of node k, due to the mobilised shear stresses. The SRC at the origin, O, or the centre of the loaded area is defined as $I_{sc}$.

The vector of the SRC along the surface is

$$\left\{ I_s \right\} = \frac{1}{B_f} \frac{G_s}{q} \left\{ \rho_z \right\} \qquad (3.37)$$

where $\left\{ I_s \right\}$ is obtained as

$$\left\{ I_s \right\} = \left[ I_s^r \right] \left\{ \tau \right\} \qquad (3.38)$$

where the matrix, $\left[ I_s^r \right]$ and vector, $\left\{ \tau \right\}$ are known.

## 3.3 Two Strips at Depth, $U_o$



### 3.3.1 Problem Definition

In this case, two strips of size, $2L_r \times 2B_r$, are placed symmetrically about the x-axis at a depth, $U_o$, within the soil mass (Fig. 3.8). Each strip is placed at a distance, $S_y$, from the x-axis. The mechanism through which shear stresses are developed along the soil-strip interface is the same as that mentioned in the section for a single strip. The discretizations of the surface loaded area and the strip are the same as in the previous case. Since the strips are placed equidistant from the x-axis, the lateral displacements along both the strips due to the surface loading are equal. Consequently, the shear stresses mobilised at the interfaces are also equal.

The horizontal displacements along the length of one strip due to shear stresses are not only influenced by the stresses along itself but also by the stresses mobilised along the second strip. In calculating the horizontal displacement of node i, due to stress on element j, (Fig. 3.9), in addition to the stresses on element j, and its image j′, stresses on elements j′′ and its image j′′′, along the second strip are also to be considered.

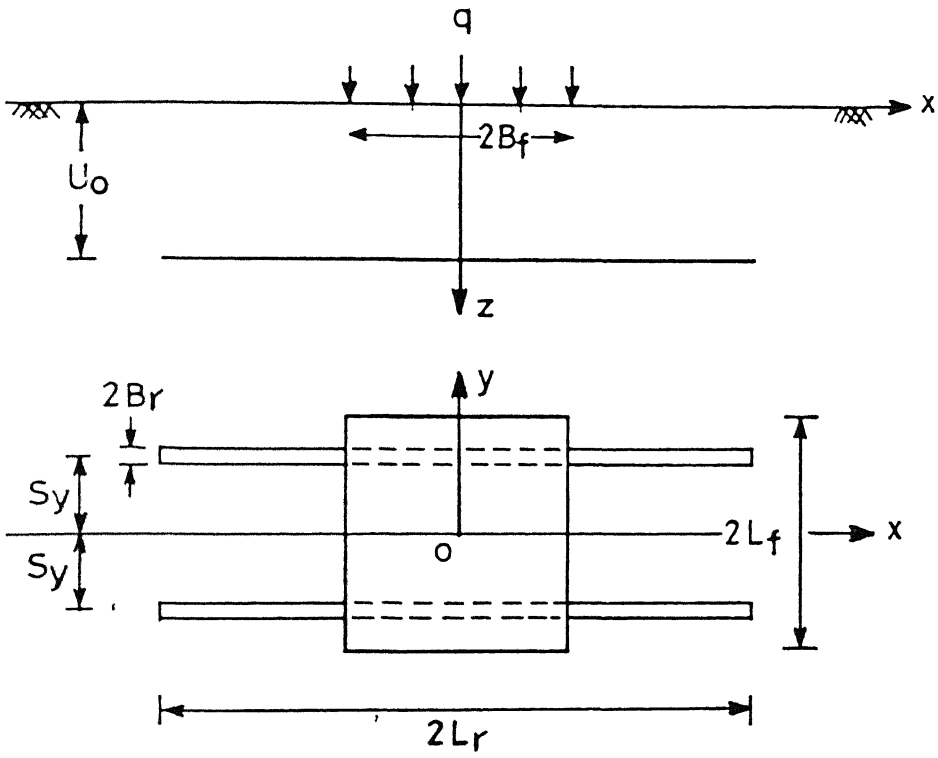


Fig. 3.8 Definition Sketch — Two Strips at Depth $U_o$

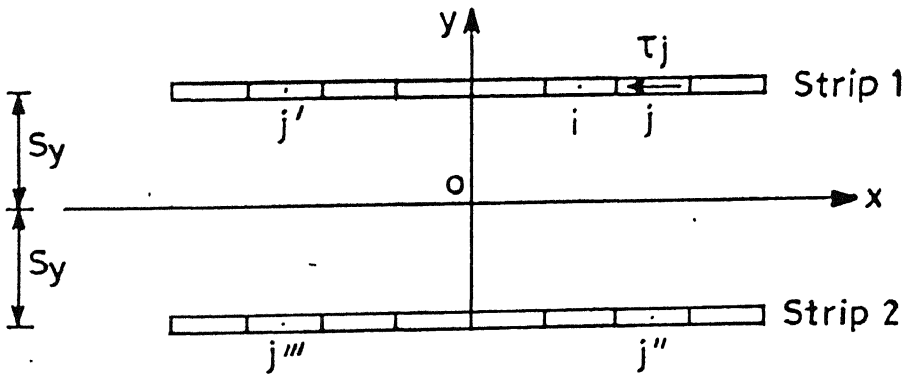


Fig. 3.9 Discretization of the Strips

Incidentally, the stresses on all these elements are the same due to symmetry.

### 3.3.2 Analysis

Due to symmetry, the horizontal displacements only along half the strip length due to applied loading are calculated. The displacements are computed from Eq. 3.7 with the modification, $r = \sqrt{x^2 + (S_y - y)^2}$. Non-dimensionalising all length parameters with the half-width of the loaded area, $B_f$, Eq. 3.7 is written as

$$\rho^f_{xi} = \frac{B_f}{E_s} I^f_i \, q \qquad (3.39)$$

where $I^f_i$ is a dimensionless influence coefficient that depends on the ratios, $L_f/B_f$, $U_o/B_f$, $S_y/B_f$, $\nu_s$ and the location of node i. $\rho^f_{xi}$ is the horizontal displacement of node i due to the surface loading. The vector of the displacements of all nodes is expressed as in Eq. 3.9 as

$$\left\{ \rho^f_x \right\} = \frac{B_f}{E_s} \left\{ I^f \right\} q \qquad (3.40)$$

where vectors $\left\{ \rho^f_x \right\}$ and $\left\{ I^f \right\}$ are of size N.

The horizontal displacements due to shear stresses along the strip are calculated using Mindlin's solution as described in Eq. 3.10. The displacements of node i due to shear stresses, acting on elements j, j′, j′′ and j′′′, as explained in Fig. 3.9 are obtained from Eq. 3.12 and are expressed in a dimensionless form as

$$\rho_{xij}^{r_1} = \frac{B_f}{E_s} I_{ij}^{r_1} \tau_j \qquad (3.41)$$

$$\rho_{xij}^{r_2} = \frac{B_f}{E_s} I_{ij}^{r_2} \tau_j \qquad (3.42)$$

$$\rho_{xij}^{r_3} = \frac{B_f}{E_s} I_{ij}^{r_3} \tau_j \qquad (3.43)$$

and

$$\rho_{xij}^{r_4} = \frac{B_f}{E_s} I_{ij}^{r_4} \tau_j \qquad (3.44)$$

where $I_{ij}^{r_1}$, $I_{ij}^{r_2}$, $I_{ij}^{r_3}$, and $I_{ij}^{r_4}$ are displacement influence coefficients for the influence of the shear stresses on elements j, j′, j′′ and j′′′ respectively, and are functions of $L_r/B_f$, $U_o/B_f$, $S_y/B_f$, $\nu_s$ and the location of the respective elements.

Combining equations 3.41 through 3.44, the lateral displacement of node i, due to shear stresses on all N elements is

$$\rho_{xi}^{r} = \sum_{j=1}^{N} \frac{B_f}{E_s} \left\{ I_{ij}^{r_1} - I_{ij}^{r_2} + I_{ij}^{r_3} - I_{ij}^{r_4} \right\} \tau_j \qquad (3.45)$$

where the summation is carried out for stresses acting on all N elements. The vector of horizontal displacements is

$$\left\{ \rho_x^r \right\} = \frac{B_f}{E_s} \left[ I^r \right] \left\{ \tau \right\} \qquad (3.46)$$

where the vectors, $\left\{ \rho_x^r \right\}$ and $\left\{ \tau \right\}$ are of size N, $\left[ I^r \right]$ is a square matrix of size N. The difference in the matrix, $\left[ I^r \right]$, in this case as compared to a single strip is that the matrix here is

a function of the distance, $S_y/B_f$, of the strips from the x-axis also, while it was not in the former case.

The net lateral displacement for a rigid strip is zero. Satisfying compatibility of displacements as in Eq. 3.20, shear stresses are obtained from Eq. 3.22, written again as

$$\left[ I^r \right] \left\{ \tau/q \right\} = \left\{ I^f \right\} \qquad (3.47)$$

Eq. 3.47 is solved for the N values of $\tau/q$ on all the elements.

Once the interfacial shear stresses are computed, the tension along the strips and settlement reduction coefficients for points on the surface are obtained based on the formulation discussed for the single strip. The tension in the strips is arrived at using equations 3.22 through 3.25.

In calculating the settlement reduction coefficients, appropriate modification for the influence of the two strips, i.e, for the distance, $S_y$, is to be made. The vertical displacement at any point, k, on the surface due to the shear stress on element j, on the strip is given by Eq. 3.29 wherein $y_{kj}$ now includes the parameter, $S_y$, while all other parameters remain unaltered.

The vertical displacements of point k, due to shear stresses on elements j, j′, j′′ and j′′′ (Fig. 3.9) are given by

$$\rho^{r_1}_{zkj} = \frac{B_f}{G_s} I^{r_1}_{skj} \tau_j \qquad (3.48)$$

$$\rho^{r_2}_{zkj} = \frac{B_f}{G_s} I^{r_2}_{skj} \tau_j \qquad (3.49)$$

$$\rho^{r_3}_{zkj} = \frac{B_f}{G_s} I^{r_3}_{skj} \tau_j \qquad (3.50)$$

and

$$\rho^{r_4}_{zkj} = \frac{B_f}{G_s} I^{r_4}_{skj} \tau_j \qquad (3.51)$$

where $I^{r_1}_{skj}$, $I^{r_2}_{skj}$, $I^{r_3}_{skj}$, and $I^{r_4}_{skj}$ are dimensionless coefficients for the influence of the shear stresses on the elements j, j′, j′′ and j′′′ respectively and are functions of $L_r/B_f$, $U_o/B_f$, $S_y/B_f$, $\nu_s$ and the location of the respective elements. Combining equations 3.48 through 3.51, the vertical displacement, $\rho^r_{zk}$, of node k, due to shear stresses on all N elements is

$$\rho^r_{zk} = \sum_{j=1}^{N} \frac{B_f}{G_s} \left\{ I^{r_1}_{skj} + I^{r_2}_{skj} + I^{r_3}_{skj} + I^{r_4}_{skj} \right\} \tau_j \qquad (3.52)$$

The vector of the vertical displacements of $N_f$ points along the surface is

$$\left\{ \rho_z \right\} = \frac{B_f}{G_c} \left[ I^r_s \right] \left\{ \tau \right\} \qquad (3.53)$$

$$\left\{ \rho_z \right\} = \frac{B_f}{G_s} \left[ I^r_s \right] \left\{ \tau \right\} \qquad (3.53)$$

The SRC at point k on the surface, due to the stresses along the

$$I_{sk} = \frac{\rho_{zk}}{B_f} \frac{G_s}{q} \qquad (3.54)$$

The vector of the SRC along the surface is expressed as

$$\left\{ I_s \right\} = \frac{1}{B_f} \frac{G_s}{q} \left\{ \rho_z \right\} \qquad (3.55)$$

where $\left\{ I_s \right\}$ is obtained as

$$\left\{ I_s \right\} = \left[ I_s^r \right] \left\{ \tau \right\} \qquad (3.56)$$

where the matrix, $\left[ I_s^r \right]$ and vector, $\left\{ \tau \right\}$ are known.

## 3.4 Two Strips - One Below the Other

### 3.4.1 Problem Definition

Two strips of size, $2L_r \times 2B_r$, placed beneath the centre of the loaded area along the x-axis, one at a depth, $U_o$, and the other at a depth, $U_i$ are considered (Fig. 3.10). The interference of one strip on the other is studied. It is assumed that the horizontal displacements at depths, $U_o$ and $U_i$, due to the surface loading remain unaffected by the presence of the other strip, i.e the Boussinesq's equation is applicable for both the depths.

Since the strips are placed at two different depths, the horizontal displacements at the two levels are different and consequently, the stresses mobilised are also different. The stresses are symmetric about the z-axis. The stresses mobilised

along each strip influence the horizontal displacements of points along the length of the other. In computing the horizontal displacement at node i (Fig. 3.11), of strip 1, the influences of stresses, $\tau_j^1$, on elements, j and its image j′, along strip 1, and the stresses, $\tau_j^2$, on elements, j and its image j′, along strip 2 are to be considered. Similarly, for horizontal displacements of points along strip 2, the influence of stresses along strip 1 and strip 2 are to be accounted for.

### 3.4.2 Analysis

Eq. 3.7 is used to calculate the horizontal displacements of points at depths, $U_o$ and $U_1$. The vector of horizontal displacements of the N nodes along the half-length of strip 1 is

$$\left\{ \rho_{x1}^f \right\} = \frac{B_f}{E_s} \left\{ I_1^f \right\} q \qquad (3.57)$$

where $\left\{ I_1^f \right\}$ is a dimensionless influence coefficient vector of size, N, that depends on the parameters, $L_f/B_f$, $U_o/B_f$, $\nu_s$ and the location of the nodes.

The vector of horizontal displacements at N nodes along the half-length of strip 2 is

$$\left\{ \rho_{x2}^f \right\} = \frac{B_f}{E_s} \left\{ I_2^f \right\} q \qquad (3.58)$$

where $\left\{ I_2^f \right\}$ is a dimensionless influence coefficient vector of size, N, that depends on the parameters, $L_f/B_f$, $U_1/B_f$ and $\nu_s$ and

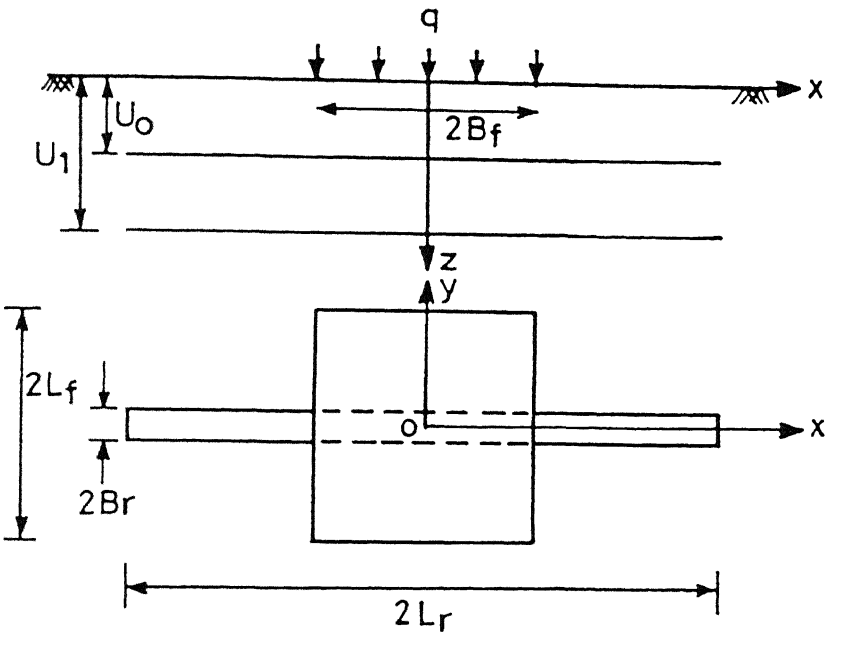


Fig. 3.10 Definition Sketch – Two Strips One Below the Other

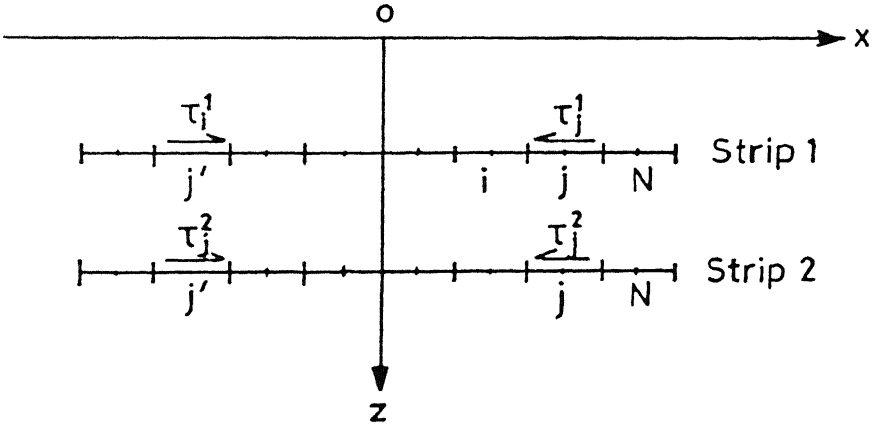


Fig. 3.11 Discretization of the Strips

the location of the nodes.

Eq. 3.10 is used to compute the horizontal displacements of points along the lengths of the strips due to the mobilised shear stresses on them. The horizontal displacement of node i of strip 1 (Fig. 3.11), due to shear stresses on all elements along strip 1 is

$$\rho_{xi}^{r_{11}} = \sum_{j=1}^{N} \frac{B_f}{E_s} \left( I_{ij}^{r_1} - I_{ij}^{r_2} \right) \tau_j^1 \qquad (3.59)$$

and that due to stresses on all elements along strip 2 is

$$\rho_{xi}^{r_{12}} = \sum_{j=1}^{N} \frac{B_f}{E_s} \left( I_{ij}^{r_3} - I_{ij}^{r_4} \right) \tau_j^2 \qquad (3.60)$$

where $I_{ij}^{r_1}$ and $I_{ij}^{r_2}$ are dimensionless coefficients for the influence of shear stress, $\tau_j^1$, on elements j and its image j′ respectively, of strip 1. $I_{ij}^{r_3}$ and $I_{ij}^{r_4}$ are dimensionless coefficients for the influence of shear stress, $\tau_j^2$, on elements j and its image j′ respectively, of strip 2. Apart from being functions of $L_r/B_f$, $\nu_s$ and the locations of the elements, $I_{ij}^{r_1}$ and $I_{ij}^{r_2}$ are functions of the depth ratios $U_o/B_f$ and, $I_{ij}^{r_3}$ and $I_{ij}^{r_4}$ are functions of the depth ratios, $U_o/B_f$ and $U_1/B_f$. From Eq. 3.59, the vector of horizontal displacements, $\left\{ \rho_x^{r_{11}} \right\}$ of all N nodes along strip 1 due to shear stresses along strip 1 is written as

$$\left\{ \rho_x^{r_{11}} \right\} = \frac{B_f}{E_s} \left[ I^{r_{11}} \right] \left\{ \tau^1 \right\} \qquad (3.61)$$

where $\left[ I^{r_{11}} \right]$ is the coefficient matrix for the influence of shear stresses, $\left\{ \tau^{1} \right\}$, along strip 1 on displacements of nodes along strip 1 itself.

The vector of horizontal displacements, $\left\{ \rho_x^{r_{12}} \right\}$, of N nodes along strip 1 due to shear stresses along strip 2, from Eq. 3.60 is

$$\left\{ \rho_x^{r_{12}} \right\} = \frac{B_f}{E_s} \left[ I^{r_{12}} \right] \left\{ \tau^{2} \right\} \tag{3.62}$$

where $\left[ I^{r_{12}} \right]$ is a coefficient matrix for the influence of shear stresses, $\left\{ \tau^{2} \right\}$, along strip 2, on the displacements of the nodes along strip 1.

Similarly for strip 2, the vectors, $\left\{ \rho_x^{r_{21}} \right\}$ and $\left\{ \rho_x^{r_{22}} \right\}$, of horizontal displacements are written as

$$\left\{ \rho_x^{r_{21}} \right\} = \frac{B_f}{E_s} \left[ I^{r_{21}} \right] \left\{ \tau^{1} \right\} \tag{3.63}$$

and

$$\left\{ \rho_x^{r_{22}} \right\} = \frac{B_f}{E_s} \left[ I^{r_{22}} \right] \left\{ \tau^{2} \right\} \tag{3.64}$$

where $\left[ I^{r_{21}} \right]$ and $\left[ I^{r_{22}} \right]$ are coefficient matrices for the influence of shear stresses, $\left\{ \tau^{1} \right\}$, along strip 1, and $\left\{ \tau^{2} \right\}$ along strip 2 respectively, on the displacements of the N nodes along strip 2. All the matrices, viz. $\left[ I^{r_{11}} \right]$, $\left[ I^{r_{12}} \right]$, $\left[ I^{r_{21}} \right]$ and $\left[ I^{r_{22}} \right]$ are square matrices of size N, and the displacement

and stress vectors are of size N

Combining Eqs. 3.61 through 3.64 the vectors of horizontal displacements of N nodes, each along strips 1 and 2 are

$$\left\{ \rho_x^r \right\} = \frac{B_f}{E_s} \left[ I^r \right] \left\{ \tau \right\} \tag{3.65}$$

where $\left\{ \rho_x^r \right\}$ and $\left\{ \tau \right\}$ are vectors of size 2N and $\left[ I^r \right]$ is a square matrix of size 2N.

The vector, $\left\{ \rho_x^r \right\}$ comprises of vectors, $\left\{ \rho_x^{r_1} \right\}$ and $\left\{ \rho_x^{r_2} \right\}$ and is written as

$$\left\{ \rho_x^r \right\}^T = \left\lfloor \left\lfloor \rho_x^{r_1} \right\rfloor \left\lfloor \rho_x^{r_2} \right\rfloor \right\rfloor \tag{3.66}$$

where $\left\{ \rho_x^{r_1} \right\} = \left\{ \rho_x^{r_{11}} \right\} + \left\{ \rho_x^{r_{12}} \right\}$

and

$$\left\{ \rho_x^{r_2} \right\} = \left\{ \rho_x^{r_{21}} \right\} + \left\{ \rho_x^{r_{22}} \right\}$$

The vector $\left\{ \tau \right\}$ comprises of vectors $\left\{ \tau^1 \right\}$ and $\left\{ \tau^2 \right\}$ and is written as

$$\left\{ \tau \right\}^T = \left\lfloor \left\lfloor \tau^1 \right\rfloor \left\lfloor \tau^2 \right\rfloor \right\rfloor = \left\lfloor \tau_1^1 \ldots\ldots \tau_N^1 \; \tau_1^2 \ldots\ldots \tau_N^2 \right\rfloor \tag{3.67}$$

The matrix, $\left[ I^r \right]$ is written as

$$\left[ I^r \right] = \left[ \begin{array}{c|c} I^r_{11} & I^r_{12} \\ \hline I^r_{21} & I^r_{22} \end{array} \right] \tag{3.68}$$

Combining equations 3.57 and 3.58 the vector of horizontal displacements of the nodes along strips 1 and 2, is

$$\left\{ \rho^f_x \right\} = \frac{B_f}{E_s} \left\{ I^f \right\} q \tag{3.69}$$

where $\left\{ \rho^f_x \right\}$ and $\left\{ I^f \right\}$ are vectors of size 2N.

Vector, $\left\{ \rho^f_x \right\}$ is expressed as

$$\left\{ \rho^f_x \right\}^T = \lfloor \lfloor \rho^f_{x1} \rfloor \lfloor \rho^f_{x2} \rfloor \rfloor = \lfloor \rho^f_{x11} \ldots\ldots \rho^f_{x1N} \; \rho^f_{x21} \ldots\ldots \rho^f_{x2N} \rfloor \tag{3.70}$$

$\left\{ I^f \right\}$ comprises of vectors $\left\{ I^f_1 \right\}$ and $\left\{ I^f_2 \right\}$

**For rigid strips, the net lateral displacement is zero. Satisfying compatibility of displacements at all nodes, it can be written that**

$$\left\{ \rho^f_x \right\} - \left\{ \rho^r_x \right\} = \left\{ 0 \right\} \tag{3.71}$$

**or**

$$\left[ I^r \right] \left\{ \tau/q \right\} = \left\{ I^f \right\} \tag{3.72}$$

The solution of these 2N equations gives the shear stresses on N elements along strips 1 and 2 respectively.

The tensile forces along the strips and the settlement reduction coefficients due to these stresses are calculated on similar lines as explained in the earlier sections.

## 3.5 Multiple Strips

The performance of multiple strips are studied here. Two pairs of strips of the same dimensions ($2L_r \times 2B_r$) are placed below the loaded area, symmetrically about the x-axis at a depth, $U_o$, (Fig. 3.12). One pair consists of two contiguous strips each at a distance, $S_{y1}=B_r$, from the x-axis. This pair is equivalent to a single strip of width, $2B_r$, placed symmetrically below the loaded area (the width of each strip in the pair is half that of a single strip). Each strip of the second pair of strips is placed at a distance, $S_{y2}$, from the x-axis. The interference of one strip on the other is studied in this case.

### 3.5.1 Analysis

As explained in the previous section, the horizontal displacement vector of N nodes along the length, $L_r$, of the first pair of strips is

$$\left\{ \rho^f_{x1} \right\} = \frac{B_f}{E_s} \left\{ I^f_1 \right\} q \qquad (3.73)$$

where $\left\{ \rho^f_{x1} \right\}$ and $\left\{ I^f_1 \right\}$ are vectors of size N, and $\left\{ I^f_1 \right\}$ is a non-dimensional vector of influence coefficients that depends on

the parameters, $L_f/B_f$, $U_o/B_f$, $S_{y1}/B_f$, $\nu_s$ and the location of node i. Again, due to symmetry only one strip of each pair is considered.

The horizontal displacement vector of the N nodes along the half-length, $L_r$, for the second pair of strips at a distance, $S_{y2}$, from the x-axis, in non-dimensional terms is

$$\left\{ \rho^f_{x2} \right\} = \frac{B_f}{E_s} \left\{ I^f_2 \right\} q \qquad (3.74)$$

where $\left\{ \rho^f_{x2} \right\}$ and $\left\{ I^f_2 \right\}$ are vectors of size N and $\left\{ I^f_2 \right\}$ is a dimensionless vector of influence coefficients that depends on the parameters, $L_f/B_f$, $U_o/B_f$, $S_{y2}/B_f$, $\nu_s$ and the location of node i.

Combining Eqs. 3.73 and 3.74, the vector of horizontal displacements for both the pairs of strips is written as

$$\left\{ \rho^f_x \right\} = \frac{B_f}{E_s} \left\{ I^f \right\} q \qquad (3.75)$$

where $\left\{ \rho^f_x \right\}$ and $\left\{ I^f \right\}$ are vectors of size 2N. $\left\{ \rho^f_x \right\}$ comprises of vectors, $\left\{ \rho^f_{x1} \right\}$ and $\left\{ \rho^f_{x2} \right\}$, while $\left\{ I^f \right\}$ comprises of vectors $\left\{ I^f_1 \right\}$ and $\left\{ I^f_2 \right\}$.

The horizontal displacement of node i (Fig. 3.13) along the first pair of strips due to the shear stresses on the N elements of the first pair can be written as mentioned in Eq. 3.45 as

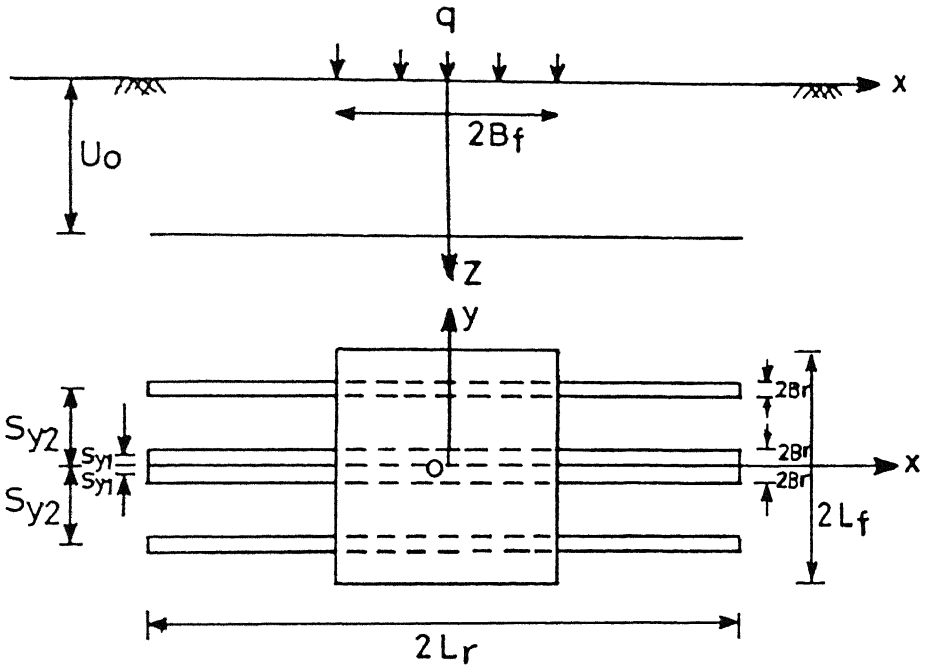


Fig. 3.12 Definition Sketch – Multiple Strips

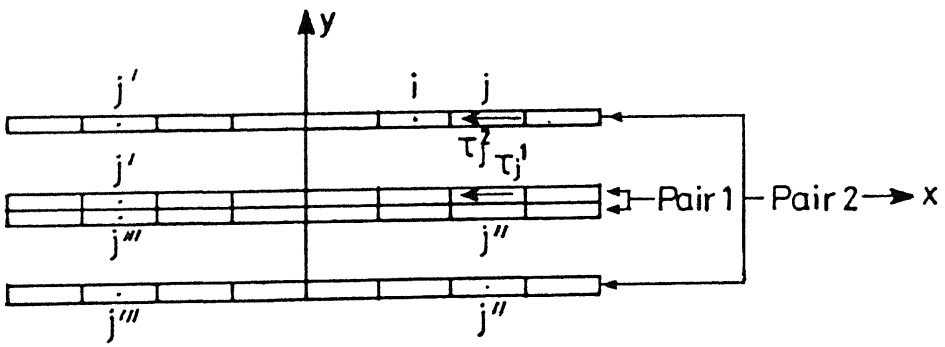


Fig. 3.13 Discretization of the Strips

$$\rho_{xi}^{r_{11}} = \sum_{j=1}^{N} \frac{B_f}{E_s} \left\{ I_{ij}^{r_1} - I_{ij}^{r_2} + I_{ij}^{r_3} - I_{ij}^{r_4} \right\} \tau_j^1 \qquad (3.76)$$

where $I_{ij}^{r_1}$, $I_{ij}^{r_2}$, $I_{ij}^{r_3}$, and $I_{ij}^{r_4}$ are the influence coefficients for the displacement of node i due to shear stress, $\tau_j^1$, on elements j, j′, j′′ and j′′′, the meanings of which are as discussed in section 3.3.2. The vector of horizontal displacements of all N nodes then is

$$\left\{ \rho_x^{r_{11}} \right\} = \frac{B_f}{E_s} \left[ I^{r_{11}} \right] \left\{ \tau^1 \right\} \qquad (3.77)$$

where $\left[ I^{r_{11}} \right]$ is a square matrix of size N and $\left[ I^{r_{11}} \right]$ is a matrix of the influence of shear stresses along the first pair of strips on the displacements of N nodes along the first pair of strips. $\left\{ \tau^1 \right\}$ and $\left\{ \rho_x^{r_{11}} \right\}$ are vectors of size N, $\left\{ \tau^1 \right\}$ being the vector of shear stresses along the first pair of strips.

Similarly, the vector of horizontal displacements of N nodes along the first pair of strips due to shear stresses along the second pair is written as

$$\left\{ \rho_x^{r_{12}} \right\} = \frac{B_f}{E_s} \left[ I^{r_{12}} \right] \left\{ \tau^2 \right\} \qquad (3.78)$$

where $\left[ I^{r_{12}} \right]$ is a square matrix of the influence of shear stresses, $\left\{ \tau^2 \right\}$, along the second pair of strips on displacements of N nodes along the first pair.

The vector of horizontal displacements of N nodes along the second pair of strips due to shear stresses along the first pair is

$$\left\{ \rho_x^{r_{21}} \right\} = \frac{B_f}{E_s} \left[ I^{r_{21}} \right] \left\{ \tau^1 \right\} \tag{3.79}$$

where $\left[ I^{r_{21}} \right]$ is a square matrix of the influence of shear stresses, $\left\{ \tau^1 \right\}$, along the first pair of strips on the displacements of N nodes along the second pair of strips. The vector of horizontal displacements of N nodes along the second pair due to shear stresses along the second pair is

$$\left\{ \rho_x^{r_{22}} \right\} = \frac{B_f}{E_s} \left[ I^{r_{22}} \right] \left\{ \tau^2 \right\} \tag{3.80}$$

where $\left[ I^{r_{22}} \right]$ is a square matrix of the influence of shear stresses, $\left\{ \tau^2 \right\}$, along the second pair of strips on the displacements of N nodes along the second pair.

All the matrices mentioned in Eq. 3.77 through 3.80 are functions of the parameters, $L_r/B_f$, $U_o/B_f$, $\nu_s$ and the respective relative distances between the pairs of strips under consideration. Eqs. 3.77 through 3.80 are combined to form a vector of horizontal displacements along both pairs of strips as

$$\left\{ \rho_x^r \right\} = \frac{B_f}{E_s} \left[ I^r \right] \left\{ \tau \right\} \tag{3.81}$$

where $\left[ I^r \right] = \begin{bmatrix} I^{r}_{11} & I^{r}_{12} \\ I^{r}_{21} & I^{r}_{22} \end{bmatrix}$

and

$$\left\{ \tau \right\}^T = \left\lfloor \left\lfloor \tau^1 \right\rfloor \left\lfloor \tau^2 \right\rfloor \right\rfloor$$

$$\left\{ \rho_x^r \right\}^T = \left\lfloor \left\lfloor \rho_x^{r_1} \right\rfloor \left\lfloor \rho_x^{r_2} \right\rfloor \right\rfloor \tag{3.82}$$

where $\left\{ \rho_x^{r_1} \right\} = \left\{ \rho_x^{r_{11}} \right\} + \left\{ \rho_x^{r_{12}} \right\}$

and

$$\left\{ \rho_x^{r_2} \right\} = \left\{ \rho_x^{r_{21}} \right\} + \left\{ \rho_x^{r_{22}} \right\}$$

Compatibility of displacements at 2N nodes is satisfied for rigid strips by equating the net displacements to zero, i.e,

$$\left\{ \rho_x^f \right\} - \left\{ \rho_x^r \right\} = \left\{ 0 \right\} \tag{3.83}$$

Substituting for the vectors, a set of 2N simultaneous equations are obtained as

$$\left[ I^r \right] \left\{ \tau/q \right\} = \left\{ I^f \right\} \tag{3.84}$$

The stresses along both pairs of strips are obtained by solving Eq. 3.84.

The settlement reduction coefficients of points along the surface due to these shear stresses are obtained as discussed in the earlier sections.

## 3.6 Results and Discussions

The main objective of this analysis is to evaluate the interaction stresses between a reinforcing strip and the soil, to obtain the distribution of the tensile forces in the strip, and to estimate the reduction in settlement due to these stresses. As described in the section on formulation and analysis, Boussinesq's equation for displacements due to a point load on surface and Mindlin's equation for horizontal displacement due to a point load within the soil mass are integrated over the respective areas.

For the purpose of numerical integration of the Boussinesq's equation, the rectangular loaded area on the surface is divided into sub-elements of size, $0.025B_f \times 0.025B_f$. For centrally placed strips the strip half-width, $B_r$, is kept constant at $0.05B_f$ whereas for strips which are not centrally placed, it is maintained at $0.025B_f$. The half width of $0.05B_f$ was selected in order to highlight the influence of the interacting shear stresses acting in the longitudinal direction of the strip only.

The influence coefficient, $I^r_{ij}$, for the horizontal displacement of node i due to shear stress on element j is evaluated by dividing the element j into 20x20 subareas for $|i-j| \leq 2$. Coarser subdivision was found to be adequate for cases, $|i-j| > 2$. Settlement reduction coefficients obtained considering elements of length equal to $0.1B_f$ were compared with those with element lengths of $0.05B_f$ and found to agree very well (Table 3.1). Based on this, the lengths of the elements along the strip are maintained at $0.1B_f$. The size of the elements are, therefore

$0.1B_f \times 0.1B_f$ for centrally placed strips and $0.1B_f \times 0.05B_f$, $B_f$ being the half-width of the loaded area, for strips which are off-centre. Thus, an element of length equal to $0.1B_f$ would imply that a strip with length, $L_r/B_f=2.0$, will have 20 elements along half its length, i.e N = 20.

To check the accuracy of the numerical integration, SRC obtained at the origin for uniform stresses at depth are compared with those from the exact solution given by Vaziri et. al., (Table 3.2) and found to agree closely.

A parametric study is carried out in order to bring out the effects of length, depth, and distance of the reinforcing strip from the x-axis, the aspect ratio of the loaded area and the Poisson's ratio of the soil on the interaction stresses and the settlement reduction coefficients of points along the surface. The ranges of the parameters considered are

1. $L_f/B_f$ : 1 to 10 (aspect ratio of loaded area)
2. $L_r/B_f$ : 1 to 5 (length of reinforcement)
3. $U_o/B_f$ : 0.25 to 2 (depth of reinforcement)
4. $S_y/B_f$ : 0.025 to 2 (distance of reinforcement from x-axis)
5. $\nu_s$ : 0.1 to 0.5 (Poisson's ratio of soil)
6. $B_r/B_f$ : 0.025 for $S_y/B_f > 0$ (width of reinforcement)
   : 0.05 for $S_y/B_f = 0$

Except for cases where the effect of Poisson's ratio, $\nu_s$ is studied or unless mentioned, all results are for $\nu_s = 0.3$

Table 3.1 Comparison of Settlement Reduction Coefficients for Different Element Sizes

| El. Size \ $U_o/B_f$ | $I_{sc}$ for $L_r/B_f$=2, $L_f/B_f$=1, $B_r/B_f$=0.05, $\nu_e$=0.3 | | | | | CPU Sec. |
|---|---|---|---|---|---|---|
| | 0.25 | 0.5 | 1.0 | 1.5 | 2.0 | |
| $0.1B_f \times 0.1B_f$ | .000071 | .001647 | .003357 | .002701 | .001844 | 0.7 |
| $0.05B_f \times 0.1B_f$ | .000076 | .001662 | .003385 | .002727 | .001865 | 1.6 |

Table 3.2 Comparison of Computed Values of $I_{sc}$ with the Exact Solution for Uniform Stresses (Vaziri et. al., 1982)

| $U_o/B_f$ | $I_{sc}$ for $L_r/B_f$=1, $B_r/B_f$=0.1 | |
|---|---|---|
| | Exact Solution (Vaziri et. al.) | Computed Values |
| 0.25 | 0.0115016 | 0.011520 |
| 0.50 | 0.0113095 | 0.011315 |
| 1.00 | 0.0068968 | 0.006898 |
| 1.50 | 0.0041129 | 0.004113 |
| 2.00 | 0.0026271 | 0.002627 |

### 3.6.1 Shear Stresses - Single Strip

Fig. 3.14 shows the variation of the normalised shear stress, $\tau/q$, with the distance, $x/B_f$, along the strip for various depths of placement, $U_o/B_f$, and for a strip of length, $L_r/B_f=2.0$, placed below a square loaded area ($L_f/B_f=1.0$). The stresses in this figure and all other figures depicting the stresses, are the total stresses mobilised at the soil-strip interface. These stresses may be assumed to be acting in equal proportion over the top and bottom surfaces of the reinforcing strip. Due to symmetry, stresses along half the length of the strip are only considered. A positive shear stress is one that prevents outward lateral movement and as such is directed inwards.

In the figure, as intutively felt, the shear stress at the centre, i.e. $x/B_f=0$, is zero. For strips at shallower depths, i.e. $U_o/B_f=0.25$, the shear stresses are negative over a large portion of the strip. Positive shear stresses are mobilised only for $x/B_f$ in the range 0.85 to 1.1. With increasing depths of placement, the shear stresses are positive over most of the length of the strip. The sharp increase in shear stresses observed at the extreme end of the strip, i.e at $x/B_f=2.0$, is because the strip is assumed to be rigid. This is in consonance with infinite contact stresses observed at the edges of rigid footings on soils. For depths of placement, $U_o/B_f$, upto 1.0, the shear stresses increase upto a distance, $x/B_f=1.0$, along the strip and then decrease gradually. The increase in stresses is attributed to increasing displacements over the distance, $x/B_f=0$ to 1. Larger the displacement, higher is the shear stress to be mobilised. Beyond $x/B_f=1$, the displacements reduce for depths, $U_o/B_f\leq1.0$, and

hence the stresses mobilised are also smaller. For strips placed at a depth, $U_o/B_f$=1.0, the stresses mobilised are a maximum and the maximum stress, $\tau/q$=0.8 is observed near $x/B_f$=1.0. With further increase in the depth of reinforcement, i.e. for $U_o/B_f$>1.0, the shear stresses are smaller than those for $U_o/B_f$=1.0 over most of the length of the strip. This is because the displacements for depths, $U_o/B_f$>1 are smaller than those for $U_o/B_f$=1. Further, there is a gradual increase in displacements with distance, $x/B_f$ for strips placed at greater depths. As a result, shear stresses increase monotonically with the distance, $x/B_f$, along the strip. A positive peak or a sharp increase in the shear stress is observed at the edge for $U_o/B_f \geq 1.5$.

The effect of the length of strip, $L_r/B_f$, on the shear stresses for a depth, $U_o/B_f$=1.0, beneath a square area ($L_f/B_f$=1.0) is depicted in Fig. 3.15. For short strips, i.e. $L_r/B_f$=1.0, the shear stresses increase almost linearly over the length of the strip. For strips with $L_r/B_f$>1.0, it is interesting to note that the stresses increase to a value of about 0.8q at a distance, $x/B_f$=1.0, i.e beneath the edge of the loaded area and then decrease monotonically. For strips of length, $L_r/B_f$=2.0, the stresses are positive over the whole length of the strip. For strips longer than $2.5B_f$ the mobilised shear stresses become negative over the distance, $x/B_f$>2.5. It is also worthwhile to note that for any length of the strip ($L_r > B_f$), the stresses are positive upto a maximum distance of $2.5B_f$ and are independent of the ratio, $L_r/B_f$. At distances, $x/B_f$>2.5 and depths, $U_o/B_f$=1.0, the soil displacements due to the surface loading are inward i.e. towards the centre. As a result the stresses mobilised are also

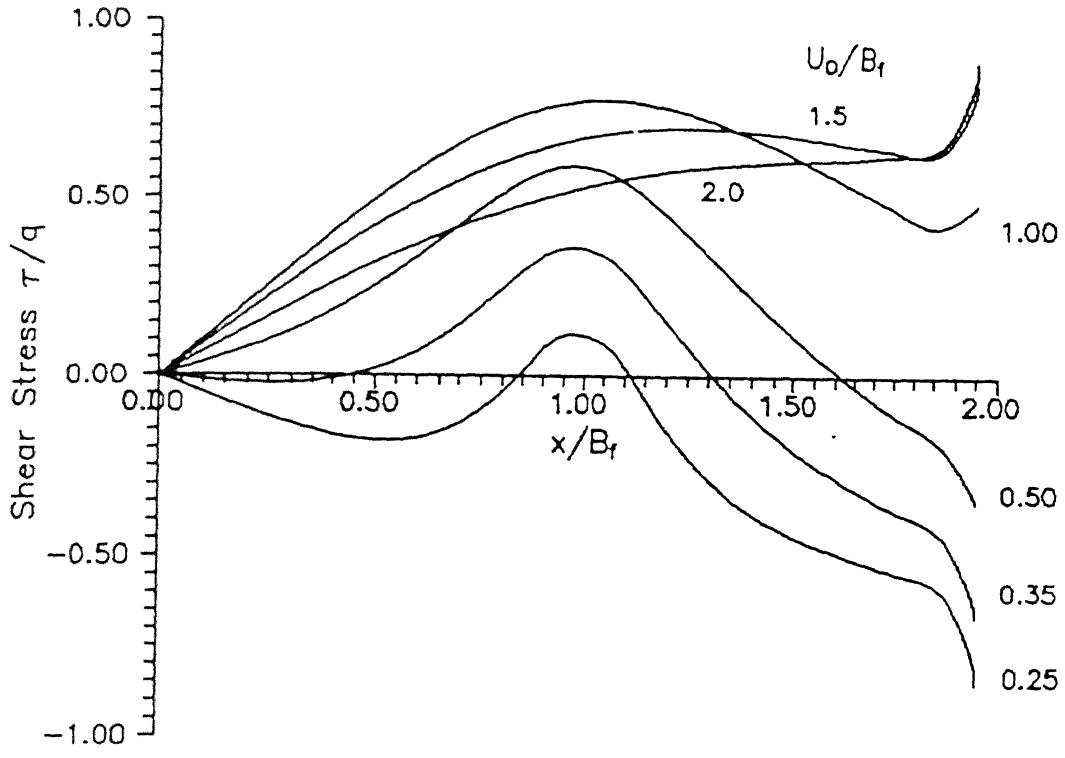


Fig. 3.14 Variation of Shear Stress with Distance for Various Depths of Placement of Strip ($L_r/B_f$=2, $L_f/B_f$=1, $\nu_s$=0.3)

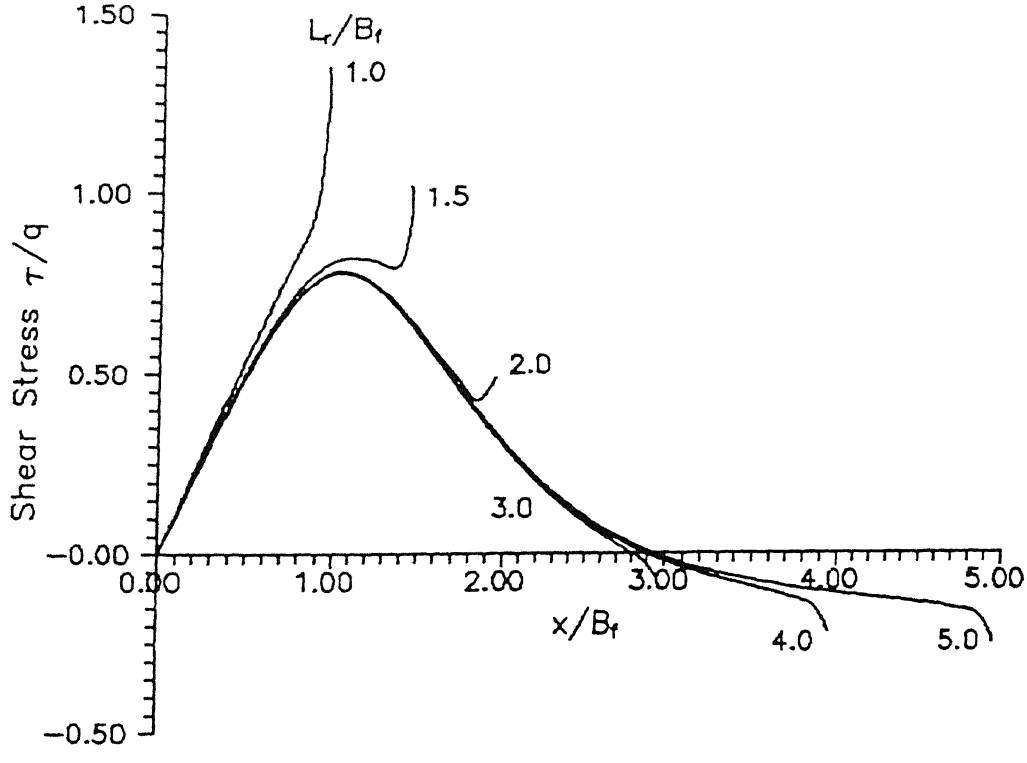


Fig. 3.15 Variation of Shear Stress with Distance for Different Lengths of Strip ($L_f/B_f$=1, $U_0/B_f$=1, $\nu_s$=0.3)

in the same direction, i.e. negative. A sharp increase in the negative stresses at the edge is noted.

The effect of the aspect ratio of the loaded area, $L_f/B_f$, on the normalised shear stresses is presented in Fig. 3.16, for depth, $U_o/B_f$=1.0, and length, $L_r/B_f$=2.0, of the strip. For all values of $L_f/B_f$ the shear stresses increase from 0 to a maximum value and then decrease. The maximum stress is observed at a distance of about $x=B_f$ for all curves. The stresses are a maximum for a rectangular area with an aspect ratio, $L_f/B_f$=2.0, and a maximum stress, $\tau/q$, of 1.0 is observed at a distance, $x/B_f$=1.0. Stresses mobilised for areas with aspect ratio, $L_f/B_f$=5.0, are slightly smaller than those for a rectangle with $L_f/B_f$=2.0 but are higher as compared to stresses for a square area ($L_f/B_f$=1) or a strip with $L_f/B_f$=10. Stresses for an area with $L_f/B_f$=10 are much smaller than those for other rectangles over distances, $x/B_f>1.5$. As the aspect ratio, $L_f/B_f$, increases beyond 2, the horizontal displacements start decreasing beyond a depth, $U_o/B_f$=1. This results in reduced stress mobilisation. For areas with $L_f/B_f$=10, displacements at $x/B_f>1.5$ are negligibly small resulting in very low shear stresses.

Fig. 3.17 shows the effect of Poisson's ratio, $\nu_s$, on the normalised shear stresses, $\tau/q$, for a length, $L_r/B_f$=2, depth, $U_o/B_f$=1, and an aspect ratio, $L_f/B_f$=1 of the loaded area. As can be intutively felt, the shear stresses increase with increase in Poisson's ratio, $\nu_s$. If $\nu_s$ is small, the lateral displacement due to surface loading is small and hence shear stresses mobilised are also small. The lateral displacements increase with $\nu_s$ and are a

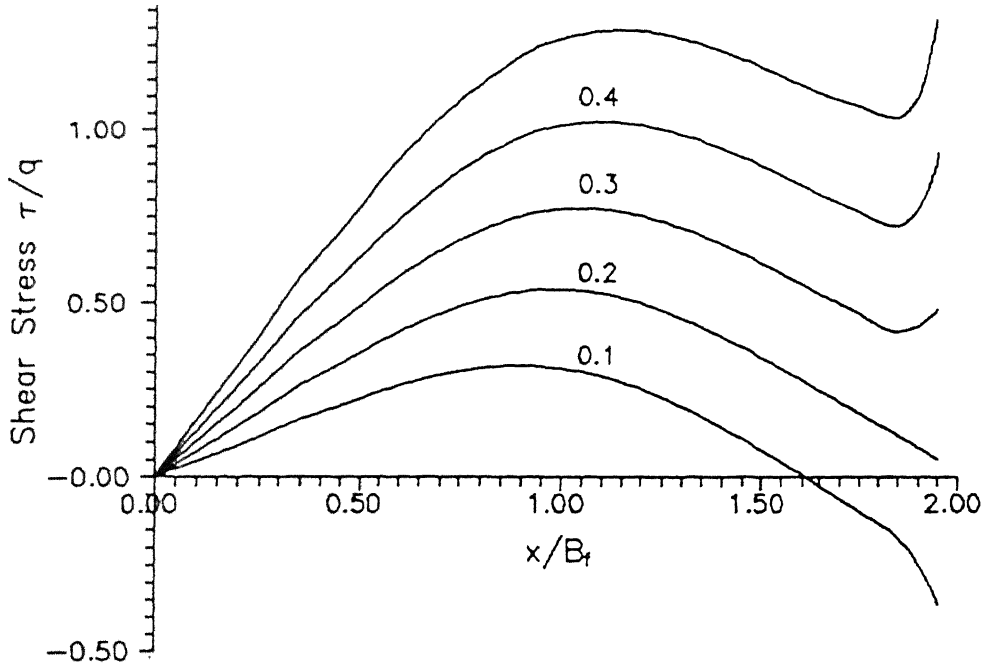


Fig. 3.16 Variation of Shear Stress with Distance for Various Aspect Ratios of Loaded Area ($L_r/B_f$=2, $U_0/B_f$=1, $\nu_s$=0.3)

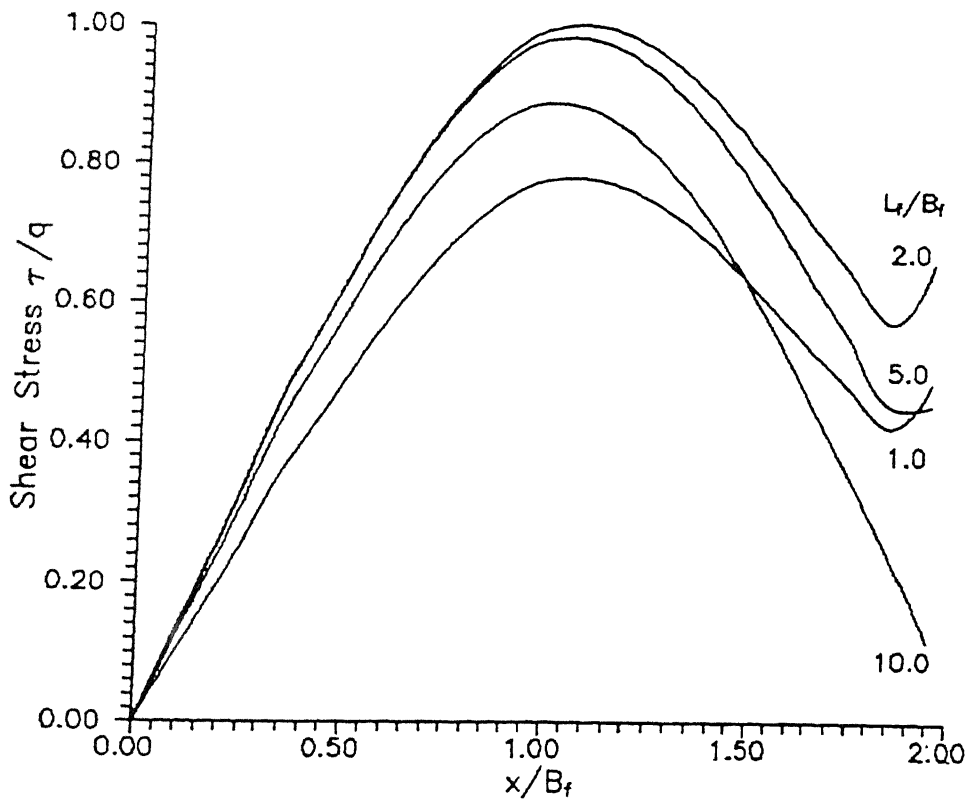


Fig. 3.17 Variation of Shear Stress with Distance for Various Poisson's Ratios of soil ($U_0/B_f$=1, $L_r/B_f$=2, $L_f/B_f$=1)

maximum for $\nu_s$=0.5 (undrained case). Consequently the stresses mobilised are also a maximum.

So far, the effect of the various parameters cited earlier on the shear stresses mobilised at the interface were studied. As stated in section 3.2 these shear stresses in turn produce tension in the reinforcing strip. The formulation for the computation of tensile forces is dealt with in section 3.2.2.

The variation of the normalised tension in the reinforcement strip, $T/qB_f^2$, along the length of the strip for lengths, $L_r/B_f$=2, and aspect ratio, $L_f/B_f$=1, of the loaded area and various values of depth ratio, $U_o/B_f$, are depicted in Fig. 3.18. A negative value of the normalised tension, $T/qB_f^2$, indicates compression. It is clear from this figure that for a depth, $U_o/B_f$<0.35, the reinforcing strip is subjected to compression throughout its length. Strips at a depth, $U_o/B_f$=0.5, are subjected to compression beyond a distance, x of $1.4B_f$. The maximum tension at the centre is observed at a depth, $U_o/B_f$=1.0 and is equal to $0.105qB_f^2$. This maximum value decreases with further increase in depth, i.e. for $U_o>B_f$. It is also evident from the figure that strips placed beyond a depth of $0.5B_f$ are subjected to tension over their full lengths. This is corroborated in Fig. 3.14 which shows the effect of depth on shear stresses. The stresses are predominantly negative for strips at depth, $U_o/B_f \leq 0.35$, while they are positive for strips at greater depths. Consequently, strips at shallower depths ($U_o/B_f$<0.35) are ineffective in providing restraint to the soil.

The effect of the various parameters mentioned at the outset of this discussion on the mobilised interaction stresses and tension in the strips are brought out through the figures illustrated so far. It is due to these stresses that the surface settlement is affected. The improvement in the soil-foundation response due to strip reinforcement can well be appreciated if the effect of the various parameters on the settlement reduction coefficients (SRC) are studied. Hence more emphasis is laid in presenting the effect of the considered parameters on the SRC. From the study of the stresses it is more or less clear that strips placed in the depth range ($U_o/B_f$) of 0.75 to 1.5 below rectangular areas are most effective.

### 3.6.2 Settlement Reduction - Single Strip

To study the effect of shear stresses on the SRC along the surface, it is essential to look into the basic solution given by Mindlin for vertical displacements due to a horizontal force at depth. The vertical displacement of any point, B(x,0,0) (Fig. 3.4) is given by Eq. 3.27. Non-dimensionalising all parameters with the depth, c of the load, Eq. 3.27 is written as

$$\rho_z = \frac{Q\,c}{G_s} I_z \qquad (3.85)$$

where $G_s=E_s/2(1+\nu_s)$ and all parameters are the same as defined in Eq. 3.27. $I_z$ is an influence coefficient dependent on x/c and $\nu_s$.

The plot of $I_z$ versus the normalised distance, $\bar{x}=x/c$, for different values of Poisson's ratio, $\nu_s$, is shown in Fig. 3.19. For all values of $\nu_s$ the coefficient, $I_z$ increases from zero,

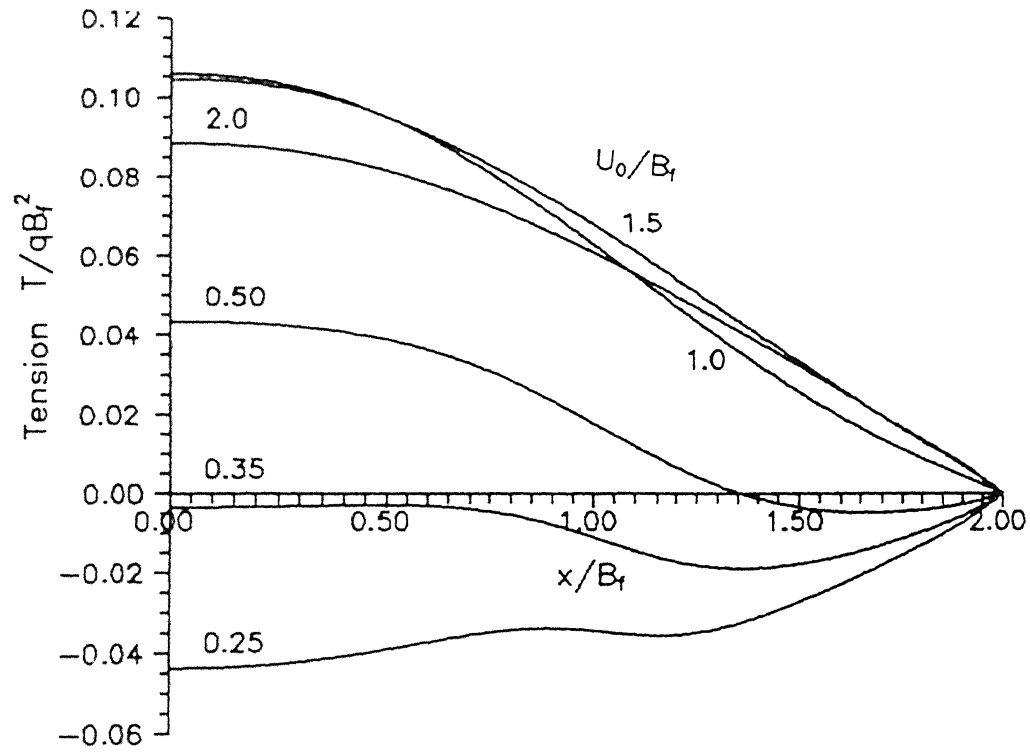


Fig. 3.18 Variation of Tension with Distance for Various Depths of Placement of Strip ($L_r/B_f$=2, $L_f/B_f$=1, $\nu_s$=0.3)

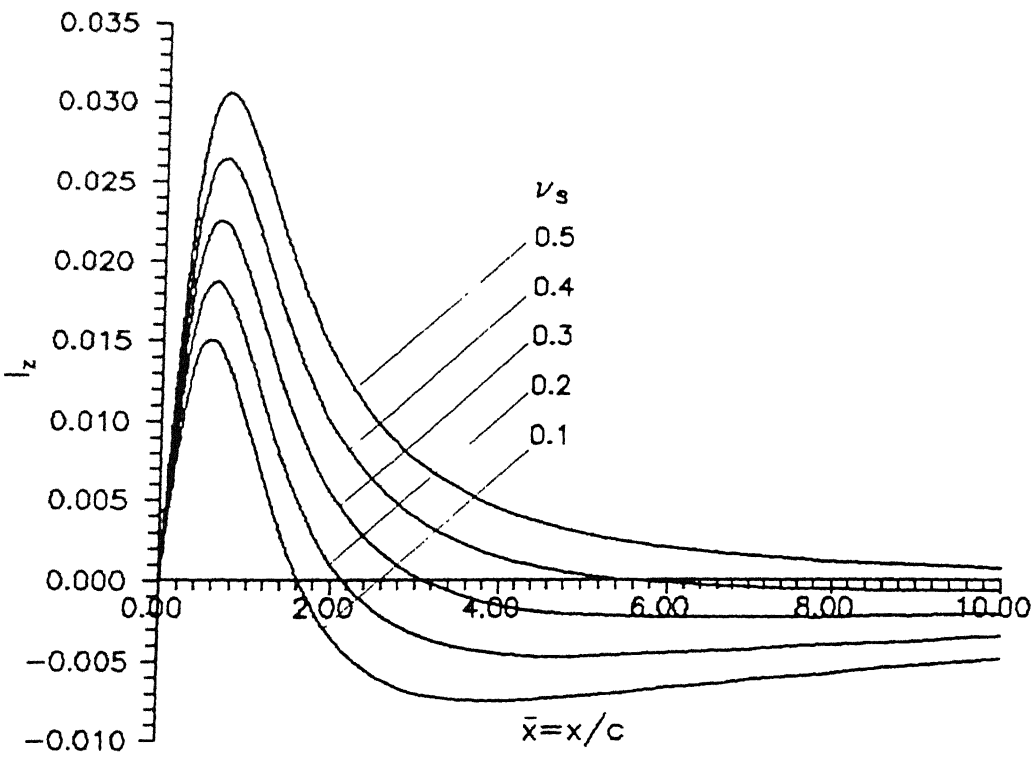


Fig. 3.19 Influence Coefficient for Vertical Surface Displacemen due to Horizontal Force at Depth (Mindlin Solution)

reaches a maximum value, and then decreases. For $\nu_s \leq 0.3$, $I_z$ becomes negative at larger values of x/c. In all cases $I_z$ tends to zero at very large values of x/c. For undrained soils ($\nu_s=0.5$), $I_z$ values are positive for all distances indicating surface heave throughout. The maximum value of $I_z$ ranges from 0.015 for $\nu_s=0.1$ to 0.03 for $\nu_s=0.5$. The distance $\bar{x}$, at which the maximum heave occurs increases from 0.5 for $\nu_s=0.1$ to about 0.7 for $\nu_s=0.5$. The distance, $\bar{x}$, beyond which settlement occurs for $\nu_s<0.5$ is again a function of $\nu_s$. For $\nu_s \leq 0.4$, distances beyond which points settle (i.e. negative $I_z$) get closer to the point force.

Fig. 3.19 gives an insight into the fundamental solution given by Mindlin. It is this equation that has been used to calculate the SRC on the surface for the various shear stress distributions arrived at from the interaction analysis. This figure will help in understanding the variation of SRC due to the stresses presented in the following figures.

Fig. 3.20 depicts the variation of SRC along the x-axis on the surface for strips of various lengths, and for a depth of placement, $U_o/B_f=1.0$, beneath a square loaded area ($L_f/B_f=1.0$). $x_f/B_f=0$ is the origin O, or the centre of the loaded area, while $x_f/B_f=1.0$ is the edge. For all lengths of reinforcement, the settlement reduction is maximum at the centre of the loaded area, O. SRC reduces with increasing distances from the centre i.e. with $x_f/B_f$. The SRC increases with increasing lengths of the strips. The improvement in SRC for the length ratio, $L_r/B_f$ increasing from 1 to 2 is significant. As the length ratio, $L_r/B_f$ increases from 2 to 5, the increase in SRC is insignificant. The

SRC at $x_f/B_f=0$, for $L_r/B_f=2$, is 0.00335 while it is 0.0035 for $L_r/B_f=5$. Thus at a depth, $U_o/B_f=1.0$, no advantage accrues by providing reinforcements of lengths greater than twice the width of the loaded area. A strip of length equal to $B_f$ gives a SRC of 0.0023 at the origin and -0.0003 at the edge, the latter indicating a small additional settlement. For strips of lengths equal to $2B_f$ to $5B_f$, the SRC at the origin is around 0.0034 and at the edge around 0.001. The reasoning for this trend is explained as follows. The positive shear stresses along the strip of length equal to $B_f$ cause the origin to move up while they try to pull the edge down. Hence a small settlement at the edge is observed in Fig. 3.20. For strips with longer lengths, stresses beyond a distance, $x/B_f=2.5$ (Fig. 3.14) are negative. The additional positive stresses (as compared to those for $L_r/B_f=1.0$) beyond a distance, $x/B_f=1.0$, help in pushing the points from the origin to the edge further upward and hence the SRC values at all points, i.e. $x_f/B_f$ varying between 0 and 1.0 are higher as compared to those for $L_r/B_f=1.0$.

Fig. 3.21 presents the effect of depth, $U_o/B_f$, on the SRC for strips of length, $L_r/B_f=2$, and for a rectangular loaded area with aspect ratio, $L_f/B_f=2$. It is seen that except for $U_o/B_f=0.25$, for all other depths the SRC is maximum at the centre of the loaded area, i.e. at $x_f/B_f=0$ and decreases gradually with increasing $x_f/B_f$. It is interesting to note that for a depth ratio, $U_o/B_f=0.25$, the maximum SRC is observed at a distance, $x_f/B_f=0.75$. This is because, for this depth the stresses are predominantly negative. As a result, the points away from the

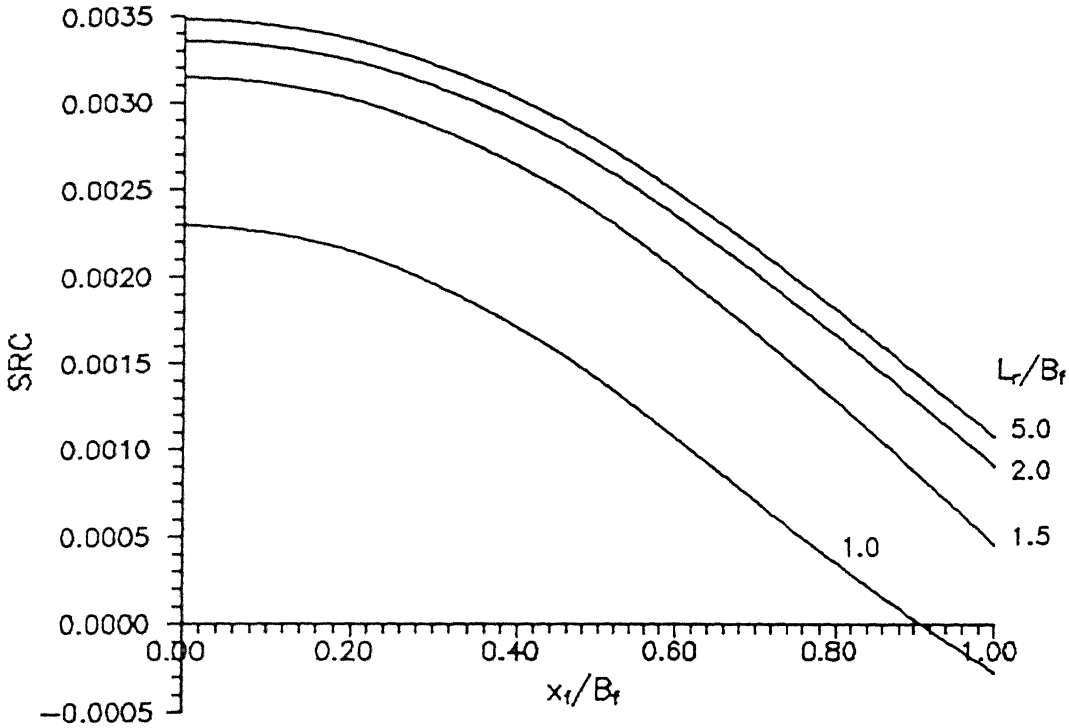


Fig. 3.20 Variation of SRC with Distance along Surface for Different Lengths of Strip ($U_o/B_f$=1, $L_f/B_f$=1, $\nu_s$=0.3)

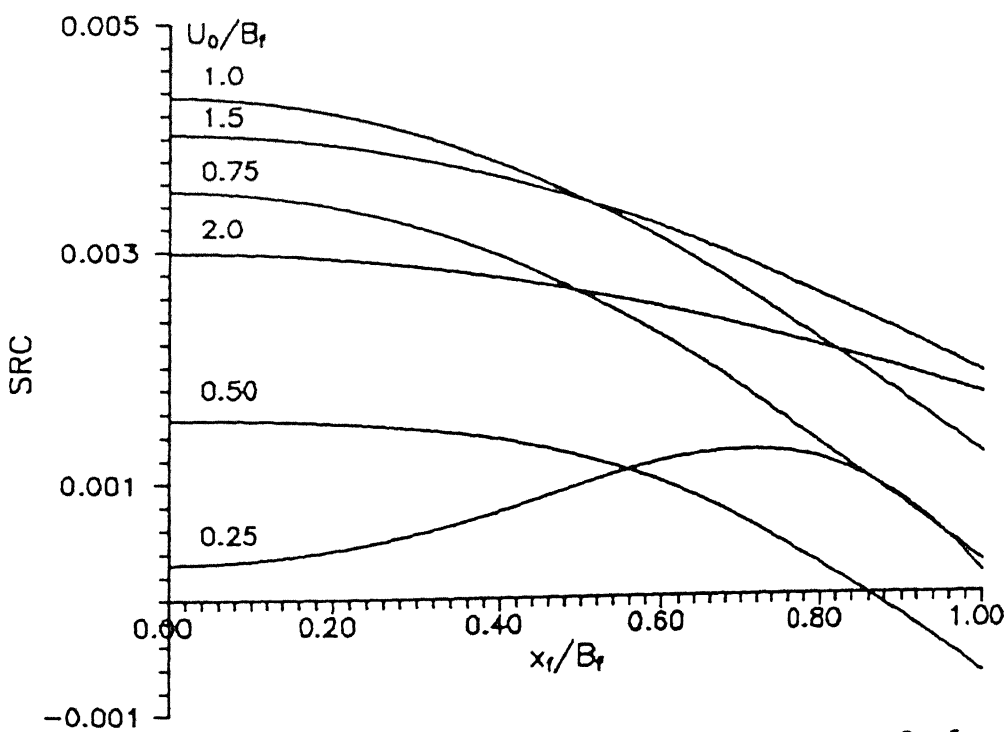


Fig. 3.21 Variation of SRC with Distance along Surface for Different Depths of Placement of Strip ($L_r/B_f$=2, $L_f/B_f$=1, $\nu_s$=0.3)

origin on the surface are pushed up by a larger amount as compared to the centre. Hence SRC increases upto a distance of $x_f/B_f=0.75$. The negative stresses beyond a distance, $x/B_f=1$ along the strip cause the edge of the loaded area ($x_f/B_f=1$) to move downwards and hence SRC decreases beyond $x_f/B_f=0.75$. With increasing depths, the SRC are positive and the rate of decrease in SRC with $x_f/B_f$ decreases.

The effect of aspect ratio of the loaded area, $L_f/B_f$, on SRC for different depths, $U_o/B_f$, and for strips of length, $L_r/B_f=2.0$, is presented in Figs. 3.22 and 3.23. In Fig. 3.22 the plot of SRC versus the distance, $x_f/B_f$, along the surface is shown for strips at depth, $U_o/B_f=1.0$. For all $L_f/B_f$ values, SRC is maximum at the centre and decreases gradually with increase in $x_f/B_f$. It is interesting to note that SRC values increase with $L_f/B_f$ and attain maximum values for rectangles with aspect ratio $L_f/B_f=2.0$. With further increase in $L_f/B_f$, the SRC values decrease. The maximum SRC at the centre of the loaded area or origin is for a rectangle with an aspect ratio, $L_f/B_f=2$, and it equals 0.00435 while the least improvement is for a square which equals 0.00335.

For strips of length, $L_r/B_f=2$, at a larger depth of $U_o/B_f=2$, the variation of SRC with distance, $x_f/B_f$, along the surface is presented in Fig. 3.23. In this figure, as compared to the previous one, the variation in the SRC with $x_f/B_f$ or with the aspect ratio of the loaded area, ($L_f/B_f$) is smaller. Further, SRC is maximum for a longer rectangle with $L_f/B_f=5$. The SRC at the centre of the loaded area, i.e. at $x_f/B_f=0$, for rectangular areas

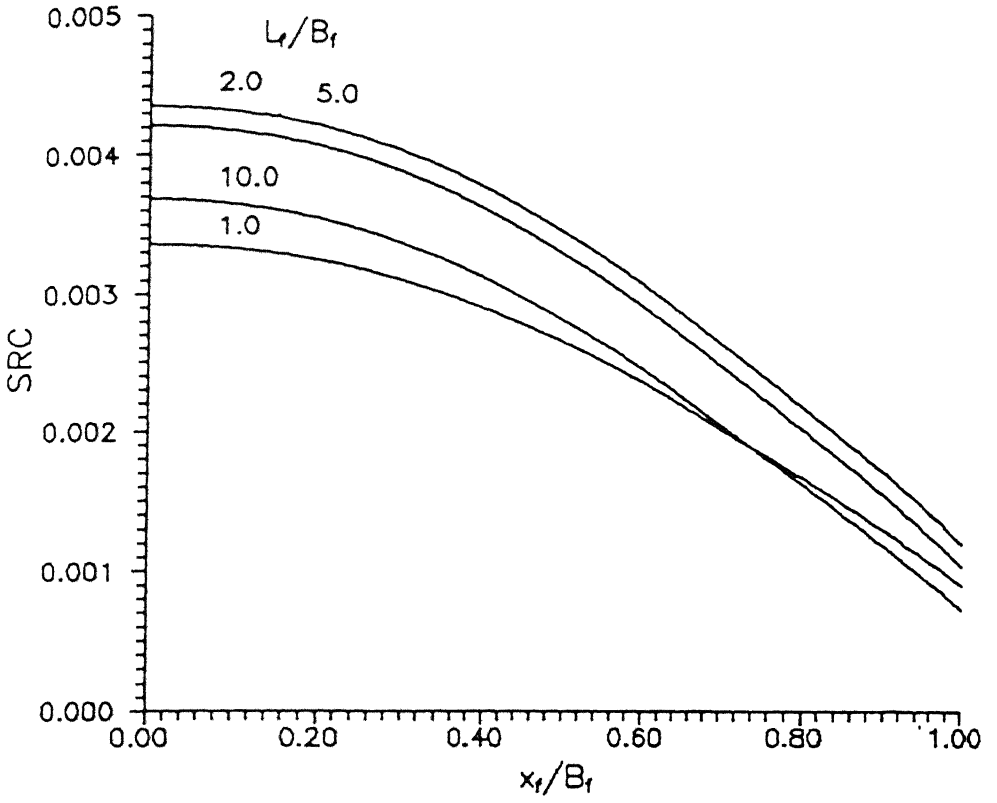


Fig. 3.22 Variation of SRC with Distance along Surface for Different Aspect Ratios of Loaded Area ($L_f/B_f=2$, $U_0/B_f=1$, $\nu_s=0.3$)

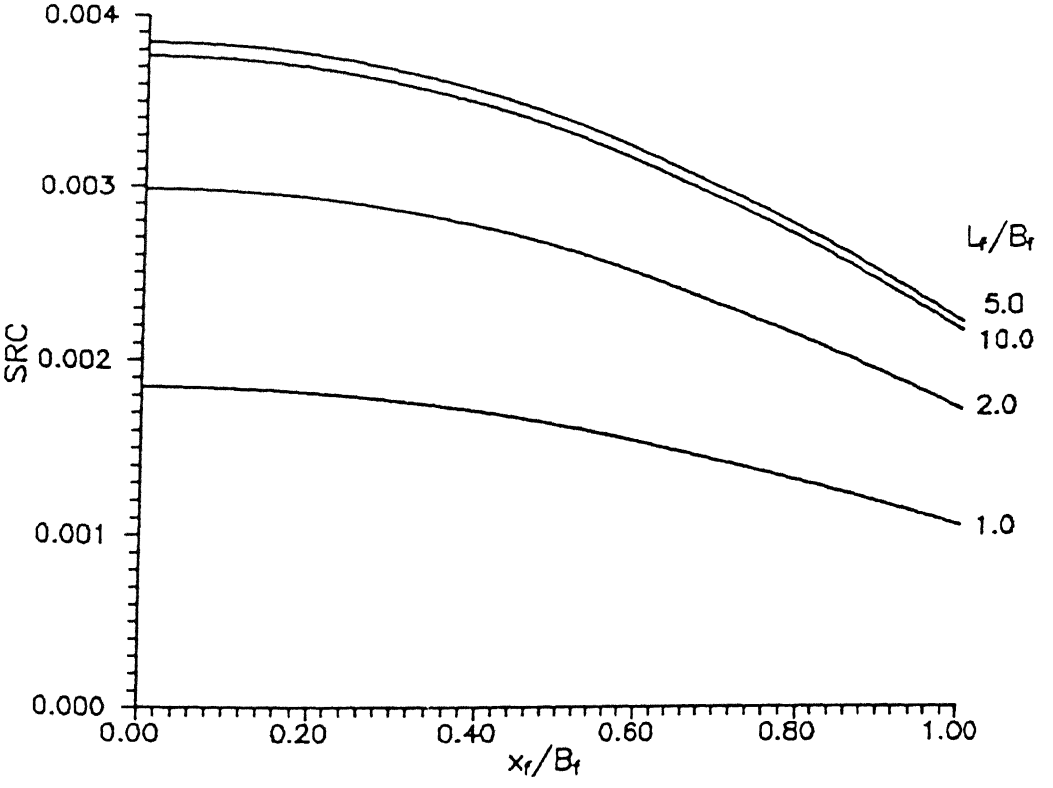


Fig. 3.23 Variation of SRC with Distance along Surface for Different Aspect Ratios of Loaded Area ($L_f/B_f=2$, $U_0/B_f=2$, $\nu_s=0.3$)

with $L_f/B_f$=5 is 0.00385 and that for a square ($L_f/B_f$=1) is 0.00185.

From these two figures, viz. Figs. 3.22 and 3.23, the settlement reduction for strips of length, $L_r/B_f$=2, is observed to be maximum if placed at intermediate depths, i.e. for $U_o/B_f$ of around 1 beneath rectangular areas with aspect ratio ($L_f/B_f$) of 2. At shallower depths the negative shear stresses are responsible for low SRC values whereas at greater depths the shear stresses are too deep to bring about any significant improvement in the SRC values. These results emphasize the fact that strips of length, $L_r/B_f$=2, placed at intermediate depths ($U_o/B_f$=1.0) are advantageous as compared to those placed at very shallow or at great depths.

Thus far, the variation of SRC with the distance, $x_f/B_f$, along the surface was studied and the effects of the various parameters on SRC were looked into. From this study it is clear that except for strips placed at very shallow depths, the centre of the loaded area, O, experiences the maximum settlement reduction. In the next couple of paragraphs the effect of the parameters on the SRC at the centre of the loaded area defined as $I_{sc}$ is analysed.

Fig. 3.24 shows the variation of $I_{sc}$ with depth, $U_o/B_f$, for various aspect ratios of the loaded area and for a strip of length, $L_r/B_f$=2.0. It is observed that for square areas ($L_f/B_f$=1.0), $I_{sc}$ increases with depth and reaches a maximum value

of 0.0034 at a depth of $0.9B_f$. A similar trend is observed for areas with $L_f/B_f=2.0$ for which the maximum value of $I_{sc}$ is 0.0044 occuring at a depth of 1.1 $B_f$. In the case of areas with aspect ratio of 5, the $I_{sc}$ versus $U_o/B_f$ curve is flatter for depths upto $0.5B_f$ beyond which the values of $I_{sc}$ increase upto depths in the range $1.4B_f$ to $1.5B_f$ and then decrease with $U_o/B_f$. A maximum value of $I_{sc}$ equal to 0.00465 is observed for areas with $L_f/B_f=5$ at a depth of $1.4B_f$. In case of long rectangular areas ($L_f/B_f=10$), the reduction in settlement due to a single strip is less than the reduction for an area with $L_f/B_f=5.0$. The depth of the strip to cause maximum reduction in settlement however, is more ($=1.5B_f$).

These trends can be explained with the help of figure 3.25. At a depth of $0.5B_f$ a maximum positive stress of 0.35q and a maximum negative stress of -1.4q are observed for areas with $L_f/B_f=5$. On the other hand, areas with $L_f=10B_f$ show a maximum positive stress of 0.2q and a maximum negative stress of -1.9q. These stresses lead to a lesser settlement reduction for areas with $L_f/B_f=10$ as compared to areas with $L_f/B_f=5$, at the same depth of $0.5B_f$.

The change in the rate of variation of $I_{sc}$ with $U_o/B_f$ for areas with $L_f/B_f=5$ and 10 at shallow depths can be explained with the help of Fig. 3.19. It can be seen from this figure that for $\nu_s=0.3$, the coefficient $I_z$ is negative for distance, $x>3c$ indicating settlement of soil. This implies that for a strip at a depth of $0.25B_f$, negative stresses beyond a distance of $0.75B_f$ ($3x0.25B_f$) push the soil at the origin upwards while for a strip

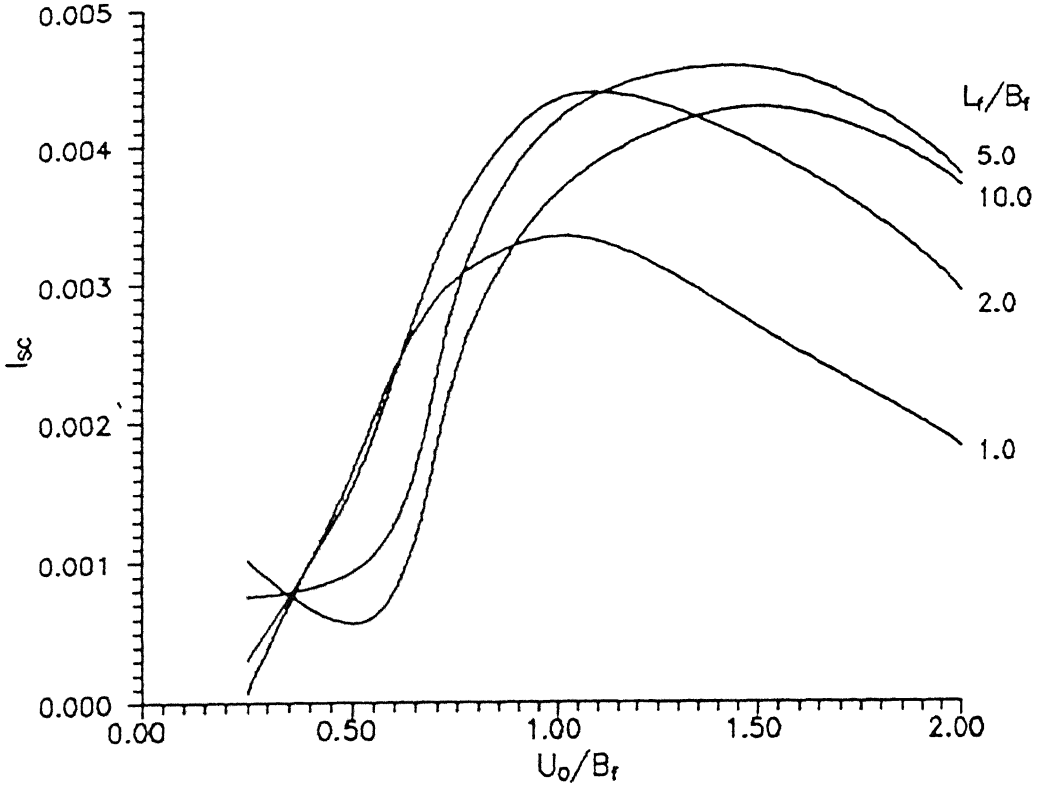


Fig. 3.24 Effect of Depth of Placement of Strip on $I_{sc}$ for Different Aspect Ratios of Loaded Area ($L_f/B_f$=2, $\nu_s$=0.3)

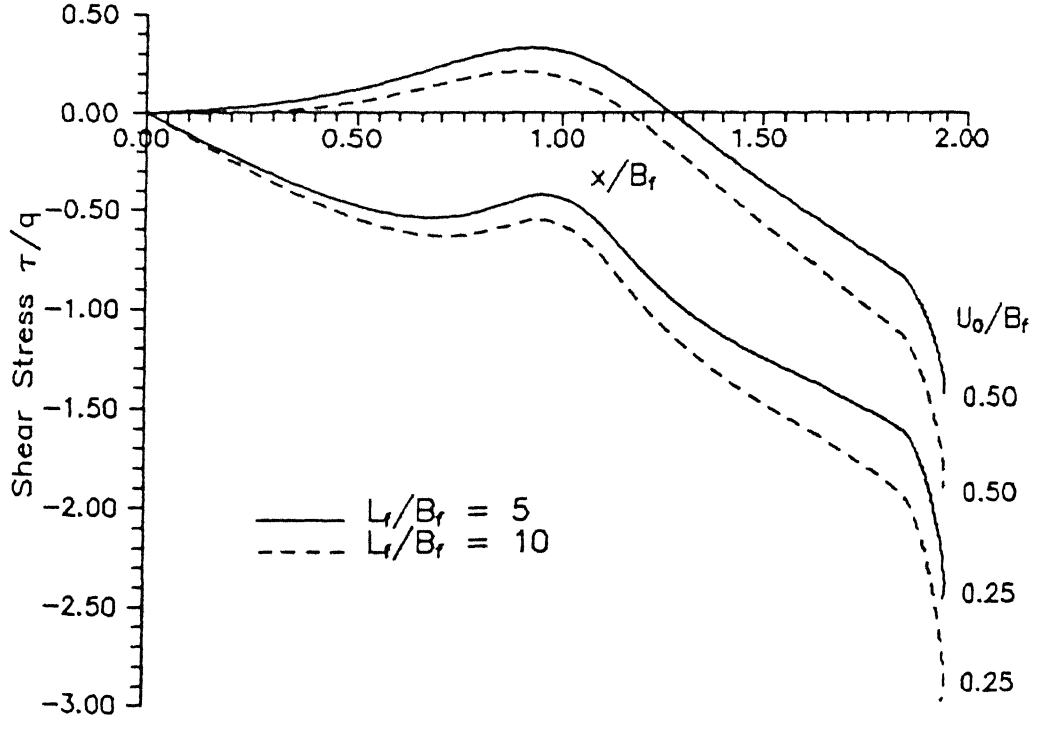


Fig. 3.25 Variation of Shear Stress with Distance for Different Depths of Placement of Strip ($L_f/B_f$=2, $\nu_s$=0.3)

at a depth of $0.5B_f$, the negative stresses beyond a distance of $1.5B_f$ cause upward movement of soil at the origin. From Fig. 3.25 it is evident that for an area with $L_f=10B_f$, the negative stresses for a strip at a depth of $0.25B_f$ are much larger than those for a strip below an area with an aspect ratio, $L_f/B_f=5$, and hence give rise to a higher $I_{sc}$ value.

Fig. 3.26, 3.27 and 3.29 present the variation of $I_{sc}$ with length of the strip, $L_r/B_f$, for various values of the aspect ratio, $L_f/B_f$, of the laoded area. The effect of $L_f/B_f$ on $I_{sc}$ for a strip placed at a depth $U_o/B_f=0.25$ is depicted in Fig. 3.26. For all $L_f/B_f$ values, the $I_{sc}$ increases gradually with increase in the length, $L_r/B_f$, of the strip. $I_{sc}$ for a short strip ($L_r/B_f=1$), for all $L_f/B_f$ values is negative. It is also evident that the $I_{sc}$ values increase with increase in the aspect ratio, $L_f/B_f$. It is worth noting that for smaller aspect ratios of the loaded area ($L_f/B_f<2$) increase in the length of strip does not improve the $I_{sc}$ values whereas for longer rectangular areas ($L_f/B_f>3$) longer strips show higher $I_{sc}$ values. For square loaded areas ($L_f/B_f=1$), $I_{sc}$, for strips of length, $L_r/B_f=1$ and 5 are -0.0008 and 0.0012 respectively. For longer rectangles ($L_f/B_f=10$), $I_{sc}$ for strips of length, $L_r/B_f=1$ and 5 are -0.002 and 0.006 respectively.

In Fig. 3.27, the plot of $I_{sc}$ versus the length, $L_r/B_f$, of the strip for different aspect ratios, $L_f/B_f$, of the loaded area and for a depth ratio, $U_o/B_f=1$, is presented. For $L_f/B_f<3$, $I_{sc}$ increases upto a length, $L_r$ of 2Bf. With further increase in $L_r/B_f$, no significant increase in $I_{sc}$ values is observed. In case

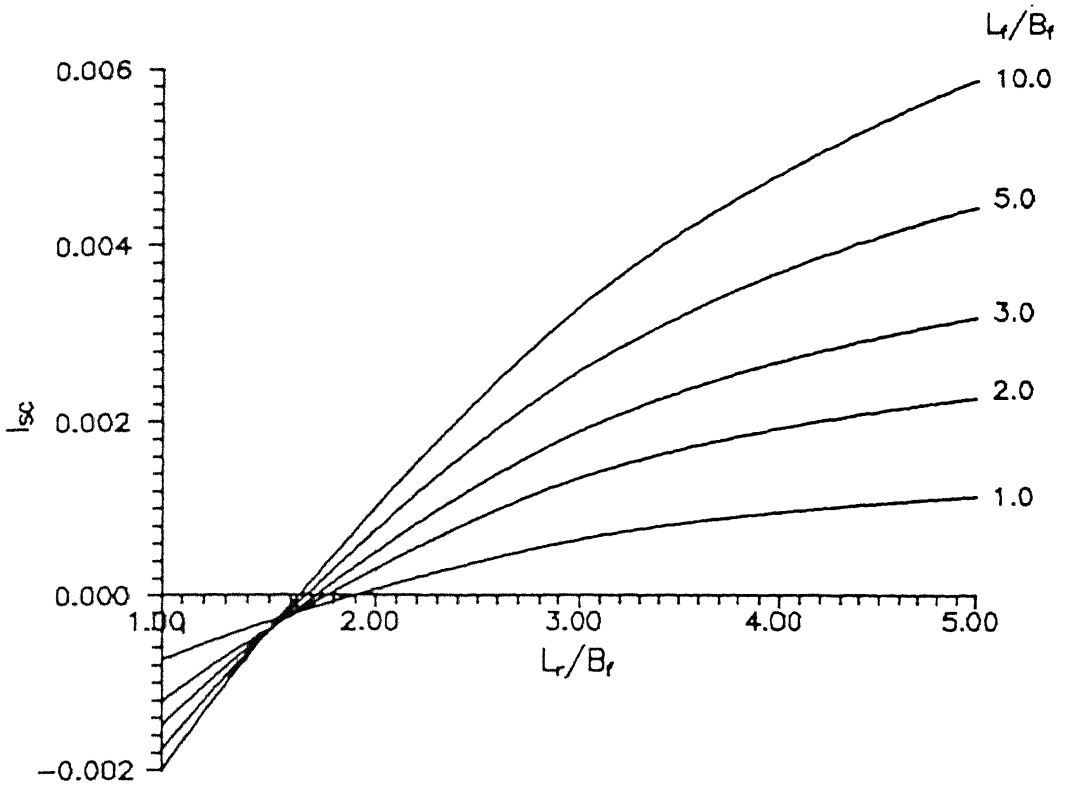


Fig. 3.26 Effect of Length of Strip on $I_{sc}$ for Different Aspect Ratios of Loaded Area ($U_0/B_f$=0.25, $\nu_s$=0.3)

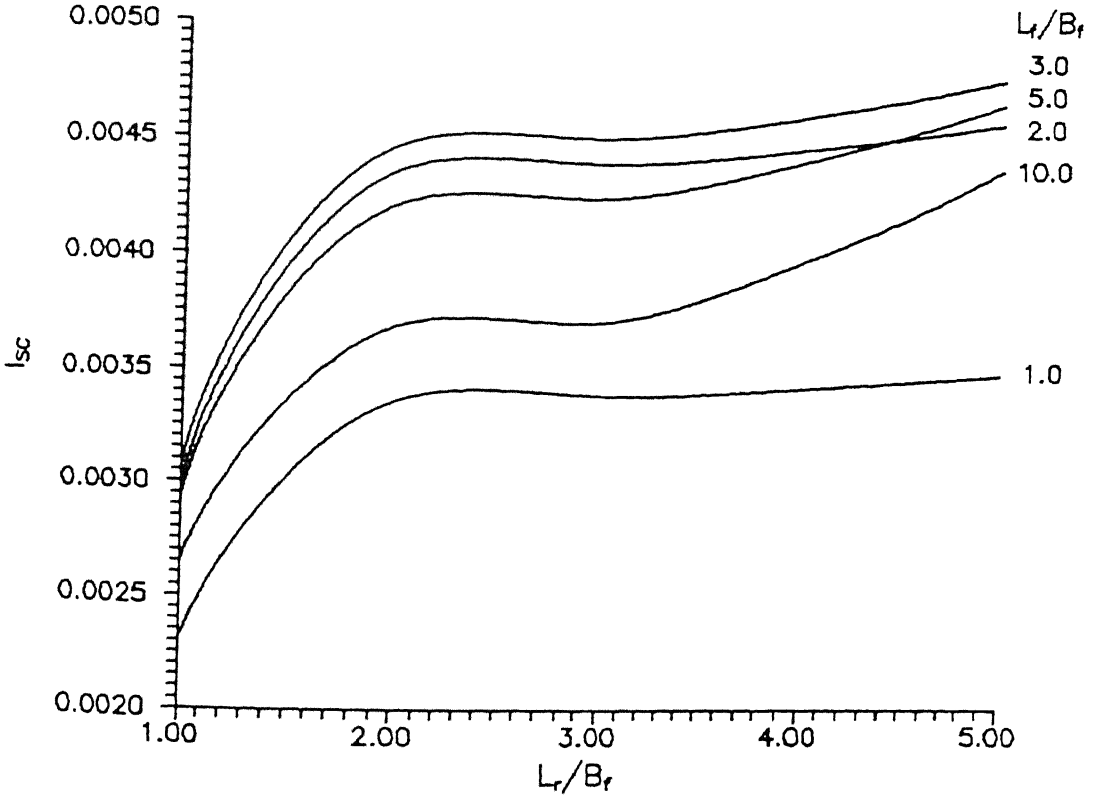


Fig. 3.27 Effect of Length of Strip on $I_{sc}$ for Different Aspect Ratios of Loaded Area ($U_0/B_f$=1, $\nu_s$=0.3)

of areas with $L_f/B_f \geq 3$, $I_{sc}$ increases for strip lengths upto $2B_f$, is almost constant for $L_r=2B_f$ to $L_r=3B_f$, and then shows a rapid increase beyond this length. Further, for $L_f/B_f=3.0$, $I_{sc}$ values are a maximum. There is a drop in $I_{sc}$ values with further increase in $L_f/B_f$ values, while the rate of increase in $I_{sc}$ values beyond $L_f/B_f=3$ is higher.

Fig. 3.28 helps in explaining these patterns. It is observed from this figure that beyond a distance of $2.7B_f$ for areas with $L_f/B_f=3$, and $2.25B_f$ for areas with $L_f=10B_f$, the shear stresses are negative. The negative stresses act over longer lengths for longer strips. Again, from Fig. 3.19 it is evident that at a depth, $U_o=B_f$, negative stresses beyond a length of $3B_f$ cause the origin on the surface to move up, thus facilitating settlement reduction. Hence a continuous increase in $I_{sc}$ values with increase in the lengths of the strip for $L_f/B_f>3$ is observed.

Fig. 3.29 presents the variation of $I_{sc}$ with the length, $L_r/B_f$, of the strip for strips placed at a depth, $U_o/B_f=2$. In this plot, unlike the earlier plots no significant improvement in $I_{sc}$ with increase in $L_r/B_f$ beyond 3 and for all $L_f/B_f$ is observed. Further, $I_{sc}$ is maximum for $L_f/B_f=5$. The value of $I_{sc}$ for strips of length, $L_r/B_f=5$ and for aspect ratios of the loaded area, $L_f/B_f=1$, 5 and 10 are 0.0024, 0.0052 and 0.0050 respectively.

From the results presented in Figs 3.27 and 3.29 it can be noted that longer strips placed under longer rectangles prove more beneficial. Increasing the length of the strips beyond $2.5B_f$

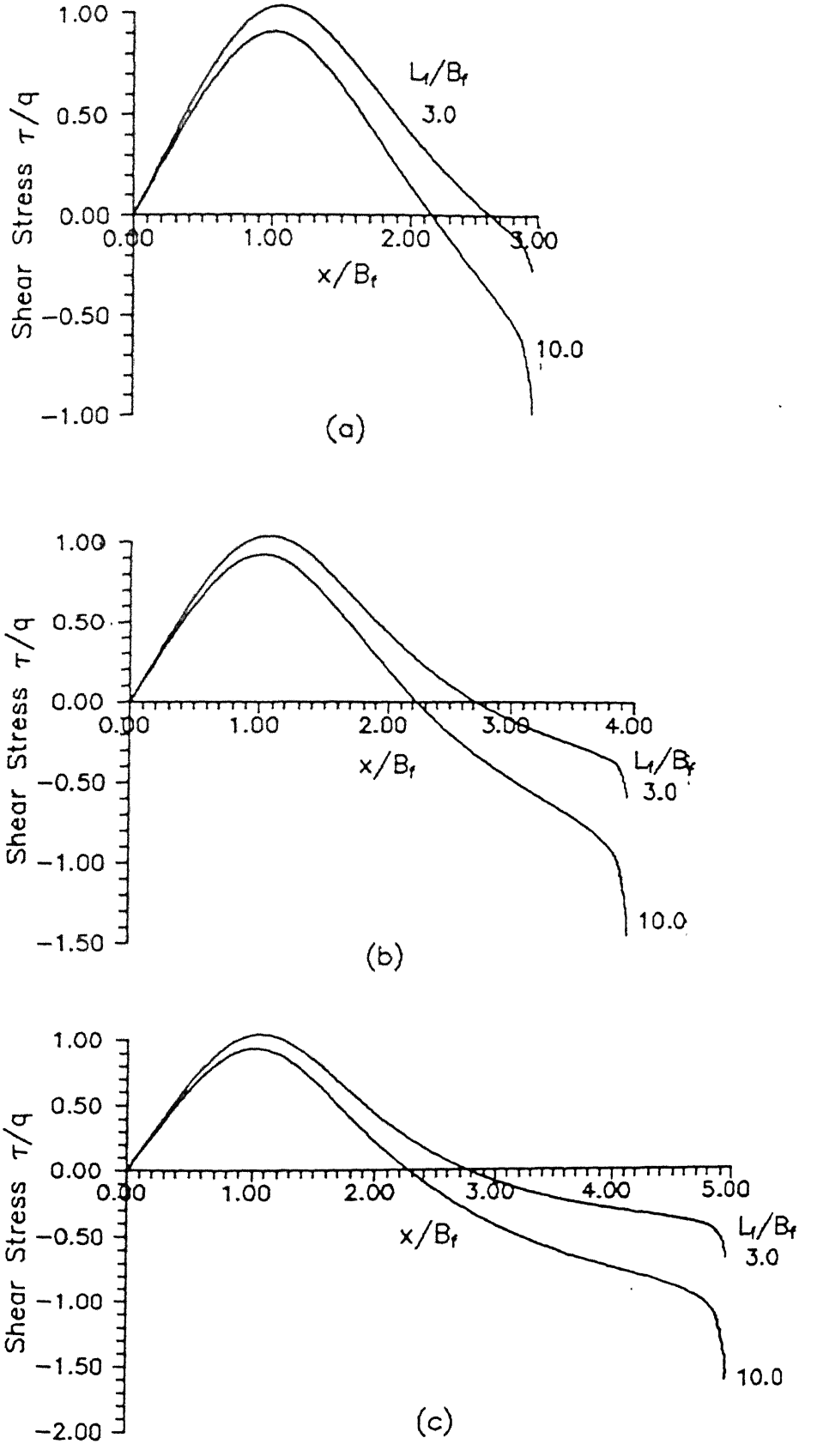


Fig. 3.28 Variation of Shear Stress with Distance for Different Aspect Ratios of Loaded Area ($U_o/B_f=1$) a) $L_r/B_f=3$, b) $L_r/B_f=4$, c) $L_r/B_f=5$

under areas with smaller aspect ratios ($L_f/B_f<2$) and at greater depths is not advantageous.

The effect of Poisson's ratio, $\nu_s$, on $I_{sc}$ is studied in Fig. 3.30 which presents the variation of $I_{sc}$ with the length, $L_r/B_f$, of the strip for different values of $\nu_s$ and for the strip placed at a depth, $U_o/B_f=1$, below a square area ($L_f/B_f=1$). It is evident from the figure that with increase in $\nu_s$, there is an increase in the $I_{sc}$ values. For $\nu_s \geq 0.2$ there is no significant improvement in $I_{sc}$ values for strips with lengths, $L_r/B_f>2.5$ or 3. This again reiterates the fact mentioned earlier that longer strips ($L_r/B_f>2.5$) under smaller areas do not prove advantageous. The increase in $I_{sc}$ values with increasing values of $\nu_s$ is due to the fact that at a depth, $U_o/B_f=1$, the stresses are predominantly positive. Higher interfacial stresses are possible for soils with higher values of Poisson's ratio since lateral displacements are higher. As a result, soils with $\nu_s=0.5$ show maximum $I_{sc}$ values.

So far, single strips placed centrally below the loaded area were studied. Strips placed away from the centre and in groups also affect the SRC considerably. In the next two sections, effects due to two strips and effects of multiple strips are studied.

### 3.6.3 Two Strips at Depth $U_o$

The half-width of the strip in this case is $0.025B_f$. A single strip of half-width, $0.05B_f$, placed centrally below the loaded area, as was studied in the previous section is equivalent

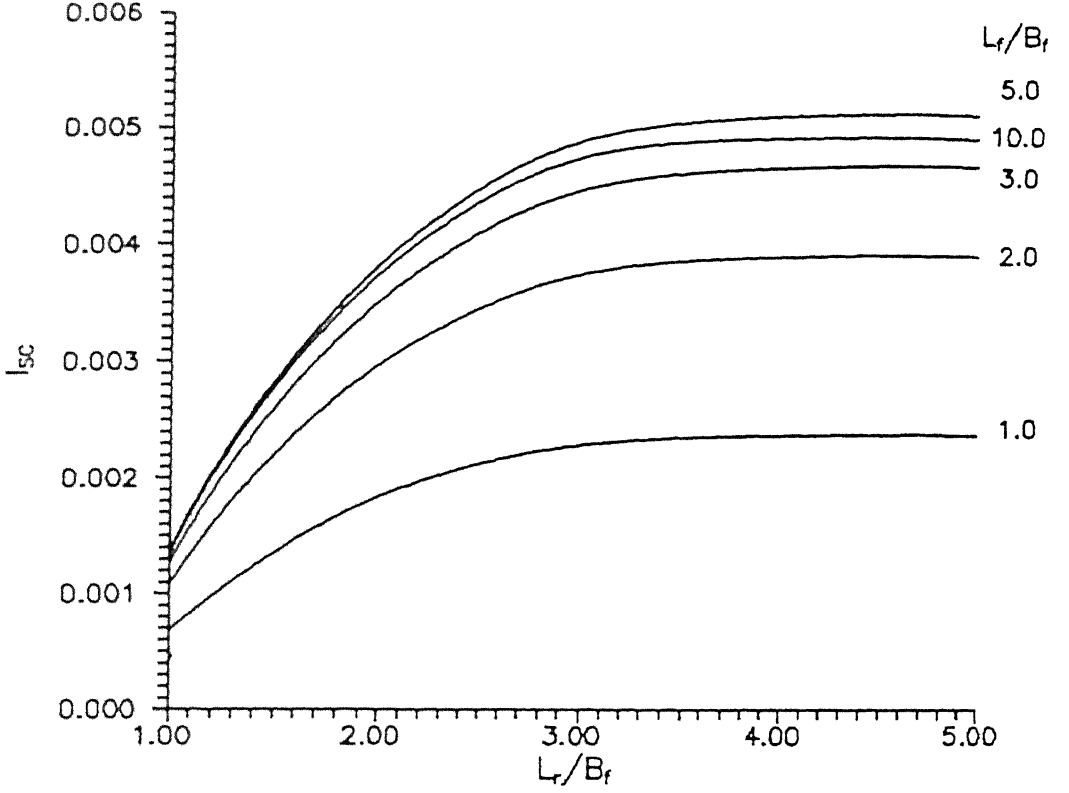


Fig. 3.29 Effect of Length of Strip on $I_{sc}$ for Different Aspect Ratios of Loaded Area ($U_0/B_f=2$, $\nu_s=0.3$)

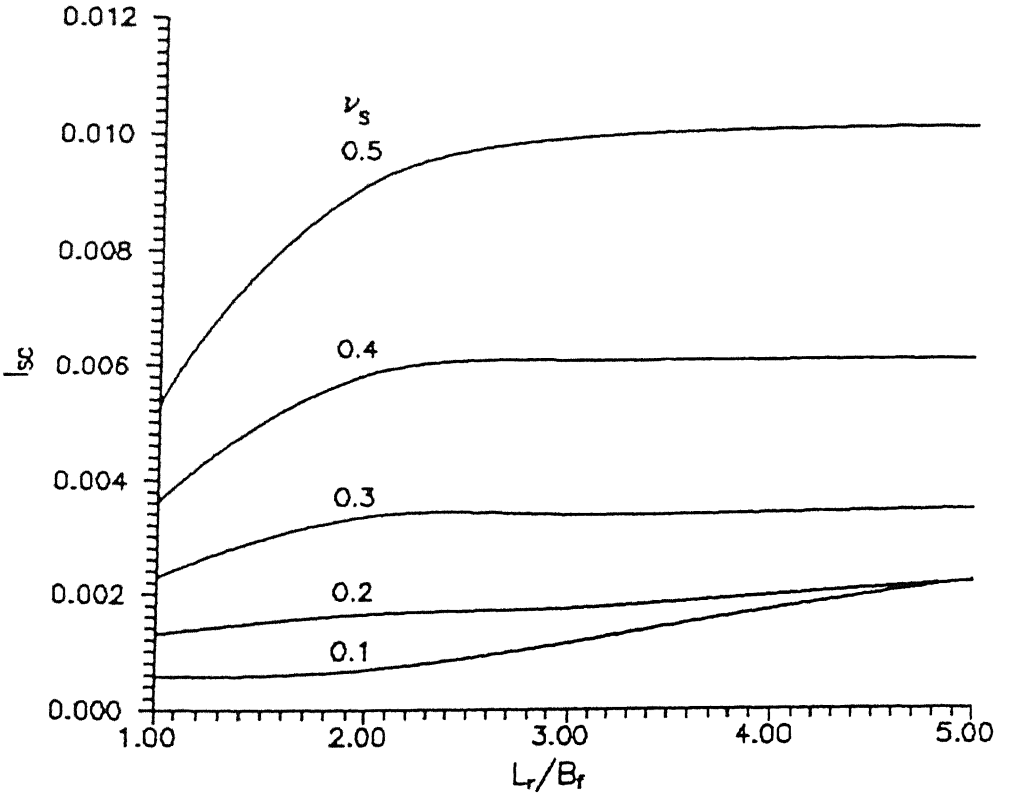


Fig. 3.30 Effect of Length of Strip on $I_{sc}$ for Different values of Poisson's Ratio of Soil ($U_0/B_f=1$, $L_f/B_f=1$)

to two strips of half-width, $0.025B_f$, placed at a distance, $S_y$, equal to $0.025B_f$, i.e. the half-width of the strip, from the x-axis. At this spacing the two strips are contiguous. Settlement reduction coefficients obtained for two strips placed touching each other at the centre are compared with those obtained for a single strip (Table 3.3). The results agree well. Table 3.3 implies that a single strip of half-width equal to $0.05B_f$ and two contiguous strips of half-width, $0.025B_f$ give the same $I_{sc}$ values.

Table 3.3 $I_{sc}$ Values for a Strip Considered as Single and as Two Contiguous Ones

| | $I_{sc}$ for $U_o/B_f=1$, $L_f/B_f=1$, $\nu_s=0.3$ | | |
|---|---|---|---|
| $L_r/B_f$ | Single Strip $B_r/B_f=0.05$ | Two Strips $B_r/B_f=S_y/B_f=0.025$ | Difference % |
| 1.0 | 0.002296 | 0.002390 | 4.10 |
| 2.0 | 0.003357 | 0.003474 | 3.50 |
| 3.0 | 0.003381 | 0.003495 | 3.46 |
| 4.0 | 0.003417 | 0.003536 | 3.48 |
| 5.0 | 0.003480 | 0.003600 | 3.45 |

It is to be noted that SRC values presented in the figures are the settlement reduction coefficients due to one of the strips among the pair at a distance, $S_y$. To obtain the SRC due to both the strips, the SRC values from the figures are to be doubled since the strips are symmetrically placed about the x-axis.

Fig. 3.31 shows the plot of the normalised shear stresses, $\tau/q$, versus the distance, $x/B_f$, along the strips for different

values of the distance, $S_y/B_f$, of the strips from the x-axis and for strips of length, $L_r/B_f=2$, placed at a depth, $U_o/B_f=1$, beneath a square area. For all $S_y/B_f$ values the stresses originate from 0, and reach a maximum at a distance, $x/B_f$ of around 1. An interesting point worth noting is that maximum stresses are observed for the distance, $S_y/B_f=0.25$, while strips placed closer to the x-axis ($S_y/B_f=0.1$) show lesser values of stresses. The maximum shear stress, $\tau/q$, for $S_y/B_f=0.25$ is of the order of 1.13 at a distance, $x/B_f=1$. Further, if this figure is compared with Fig. 3.14 and the curve of shear stresses for a single centrally placed strip ($U_o/B_f=1$) is superimposed on Fig. 3.31, it is seen that the shear stresses for the single strip case lie slightly below the curve for $S_y/B_f=1$. As $S_y/B_f$ increases beyond 0.25 the stresses decrease quite rapidly, the stresses for the distance of the strip, $S_y/B_f$, from the x-axis equal to 2 being very small. This trend of the stresses can be explained as follows. For strips placed closer to the x-axis ($S_y/B_f<0.25$) the interference of one strip on the other is high due to close spacing. For $S_y/B_f=0.025$ (contiguous strips) the interference is maximum. As this distance increases from 0.025 to 0.25, the influence of one strip on the other decreases. Consequently there is an increase in the stresses. Beyond a distance, $S_y$, of $0.25B_f$ the lateral displacements due surface loading decrease resulting in lower shear stress mobilisation. For large $S_y/B_f$ values ($S_y/B_f>1.5$) the lateral displacement is negligibly small and hence stresses are relatively smaller compared to closer spacings.

The variation of the normalised tension, $T/qB_f^2$, with the distance, $x/B_f$, along the strip for different values of the

distance, $S_y/B_f$, of the strip from the x-axis and for strips of length, $L_r/B_f=2$, placed beneath a square area ($L_f/B_f=1$) at a depth, $U_o/B_f=1$, is depicted in Fig. 3.32. The stresses being positive over the full length (Fig. 3.31), the strip is subjected to pure tension throughout its length. As a consequence of these stresses, tension is maximum for strips placed at a distance, $S_y/B_f=0.25$, and minimum for $S_y/B_f=2.0$. The maximum tension, $T/qB_f^2$, at the centre for strips at a distance, $S_y/B_f=0.25$ is 0.076 while the same for strips at a distance, $S_y/B_f=2$ is 0.014.

The effect of the distance of the strips from the x-axis ($S_y/B_f$) on $I_{sc}$ for various depths, $U_o/B_f$, and for strips of length, $L_r/B_f=2$, placed beneath a square area is presented in Fig. 3.33. For closer spacing from the x-axis, i.e. $S_y \leq 0.25B_f$, $I_{sc}$ increases monotonically upto a depth, $U_o=B_f$ and then decreases with increase in depth upto $2B_f$. $I_{sc}$ for a distance, $S_y=0.25B_f$ increases from 0.00025 at a depth of $0.25B_f$ to 0.0023 at depth of $B_f$ and then decreases to 0.0013 at $U_o/B_f=2$. As the distance, $S_y$, increases beyond $0.25B_f$, there is a change in slope at shallow depths and a decrease in the maximum value of $I_{sc}$. The depth at which maximum settlement reduction occurs also increases with the increase in the distance, $S_y/B_f$. The $I_{sc}$ values decrease with increase in $S_y/B_f$ since the stresses decrease with increase in $S_y/B_f$ (Fig. 3.31). In reasoning for slope changes at shallow depths, apart from the aspects considered in Fig. 3.19, the ratio $S_y/B_f$ also plays an important role. It is interesting to note that larger settlement reduction results from relatively distantly spaced strips placed at greater depths ($U_o/B_f>1.5$).

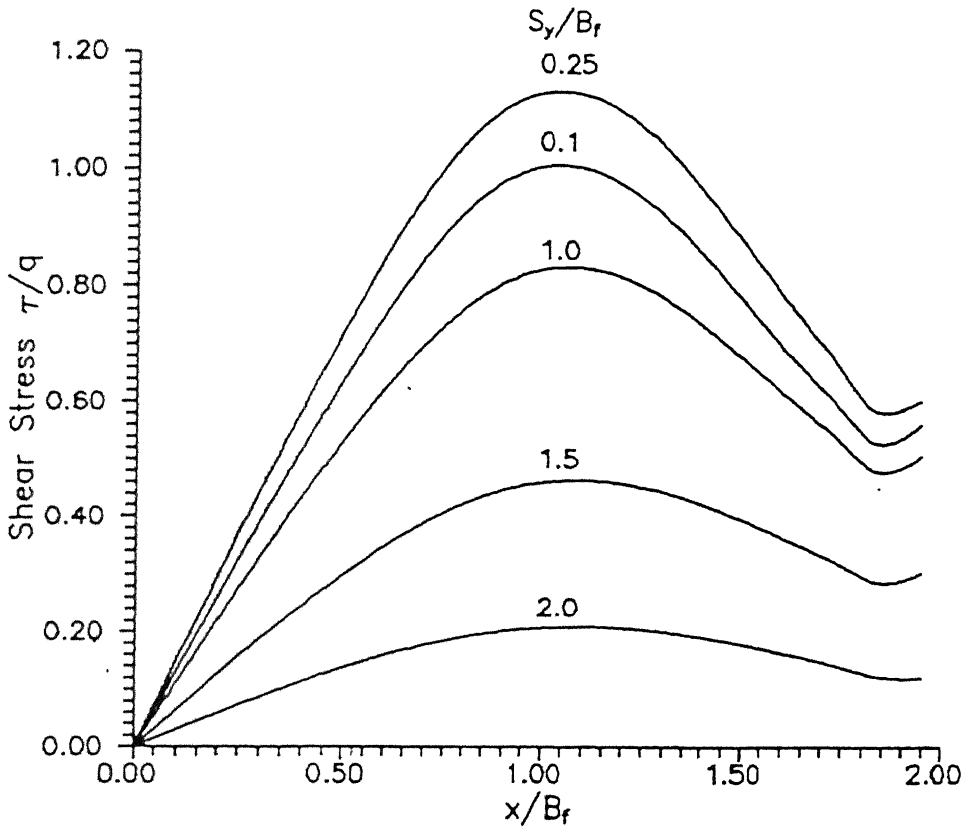


Fig. 3.31 Variation of Shear Stress with Distance for Different Distances of Strip from x–axis ($L_r/B_f$=2, $L_t/B_f$=1, $U_0/B_f$=1, $\nu_s$=0.3)

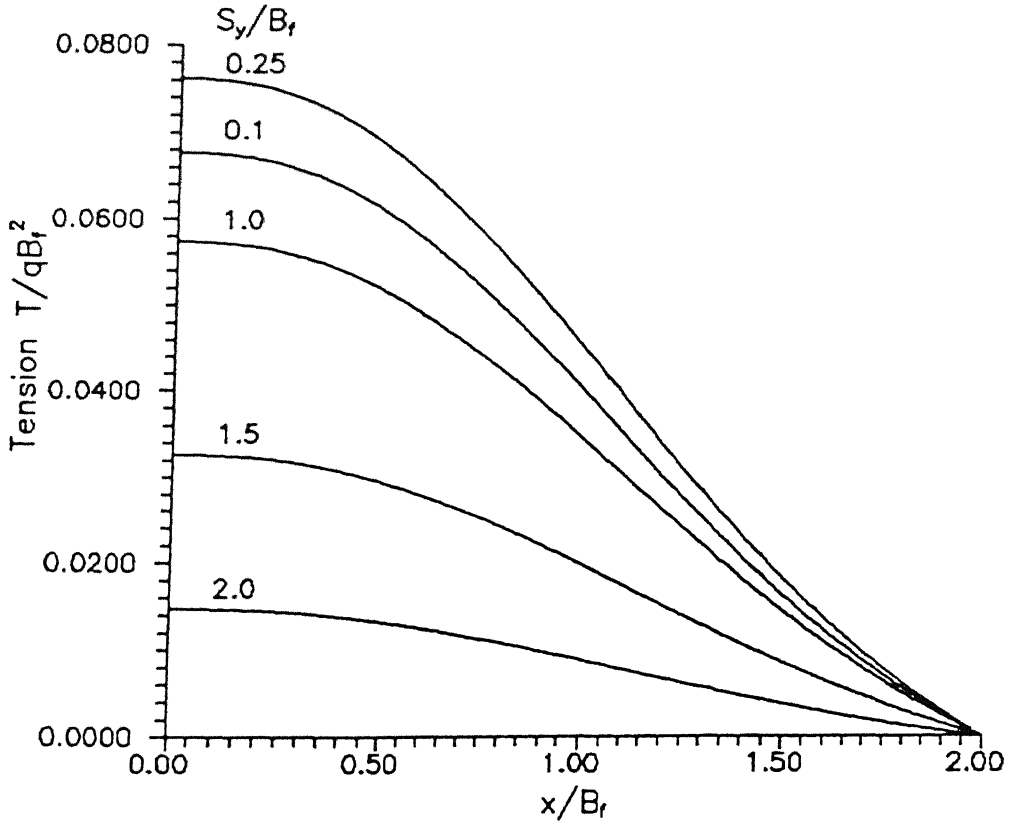


Fig. 3.32 Variation of Tension with Distance for Different Distances of Strip from x–axis

Fig. 3.34 presents the variation of $I_{sc}$ with the distance, $S_y/B_f$, for different lengths of the strip, $L_r/B_f$, placed at a depth, $U_o/B_f$=1.0, below a square loaded area. It is observed that the $I_{sc}$ values increase with $S_y/B_f$ upto $S_y/B_f$ equal to 0.25. For larger values of $S_y/B_f$, $I_{sc}$ values reduce sharply with increase in $S_y/B_f$. At distances beyond $1.75B_f$, the settlement reduction is negligible. For all lengths ($L_r/B_f$) a maximum $I_{sc}$ is observed at a distance of $S_y/B_f$=0.25. This is because the shear stresses for strips at this distance are maximum (Fig. 3.31). The variation in $I_{sc}$ values with $S_y/B_f$ is a direct outcome of the variation of stresses. The maximum $I_{sc}$ values are 0.0016 for $L_r/B_f$=1, 0.0023 for $L_r/B_f$=2 and 0.0024 for $L_r/B_f$=5.0. The increase in $I_{sc}$ for $L_r/B_f$>2.0 is minimal which indicates that there is no advantage in providing strips longer than $2B_f$ at a depth of $B_f$.

In studying the effect of $S_y/B_f$ on settlement reduction it is imperative that for maximum benefit from strips of length, $L_r/B_f$=2, placed at a depth, $U_o/B_f$=1, under square areas, the optimal choice of the distance from the x-axis, $S_y/B_f$ is 0.25.

### 3.6.4 Two Strips One Below the Other

The interference of two strips one below the other and the consequent effect on the shear stresses mobilised are studied here under. The settlement reduction resulting from these stresses are compared with those obtained from the principle of superposition, i.e. $I_{sc}$ values obtained by considering each strip as a single strip. The ratio of the $I_{sc}$ obtained for the present case with that obtained from the principle of superposition is termed as $I_D$.

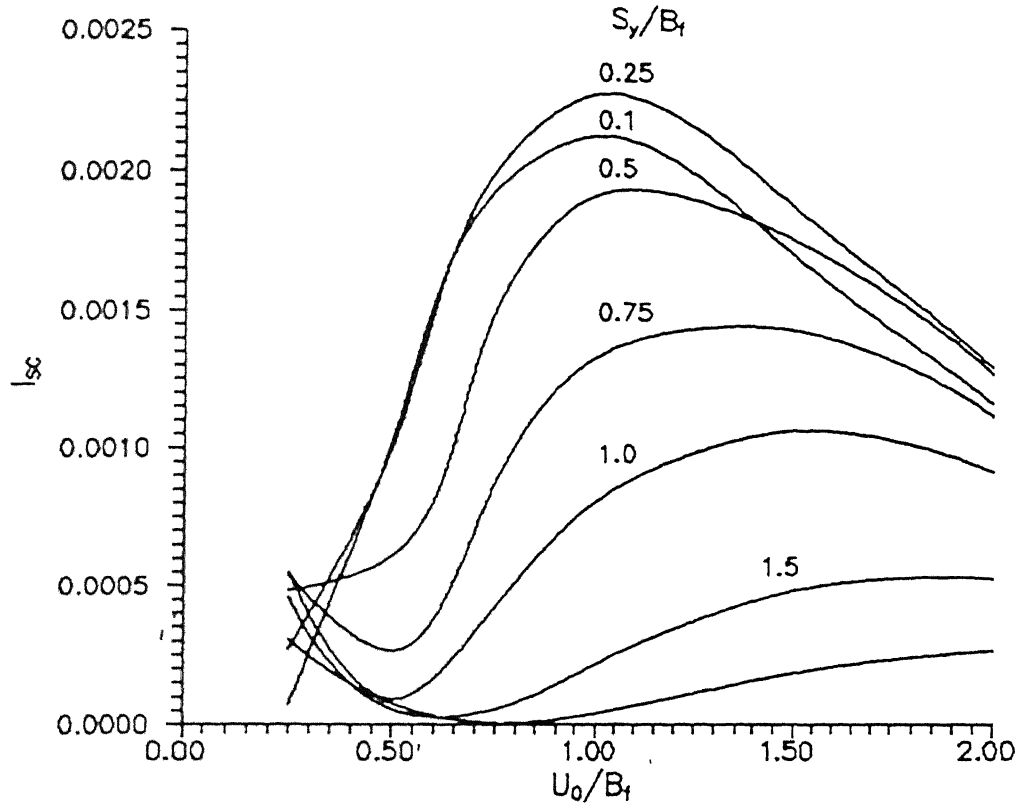


Fig. 3.33 Effect of Depth of Placement on $I_{sc}$ for Different Distances of Strip from x–axis ($L_r/B_f$=2, $L_t/B_f$=1, $\nu_s$=0.3)

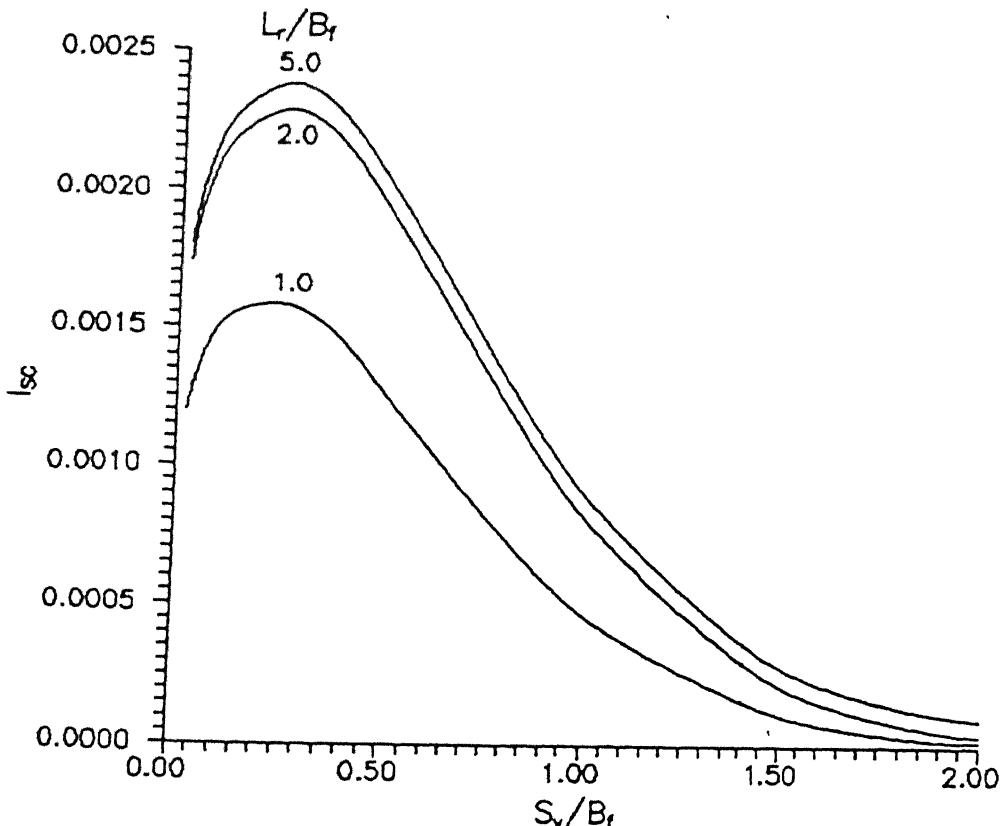


Fig. 3.34 Effect of Distance from x–axis on $I_{sc}$ for Different Lengths of Strip ($U_0/B_f$=1, $L_t/B_f$=1, $\nu_s$=0.3)

Fig. 3.35 depicts the shear stress variation for two strips of length, $L_r/B_f=2$, at depths, $U_o/B_f=0.5$ and $U_i/B_f=1.0$ below a square loaded area. The dotted lines are the shear stresses for single strips at the respective depths. It is evident that the stresses for the two strips, one below the other are smaller than those for single strips. The difference in the stresses is much higher for the strip at a shallower depth ($U_o/B_f=0.5$). The decrease in the shear stresses is due to the interference of one strip on the other. As a consequence the settlement reduction coefficients of points on the surface are smaller.

Table 3.4 presents the $I_D$ values for two strips placed one below the other at depths, $U_o/B_f$ and $U_i/B_f$, for various lengths, $L_r/B_f$, of the strips. Two sets of results are presented. In the first set, one strip is placed at a depth, $U_o/B_f=0.75$ and in the second it is placed at a depth, $U_o/B_f=1.5$. The depth, $U_i/B_f$, in both sets is varied from 0.25 to 2. It is seen that the least value of $I_D$ in the first set is when the second strip of length, $L_r/B_f=2$ is placed at a depth, $U_i/B_f=1$ and equals 0.769. The corresponding value for the second set is for a strip of length, $L_r/B_f=5$ at a depth, $U_i/B_f=2$ and equals 0.825. In both the sets it is observed that at shallow depths the ratio, $I_D$, is marginally greater than 1 which indicates that the $I_{sc}$ values obtained by considering the interference of each strip on the other is greater than that obtained from the principle of superposition. This small increase is because of the following reason. The shear stresses on the second strip at shallow depths ($U_i/B_f \leq 0.25$) are predominantly negative. These negative stresses cause the points

Table 3.4 $I_D$ Values for Two Strips Placed Centrally Below the Other

| $U_i/B_f$ \ $L_r/B_f$ | $U_o/B_f$ = 0.75 | | | $U_i/B_f$ \ $L_r/B_f$ | $U_o/B_f$ = 1.5 | | |
|---|---|---|---|---|---|---|---|
| | 1 | 2 | 5 | | 1 | 2 | 5 |
| 0.25 | 0.956 | 1.1 | 1.09 | 0.25 | 0.99 | 1.04 | 1.1 |
| 0.50 | 0.800 | 0.8 | 0.815 | 0.50 | 0.976 | 0.96 | 1.02 |
| 1.00 | 0.818 | 0.769 | 0.785 | 0.75 | 0.962 | 0.917 | 0.94 |
| 1.50 | 0.962 | 0.917 | 0.942 | 1.00 | 0.926 | 0.86 | 0.863 |
| 2.00 | 0.991 | 0.965 | 0.984 | 2.00 | 0.93 | 0.858 | 0.825 |

on the first strip at depth $U_o/B_f$ to move away from the centre. Hence, the net horizontal displacements of points along the first strip are higher than the corresponding displacements for a single strip. As a result the stresses mobilised are higher. Consequently, the settlement reduction of points along the surface are also higher. This results in $I_D$ value greater than 1.

### 3.6.5 Multiple Strips

Settlement reduction due to two pairs of strips at the same depth is studied herein. $I_{sc}$ values due to these two pairs, one separated by a distance, $2S_{y1}/B_f$, and the other by a distance, $2S_{y2}/B_f$, are computed. $I_{sc}$ values for strip pairs at $S_{y1}/B_f$ and $S_{y2}/B_f$ from x-axis are computed independently and summed up. The ratio ($I_D$) of $I_{sc}$ for the first case with respect to the one obtained due to summation is calculated. The difference of the two spacings ($S_{y2}-S_{y1}$) is termed as $S_{yD}$. It is checked whether

the principle of superposition is valid for multiple strips.

The variation of shear stresses, $\tau/q$ with distance, $x/B_f$ for multiple strips of length, $L_r/B_f=2$, placed at a depth, $U_o/B_f=1$, below a square area is presented in Fig. 3.36. The solid lines indicate shear stresses for multiple strips, placed at distances, $S_{y1}/B_f=0.025$ and $S_{y2}/B_f=0.5$, and the dotted lines are the shear stresses for a single pair of strips at the respective distances, $S_y/B_f$, from the x-axis. The shear stresses mobilised for multiple strips are smaller than those for a single pair of strips. Stresses on one pair influence the displacements of nodes along the second pair resulting in smaller net displacements of the nodes. As a result the stresses mobilised are smaller. These, in turn affect the settlement reduction of points along the surface, as can be seen in the following figures.

Fig. 3.37 depicts the variation of $I_D$ with $S_{yD}$ for different lengths, $L_r/B_f$, of the strip placed at a depth, $U_o/B_f=1$, below a square area. $I_D$ values increase from about 0.54 to 0.99 with increasing values of $S_{yD}$. For strips with length, $L_r/B_f=1$, $I_D$ equals 0.9 for $S_{yD}=0.5$, whereas for strips with $L_r/B_f\geq2$, $I_D$ equals 0.9 for $S_{yD}=1$. It is clear that for multiple strips the principle of superposition is not valid unless $S_{yD}$ is greater than about 0.7 for $L_r/B_f=1$ and around 1 for $L_r/B_f\geq2$. When the $S_{yD}$ is small, all the four strips have equally high influences on each other resulting in low shear stresses.

Fig. 3.38 shows the variation of $I_D$ with $S_{yD}$ for different

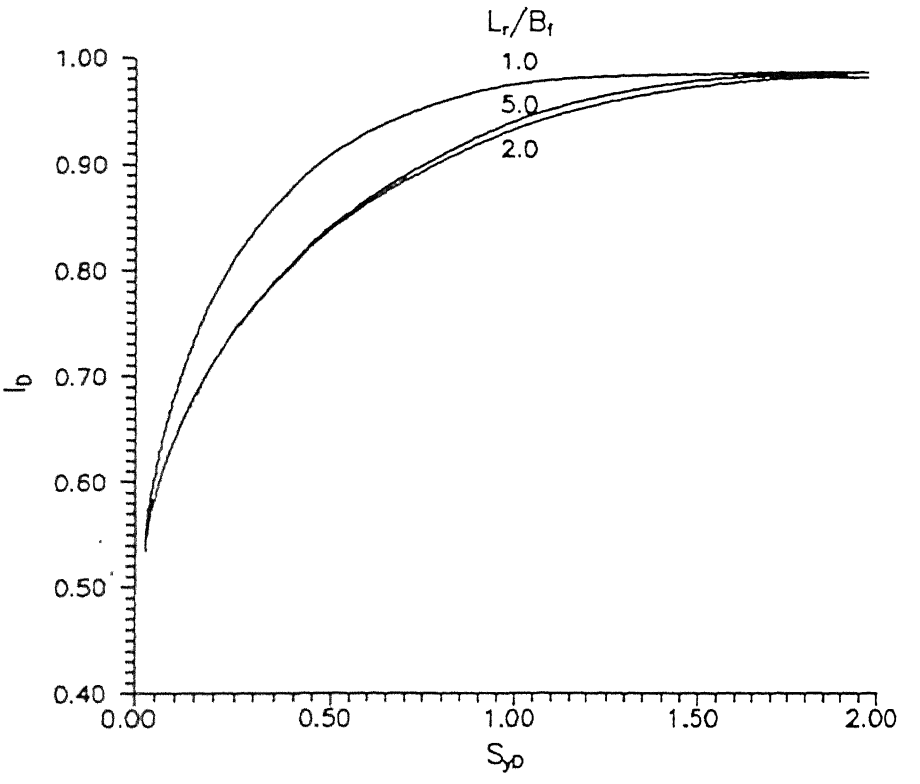


Fig. 3.37 Effect of Difference of Spacing on $I_\rho$ for Different Lengths of Strip ($U_0/B_f=1$, $L_f/B_f=1$, $\nu_s=0.3$)

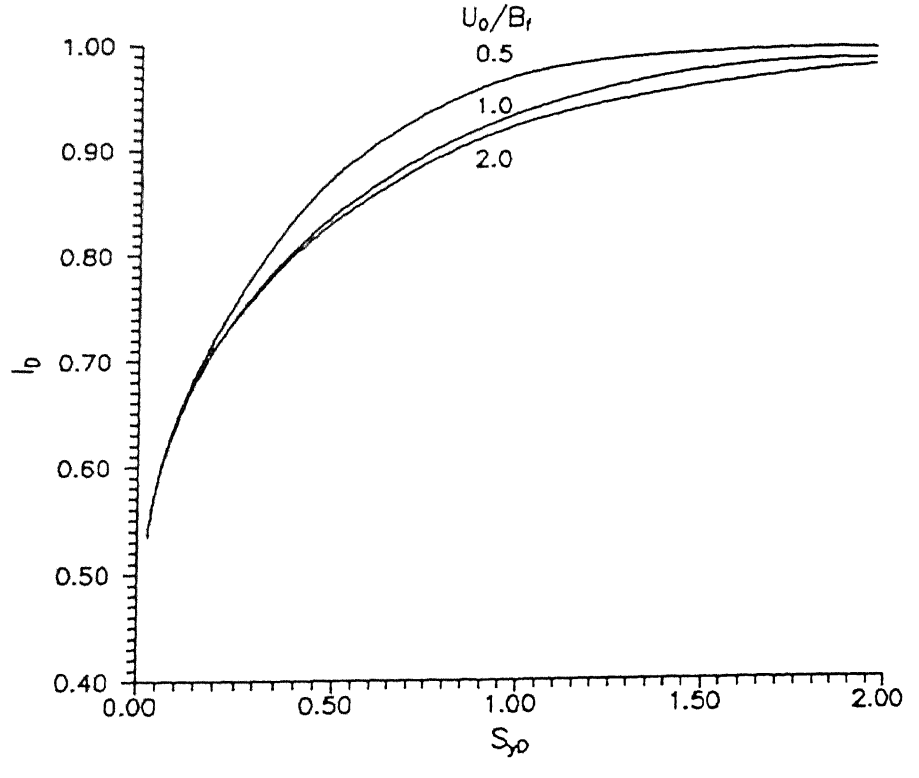


Fig. 3.38 Effect of Difference of Spacing on $I_\rho$ for Different Depths of Placement of strip ($L_r/B_f=2.0$, $L_f/B_f=1$, $\nu_s=0.3$)

depths of placement, $U_o/B_f$, of strips of length, $L_r/B_f=2$, beneath a square area. $I_D$ increases from 0.53 to 0.99 with $S_{yD}$ for all depths. With depth, $U_o/B_f$ increasing from 0.5 to 1 the decrease in the $I_D$ values is noticable while it is marginal with further increase in depth. The principle of superposition appears to be valid for $S_{yD}>0.7$ for $U_o/B_f<1$ and for $S_{yD}>1$ for $U_o/B_f>1$.

From these two figures it is clear that for close spacing of strips the principle of superposition is not valid. An appropriate correction factor based on the spacing of strips is to be considered in order to obtain the settlement reduction coefficients due to multiple strips from those of single strips.

## 3.7 Conclusions

A parametric study, using the elastic continuum approach has been developed to study the effects of the aspect ratio of the loaded area, length and depth of a strip reinforcement on the shear stresses mobilised at its interface with soil and on the reduction of surface settlements. The effects of the distance of the strip from the centre and the Poisson's ratio of the soil on the quantities mentioned above have also been examined. The shear stresses mobilised at the interface oppose the displacements of the soil due to the surface load. It is perceived that these stresses are responsible for the reduction in surface settlements. The results obtained from the parametric study depict that an optimum choice of the parameters has to be made in order to extract the maximum benefit from rigid strip reinforcements. Based on the results, the following conclusions are enumerated.

1. A short strip placed at a shallow depth ($U_o/B_f \leq 0.35$) is ineffective in reducing settlement at the surface. It is subjected to compression since the shear stresses mobilised are negative, i.e., they are directed outward.
2. Maximum settlement reduction of the centre of the loaded area due to a single strip is observed for a strip placed at a depth in the range of $0.75B_f$ to $1B_f$ below an area with aspect ratio upto 3, and at about $1.5B_f$ below longer rectangles.
3. For a strip placed at a depth equal to $B_f$ below a loaded area with aspect ratio upto 3, the settlement reduction coefficient increases appreciably with the length of strip upto $L_r=2B_f$. With further increase in the length of the strip the increase in SRC is marginal.
4. As expected, the results show that a longer strip ($L_r/B_f \geq 3$) is effective if placed below a longer rectangular area upto a depth equal to $B_f$.
5. At depths, $U_o/B_f \geq 2$, increasing the length of the strip beyond $3B_f$, for any aspect ratio of the loaded area does not contribute to any increase in the settlement reduction coefficients.
6. As expected, strips placed in incompressible soils (saturated undrained condition) show maximum reduction.
7. For a pair of rigid strips of length, $L_r/B_f=2$, placed symmetrically about the x-axis and at a depth, $U_o>0.5B_f$, maximum reduction in surface settlements is observed if the centre of each strip lies at a distance of $0.25B_f$ from the x-axis.
8. For two strips placed one below the other the principle of

superposition is valid if the vertical spacing of the strips is greater than $0.5B_f$. A suitable correction factor will have to be used for closer vertical spacings.

9. For multiple strips at the same depth, the principle of superposition is valid if the difference in the distances of each pair from the x-axis is greater than $0.7B_f$. For closer spacings ($S_y/B_f<0.7$) a suitable correction factor has to be used.

# CHAPTER 4

# SOIL-RIGID STRIP REINFORCEMENT INTERACTION - NORMAL STRESSES

## 4.1 Introduction

In chapter 3, the rigidity of the strip in the axial direction was considered. In this chapter the strip is assumed to be rigid in the vertical (normal) direction. As seen earlier, the applied load on the surface causes the soil below to move downward and outward. A deformable strip will deform as shown in Fig. 4.1 (dotted line) but a strip assumed to be rigid undergoes a rigid body displacement in the vertical direction. As a result, normal stresses are mobilised along the soil-strip interface. The stressess are symmetric about the z-axis due to the symmetry of the loading. Since the normal stresses alone are considered it is assumed that the rigidity of the strip in the horizontal (axial) direction (i.e. the shear interaction) has no effect on the normal displacements.

The mobilised interfacial normal stresses represent the difference between the normal stresses on the top and the bottom faces of the strip. Because of the rigidity of the strip, the normal stresses act upward near the centre and downward at the edges, thus forcing the strip to undergo a uniform displacement. The net result of these stresses is to push the soil on the surface upward near the centre of the loaded area. Consequently, there is a reduction in the settlement of the surface. Thus, the reinforcing strip helps in reducing foundation settlements.

## 4.2 Single Strip

### 4.2.1 Problem Definition

The analysis of soil-reinforcement strip interaction for normal stresses is very similar to the analysis for shear stresses discussed in chapter 3, but with a difference in the mechanism. In this chapter the normal stresses only are considered. A rigid reinforcing strip of size, $2L_r \times 2B_r$, is placed at a depth, $U_o$, centrally below a rectangular area of size, $2L_f \times 2B_f$, transmitting a uniform load of intensity, q, (Fig. 4.2). The width of the strip ($0.1B_f$) is relatively small and its thickness, $t_r$, negligible.

### 4.2.2 Analysis

The elastic continuum approach is resorted to in modelling the soil-strip interaction. The vertical displacements of the points at the soil-strip interface are calculated using Boussinesq's solution for vertical displacement at a point within an elastic half-space due to a point load acting on the surface. The Boussinesq's problem is as shown in Fig. 4.3. The vertical displacement of point, A, as shown in the figure, due to load P is

$$\rho_z = \frac{P(1+\nu_s)}{2\pi E_s R}\left[2(1-\nu_s) + \frac{z^2}{R^2}\right] \qquad (4.1)$$

where $R=\sqrt{r^2 + z^2}$, r and z are respectively the radial distance and depth of point A, with respect to the load P, $E_s$ and $\nu_s$ are respectively the modulus of deformation and Poisson's ratio of the soil.

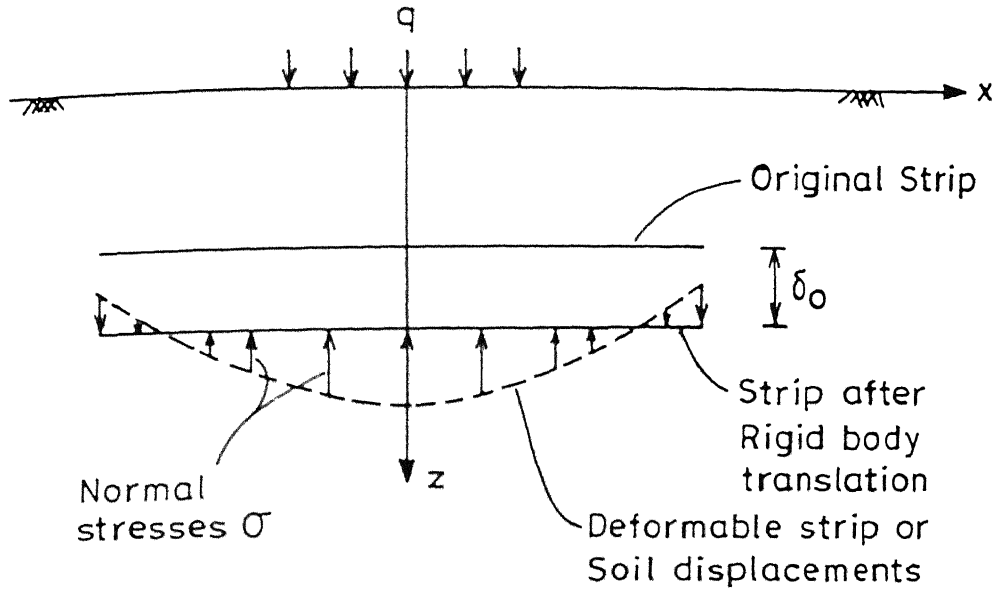


Fig. 4.1 Strip Deformation

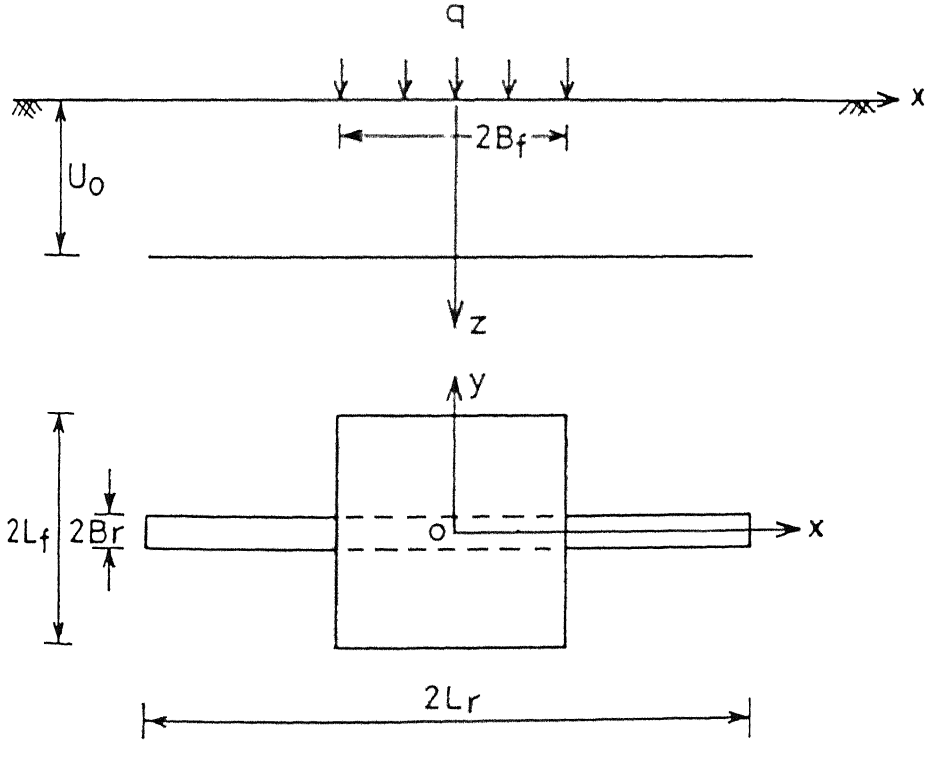


Fig. 4.2 Definition Sketch – Single Strip

The vertical displacements, $\rho_z^f$, of points along the reinforcement strip, due to the uniform surface load, q, is calculated by integrating Eq. 4.1 over the loaded area as

$$\rho_z^f = \int_{-B_f}^{B_f} \int_{-L_f}^{L_f} \frac{q(1+\nu_s)}{2\pi E_s R} \left[ 2(1-\nu_s) + \frac{z^2}{R^2} \right] dA \qquad (4.2)$$

where dA is an elemental area on the loaded surface.

The discretization of the loaded area is the same as in section 3.2.2. The vertical displacement, $\rho_{zi}^f$, of the centre of element i (Fig. 4.4), due to the surface load is obtained by carrying out the integration of Eq. 4.2 numerically as

$$\rho_{zi}^f = \sum_{i_f=1}^{n_B} \sum_{j_f=1}^{n_L} \frac{q(1+\nu_s)}{2\pi E_s R} \left[ 2(1-\nu_s) + \frac{U_o^2}{R^2} \right] dA \qquad (4.3)$$

where $r=\sqrt{x^2 + y^2}$, and $R=\sqrt{r^2 + U_o^2}$. Non-dimensionalising all length parameters with half the width, $B_f$, of the loaded area, Eq. 4.3 is expressed as

$$\rho_{zi}^f = \frac{B_f}{E_s} I_i^f q \qquad (4.4)$$

where $I_i^f$ is a dimensionless influence coefficient that depends on the aspect ratio, $L_f/B_f$, of the loaded area, the depth, $U_o/B_f$, of the strip, the Poisson's ratio, $\nu_s$, of the soil and the location of node i. The vector of the vertical displacements of all the N nodes along the half-length of the strip is obtained by evaluating

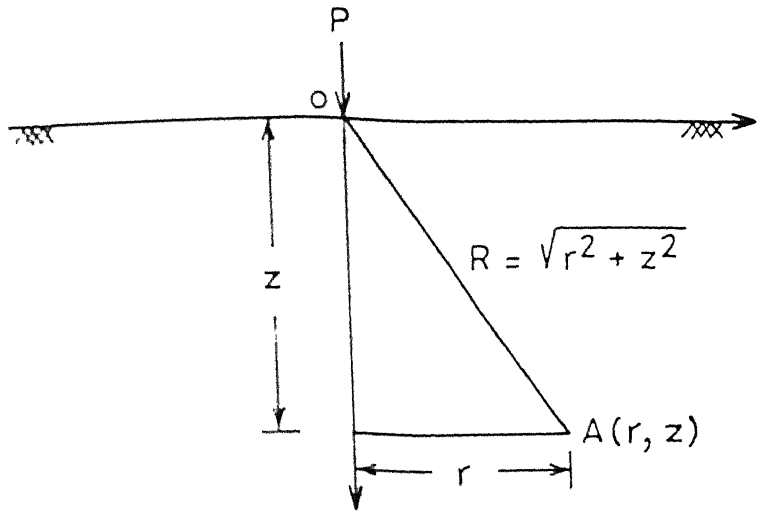


Fig. 4.3 Boussinesq Problem

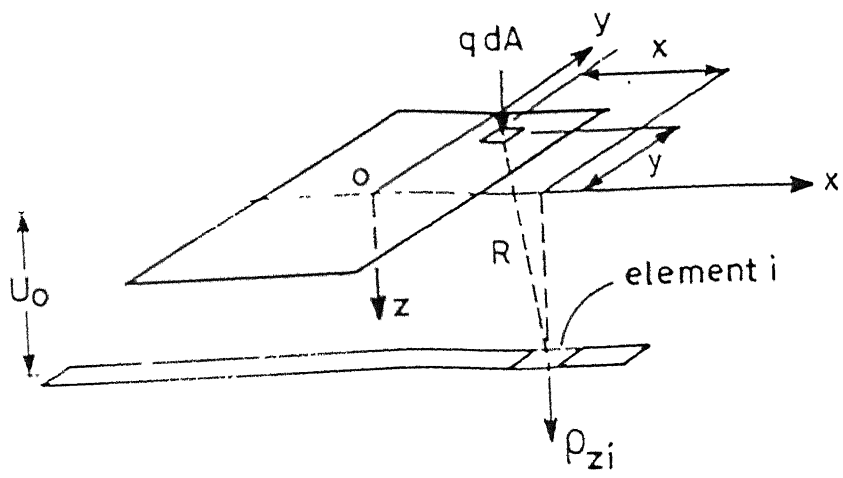


Fig. 4.4 Vertical Displacement along Strip due to Surface Load

Eq. 4.4 for all the nodes as

$$\left\{ \rho_z^f \right\} = \frac{B_f}{E_s} \left\{ I^f \right\} q \qquad (4.5)$$

where the vectors $\left\{ \rho_z^f \right\}$ and $\left\{ I^f \right\}$ are of size N.

Eq. 4.5 gives the vertical displacement profile of the soil without any reinforcement at depth $U_o$. If a rigid strip is placed at this depth, normal stresses are mobilised at the soil-strip interface so that the strip undergoes a rigid body displacement. To obtain these stresses, the vertical displacements due to these stresses are to be computed. It is achieved by using Mindlin's solution for vertical displacements due to a vertical force acting within an elastic half-space. The vertical displacement of a point, A(x,y,z) due to a vertical force, Q, (Fig 4.5) acting at a depth, c, in a semi-infinite elastic continuum is

$$\rho_z = \frac{Q(1+\nu_s)}{8\pi E_s (1-\nu_s)} \left[ G \right] \qquad (4.6)$$

where $$G = \frac{(3-4\nu_s)}{R_1} + \frac{[8(1-\nu_s)^2-(3-4\nu_s)]}{R_2} + \frac{(z-c)^2}{R_1^3} + \frac{(3-4\nu_s)[(z+c)^2-2cz]}{R_2^3} + \frac{6cz(z+c)^2}{R_2^5}$$

$$R_1 = \sqrt{x^2 + y^2 + (z-c)^2}\ , \quad R_2 = \sqrt{x^2 + y^2 + (z+c)^2}$$

and x, y, z are the co-ordinates of point A. The vertical displacement of any point along the strip due to normal stress, $\sigma$, on an elemental area, dA, is

$$d\rho_z = \frac{\sigma dA(1+\nu_s)}{8\pi E_s(1-\nu_s)} \left[ G \right] \qquad (4.7)$$

To obtain the vertical displacements, $\rho_z^r$, along the reinforcing strip due to the mobilised normal stresses, Eq. 4.7 is integrated over the area of the reinforcing strip.

The vertical displacement, $\rho_{zij}^r$, of node i, due to normal stress, $\sigma_j$, acting on element j (Fig. 4.6) is

$$\rho_{zij}^r = \int_{dA} \frac{(1+\nu_s)}{8\pi E_s(1-\nu_s)} \left[ G \right] \sigma_j \, dA \qquad (4.8)$$

where all the parameters are as mentioned in Eq. 4.6 with $c=U_o=z$, and x and y being the horizontal distances of node i with respect to the elemental area dA of the $j^{th}$ element.

Eq. 4.8 is integrated numerically to obtain the influence of the normal stress, $\sigma_j$, on the displacements of the N nodes. As in the case of shear stresses, the vertical displacement of node i is not only affected by the normal stress on element j alone but also by its image on element j'. The vertical displacements of node i due to stresses on both these elements are written as

$$\rho_{zij}^{r_i} = \frac{B_f}{E_s} I_{ij}^{r_i} \sigma_j \qquad (4.9)$$

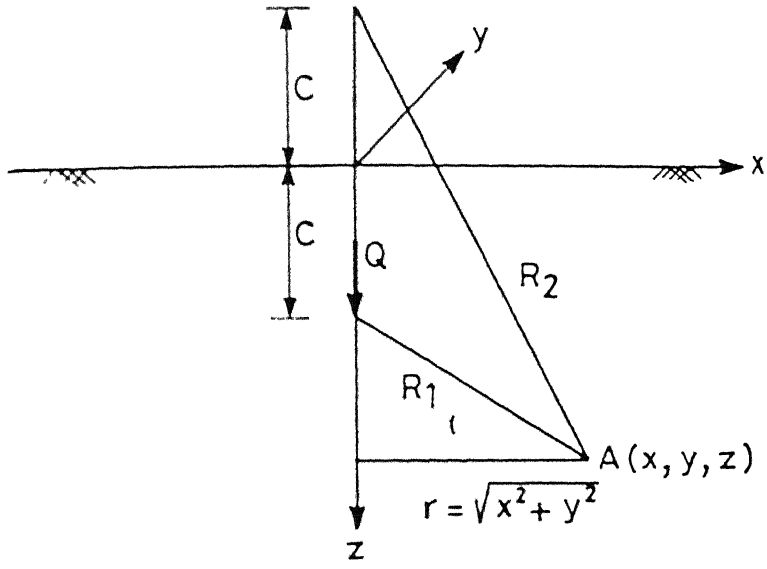


Fig. 4.5 Mindlin Problem

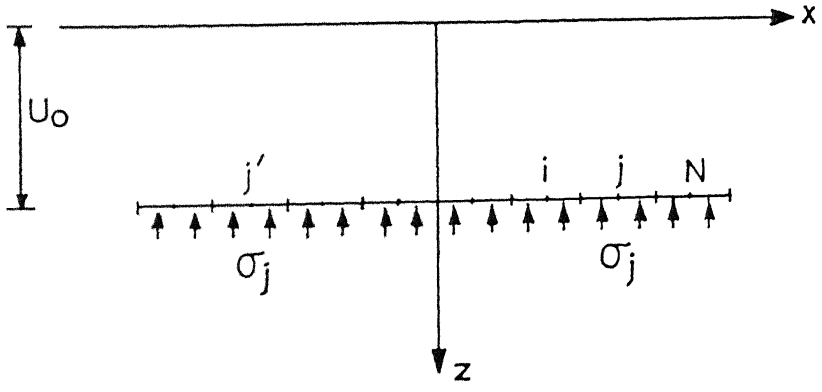


Fig. 4.6 Normal Stresses at Soil–Strip Interface

and

$$\rho_{zij}^{r_2} = \frac{B_f}{E_s} I_{ij}^{r_2} \sigma_j \qquad (4.10)$$

where $\rho_{zij}^{r_1}$ and $\rho_{zij}^{r_1}$ are displacements of node i and, $I_{ij}^{r_1}$ and $I_{ij}^{r_2}$ are respectively the dimensionless influence coefficients due to normal stresses acting on elements j and j'. $I_{ij}^{r_1}$ and $I_{ij}^{r_2}$ are functions of the parameters, $L_r/B_f$, $U_o/B_f$, $\nu_s$ and the locations of node i and element j. The vertical displacements, $\rho_{zij}^{r_1}$ and $\rho_{zij}^{r_2}$, act in the same direction and hence are additive.

Combining Eqs. 4.9 and 4.10, the vertical displacement at node i is obtained as

$$\rho_{zij}^{r} = \frac{B_f}{E_s} \left( I_{ij}^{r_1} + I_{ij}^{r_2} \right) \sigma_j \qquad (4.11)$$

The displacement, $\rho_{zi}^{r}$, at node i due to stresses on all the N elements is

$$\rho_{zi}^{r} = \sum_{j=1}^{N} \frac{B_f}{E_s} \left( I_{ij}^{r_1} + I_{ij}^{r_2} \right) \sigma_j \qquad (4.12)$$

The vector of the vertical diplacements of all the nodes along the half-length of the strip is

$$\left\{ \rho_z^r \right\} = \frac{B_f}{E_s} \sum_{j=1}^{N} \left( I_{ij}^{r_1} + I_{ij}^{r_2} \right) \left\{ \sigma \right\} \qquad (4.13)$$

Eq. 4.13 is rewritten as

$$\left\{ \rho_z^r \right\} = \frac{B_f}{E_s} \left[ I^r \right] \left\{ \sigma \right\} \qquad (4.14)$$

where the vectors, $\left\{ \rho_z^r \right\}$ and $\left\{ \sigma \right\}$, are of size N, $\left[ I^r \right]$ is a square matrix of size N.

The solution for the normal stresses are obtained by satisfying the compatibility of displacements at all the nodes at the soil-strip interface. In section 4.2.1, it was stated that since the strip is rigid it undergoes a uniform displacement in the vertical direction. Hence, the net vertical displacement of the strip is equal to the rigid body displacement, $\delta_o$, i.e.

$$\left\{ \rho_z^f \right\} - \left\{ \rho_z^r \right\} = \left\{ \delta_o \right\} = \delta_o \left\{ 1 \right\} \qquad (4.15)$$

Combining Eqs. 4.5, 4.14 and 4.15, one gets

$$\frac{B_f}{E_s} \left\{ I^f \right\} q - \frac{B_f}{E_s} \left[ I^r \right] \left\{ \sigma \right\} = \delta_o \left\{ 1 \right\} \qquad (4.16)$$

Eq. 4.16 gives N equations while there are N+1 unknowns, viz. N normal stresses and one rigid body displacement, $\delta_o$. The additional equation is obtained by satisfying equilibrium at the strip-soil interface, i.e.

$$\sum F_z = \sum_{i=1}^{N} \sigma_i \, dA = 0 \qquad (4.17)$$

where $\sum F_z$ is the summation of all forces acting on one half of the strip in the z-direction and dA is area of each element along

the strip. Since the stresses are symmetrical about the z-axis, the summation is carried out along half the length of the strip only. Eqs. 4.16 and 4.17 are rearranged and written as

$$\left[ I^r \right] \left\{ \sigma/q \right\} + \frac{\delta_o E_s}{B_f q} = \left\{ I^f \right\} \qquad (4.18)$$

$$\sum \sigma/q = 0 \qquad (4.19)$$

Eqs. 4.18 and 4.19 give N+1 equations for N+1 unknowns. They are solved by the Guass elimination technique for N values of normalised stresses, and the value of the normalised rigid body displacement, $\delta_o E_s / B_f q$.

Once the normal stresses mobilised at the strip-soil interface are computed, the settlement reduction coefficients along the surface are calculated on the same lines as in the previous chapter. The mechanism for settlement reduction is that, since the stresses are acting in the upward direction over the middle of the strip they cause the soil above the strip to move upward. As a result the surface heaves with a maximum heave at the origin, O. In order to arrive at this heave profile of the surface, Mindlin's solution for vertical displacements due to a vertical point load within an elastic half space is used. Referring to Fig. 4.5, the vertical displacement of point A, due to a vertical load, Q, is given by Eq. 4.6. The vertical displacement of point, B (x,0,0), on the surface is arrived at by substituting z=0 in Eq. 4.6 which reduces to

$$\rho_z = \frac{Q(1+\nu_s)}{8\pi E_s(1-\nu_s)}\left[\frac{8(1-\nu_s)^2}{R} + \frac{4(1-\nu_s)c^2}{R^3}\right] \qquad (4.20)$$

where $R = \sqrt{x^2 + c^2}$

Eq. 4.20 is integrated over the area of the reinforcing strip in order to evaluate the vertical displacements of points on the surface due to normal stresses at a depth, $U_o$, as

$$\rho_z = \frac{1}{16\pi G_s(1-\nu_s)} \int_{-L_r}^{L_r}\int_{-B_r}^{B_r} \sigma\left[\frac{8(1-\nu_s)^2}{R} + \frac{4(1-\nu_s)U_o^2}{R^3}\right] dA \qquad (4.21)$$

where $R = \sqrt{x^2 + U_o^2}$ and $G_s = \frac{E_s}{2(1+\nu_s)}$

The vertical displacement of any point k, on the surface due to normal stress, $\sigma_j$, on element j is given by

$$\rho_{zkj} = \frac{1}{16\pi G_s(1-\nu_s)} \int_{A_j}\left[\frac{8(1-\nu_s)^2}{R} + \frac{4(1-\nu_s)U_o^2}{R^3}\right]\sigma_j\, dA \qquad (4.22)$$

where $R = \sqrt{x_{kj}^2 + U_o^2}$, $x_{kj}$ being the distance along the x-axis between point k, and the centre of element j. Eq. 4.22 is rewritten as

$$\rho_{zkj}^{r_1} = \frac{B_f}{G_s} I_{nkj}^{r_1}\, \sigma_j \qquad (4.23)$$

Displacement at point k, due to normal stress on the image element, j′ on the left half of the strip is

$$\rho^{r_2}_{zkj} = \frac{B_f}{G_s} I^{r_2}_{nkj} \sigma_j \qquad (4.24)$$

where $I^{r_1}_{nkj}$ and $I^{r_2}_{nkj}$ are dimensionless displacement coefficients for the influence of normal stresses on the elements j and j′ and are functions of the ratios, $L_r/B_f$, $U_o/B_f$, $\nu_s$ and the location of the respective elements.

Combining Eqs. 4.23 and 4.24 and summing up for stresses on all the elements along the strip, the displacement of point k, is written as

$$\rho_{zk} = \sum_{j=1}^{N} \frac{B_f}{G_s} \left( I^{r_1}_{nkj} + I^{r_2}_{nkj} \right) \sigma_j \qquad (4.25)$$

The vector of the vertical surface displacements is

$$\left\{ \rho_z \right\} = \frac{B_f}{G_s} \left[ I^r_n \right] \left\{ \sigma \right\} \qquad (4.26)$$

As mentioned in chapter 3, the vector, $\left\{ \rho_z \right\}$ is of size, $N_f$ and vector, $\left\{ \sigma \right\}$ of size N. The matrix $\left[ I^r_n \right]$ is of size $N_f \times N$.

Eq. 4.26 is rewritten as

$$\left\{ \rho_z \right\} = \frac{B_f}{G_s} \left\{ I_n \right\} q \qquad (4.27)$$

where $\left\{ I_n \right\}$ is a vector of the Settlement Reduction Coefficients, defined in chapter 3 as

$$SRC_k = I_{nk} = \frac{\rho_{zk}}{B_f} \frac{G_s}{q} \qquad (4.28)$$

The vector of the SRC for points on the surface is

$$\left\{ I_n \right\} = \frac{1}{B_f} \frac{G_s}{q} \left\{ \rho_z \right\} \qquad (4.29)$$

where $\left\{ I_n \right\}$ is obtained as

$$\left\{ I_n \right\} = \left[ I_n^r \right] \left\{ \sigma \right\} \qquad (4.30)$$

where matrix $\left[ I_n^r \right]$ and vector $\left\{ \sigma \right\}$ are known.

## 4.3 Two Strips at Depth, $U_o$

### 4.3.1 Problem Definition

Two strips of size, $2L_r \times 2B_r$ (Fig. 4.7), are placed symmetric about the x-axis at a depth, $U_o$, within the soil mass. Each strip is placed at a distance, $S_y$, from the x-axis. The problem definition is the same as in section 3.3.1 with the only difference being that the vertical displacements of the strips are considered.

The normal stresses mobilised along both the strips are equal due to the symmetry of placement of the strips. The vertical displacements of the nodes along the length of one strip are influenced by the stresses acting on the second strip, in addition to the influence of the stresses acting on the first strip itself.

### 4.3.2 Analysis

Eq. 4.3 is used to calculate the vertical displacements along the length of the strips due to surface loading with $r=\sqrt{x^2 + (S_y - y)^2}$. These displacements being identical for both strips, computations are made for one strip alone. The vector of the displacements of all N nodes is given by

$$\left\{ \rho_z^f \right\} = \frac{B_f}{E_s} \left\{ I^f \right\} q \qquad (4.31)$$

where vectors $\left\{ \rho_z^f \right\}$ and $\left\{ I^f \right\}$ are of size N. Elements of $\left\{ I^f \right\}$ in this case are dependent, in addition to the parameters, $U_o/B_f$, $L_f/B_f$, and $\nu_s$, on the ratio, $S_y/B_f$.

The vertical displacements of the nodes due to normal stresses acting on the strips are calculated using Eq. 4.6. The vertical displacements of node i, due to normal stresses, acting on elements j, and its image j′ (strip 1), j′′ and its image j′′′ (strip 2) (Fig. 4.8), are obtained as

$$\rho_{zij}^{r_1} = \frac{B_f}{E_s} I_{ij}^{r_1} \sigma_j \qquad (4.32)$$

$$\rho_{zij}^{r_2} = \frac{B_f}{E_s} I_{ij}^{r_2} \sigma_j \qquad (4.33)$$

$$\rho_{zij}^{r_3} = \frac{B_f}{E_s} I_{ij}^{r_3} \sigma_j \qquad (4.34)$$

and

$$\rho_{zij}^{r_4} = \frac{B_f}{E_s} I_{ij}^{r_4} \sigma_j \qquad (4.35)$$

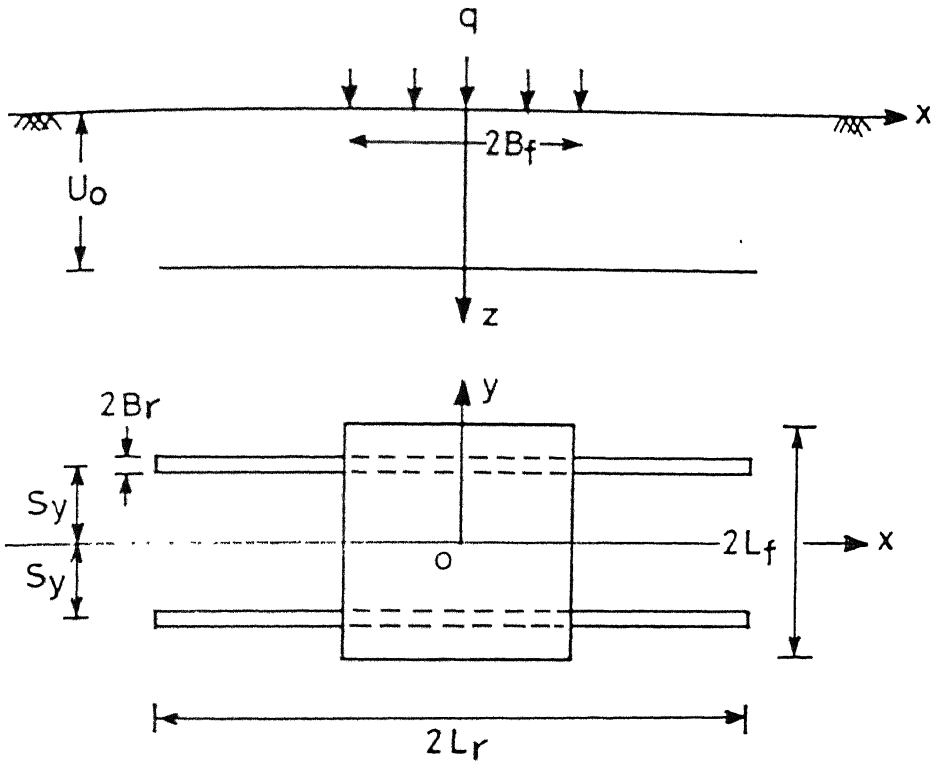


Fig. 4.7 Definition Sketch – Two Strips at Depth $U_o$

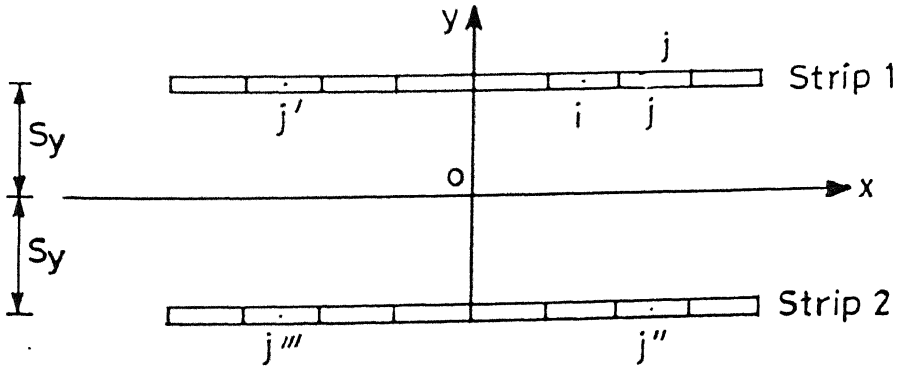


Fig. 4.8 Discretization of the Strips

where $I_{ij}^{r_1}$, $I_{ij}^{r_2}$, $I_{ij}^{r_3}$ and $I_{ij}^{r_4}$ are dimensionless coefficients for the influence of the normal stresses on elements j, j', j'' and j''' on the displacements of node i and are functions of the parameters $L_r/B_f$, $U_o/B_f$, $S_y/B_f$, $\nu_s$ and the locations of the node i and element j. The vector of the vertical displacements of the N nodes due to normal stresses on all the elements is

$$\left\{ \rho_z^r \right\} = \frac{B_f}{E_s} \left[ I^r \right] \left\{ \sigma \right\} \tag{4.36}$$

The vectors $\left\{ \rho_z^r \right\}$ and $\left\{ \sigma \right\}$ are of size N, and $\left[ I^r \right]$ is a square matrix of size N with $I_{ij}^r = I_{ij}^{r_1} + I_{ij}^{r_2} + I_{ij}^{r_3} + I_{ij}^{r_4}$

Satisfying the compatibility of displacements at the nodes as in Eq. 4.16 one obtains

$$\frac{B_f}{E_s} \left\{ I^f \right\} q - \frac{B_f}{E_s} \left[ I^r \right] \left\{ \sigma \right\} = \delta_o \left\{ 1 \right\} \tag{4.37}$$

The additional equation of force equilibrium as in Eq. 4.17 is

$$\sum_{i=1}^{N} \sigma_i \, dA = 0 \tag{4.38}$$

where the parameters have the same meaning as in Eqs. 4.16 and 4.17. On rearranging Eqs. 4.37 and 4.38, N+1 equations for N unknown stresses, and 1 unknown rigid body displacement, $\delta_o$, become available as

$$\left[ I^{r} \right] \left\{ \sigma/q \right\} + \frac{\delta_o E_s}{B_f q} = \left\{ I^{f} \right\} \tag{4.39}$$

$$\sum \sigma/q = 0 \tag{4.40}$$

Solution of these equations yields the N values of the normalised normal stresses, $\sigma/q$, and the normalised rigid body displacement, $\delta_o E_s/B_f q$.

Having calculated the normal stresses, the settlement reduction coefficients are computed based on the formulations discussed for a single strip. The vertical displacement of the points on the surface due to the normal stresses are calculated using Eq. 4.20 with $R = \sqrt{x^2 + S_y^2 + U_o^2}$. The vertical displacement of point k, on the surface due to normal stresses on the elements j, j′, j′′, j′′′ (Fig. 4.8) is

$$\rho_{zkj}^{r_1} = \frac{B_f}{G_s} I_{nkj}^{r_1} \sigma_j \tag{4.41}$$

$$\rho_{zkj}^{r_2} = \frac{B_f}{G_s} I_{nkj}^{r_2} \sigma_j \tag{4.42}$$

$$\rho_{zkj}^{r_3} = \frac{B_f}{G_s} I_{nkj}^{r_3} \sigma_j \tag{4.43}$$

and

$$\rho_{zkj}^{r_4} = \frac{B_f}{G_s} I_{nkj}^{r_4} \sigma_j \tag{4.44}$$

where $I_{nkj}^{r_1}$, $I_{nkj}^{r_2}$, $I_{nkj}^{r_3}$, and $I_{nkj}^{r_4}$ are displacement coefficients for the influence of the normal stresses on elements j, j′, j′′, and j′′′ respectively and are functions of the parameters, $L_r/B_f$,

$U_o/B_f$, $S_y/B_f$, $\nu_s$ and the location of the nodes.

Combining Eqs. 4.41 through 4.44, the vertical displacement, $\rho^r_{zk}$, of node k due to normal stresses on all N elements is

$$\rho^r_{zk} = \sum_{j=1}^{N} \frac{B_f}{G_s} \left( I^{r_1}_{nkj} + I^{r_2}_{nkj} + I^{r_3}_{nkj} + I^{r_4}_{nkj} \right) \sigma_j \qquad (4.45)$$

The vector of the vertical displacements of $N_f$ points along the surface is

$$\left\{ \rho_z \right\} = \frac{B_f}{G_s} \left[ I^r_n \right] \left\{ \sigma \right\} \qquad (4.46)$$

Eq. 4.46 gives the heave profile of the surface. The SRC are obtained on similar lines as in Eqs. 4.27 through 4.30.

## 4.4 Two Strips - One Below the Other

### 4.4.1 Problem Definition

As in chapter 3, two strips of size, $2L_r \times 2B_r$, placed beneath the centre of the loaded area along the x-axis, one at a depth, $U_o$, and the other at a depth, $U_1$, are considered (Fig. 4.9). The assumption regarding the applicability of Boussinesq's solution remains the same. The normal stresses mobilised along each strip are different since they are placed at different depths. In calculating the vertical displacements of the nodes along each strip due to mobilised normal stresses, the influences of both the strips on each other are to be considered.

### 4.4.2 Analysis

The analysis is similar to the one described for shear stresses in chapter 3. The vectors of vertical displacements at N nodes along strips 1 and 2 due to surface load, q, as calculated from Eq. 4.3 are

$$\left\{ \rho_{z1}^{f} \right\} = \frac{B_f}{E_s} \left\{ I_1^f \right\} q \tag{4.47}$$

and

$$\left\{ \rho_{z2}^{f} \right\} = \frac{B_f}{E_s} \left\{ I_2^f \right\} q \tag{4.48}$$

where and $\left\{ I_1^f \right\}$ and $\left\{ I_2^f \right\}$ are vectors of size N and depend on the parameters $L_f/B_f$, $\nu_s$ and the location of the nodes. $\left\{ I_1^f \right\}$ and $\left\{ I_2^f \right\}$ are also functions of $U_o/B_f$ and $U_1/B_f$, respectively.

The vertical displacements of the nodes along each strip due to normal stresses on them are computed using Eq. 4.6. The vertical displacements of node i due normal stresses on element j along each strip are calculated on the same lines as in section 3.4.2. The vector of the displacements at N nodes along strips 1 and 2 due to the normal stresses along each strip are

$$\left\{ \rho_z^{r_{11}} \right\} = \frac{B_f}{E_s} \left[ I^{r_{11}} \right] \left\{ \sigma^1 \right\} \tag{4.49}$$

$$\left\{ \rho_z^{r_{12}} \right\} = \frac{B_f}{E_s} \left[ I^{r_{12}} \right] \left\{ \sigma^2 \right\} \tag{4.50}$$

$$\left\{ \rho_z^{r_{21}} \right\} = \frac{B_f}{E_s} \left[ I^{r_{21}} \right] \left\{ \sigma^1 \right\} \tag{4.51}$$

and

$$\left\{ \rho_z^{r_{22}} \right\} = \frac{B_f}{E_s} \left[ I^{r_{22}} \right] \left\{ \sigma^2 \right\} \tag{4.52}$$

where $\left\{ \rho_z^{r_{11}} \right\}$ and $\left\{ \rho_z^{r_{12}} \right\}$, and $\left\{ \rho_z^{r_{21}} \right\}$ and $\left\{ \rho_z^{r_{22}} \right\}$ are displacement vectors for strips 1 and 2 due to stresses on strips 1 and 2 respectively. $\left[ I^{r_{11}} \right]$, $\left[ I^{r_{12}} \right]$, $\left[ I^{r_{21}} \right]$ and $\left[ I^{r_{22}} \right]$ are matrices for the influence of the stresses, $\left\{ \sigma^1 \right\}$ and $\left\{ \sigma^2 \right\}$ on the displacements of nodes along strips 1 and 2, $\left\{ \sigma^1 \right\}$ and $\left\{ \sigma^2 \right\}$ being the normal stress vectors along strips 1 and 2 respectively. All the vectors mentioned in Eqs. 4.49 through 4.52 are of size N and the matrices are square matrices of size N.

Combining Eqs. 4.49 through 4.52, the vector of vertical displacements of N nodes along strip 1 and N nodes along strip 2 is

$$\left\{ \rho_z^r \right\} = \frac{B_f}{E_s} \left[ I^r \right] \left\{ \sigma \right\} \tag{4.53}$$

where $\left\{ \rho_z^r \right\}$ and $\left\{ \sigma \right\}$ are vectors of size 2N, and $\left[ I^r \right]$ is a square matrix of size 2N. $\left\{ \rho_z^r \right\}$ consists of vectors $\left\{ \rho_z^{r_1} \right\} = \left\{ \left\{ \rho_z^{r_{11}} \right\} + \left\{ \rho_z^{r_{12}} \right\} \right\}$ and $\left\{ \rho_z^{r_2} \right\} = \left\{ \left\{ \rho_z^{r_{21}} \right\} + \left\{ \rho_z^{r_{22}} \right\} \right\}$ and $\left\{ \sigma \right\}$ consists of the vectors $\left\{ \sigma^1 \right\}$ and $\left\{ \sigma^2 \right\}$. The matrix $\left[ I^r \right]$ comprises of the matrices $\left[ I^{r_{11}} \right]$, $\left[ I^{r_{12}} \right]$, $\left[ I^{r_{21}} \right]$ and $\left[ I^{r_{22}} \right]$ expressed in the same fashion as in Eq. 3.68.

Combining Eqs. 4.47 and 4.48 the vector of vertical displacements of the nodes along strips 1 and 2 due to the surface load, q, is given by

$$\left\{ \rho_z^f \right\} = \frac{B_f}{E_s} \left\{ I^f \right\} q \qquad (4.54)$$

where $\left\{ \rho_z^f \right\}$ and $\left\{ I^f \right\}$ are vectors of size 2N. $\left\{ \rho_z^f \right\}$ comprises of vectors $\left\{ \rho_{z1}^f \right\}$ and $\left\{ \rho_{z2}^f \right\}$, and $\left\{ I^f \right\}$ comprises of vectors $\left\{ I_1^f \right\}$ and $\left\{ I_2^f \right\}$.

Satisfying the compatibility of displacements at all the 2N nodes, one obtains

$$\left\{ \rho_z^f \right\} - \left\{ \rho_z^r \right\} = \left\{ \delta_o \right\} \qquad (4.55)$$

where $\left\{ \delta_o \right\}$ is a vector of size 2N consisting of vectors, $\delta_{o1}\left\{ 1 \right\}$ for strip 1 and $\delta_{o2}\left\{ 1 \right\}$ for strip 2 each of size, N. Substituting Eqs. 4.53 and 4.54 in Eq. 4.55, one obtains

$$\left[ I^r \right] \left\{ \sigma/q \right\} + \left\{ \frac{\delta_o E_s}{B_f q} \right\} = \left\{ I^f \right\} \qquad (4.56)$$

Eq. 4.56 gives 2N equations in 2N unknowns for the normalised normal stresses, $\left\{ \sigma/q \right\}$, and 2 unknowns for the normalised rigid body displacements, $\delta_{o1}E_s/B_f q$ and $\delta_{o2}E_s/B_f q$. Hence the two equilibrium equations to be satisfied are

$$\sum \sigma_1/q = 0 \qquad (4.57)$$

$$\sum \sigma_2/q = 0 \qquad (4.58)$$

The solution of Eqs. 4.56 through 4.58 gives 2N values of normal stresses along strips 1 and 2 and the rigid body displacements of strips 1 and 2.

The SRC due to these stresses are computed on similar lines as explained in earlier sections.

## 4.5 Multiple Strips

The problem is similar to the one considered in chapter 3. Two pairs of strips are considered, symmetrically placed below the loaded area at a depth, $U_o$. The first pair is contiguously placed ($S_{y1}/B_f = B_r/B_f$) while each strip of the second is placed at a distance, $S_{y2}/B_f$, from the x-axis (Fig. 4.10).

### 4.5.1 Analysis

The analysis, again is similar to the one for shear stresses as explained in chapter 3. Only one strip of each pair is considered, due to symmetry. The vector of vertical displacements of all the 2N nodes along both the pairs obtained from the Boussinesq's solution for vertical displacements given by Eq. 4.1 is

$$\left\{ \rho_z^f \right\} = \frac{B_f}{E_s} \left\{ I^f \right\} q \qquad (4.59)$$

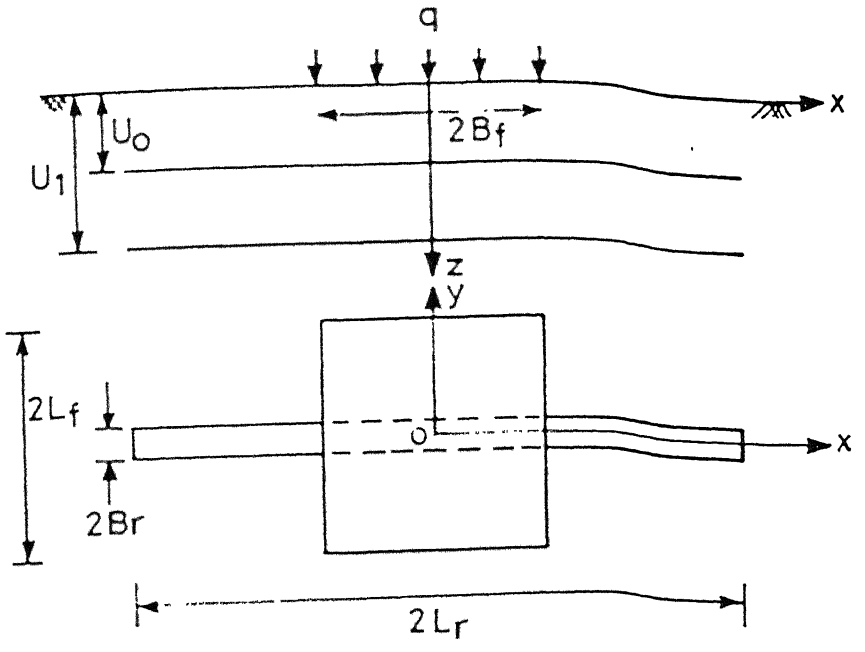


Fig. 4.9 Definition Sketch – Two Strips One Below the Other

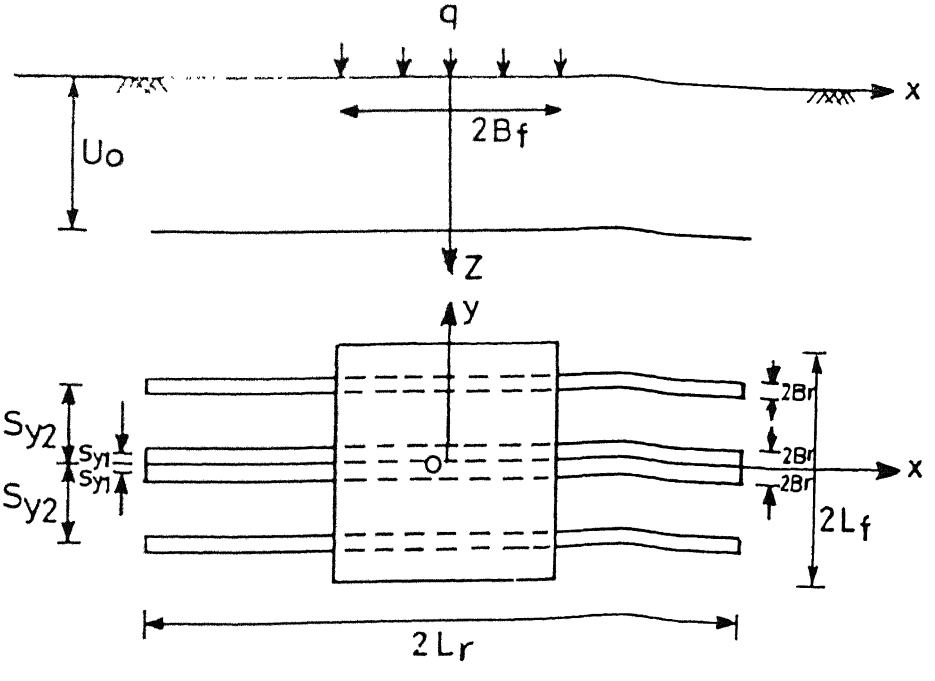


Fig. 4.10 Definition Sketch – Multiple Strips

where the vectors $\left\{ \rho_z^f \right\}$ and $\left\{ I^f \right\}$ are of size 2N.

The vector of vertical displacements of all the 2N nodes due to normal stresses acting on both pairs is obtained on similar lines as explained in chapter 3. For this purpose Mindlin's equation for vertical displacements given by Eq. 4.6 is used. In computing the vertical displacements due to normal stresses the influence of the stresses on all elements including the image elements along both the pairs of strips are to be considered. The vector of the vertical displacements of the 2N nodes due to normal stresses, $\left\{ \sigma_1 \right\}$, along the first pair and $\left\{ \sigma_2 \right\}$ along the second pair of strips is

$$\left\{ \rho_z^r \right\} = \frac{B_f}{E_s} \left[ I^r \right] \left\{ \sigma \right\} \qquad (4.60)$$

where

$$\left[ I_r \right] = \left[ \begin{array}{c|c} I^{r_{11}} & I^{r_{12}} \\ \hline I^{r_{21}} & I^{r_{22}} \end{array} \right]$$

$\left[ I^{r_{11}} \right]$ and $\left[ I^{r_{12}} \right]$ are matrices of the influences of the normal stresses, $\left\{ \sigma_1 \right\}$ and $\left\{ \sigma_2 \right\}$, along both pairs of strips on the displacement of the N nodes along the first pair of strips. $\left[ I^{r_{21}} \right]$ and $\left[ I^{r_{22}} \right]$ are matrices of the influence of the normal stresses along both the pairs of strips on the displacement of the N nodes along the second pair of strips. The vector $\left\{ \sigma \right\}$ comprises of the vectors $\left\{ \sigma_1 \right\}$ and $\left\{ \sigma_2 \right\}$.

Compatibility of displacements at the 2N nodes is satisfied as in Eq. 4.55 as

$$\left\{ \rho_z^f \right\} - \left\{ \rho_z^r \right\} = \left\{ \delta_o \right\} \tag{4.61}$$

where $\left\{ \delta_o \right\}$ is a vector of size 2N consisting of vectors, $\delta_{o1}\left\{ 1 \right\}$ for the first pair of strips and $\delta_{o2}\left\{ 1 \right\}$ for the second pair of strips. Substituting Eqs. 4.59 and 4.60 in Eq. 4.61, Eq. 4.61 is rewritten as

$$\left[ I^r \right] \left\{ \sigma/q \right\} + \left\{ \frac{\delta_o E_s}{B_f q} \right\} = \left\{ I^f \right\} \tag{4.62}$$

Eq. 4.62 gives 2N equations in 2N unknowns for the normalised normal stresses $\left\{ \sigma/q \right\}$ and 2 unknowns for the normalised rigid body displacements, $\delta_{o1}E_s/B_f q$ and $\delta_{o2}E_s/B_f q$. Hence the two equilibrium equations to be satisfied are

$$\sum \sigma_1/q = 0 \tag{4.63}$$

$$\sum \sigma_2/q = 0 \tag{4.64}$$

The solution of Eqs. 4.62 through 4.64 gives 2N values of normal stresses along pairs 1 and 2 and the rigid body displacements of pairs 1 and 2.

The SRC due to these stresses are computed on similar lines as explained in earlier sections.

## 4.6 Results and Discussion

The analysis aims to evaluate the normal stresses developed at the soil-strip interface, and estimate the settlement reduction of the surface thereof. As indicated in the analysis, integrations of the basic solutions given by Boussinesq and Mindlin are carried out numerically.

For the purpose of integration, the descretizations of the loaded area and of the reinforcing strip are the same as those for the case where shear stresses alone were considered (chapter 3). That is, the loaded area is divided into subelements of size, $0.025B_f \times 0.025B_f$, and the size of elements along the strip is $0.1B_f \times 0.1B_f$ for centrally placed strips and $0.1B_f \times 0.05B_f$ for strips placed off the centre. The influence coefficient, $I^r_{ij}$, for the vertical displacement of node i, due to normal stress on element j, is evaluated by dividing the element j into 20x20 subareas for $|i-j| \leq 2$. Coarser subdivision of 4x4 was found to be adequate for cases $|i-j| > 2$. The half-width of the strips, $B_r$, is maintained at $0.05B_f$ for centrally placed strips and $0.025B_f$ for those placed off the centre.

A parametric study brings out the effects of the depth, length and distance of the reinforcement from the x-axis, the aspect ratio of the loaded area, and Poisson's ratio of the soil on the mobilised normal stresses and the settlement reduction coefficients along the surface. The ranges of the parameters considered are the same as in chapter 3. They are

1) $L_f/B_f$ : 1 to 10 (aspect ratio of loaded area)

2) $L_r/B_f$ : 1 to 5 (length of reinforcement)

3) $U_o/B_f$ : 0.1 to 2 (depth of reinforcement)

4) $S_y/B_f$ : 0.025 to 2 (distance of reinforcement from x-axis)

5) $\nu_s$ : 0.1 to 0.5 (Poisson's Ratio of the soil)

6) $B_r/B_f$ : 0.025 for $S_y/B_f > 0$ (width of reinforcement)

: 0.05 for $S_y/B_f = 0$

Except for cases where the effect of Poisson's ratio, $\nu_s$, is studied or unless mentioned all results are for $\nu_s = 0.3$.

### 4.6.1 Normal Stresses - Single Strip

Initially, the effect of the parameters mentioned, on the mobilised normal stresses are studied. The variations of the SRC are discussed in the next section.

Fig. 4.11 presents the variation of the normalised normal stress, $\sigma/q$, with the distance, $x/B_f$, along the half-length of the strip for various depths, $U_o/B_f$, below a square area ($L_f/B_f=1$), and strip length of $L_r/B_f=2$. A positive stress is one that acts upwards. It is seen from the figure that at a distance, $x/B_f$, in the range 1 to 1.15 the stresses change sign. Further, the negative stresses at the edge of the strip increase rapidly, tending to infinity. This is due to the edge effect. Also, as expected the stresses at the centre of the strip are maximum.

It is interesting to note that for the depths studied, the stresses are maximum for a strip at depth, $U_o/B_f=0.25$. As the depth of the strip increases, the stresses decrease, the magnitude

of stresses being small at great depths ($U_o/B_f$=2). At very shallow depths of placement of strip ($U_o/B_f$<0.25), i.e. very close to the loaded area the vertical displacements due to the surface load are high. At this depth, the interference effect of the normal stresses on the displacements of points along the strip are also high. Hence, the stresses required to be mobilised so that the strip displaces uniformly is small. With increase in depth of placement of strip, $U_o/B_f$, upto 0.25, the interference effect decreases although the displacements due to the surface load are high. The stresses mobilised, therefore are higher. With further increase in $U_o/B_f$, the displacements decrease and hence stresses are small and tend to be uniform. The normalised normal stresses, $\sigma/q$, at the centre for strips at depth, $U_o/B_f$=0.25 and 2 are 4.25 and 1.3 respectively.

The effect of the length of the strip, $L_r/B_f$, on the normalised normal stresses, $\sigma/q$, for strips placed below a square area with $L_f/B_f$=1, and at a depth, $U_o/B_f$=1, is presented in Fig. 4.12. It is observed that for all lengths of the strip, the stresses decrease with the distance along the strip, $x/B_f$, and become negative beyond a certain distance. This negative stress increases with $x/B_f$ and increases very rapidly at the edge. For strips with $L_r/B_f \leq 3$, positive stresses are developed over a distance of 0.6 times the half length, $L_r$. For longer strips ($L_r/B_f$>3), stresses are negative over predominant lengths of the strips. The normalised stress at the centre of the strip, ($x/B_f$=0) for $L_r/B_f$=1 and 5 are 1.3 and 5.5 respectively. In the case of shorter strips the difference between the vertical

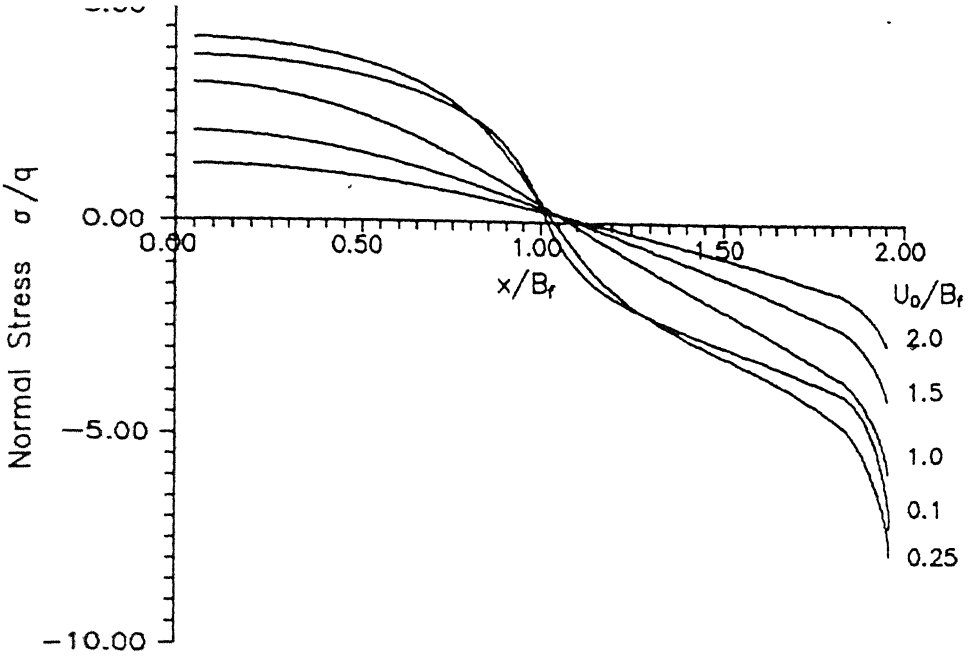


Fig. 4.11 Variation of Normal Stress with Distance for Different Depths of Placement of Strip ($L_r/B_f=2$, $L_f/B_f=1$, $\nu_s=0.3$)

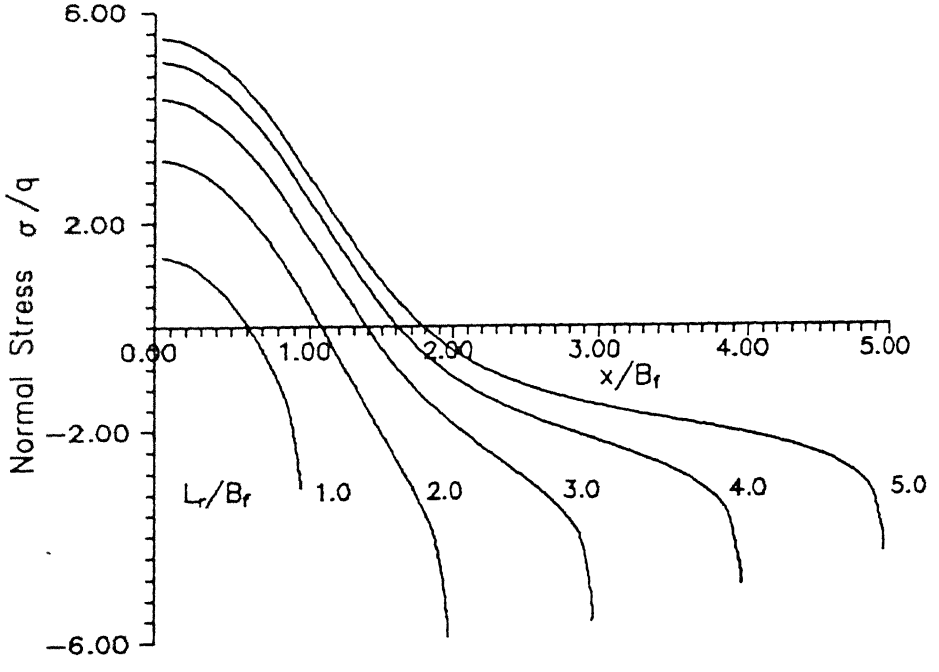


Fig. 4.12 Variation of Normal Stress with Distance for Different Lengths of Strip ($U_o/B_f=1$, $L_f/B_f=1$, $\nu_s=0.3$)

displacements of the points at the centre and the edge of the strip due to surface load is small. As a result, stresses of lesser magnitude are sufficient to force the strip to undergo a uniform rigid body displacement. On the other hand, the gradient between the vertical displacement due to surface load at the centre and edge of longer strips is high. Consequently, higher stresses are required to make the strip displace uniformly throughout its length. The stresses change sign at a distance approximately equal to 0.45 to 0.55 times the half length, $L_r$, of the strip.

The aspect ratio of the loaded area, $L_f/B_f$, appears to have a considerable influence on the mobilised stresses, $\sigma/q$ (Fig. 4.13). The figure depicts the variation of $\sigma/q$, with the distance along the strip, $x/B_f$, for various aspect ratios, $L_f/B_f$, and for strips of length, $L_r/B_f=2$, placed at a depth, $U_o/B_f=1$. For all $L_f/B_f$ values, the variation of stresses is similar. The stresses change sign at a distance, $x/B_f$, of 1.1. Longer rectangles with $L_f/B_f=10$ generate maximum stresses at the soil-reinformcement interface, the stress, $\sigma$, near the centre being 5q. The increase in stresses from square ($L_f/B_f=1$) to rectangular areas with $L_f/B_f=2$ is significant. With further increase in the aspect ratio of the loaded area ($L_f/B_f$) the increase in the interaction stresses is small. The reason for this is that as the aspect ratio increases, the loading at points farther away from the x-axis have an insignificant effect on the displacement of points along the strip.

The plot of the normalised normal stress, $\sigma/q$, with $x/B_f$ is shown in Fig. 4.14, for different values of Poisson's ratio, $\nu_s$, and for a strip of length, $L_r/B_f=2$, placed below a square area ($L_f/B_f=1$) at a depth, $U_o/B_f=1$. It is clear from the plot that Poisson's ratio does not affect the stresses mobilised along the strip appreciably. For $\nu_s=0.5$, the stresses are marginally higher than the stresses for other values of $\nu_s$. The maximum $\sigma/q$, observed at the centre is 3.4q for $\nu_s=0.5$.

From these plots of the normal stress variations it is evident that strips placed at a depth, $U_o/B_f$, of 0.25 develop maximum stresses and stresses are higher for rectangles with larger aspect ratios. The stresses are not sensitive to the value of the Poisson's ratio.

The normal stresses developed at the interface are responsible for the settlement reduction of the surface. In the next section the effect of various parameters defined earlier on the settlement reduction of the surface will be discussed.

### 4.6.2 Settlement Reduction - Single Strip

Before studying the reduction of settlements at the surface due to the normal stresses, it would be worthwhile to examine the basic solution given by Mindlin for vertical displacements due to a verical force at depth. The vertical displacement of point, B(x,0,0) (Fig. 4.5), due to a vertical force, Q, at a depth, c, is given by Eq. 4.20. Non-dimensionalising all length parameters with c, Eq. 4.20 is written as

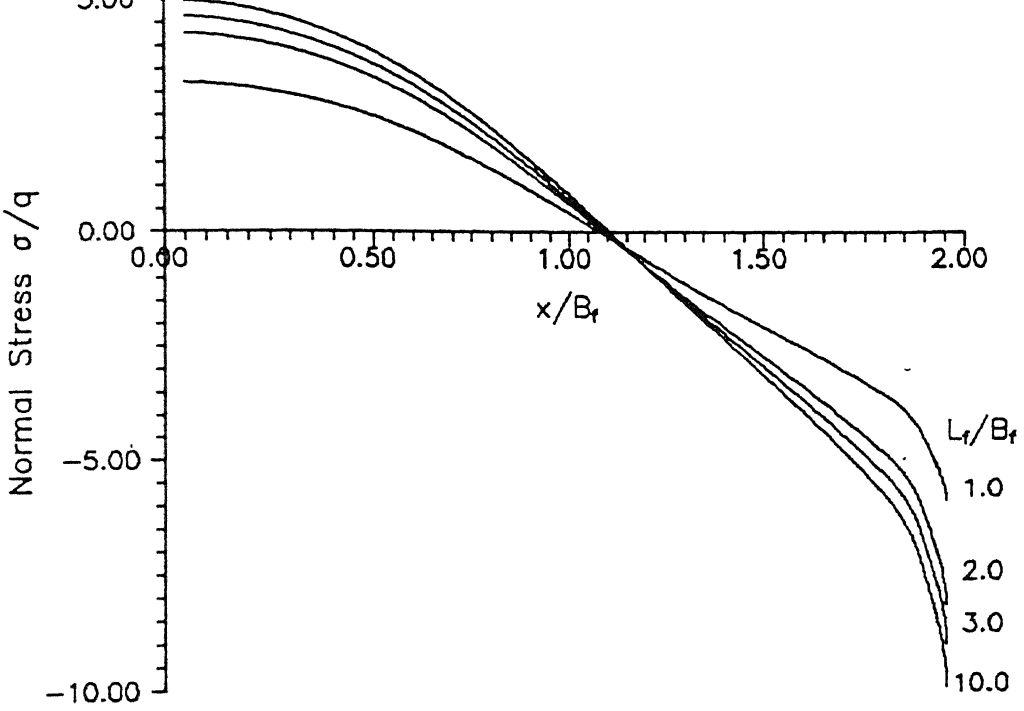


Fig. 4.13 Variation of Normal Stress with Distance for Different Aspect Ratios of Loaded Area ($L_f/B_f=2$, $U_0/B_f=1$, $\nu_s=0.3$)

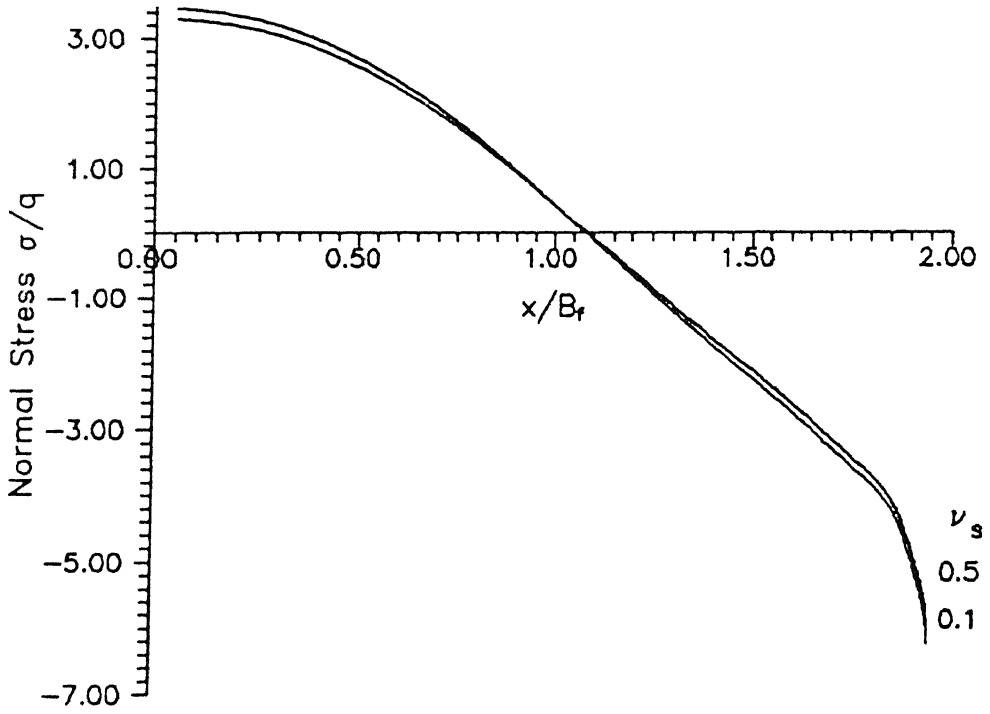


Fig. 4.14 Variation of Normal Stress with Distance for Different Poisson's Ratios of Soil ($L_f/B_f=2$, $L_f/B_f=1$, $U_0/B_f=1$)

$$\rho_z = \frac{Qc}{G_s} I_z \qquad (4.65)$$

where $G_s=E_s/2(1+\nu_s)$ and $I_z$ is an influence coefficient dependent on the normalised distance, x/c and Poisson's ratio, $\nu_s$.

The variation of $I_z$ with the normalised distance, x/c, for different values of Poisson's ratio, $\nu_s$ is presented in Fig. 4.15. For all $\nu_s$ values it is observed that $I_z$ is maximum for x/c=0 and it decreases rapidly with increase in the distance, x/c. $I_z$ values are positive for all values of $\nu_s$ indicating surface heave throughout. $I_z$ values asymtotically approach zero at large x/c values. This figure shows that the points on the surface just above the point force experience the maximum vertical displacement in the direction of the force and the points further away from the force displace by smaller amounts. It is apparent that $\nu_s$=0.1 shows the maximum $I_z$ values, and $\nu_s$=0.5 the least. This difference arises since the parameter, $G_s$, has been used in Eq. 4.65. If the modulus, $E_s$, is substituted for $G_s$ in Eq. 4.65, $I_z$ values will be less affected by $\nu_s$ values. It is also perceived that beyond a distance, x/c, of about 3, the $I_z$ values are very small as compared to the maximum value at x/c=0. This indicates that the zone of influence for the force at a depth, c in producing heave at the surface is of the order of 3c. The values of $I_z$ at x/c=0 for $\nu_s$=0.1 and 0.5, are 0.223 and 0.158 respectively. At a distance of x/c=3, the corresponding values of $I_z$ are 0.05 and 0.03 respectively.

The effect of length of the strip, $L_r/B_f$, placed below a

square area ($L_f/B_f$=1) at depth, $U_o/B_f$=1, on the SRC is presented in Fig. 4.16. The SRC values are maximum at the centre of the loaded area ($x_f/B_f$=0) and gradually decrease with increase in the distance, $x_f/B_f$, for all lengths of the strip. The edge of the loaded area shows minimum settlement reduction. It is also noted that SRC values increase with increasing lengths of the strip. The SRC at the centre for $L_r/B_f$=1 is 0.007 and for $L_r/B_f$=5 is 0.13. Strips with $L_r/B_f$=1 show a small negative SRC at the edge indicating settlement of the surface. The increase in SRC with $L_r/B_f$ is due to the fact that the stresses for longer strips are higher than for shorter ones as seen from Fig. 4.12. Further from Fig. 4.15 it is clear that points on the surface within the distance, x/c of 2 show significant heave. Beyond this distance, the $I_z$ values are comparatively small. Hence it follows that high positive stresses within a distance, $x/B_f$=1, cause high settlement reduction of the surface and this is true for longer strips (Fig. 4.12). The decrease in SRC with increase in $x_f/B_f$ is obvious because the stresses are a maximum at the centre of the strip i.e. at $x/B_f$=0 and decrease with $x/B_f$. Shorter strips ($L_r/B_f$=1) show negative SRC at the edge because the stresses beyond a distance, $x/B_f$=0.5 are negative which cause the edge of the loaded area, $x_f/B_f$=1, to settle.

Fig. 4.17 shows the variation of SRC with the distance, $x_f/B_f$, along the surface for various depths of placement of reinforcement, $U_o/B_f$, and for a length, $L_r/B_f$=2, placed below a rectangular area with aspect ratio, $L_f/B_f$=2. All the curves start off from a maximum value at $x_f/B_f$=0 and SRC decreases with

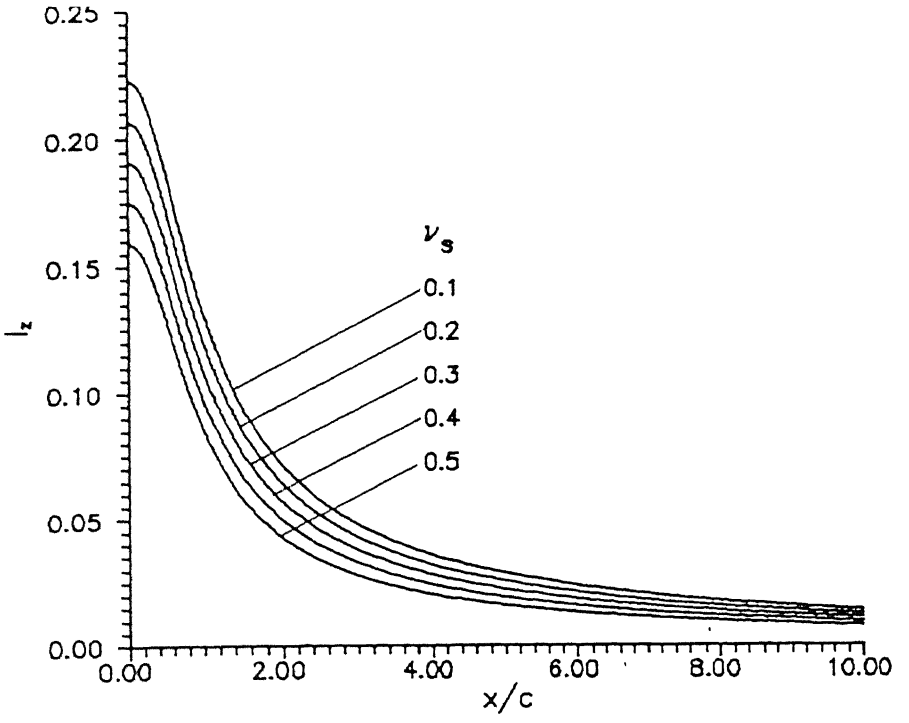


Fig. 4.15 Influence Coefficients for Vertical Surface Displacements due to Vertical Force at Depth (Mindlin Solution)

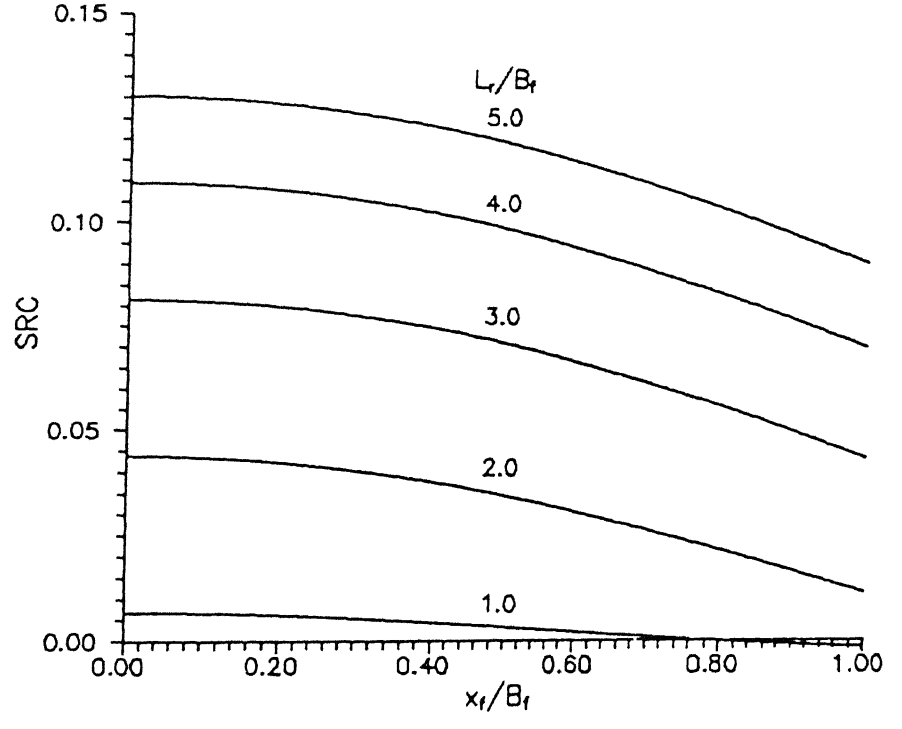


Fig. 4.16 Variation of SRC with Distance along Surface for Different Lengths of Strip ($U_o/B_f$=1, $L_f/B_f$=1, $\nu_s$=0.3)

distance from the centre. The rate of change of SRC with $x_f/B_f$ is maximum for shallow depths and it decreases with increase in $U_o/B_f$. At large depths ($U_o/B_f \geq 1.5$) the SRC curve is almost parallel to the $x_f/B_f$ axis indicating uniform heave of the surface. SRC values decrease with increase in the depth of placement of the strip. It is interesting to note that although normal stresses, $\sigma/q$, for a strip at depth, $U_o/B_f=0.25$, are marginally higher than those for $U_o/B_f=0.1$ (Fig. 4.11), the SRC values for the latter are higher. This is because the latter is closer to the surface and the stresses have a greater influence on the settlement reduction of the points on the surface. As the depth of placement of the strip increases, the influence of the mobilised stresses in reducing surface settlements decrease rapidly.

The variations in SRC for different aspect ratios, $L_f/B_f$, of the loaded area are presented in Figs. 4.18 and 4.19. The variation of SRC with the distance, $x_f/B_f$, along the surface for strips of length, $L_r/B_f=2$, placed at a depth, $U_o/B_f=1$, is depicted in Fig. 4.18. The maximum settlement reduction is for long rectangular areas ($L_f/B_f=10$) while square areas exhibit the least SRC values. It is noted that the increase in SRC is significant for an increase in the aspect ratio ($L_f/B_f$) from 1 to 2. With further increase in $L_f/B_f$ values upto 10, the increase in SRC is not as significant. The SRC at the centre of the loaded area with an aspect ratio, $L_f/B_f=10$, is about 0.07 while for a square area it is 0.044. At the edge, i.e., at $x_f/B_f=1$ the values of SRC are small and the variation with $L_f/B_f$ relatively less significant.

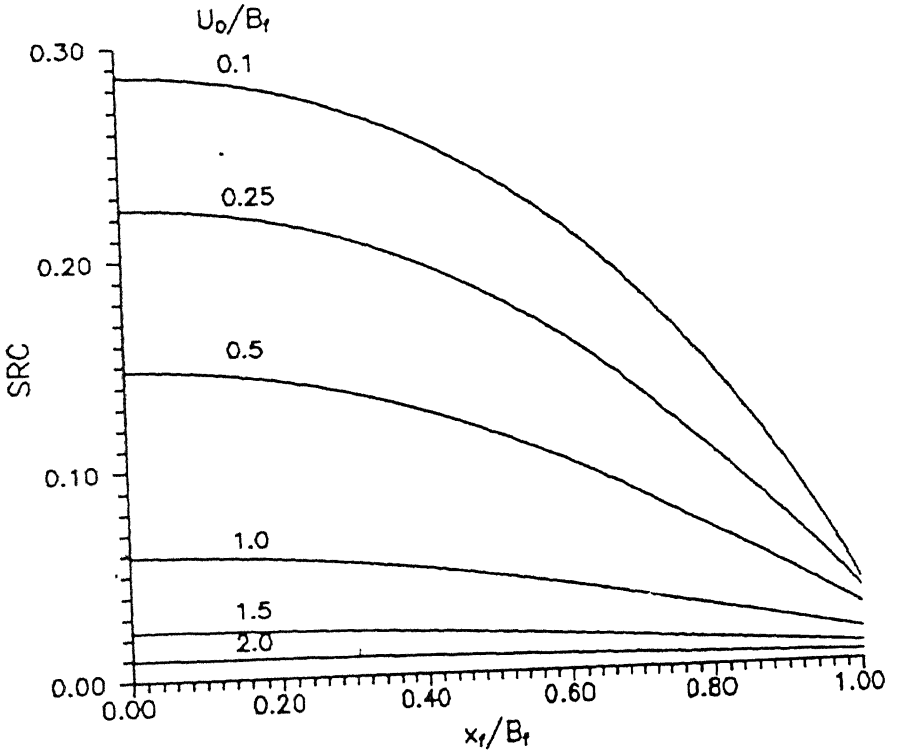


Fig. 4.17 Variation of SRC with Distance along Surface for Different Depths of Placement of Strip ($L_r/B_f=2$, $L_f/B_f=1$, $\nu_s=0.3$)

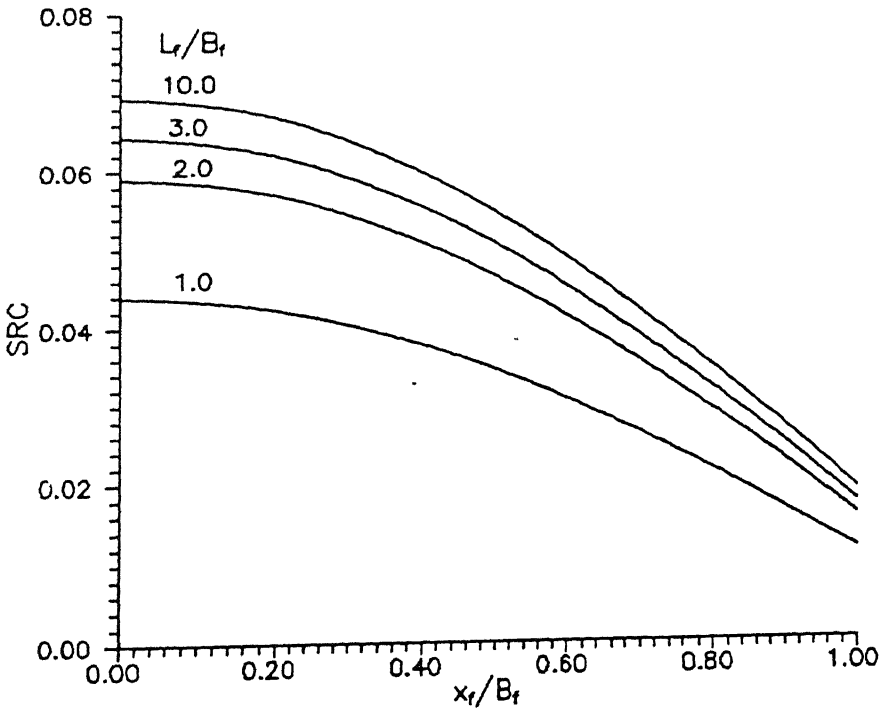


Fig. 4.18 Variation of SRC with Distance along Surface for Different Aspect Ratios of Loaded Area ($L_r/B_f=2$, $U_o/B_f=1$, $\nu_s=0.3$)

In Fig. 4.19 the variation of SRC with distance, $x_f/B_f$, for strips at depth, $U_o/B_f=2$, is depicted. The trends in this plot are similar to those observed in Fig. 4.18. The SRC values are much smaller than the corresponding values of SRC for strips at depth, $U_o/B_f=1$, as seen in the previous figure. It is seen that the increase in SRC for $L_f/B_f$ increasing from 2 to 10 is as significant as its increase from $L_f/B_f=1$ to 2. The SRC values at the centre, i.e. $x_f/B_f=0$, for square, and rectangular areas with $L_f/B_f=2$ and $L_f/B_f=10$, are 0.006, 0.0096 and 0.013 respectively.

From Figs. 4.18 and 4.19 it is evident that for all depths, long rectangular areas ($L_f/B_f=10$) show maximum SRC values. With the decrease in the aspect ratio of the loaded area the SRC values decrease, with square areas exhibiting the least SRC values.

Thus far the variation of SRC along the surface due to the effect of the various parameters was studied. It is observed from the figures that the centre of the loaded area experiences maximum settlement reduction. It would also be of practical interest to consider the settlement reduction at the centre of the loaded area. The effect of the various parameters on the SRC at the centre, defined as $I_{sc}$, is presented in the succeeding graphs.

Fig. 4.20 plots $I_{sc}$ values with the depth ratio of the strip, $U_o/B_f$, for various values of the aspect ratio, $L_f/B_f$, of the loaded area and for a strip of length, $L_r/B_f=2$. $I_{sc}$ values decrease with increase in the depth of reinforcement, $U_o/B_f$, for all $L_f/B_f$ values. They increase with the aspect ratio, $L_f/B_f$, of

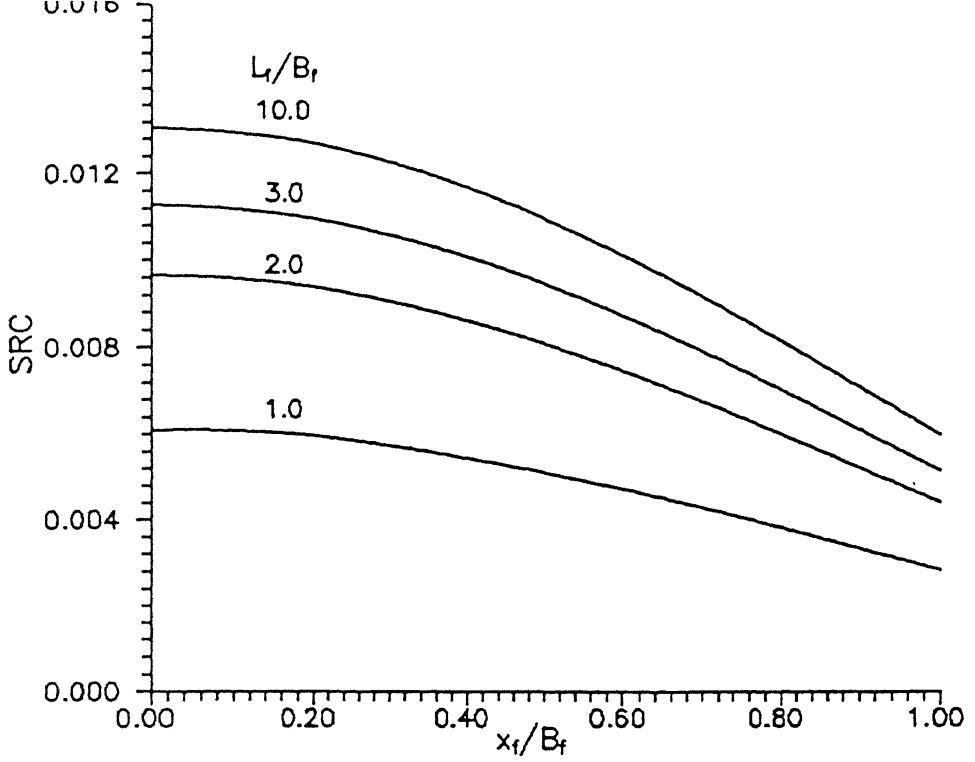


Fig. 4.19 Variation of SRC with Distance along Surface for Different Aspect Ratios of Loaded Area ($L_f/B_f$=2, $U_0/B_f$=2, $\nu_s$=0.3)

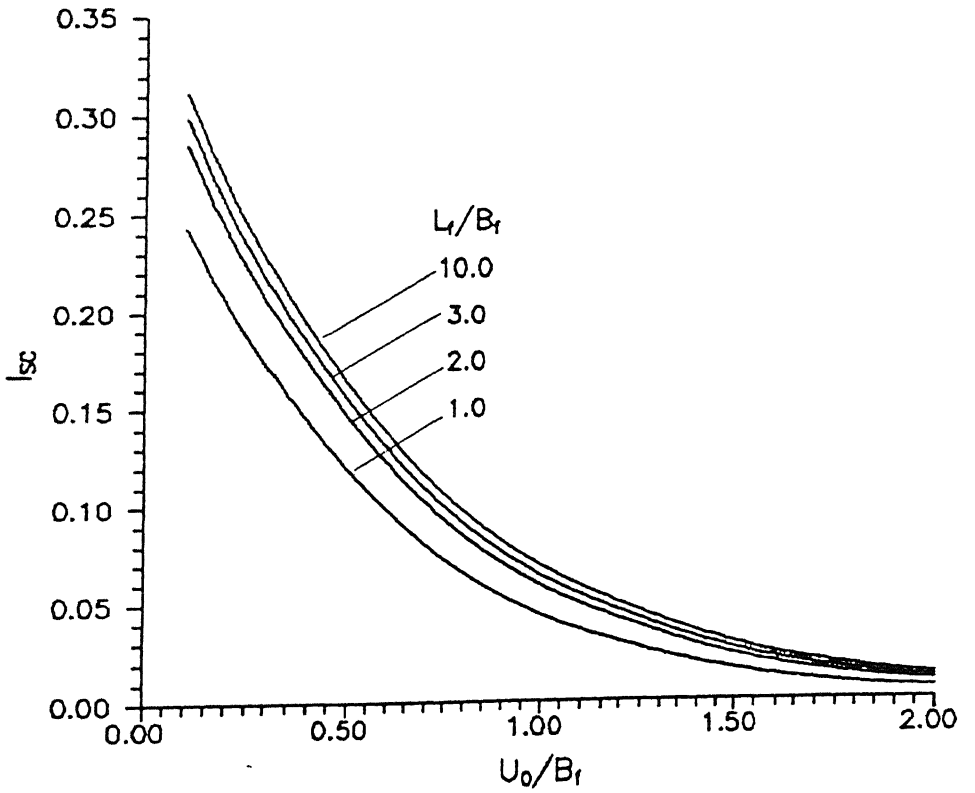


Fig. 4.20 Effect of Depth of Placement on $I_{sc}$ for Different Aspect Ratios of Loaded Area ($L_f/B_f$=2, $\nu_s$=0.3)

the loaded area, with long rectangular areas ($L_f/B_f$=10) exhibiting highest $I_{sc}$ values. The increase in $I_{sc}$ for areas with $L_f/B_f$ increasing from 2 to 10 is not as significant as the increase for areas with $L_f/B_f$ increasing from 1 to 2. At depths, $U_o/B_f \geq 1.5$, the value of $I_{sc}$ are negligible. The reason for the rapid decrease in the values of $I_{sc}$ with the depth of reinforcement is that the magnitude of stresses decreases with depth. In addition to this, with increasing depths, the stresses mobilised have a decreasing influence on the displacements of points along the surface. At a depth, $U_o/B_f$=0.1, the $I_{sc}$ values for aspect ratios, $L_f/B_f$=1 and 10 are 0.245 and 0.31 respectively. At a depth of placement, $U_o=B_f$, the difference in $I_{sc}$ values for $L_f/B_f$=1 and 10 is much smaller, the corresponding values of $I_{sc}$ being 0.04 and 0.07. This plot implies that rigid strips placed at shallow depths are advantageous in reducing settlements. Also, strips placed below longer rectangles give better results.

The effect of the aspect ratio, $L_f/B_f$, of the loaded area on $I_{sc}$ for different lengths of the strip, $L_r/B_f$, is depicted in Figs. 4.21 and 4.22. Fig. 4.21 shows the plot for the depth, $U_o/B_f$=1. $I_{sc}$ values increase with the length of the strip, and the aspect ratio of the loaded area. For shorter strips ($L_r/B_f$=1) the $I_{sc}$ values are very small and the aspect ratio, $L_f/B_f$, has a minimal effect on these values. For longer strips, e.g. $L_r/B_f$=5, the aspect ratio, $L_f/B_f$, affects the $I_{sc}$ values considerably. The $I_{sc}$ values for this length of the strip ($L_r/B_f$=5) are 0.12 and 0.25 for aspect ratios, $L_f/B_f$=1 and 10 respectively.

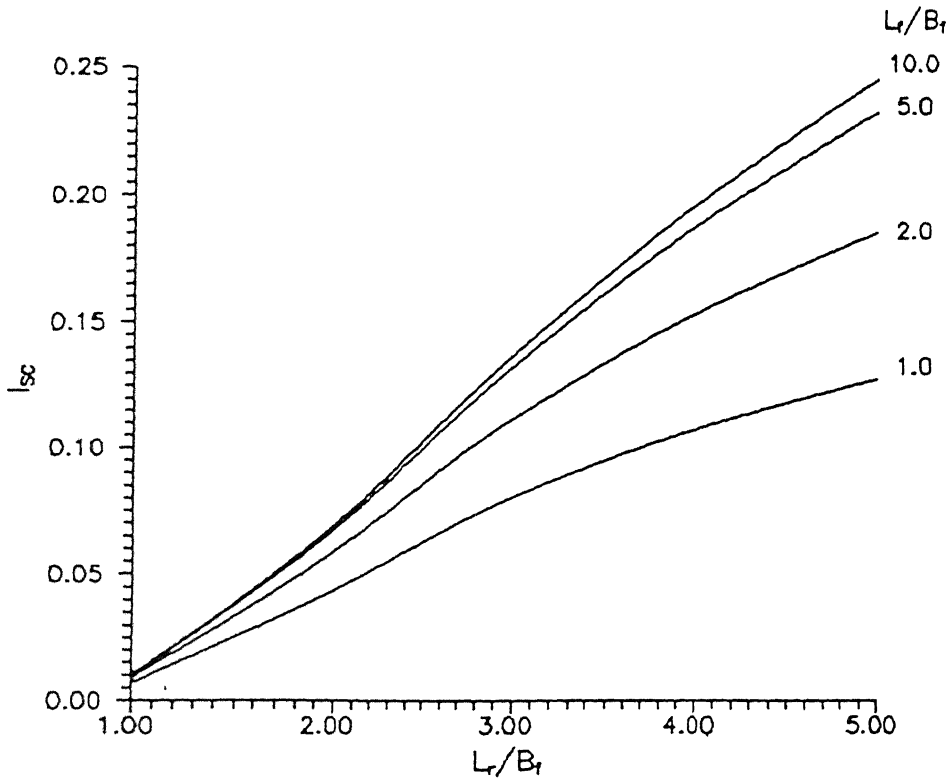


Fig. 4.21 Effect of Length of Strip on $I_{sc}$ for Different Aspect Ratios of Loaded Area ($U_o/B_f=1$, $\nu_s=0.3$)

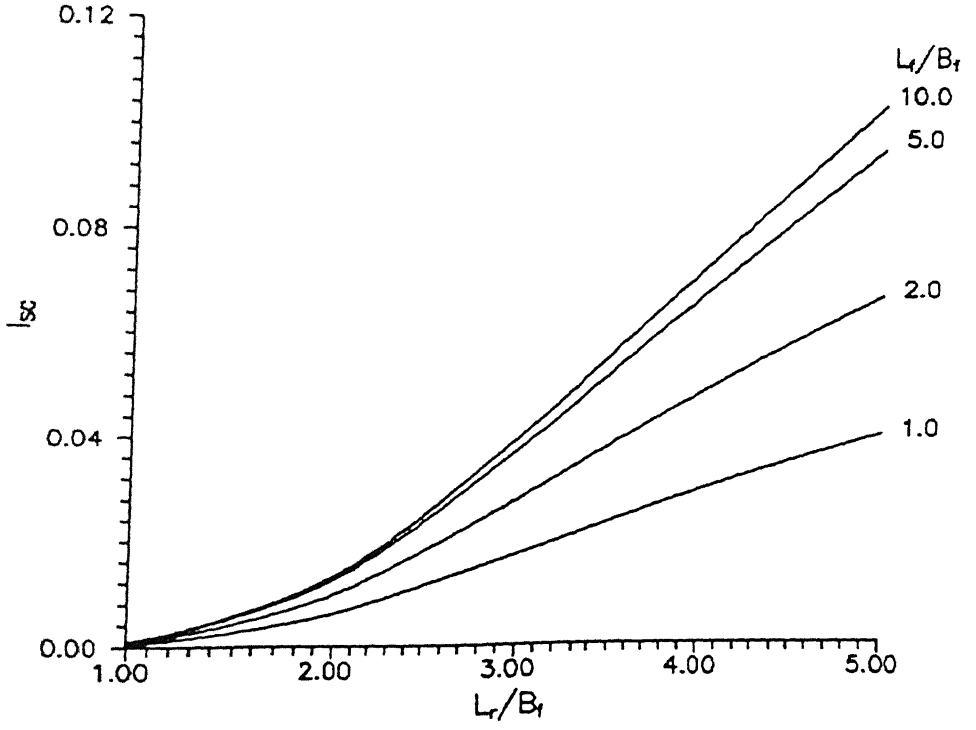


Fig. 4.22 Effect of Length of Strip on $I_{sc}$ for Different Aspect Ratios of Loaded Area ($U_o/B_f=2$, $\nu_s=0.3$)

The plot for a deeper strip, i.e. for $U_o/B_f$=2, is presented in Fig. 4.22. Here again, the $I_{sc}$ values increase with the length of the strip, $L_r/B_f$, and the aspect ratio, $L_f/B_f$, of the loaded area. There is a continuous increase in $I_{sc}$ values with $L_r/B_f$. However, they are small as compared to the values for the strips placed at a depth, $U_o/B_f$=1.0. The values of $I_{sc}$ for strips with $L_r/B_f$=5 are of the order of 0.04 for $L_f/B_f$=1 and 0.105 for $L_f/B_f$=10.

From these two figures it is evident that longer strips below longer rectangles at shallow depths result in significant settlement reduction at the centre of the loaded area. Strips at shallow depths are more advantageous as compared to strips at greater depths. As seen from Fig. 4.12, the stresses are higher for longer strips. Also, from Fig. 4.15, it is clear that the maximum heave of the surface is experienced within a distance, x/c of 2 from the point force at a depth c. Hence positive (upward) normal stresses for strips at depth, $U_o/B_f$=1, within a distance, $x=2B_f$ ($c=U_o=B_f$) and at depth, $U_o/B_f$=2, within a distance, $x=4B_f$ ($c=U_o=2B_f$) are responsible for settlement reduction of the surface. Normal stresses are positive over larger distances for longer strips. Hence longer strips result in higher $I_{sc}$ values.

The effect of Poisson's ratio, $\nu_s$, on $I_{sc}$ for strips at a depth, $U_o/B_f$=1, placed below a square area ($L_f/B_f$=1) is shown in Fig. 4.23. The $I_{sc}$ values increase with length, $L_r/B_f$, for all $\nu_s$ values. The effect of $\nu_s$ is felt only in case of strips with length, $L_r/B_f$>2. For $L_r/B_f$=5, $I_{sc}$ values for $\nu_s$=0.1 and 0.5 (saturated undrained soils) are 0.16 and 0.11 respectively.

From Figs. 4.20 to 4.23, it is evident that the settlement reduction coefficient at the centre of the loaded area, $I_{sc}$, is affected considerably by the length of the reinforcement, $L_r/B_f$, depth of reinforcement, $U_o/B_f$, the aspect ratio of the loaded area, $L_f/B_f$ and the Poisson's ratio of the soil, $\nu_s$. Hence, in designing the reinforced foundation bed, an optimum choice of all these parameters is to be made.

The effect of the length of the strip, $L_r/B_f$, on the normalised rigid body displacement of the reinforcement strip, $\delta_o E_s/B_f q$, for different depths of placement, $U_o/B_f$, and for a square loaded area ($L_f/B_f=1$), is depicted in Fig. 4.24. $\delta_o E_s/B_f q$ decreases with depth, $U_o/B_f$. It is also seen that $\delta_o E_s/B_f q$ decreases with increase in the length of the strip, $L_r/B_f$. The rate of change of rigid body displacement of strips, with depth, $U_o/B_f$, also decreases with the increase in $L_r/B_f$. For a strip of length, $L_r/B_f=1$, the values of the rigid body displacement of the strip, $\delta_o E_s/B_f q$ at depths, $U_o/B_f=0.1$ and 2 are 1.78 and 0.85 respectively. The corresponding values for longer strips with $L_r/B_f=5$ are 0.72 and 0.5 respectively. At shallow depths ($U_o/B_f<1$) the change in the rigid body displacement of the strip for lengths of strip, $L_r/B_f$, increasing from 1 to 2, is much more significant than with further increase in $L_r/B_f$. As explained earlier, the difference between the vertical displacements due to surface loading at the centre and edge of the strip is high for longer strips and low for shorter strips. The average value of displacements for a shorter strip is therefore higher than that for a longer one. The uniform displacement value which a rigid

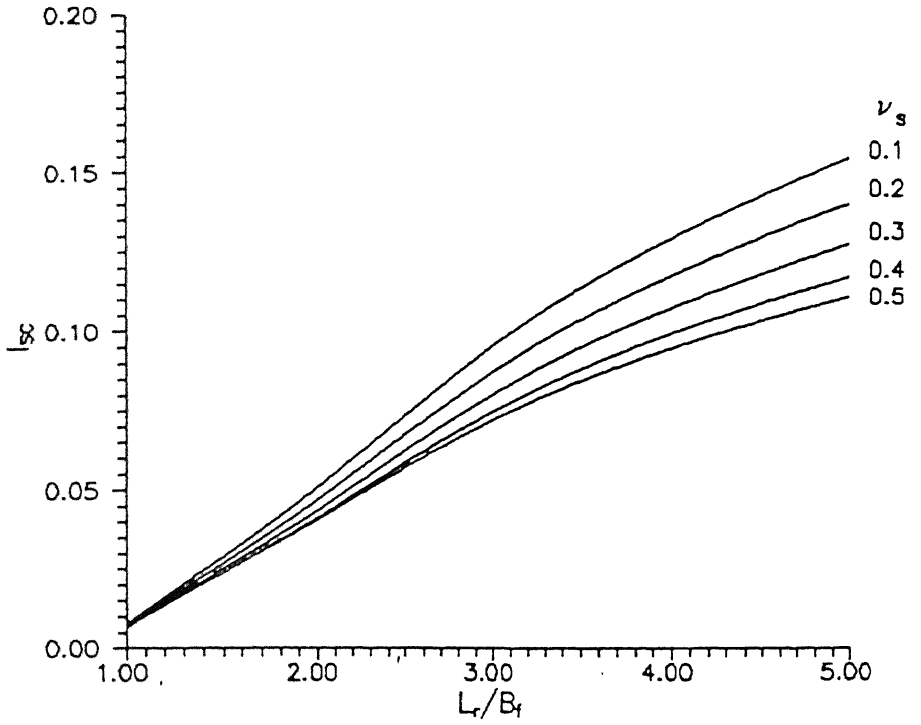


Fig. 4.23 Effect of Length of Strip on $I_{sc}$ for Different Poisson's Ratio of Soil ($U_0/B_f=1$, $L_f/B_f=1$)

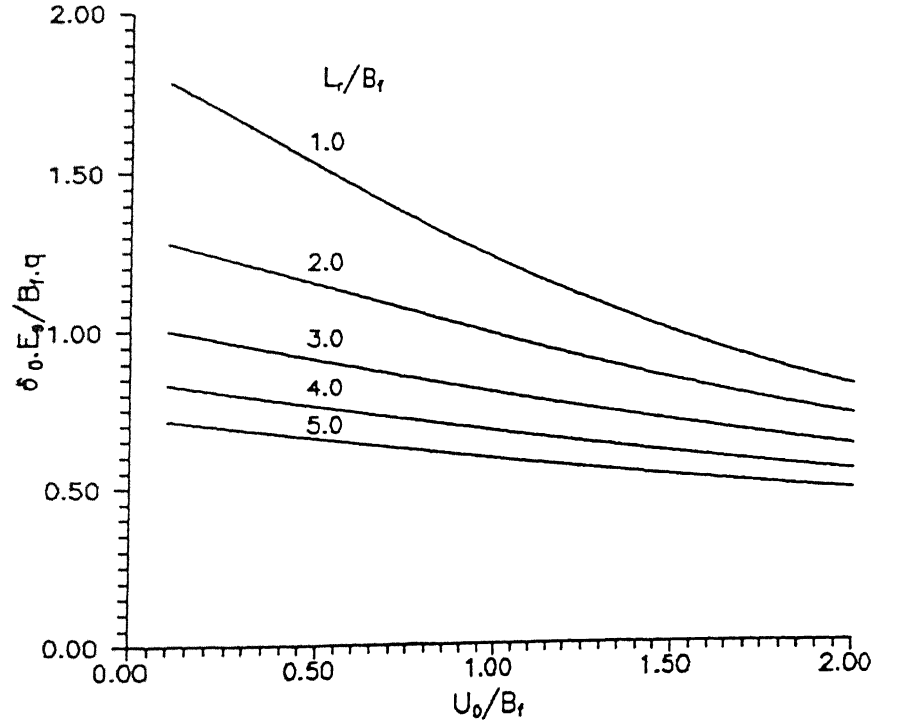


Fig. 4.24 Effect of Depth of Placement on Rigid Body Displacement for Different Lengths of Strip ($L_f/B_f=1$, $\nu_s=0.3$)

strip maintains lies in the vicinity of this average value. This explains why the rigid body displacement, $\delta_o E_s/B_f q$, is maximum for strips with lengths, $L_r/B_f=1$ and minimum for $L_r/B_f=5$. Further, as the depths of placement of strip, $U_o/B_f$, increases, the vertical displacements of points are smaller and consequently, the rigid body displacement decreases.

Fig. 4.25 presents the plot of the rigid body displacement, $\delta_o E_s/B_f q$, of the strip versus the length, $L_r/B_f$, of the strip for various aspect ratios, $L_f/B_f$, of the loaded area. This figure reiterates the observation that $\delta_o E_s/B_f q$ decrease with length, $L_r/B_f$, made with respect to the data presented in Fig. 4.24. This is true for all $L_f/B_f$ values. It is also observed from this figure that the rigid body displacement increases with $L_f/B_f$. $\delta_o E_s/B_f q$, for $L_r/B_f=1$ is 3.8 for a long rectangular area with aspect ratio, $L_f/B_f=10$ and 1.23 for a square area ($L_f/B_f=1$). The increase in $\delta_o E_s/B_f q$ with $L_f/B_f$ is because higher stresses are mobilised for strips below longer rectangles due to high vertical displacements.

### 4.6.3 Two Strips at Depth, $U_o$

Fig. 4.26 presents the effect of distance of the strip from x-axis, $S_y/B_f$, on the normalised normal stresses, $\sigma/q$, for a strip of length, $L_r/B_f=2$, placed below a square area ($L_f/B_f=1$) at a depth, $U_o/B_f=1$. For all $S_y/B_f$ values the stresses are maximum at the centre i.e. at $x/B_f=0$, decrease with the distance, $x/B_f$ and increase rapidly on the negative side towards the edge of the strip. The stresses change sign at a distance, $x/B_f$ of around 1.1. Normal stresses are maximum for $S_y/B_f=0.5$. At larger

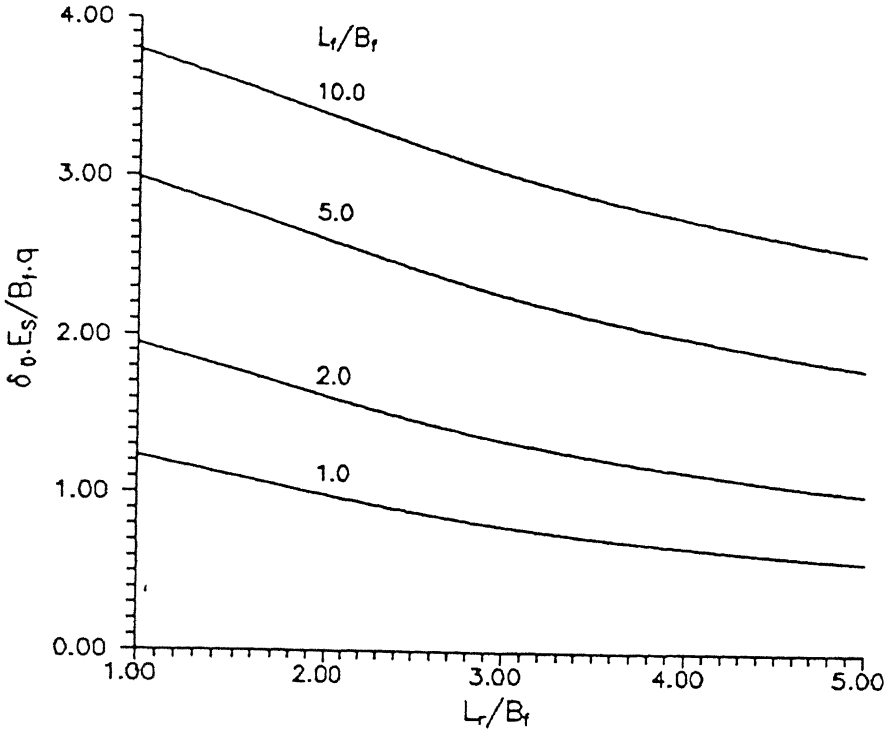


Fig. 4.25 Effect of Length on Rigid Body Displacement of Strip for Different Aspect Ratios of Loaded Area ($U_0/B_f=1$, $\nu_s=0.3$)

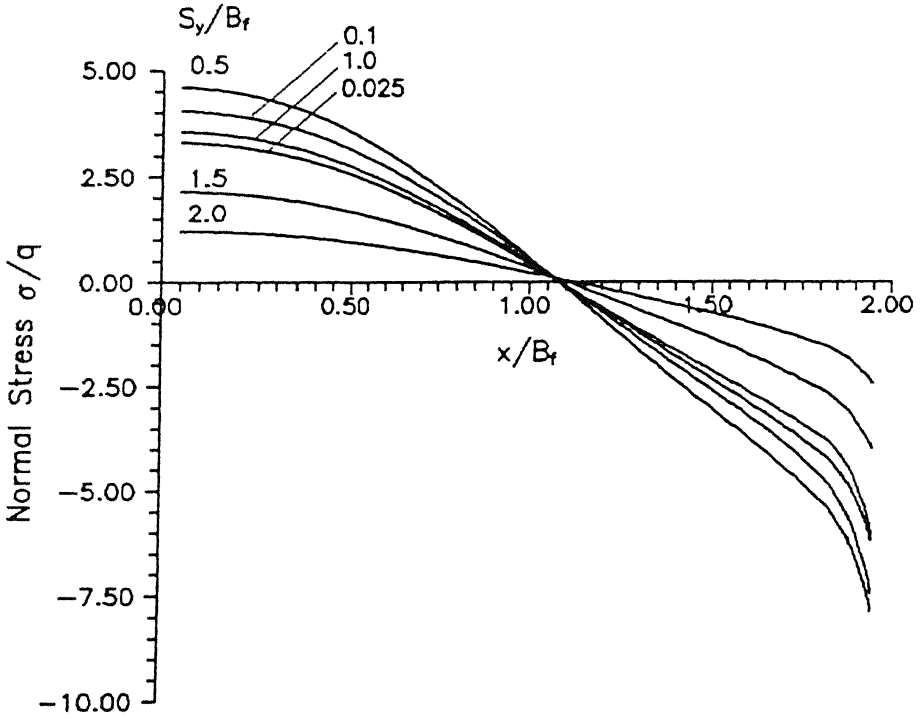


Fig. 4.26 Variation of Normal Stress with Distance for Different Distances of Strip from x−axis ($L_r/B_f=2$, $L_f/B_f=1$, $U_0/B_f=1$, $\nu_s=0.3$)

distances ($S_y/B_f$>1.5) the stresses are very small. The stress, $\sigma/q$, for two contiguous strips, i.e. $S_y/B_f$=0.025, at the centre ($x/B_f$=0) is 3.3. The stress at the centre for $S_y/B_f$=0.5 and 2 are 4.6q and 1.2 q. At closer spacings of the strips, that is for distances, $S_y/B_f$<0.5 the interference of the normal stresses over each other is high and as this distance increases upto $S_y/B_f$=0.5 the interference effect decreases. As a result stresses increase upto $S_y/B_f$=0.5. For $S_y/B_f$>0.5 the vertical displacements of the points along the strip due to the surface loading are themselves small. Consequently the stresses decrease with $S_y/B_f$.

The plot of SRC at the centre, i.e $I_{sc}$, versus the distance of the strip from x-axis, $S_y/B_f$, for various lengths, $L_r/B_f$, of the strip placed at a depth, $U_o/B_f$=1 below a square loaded area is shown in Fig. 4.27. The $I_{sc}$, for all lengths of strips, increases upto a certain value and then decreases with $S_y/B_f$. The maximum $I_{sc}$ is observed at a distance, $S_y/B_f$ of around 0.15 to 0.25, depending on the length of the strip. Further, the $I_{sc}$ values increase with $L_r/B_f$ and this is obvious because the stresses mobilised are higher for longer strips (Fig. 4.12). The maximum values of $I_{sc}$ of 0.005 and 0.081 for $L_r/B_f$=1 and 5 are observed at distances, $S_y/B_f$=0.15 and 0.25. At $S_y/B_f$=2 the $I_{sc}$ values for the corresponding lengths are practically zero and 0.01 respectively. The maximum $I_{sc}$ is observed at a distance, $S_y/B_f$ of around 0.25 because the stresses developed are maximum at this distance as perceived from Fig. 4.26. From this figure it is clear that for rigid strips at a depth, $U_o$ equal to $B_f$, maximum settlement reduction accrues if the two strips are placed each at a distance

of $0.25B_f$ from the x-axis. Further, longer strips result in higher settlement reduction.

Fig. 4.28 depicts the variation of $I_{sc}$ with depth ratio, $U_o/B_f$, for various values of the distance, $S_y/B_f$, of the strips of length, $L_r/B_f=2$, from the x-axis placed below a square area. It is seen that beyond a depth of $0.5B_f$ the $I_{sc}$ values decrease for all $S_y/B_f$ values. At shallow depths ($U_o/B_f \leq 0.25$) there is a change in the slope of the $I_{sc}$ curve with increase in the values of $S_y/B_f$ from 0.025 to 0.25. For $S_y/B_f<0.25$, the maximum $I_{sc}$ is observed at a depth of $0.1B_f$ whereas for $S_y/B_f \geq 0.25$ it occurs at a depth of $0.25B_f$. Further, in the depth range of $0.2B_f$ to $0.6B_f$, $I_{sc}$ is maximum for strips placed at a distance $S_y/B_f=0.1$ and for depths, $U_o/B_f>0.6$, it is maximum for $S_y/B_f=0.25$. This shows that the distance, $S_y/B_f$ at which maximum settlement reduction occurs is a function of depth of the strips. At a depth, $U_o/B_f=0.1$, contiguous strips ($S_y/B_f=B_r/B_f=0.025$) exhibit maximum $I_{sc}$. At greater depths ($U_o/B_f>1.5$), $I_{sc}$ values are very small and the effect of $S_y/B_f$ is insignificant.

Figs. 4.29 and 4.30 show the effect of the parameters on the normalised rigid body displacement, $\delta_o E_s/B_f q$. The variation of $\delta_o E_s/B_f q$ versus the distance, $S_y/B_f$ of the strips from the x-axis for various lengths of the strip, $L_r/B_f$, placed at a depth, $U_o/B_f=1$ below a square area is presented in Fig. 4.29. The rigid body displacement decreases with $S_y/B_f$ for all lengths. The rate of change of $\delta_o E_s/B_f q$ is maximum for shorter strips and it decreases with increase in the length of strip. The maximum value

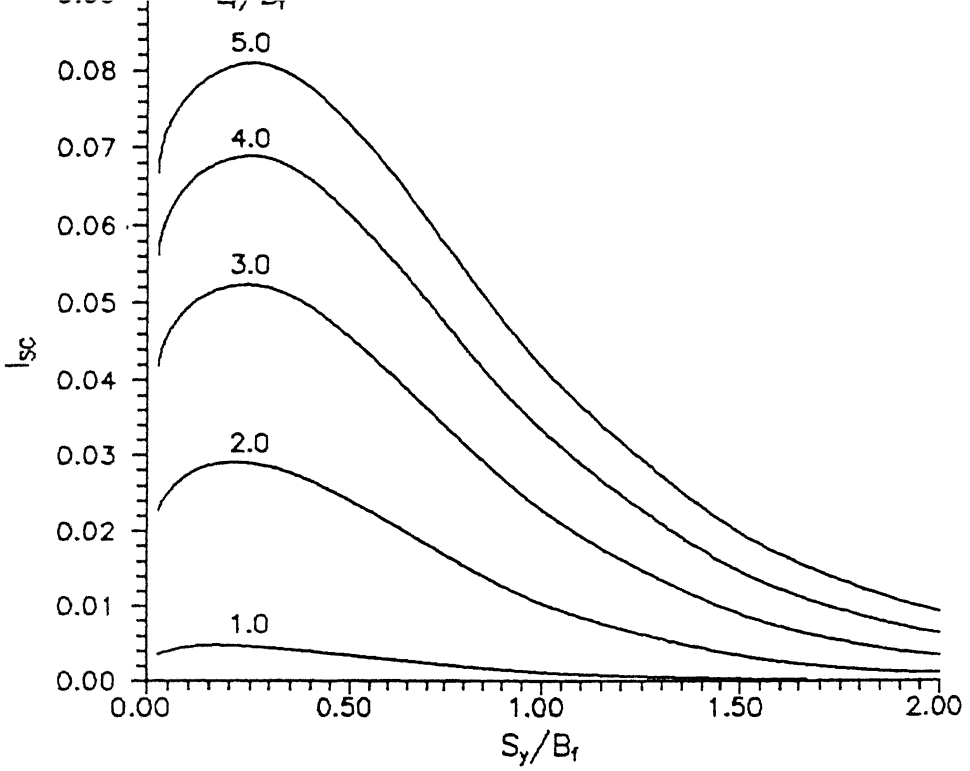


Fig. 4.27 Effect of Distance of Strip from x-axis on $I_{sc}$ for Different Lengths of the Strip ($U_0/B_f=1$, $L_f/B_f=1$, $\nu_s=0.3$)

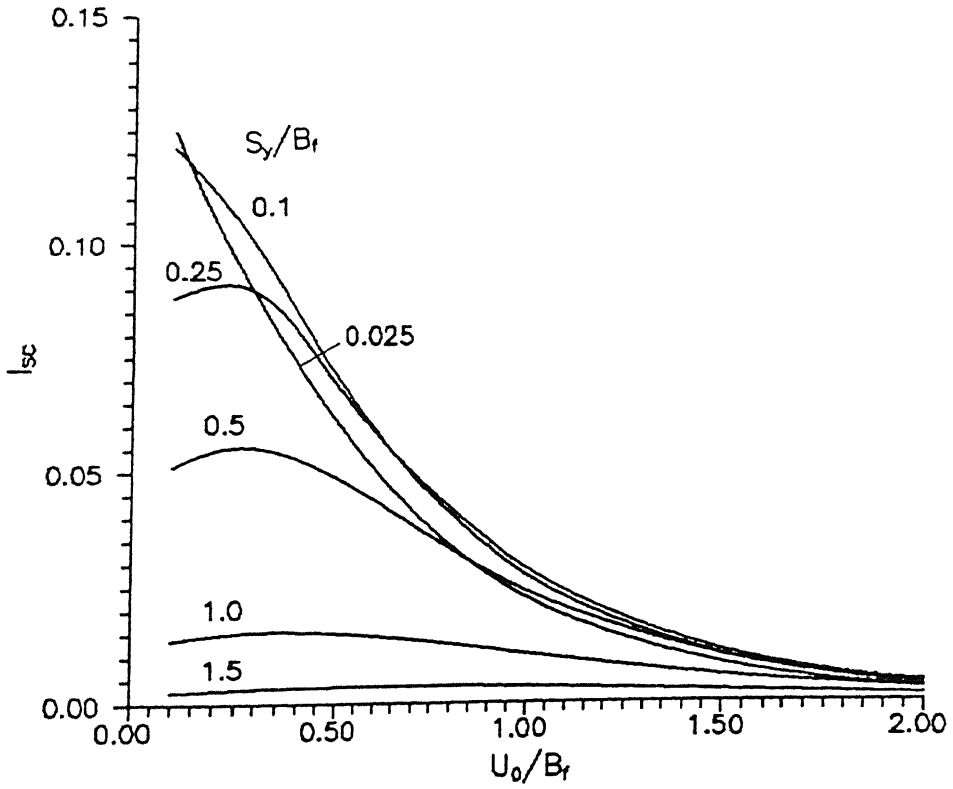


Fig. 4.28 Effect of Depth of Placement on $I_{sc}$ for Different Distances of Strip from x-axis ($L_r/B_f=2$, $L_f/B_f=1$, $\nu_s=0.3$)

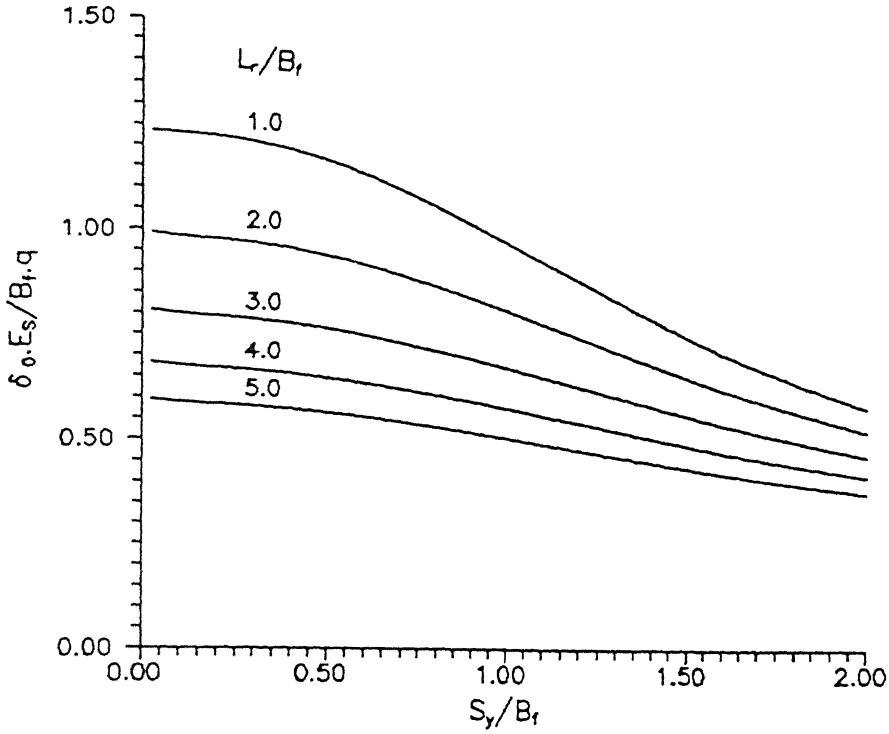


Fig. 4.29 Effect of Distance of Strip from x-axis on its Rigid Body Displacement for Different Lengths of Strip ($U_0/B_f$=1, $L_f/B_f$=1, $\nu_s$=0.3)

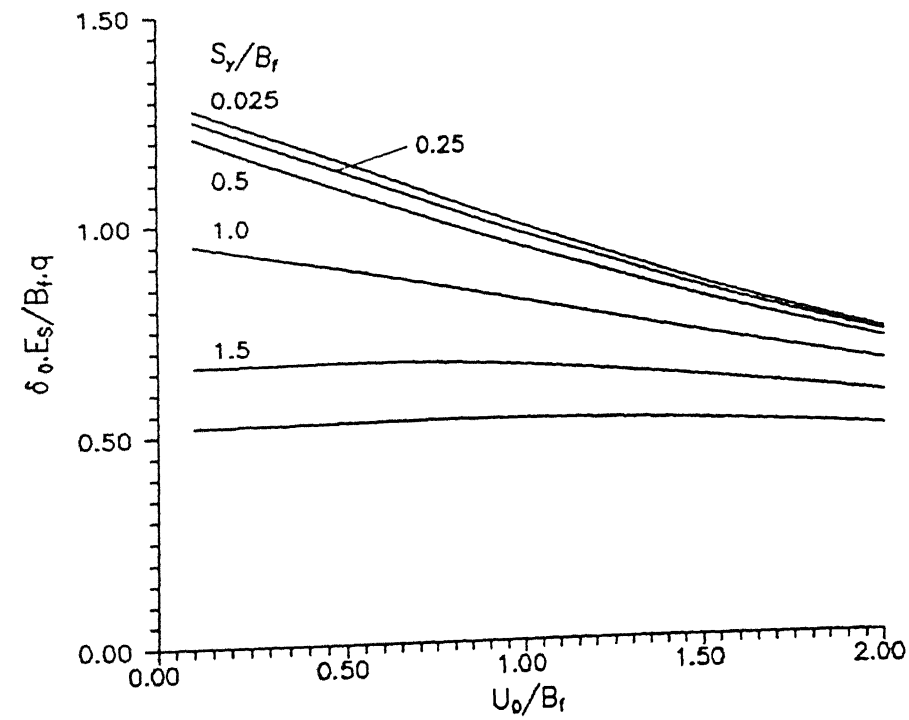


Fig. 4.30 Effect of Depth of Placement of Strip on the Rigid Body Displacement for Different Distances of Strip from x-axis ($L_r/B_f$=2, $L_f/B_f$=1, $\nu_s$=0.3)

of $\delta_o E_s/B_f q$ is observed for contiguous strips. It is also evident from the figure that the rigid body displacements decrease with increase in length, $L_r/B_f$, of the strip, as observed in Figs. 4.24 and 4.25. For contiguous strips the value of $\delta_o E_s/B_f q$ are 1.23 and 0.59 for $L_r/B_f$=1 and 5. At $S_y/B_f$=2 the corresponding values are 0.6 and 0.38 respectively. The decrease in $\delta_o E_s/B_f q$ with the distance, $S_y/B_f$, is obvious because the vertical displacement of the points along the strip decrease with $S_y/B_f$.

Fig. 4.30 shows the plot of $\delta_o E_s/B_f q$ with the depth ratio, $U_o/B_f$, for various distances from x-axis, $S_y/B_f$, and for strips of length, $L_r/B_f$=2, placed below a square area. The rigid body displacement decreases with depth for all $S_y/B_f$ values. With increase in $S_y/B_f$, $\delta_o E_s/B_f q$ decreases. The rate of change of the rigid body displacement is high for smaller distances, $S_y/B_f$, from the x-axis. The decrease in $\delta_o E_s/B_f q$ with $S_y/B_f$ is due to the fact that the vertical displacements due to surface loading decrease with increasing $S_y/B_f$ values. The decrease in rigid body displacement with depth is again due to the decrease in vertical displacements with $U_o/B_f$ values.

### 4.6.4 Two Strips One Below The Other

The interference of two strips placed one below the other is investigated next. The stresses are calculated and the corresponding effect on the settlement reduction of the centre of the loaded area on the surface studied.

The comparison for normal stresses for strips one below the other at depths, $U_o/B_f$=0.75 and $U_i/B_f$=1 with those for single

influence on each other. As a result, the stresses mobilised are smaller as compared to those mobilised if considered independently. Further, this difference in stresses is higher for longer strips. The consequence is that the settlement reduction reduces as compared to strips considered independently. It is also evident that even for a vertical spacing of $\Delta u$=1.75 the value of $I_D$ for $L_r/B_f$=1 and 5 are 0.72 and 0.66. From this table it is clear that the principle of superposition cannot be applied for two strips placed one below the other atleast for the depth range considered in the analysis. A suitable correction factor will have to be used to calculate the settlement reduction coefficients due to two strips acting together from those of strips acting independently.

### 4.6.5 Multiple Strips

Two pairs of strips are considered at the same depth and the influence of each strip on the other is investigated. One pair is contiguously placed ($S_{y1}/B_f$=0.025) while the distance of the second pair, $S_{y2}/B_f$ from the x-axis is varied. The ratio of the $I_{sc}$ for the multiple strips to that obtained from the summation of the $I_{sc}$ for a single pair is calculated. The effects of the lengths of the strips, $L_r/B_f$ and depth of placement, $U_o/B_f$ on the ratio, $I_D$ (defined subsequently), is studied in this section.

The comparison of normal stresses for multiple strips at distances, $S_{y1}/B_f$=0.025 (contiguous strips) and $S_y/B_f$=0.5 with those for a single pair of strips at the respective distances is presented in Fig. 4.32. Strips considered are of length, $L_r/B_f$=2, placed at a depth, $U_o/B_f$=1, below a square area. It is seen that

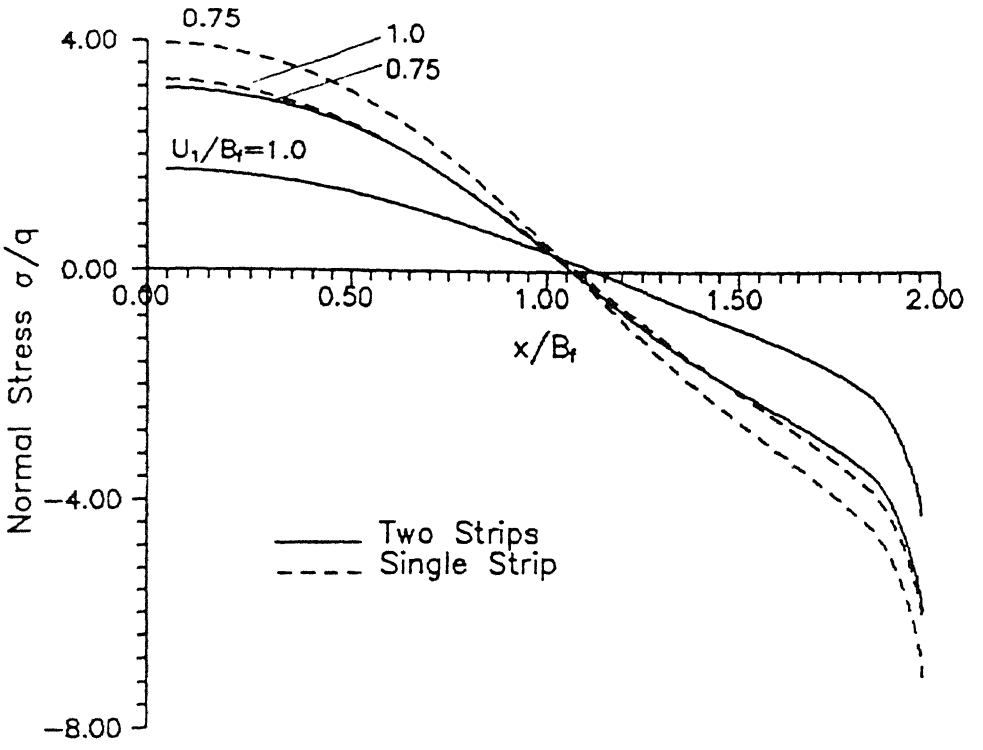


Fig. 4.31 Comparison of Normal Stresses for Strips at Depths $U_0$ and $U_1$ with those for Single Strips ($L_r/B_f$=2, $L_f/B_f$=1, $\nu_s$=0.3)

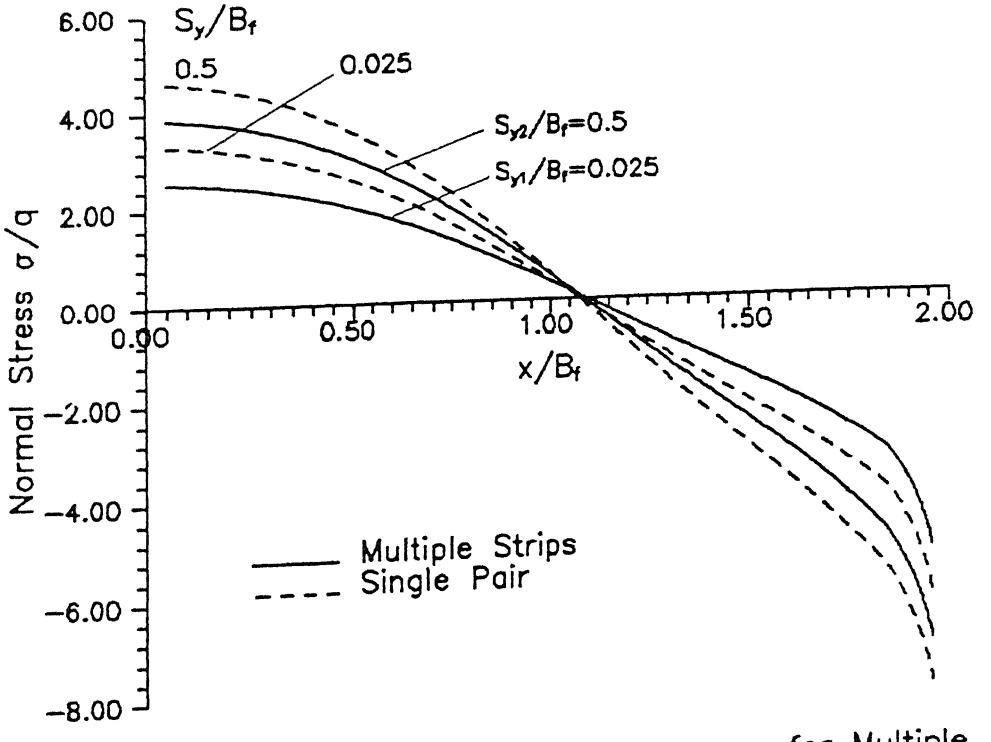


Fig. 4.32 Comparison of Normal Stresses for Multiple Strips with those for a Single Pair of Strips ($L_r/B_f$=2, $L_f/B_f$=1, $U_0/B_f$=1, $\nu_s$=0.3)

the normal stresses for the multiple strips are smaller than those for a single pair considered at the respective distances ($S_y/B_f$). This again is due to the influence of each pair of strips on the other. The vertical displacements along each pair to be counteracted by the normal stresses are reduced and as a result the normal stresses mobilised are smaller.

In this case the ratio, $I_D$, is defined as

$$I_D = \frac{I_{sc} \text{ for two pairs of strips at } S_{y1} \text{ and } S_{y2}}{I_{sc} \text{ for strips at } S_{y1} + I_{sc} \text{ for strips at } S_{y2}} \qquad (4.66)$$

Fig. 4.33 presents the variation of the ratio, $I_D$, with the horizontal spacing, $S_{yD}$ ($=S_{y1}/B_f - S_{y2}/B_f$) for various lengths of the strips, $L_r/B_f$ placed at a depth, $U_o/B_f=1$, below a square area. $I_D$ increases with increase in the spacing for all lengths of the strips. For shorter strips the increase in $I_D$ with $S_{yD}$ is rapid as compared to longer ones. At a spacing, $S_{yD}=0.4$, $I_D=0.9$ for strips of length, $L_r/B_f=1$ while for longer strips ($L_r/B_f=5$) a high value of $I_D$ is observed at large values of $S_{yD}$. This is because, at close spacings the influence of each strip on the other is high and this is particularly high for longer strips. The stresses mobilised are consequently low, resulting in smaller settlement reduction coefficients as compared to a single pair considered in an earlier section.

The variation of $I_D$ with $S_{yD}$ for various depths, $U_o/B_f$, of placement of the strips of length, $L_r/B_f=2$, below a square area is presented in Fig. 4.34. It is interesting to note that at closer

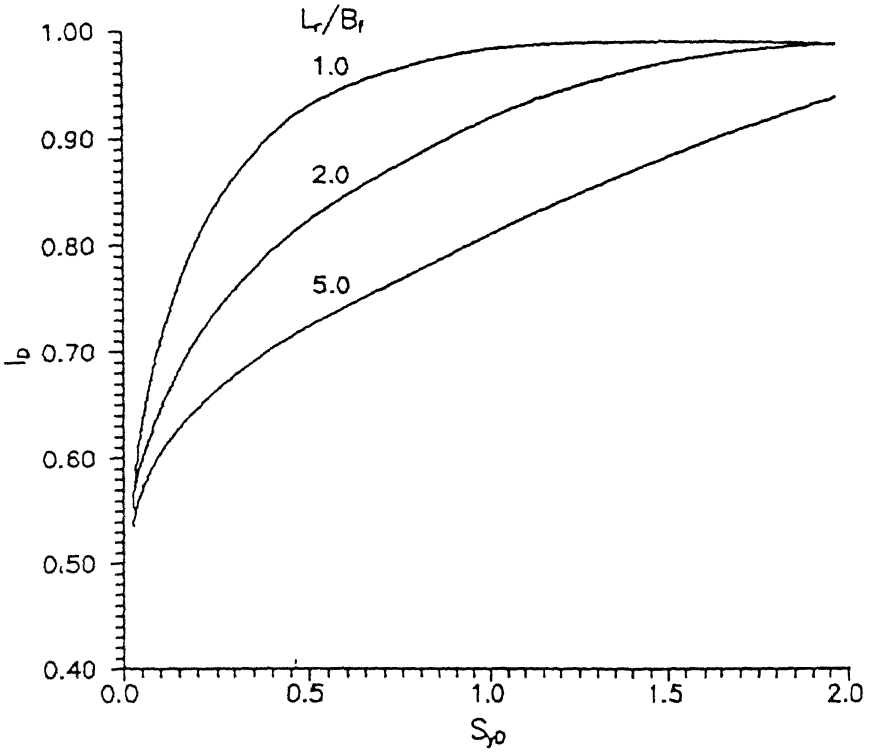


Fig. 4.33 Effect of Spacing Difference on $I_\rho$ for Different Lengths of strip ($U_o/B_f=1$, $L_f/B_f=1$, $\nu_s=0.3$)

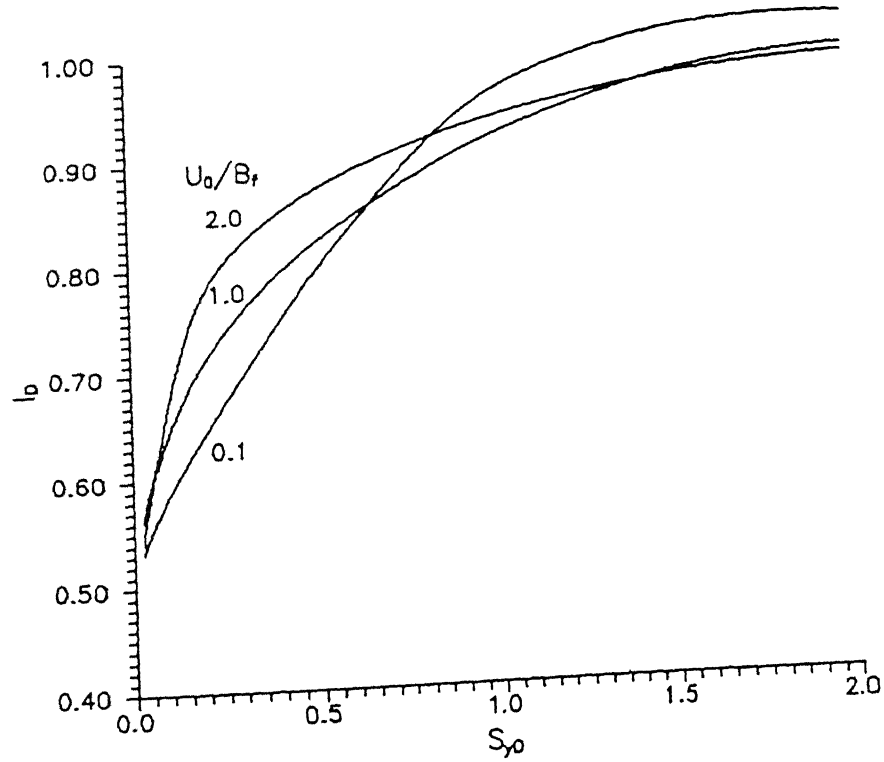


Fig. 4.34 Effect of Spacing Difference on $I_\rho$ for Different Depths of Placement of strip ($L_r/B_f=2.0$, $L_f/B_f=1$, $\nu_s=0.3$)

spacings, $I_D$ for greater depths is higher while this trend reverses with increase in the spacing, $S_{yD}$. The reason for this is that at shallow depths, strips placed at closer spacings have a higher influence on each other as compared to distantly spaced strips. On the other hand, the effect of distantly spaced strips becomes predominant at greater depths, as seen in Fig. 4.28.

From these two figures it is clear that $I_D$ is a function of the length, $L_r/B_f$, depth, $U_o/B_f$ of the strips and the spacing between them. Based on these parameters a suitable factor is to be selected from these figures to obtain settlement reduction due to multiple strips from those obtained by summing up the coefficients for individual pairs.

## 4.7 Conclusions

An analysis using the elastic continuum theory for a rigid strip displacing uniformly in soil is proposed. The normal stress interactions are studied and evaluated. The effects of the parameters mentioned in section 4.6 viz., the aspect ratio of the loaded area, length, depth and distance of the strip from the x-axis on the normal stresses mobilised at the strip-soil interface and the reduction in surface settlements, resulting thereof have been studied. It is seen that, in forcing the strip to undergo a uniform vertical deformation normal stresses are mobilised at the strip-soil interface which act upward at the centre and downward at the strip edges. These stresses, in turn push the soil up, bringing about a reduction in surface settlements. The results of the parametric study indicate a

number of facts which are listed below.

1. A rigid strip placed close to the surface ($U_o/B_f \leq 0.1$) gives rise to maximum reduction of the settlement of the surface.
2. For any depth of placement, for shorter strips ($L_r/B_f < 3$), the increase in settlement reduction is appreciable with increase in the aspect ratio of the loaded area upto 2 while it is marginal for further increase in the aspect ratio.
3. For any depth of placement, longer strips show higher settlement reduction of the surface since the mobilised normal stresses are positive over larger lengths.
4. Similar to the results of chapter 3, for a pair of rigid strips placed symmetrically about the x-axis and at a depth $U_o \geq 0.5B_f$ maximum reduction in surface settlement is observed if the centre of each strip lies at a distance of $0.25B_f$ from the x-axis.
5. A suitable factor is to be used for obtaining the settlement reduction due to two strips placed one below the other and for multiple strips from those obtained from the principle of superposition.
6. For a rigid strip, the settlement reduction coefficients due to normal stress interactions are much higher than those due to shear stress interactions.

# CHAPTER 5

# STRIP-SOIL INTERACTION : EFFECTS OF EXTENSIBILITY, FLEXIBILITY, COUPLED SHEAR AND NORMAL STRESS INTERACTIONS AND SLIP

## 5.1 Introduction

In the preceding chapters the strip was considered to be rigid such that no axial elongation was permitted (Chapter 3) or it was forced to undergo a uniform vertical displacement (Chapter 4). The shear and normal stresses mobilised thereof, considered independently, were calculated and the consequent reduction in surface settlements computed. In this chapter, firstly the extensibility and the flexural stiffness of the strip are taken into account separately. Unlike the case of an inextensible one (Chapter 3), the horizontal displacements of the points along the extensible strip are equated to the elongations of these points due to tensions in the strip which are an outcome of the shear stresses mobilised at the interface. A flexible strip is assumed to behave like a beam and hence the flexural deformations of points along the strip are equated to the soil displacements. The shear and normal stresses mobilised thereof, were computed as also the resulting settlement reductions of points along the surface. The combined effect of the horizontal and vertical rigidity for a rigid strip is then considered wherein the inextensibility and the uniform vertical translation of the strip are incorporated simultaneously. An allowance is made for possible slip along the strip-soil interface by limiting the shear stresses mobilised to the frictional resistance available at the interface due to mobilsed normal stresses and the overburden stress at that depth.

## 5.2 Extensible Strip - Single Strip

### 5.2.1 Problem Definition

The definition of the problem is similar to the one in chapter 3 with the difference that the strip (of size, $2L_r \times 2B_r$ placed centrally beneath a loaded area of size, $2L_f \times 2B_f$ transmitting a uniform load, q, at a depth, $U_o$) is extensible (Fig. 5.1). The width of this strip, $2B_r$, as explained earlier is relatively small and its thickness, $t_r$, negligible. The strip being extensible, the net soil lateral displacements resulting from the applied surface load and the mobilised shear stresses are not zero but equal to the axial elongations of the strip. Satisfying the compatibility of displacements for points along the strip, the shear stresses mobilised at the strip-soil interface are computed.

The tension in the strip and settlement reduction coefficients of points along the surface are calculated as before. Again, the shear stresses developed are assumed to be constant over the width of the strip and to vary along its length.

### 5.2.2 Analysis

The discretization of the loaded area and the strip for numerical integrations are the same as in chapter 3. The Boussinesq's and Mindlin's equations are used in computing the lateral displacements due to the applied load on the surface and the mobilised shear stresses respectively.

The vector of horizontal displacements of the N nodes along

the half-length of the strip due to the surface load, q as obtained by integrating Boussinesq's equation over the loaded area, is

$$\left\{ \rho_x^f \right\} = \frac{B_f}{E_s} \left\{ I^f \right\} q \qquad (5.1)$$

where $\left\{ \rho_x^f \right\}$ and $\left\{ I^f \right\}$ are vectors of size N.

The vector of horizontal displacements of the N nodes along the half-length of the strip due to shear stresses mobilised along the whole length of the strip as obtained from integration of Mindlin's equation for each element is

$$\left\{ \rho_x^r \right\} = \frac{B_f}{E_s} \left[ I^r \right] \left\{ \tau \right\} \qquad (5.2)$$

where $\left[ I^r \right]$ is an influence coefficient matrix for the influence of the shear stresses on the horizontal displacements of the N nodes. It is a square matrix of size N, and $\left\{ \rho_x^f \right\}$ and $\left\{ \tau \right\}$ are vectors of size N, $\left\{ \tau \right\}$ being the vector of the mobilised shear stresses.

The net lateral displacement of all the nodes, as mentioned earlier is equal to the elongations of the strip. Thus, the compatibility equation is

$$\left\{ \rho_x^f \right\} - \left\{ \rho_x^r \right\} = \left\{ \rho_E \right\} \qquad (5.3)$$

where $\{ \rho_E \}$ is a vector of displacements of the nodes due to the elongation of each element of the strip and is of size N. The elongations are due to the tension in the strip resulting from mobilised shear stresses. The force equilibrium of the element i in Fig. 5.2 is written as

$$T_k + \Delta T_k + \tau_k dA = T_k \tag{5.4}$$

or

$$\Delta T_k = -\tau_k dA = -\tau_k dl \; 2B_r \tag{5.5}$$

The negative sign indicates that the tension in the strip decreases with distance along the x-axis. The tension, $T_k$, to the left of element k, would then be

$$T_k = \sum_{i=k}^{N} \Delta T_i = \sum_{i=k}^{N} \tau_i dl \; 2B_r \tag{5.6}$$

The elemental elongation, $\Delta\rho_{Ek}$, of the $k^{th}$ element is

$$\Delta\rho_{Ek} = \frac{T_k + (T_k + \Delta T_k)}{A_r E_r} \frac{dl}{2} \tag{5.7}$$

$$= \left( T_k + \frac{\Delta T_k}{2} \right) \frac{dl}{A_r E_r} \tag{5.8}$$

$$= \left( \frac{\tau_k}{2} + \sum_{i=k+1}^{N} \tau_i \right) \frac{dl \; 2B_r}{A_r E_r} dl \tag{5.9}$$

$A_r$ is the cross-sectional area of each element (assumed constant) and $E_r$ is the modulus of deformation of the strip. The

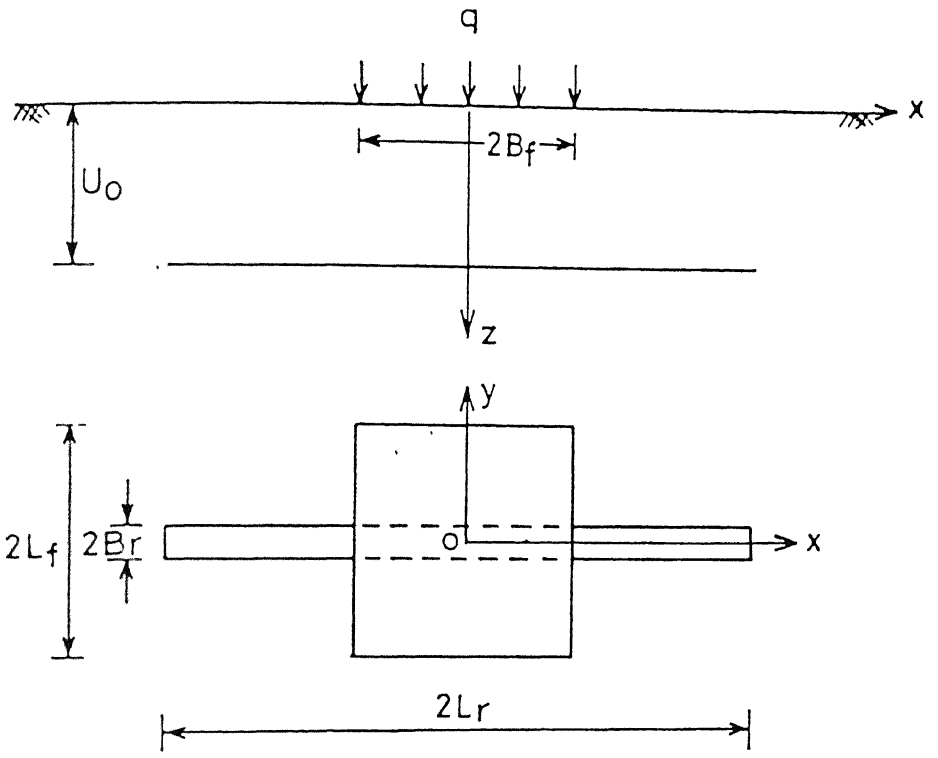


Fig. 5.1 Definition Sketch — Extensible Strip

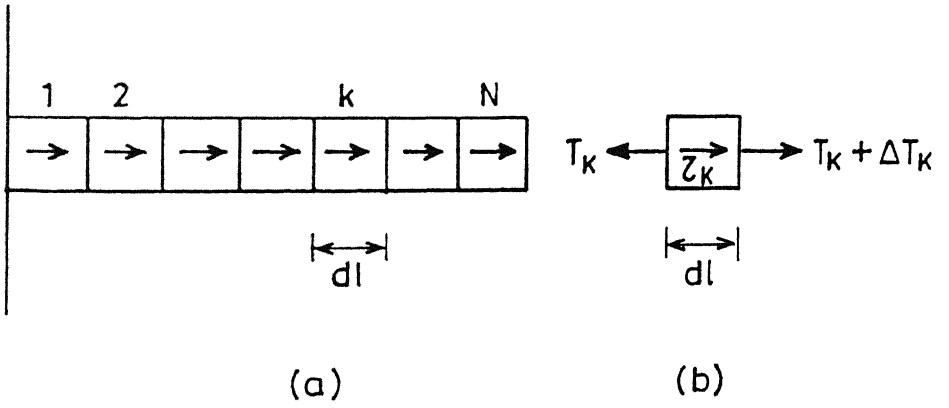


Fig. 5.2 a) Stresses on the Strip
b) Tension in an Element

cross-sectional area, $A_r$, of the strip is

$$A_r = t_r 2B_r \tag{5.10}$$

$t_r$ being the thickness of the strip. Substituting Eq. 5.10 in Eq. 5.9 and rewriting

$$\Delta\rho_{Ek} = \left( \frac{\tau_k}{2} + \sum_{i=k+1}^{N} \tau_i \right) \frac{dl^2}{t_r E_r} \tag{5.11}$$

The total elongation of node k is equal to the sum of all the elemental elongations from nodes 1 to k, and is written as

$$\rho_{Ek} = \rho_{Ek-1} + \Delta\rho_{Ek} \tag{5.12}$$

Combining Eqs. 5.11 and 5.12, the vector of the elongations of all the N nodes is written as

$$\left\{ \rho_E \right\} = \frac{dl^2}{t_r E_r} \left[ I_E \right] \left\{ \tau \right\} \tag{5.13}$$

where $\left[ I_E \right]$ is a square elongation coefficient matrix of size, N, and is given by

$$\left[ I_E \right] = \begin{bmatrix} 0.5 & 1.0 & 1.0 & 1.0 & 1.0 \\ 0.5 & 1.5 & 2.0 & 2.0 & 2.0 \\ 0.5 & 1.5 & 2.5 & 3.0 & 3.0 \\ & & & & \\ 0.5 & 1.5 & 2.5 & 3.5 & N-0.5 \end{bmatrix}$$

Non-dimensionalising the length parameters with $B_f$, Eq. 5.13 is rewritten as

$$\left\{ \rho_E \right\} = \frac{B_f (dl/B_f)^2}{(t_r/B_f)\, E_r} \left[ I_E \right] \left\{ \tau \right\} \qquad (5.14)$$

Substituting for $\left\{ \rho_E \right\}$ in Eq. 5.3

$$\frac{B_f}{E_s} \left\{ I^f \right\} q - \frac{B_f}{E_s} \left[ I^r \right] \left\{ \tau \right\} = \frac{B_f (dl/B_f)^2}{(t_r/B_f)\, E_r} \left[ I_E \right] \left\{ \tau \right\} \qquad (5.15)$$

or

$$\left[ \left[ I^r \right] + \frac{C}{K_\tau} \left[ I_E \right] \right] \left\{ \tau/q \right\} = \left\{ I^f \right\} \qquad (5.16)$$

where $C = (dl/B_f)^2$ and $K_\tau = \frac{E_r t_r}{E_s B_f}$. $K_\tau$ is the dimensionless elongation factor which takes into account the axial stiffness of the strip and the modulus of deformation of the soil.

Eq. 5.16 gives N equations for the normalised shear stresses mobilised along the N elements of the strip, which are solved by the Gauss elimination technique.

The tension in the reinforcement and the SRC are calculated as explained in chapter 3 for a single rigid strip.

## 5.3 Extensible Strip - Two Strips at Depth $U_o$

### 5.3.1 Problem Definition

The problem definition remains the same as in chapter 3.

The horizontal displacement vector for the displacements of all the N nodes of one strip due to surface load as expressed by Eq. 3.40 in chapter 3 is

$$\left\{ \rho_x^f \right\} = \frac{B_f}{E_s} \left\{ I^f \right\} q \qquad (5.17)$$

The vector of horizontal displacements due to shear stresses as expressed by Eq. 3.46 is

$$\left\{ \rho_x^r \right\} = \frac{B_f}{E_s} \left[ I^r \right] \left\{ \tau \right\} \qquad (5.18)$$

where all the vectors and matrix $\left[ I^r \right]$ have the same definitions as in Eqs. 3.40 and 3.46.

The elongation vector, $\left\{ \rho_E \right\}$, being a function of the stresses and the material properties of the strip, is the same as in Eq. 5.14. Satisfying the compatibility of displacements at all the nodes one obtains

$$\left\{ \rho_x^f \right\} - \left\{ \rho_x^r \right\} = \left\{ \rho_E \right\} \qquad (5.19)$$

or

$$\left[ \left[ I^r \right] + \frac{C}{K_\tau} \left[ I_E \right] \right] \left\{ \tau/q \right\} = \left\{ I^f \right\} \qquad (5.20)$$

the normalised shear stresses, $\left\{ \tau/q \right\}$, are obtained by solving the N equations. The difference in Eq. 5.16 and Eq. 5.20 is that the matrix $\left[ I^r \right]$ and vector $\left\{ I^f \right\}$ in Eq. 5.20 are functions of $S_y/B_f$ also, while they were functions of $U_o/B_f$, $L_r/B_f$ and $L_f/B_f$

only in Eq. 5.16.

The tension and SRC are calculated as explained in chapter 3 for the same problem.

## 5.4 Flexible Strips - Single Strip

### 5.4.1 Problem Definition

The strip considered is assumed to deform in the vertical direction, i.e., it is assumed to behave like a beam. As in chapter 4, a strip of size, $2L_r \times 2B_r$, is placed centrally at a depth, $U_o$, below a rectangular area on the surface transmitting a load of intensity, q (Fig. 5.3).

The surface load causes the strip to deform in the vertical direction as shown in Fig. 5.4. Due to this deformation, normal stresses are induced in the soil. The total vertical displacement of the soil is equal to the displacement due to the loading plus the displacement due to normal stresses generated. Satisfying the compatibility of the net displacements of the soil adjacent to the strip with those of the strip assumed to behave like a beam, the normal stresses are arrived at. The SRC along the surface due to these normal stresses are then calculated on the same lines as in chapter 4.

### 5.4.2 Analysis

The elastic continuum approach is used to obtain the vertical displacements. The loaded area is discretized in the

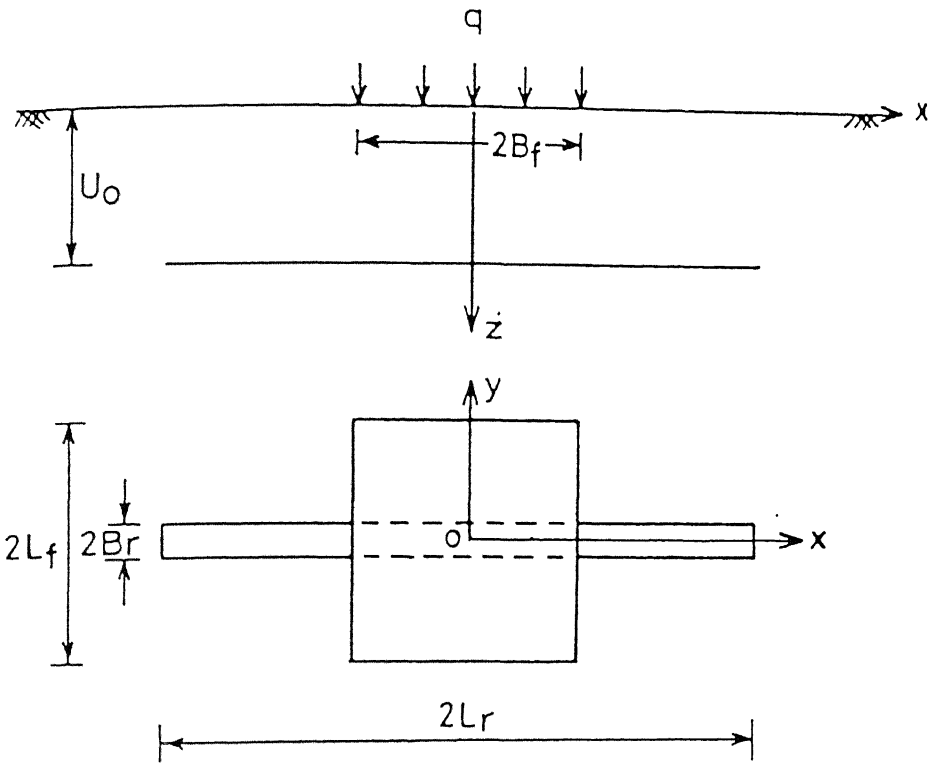


Fig. 5.3 Definition Sketch — Flexible Strip

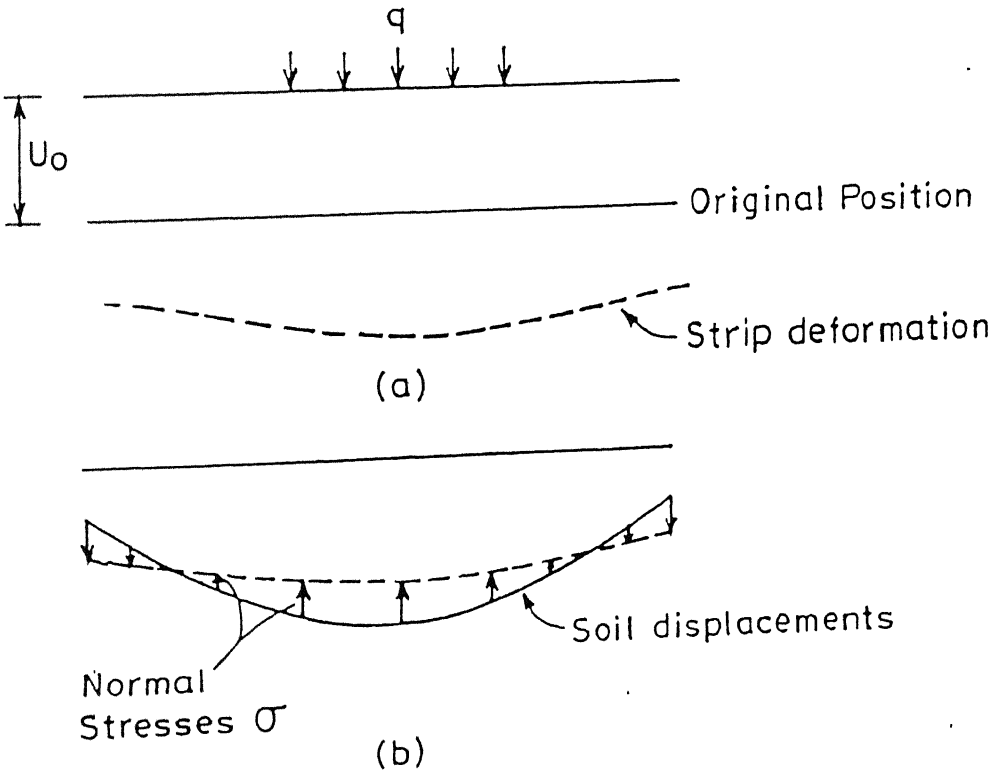


Fig. 5.4 a) Deformation of Strip
b) Stresses in Soil

same manner as in chapter 4. For the convenience of applying boundary conditions for the beam (strip), the strip is discretized as shown in Fig. 5.5. Due to symmetry, only half the length of the strip is considered. The strip is divided in such a way that two nodes are available at the two ends as shown in the figure. The other nodes are placed such that all the nodes are equidistant from each other and each node forms the centre of an element. Hence, excepting the first and the last elements, all other elements are of the same length, dl. The first and the last ones are half-elements. The number of nodes, $N = L_r/dl + 1$.

Using Boussinesq's equation, the vector of vertical displacements of all the N nodes due to the surface load as expressed in Eq. 4.5 of chapter 4, is

$$\left\{ \rho_z^f \right\} = \frac{B_f}{E_s} \left\{ I^f \right\} q \qquad (5.21)$$

The vertical displacements of all the N nodes due to the normal stresses mobilised at the interface is obtained using Mindlin's solution, and the vector of the displacements as defined in Eq. 4.14 of chapter 4, is

$$\left\{ \rho_z^r \right\} = \frac{B_f}{E_s} \left[ I^r \right] \left\{ \sigma \right\} \qquad (5.22)$$

where $\left\{ \sigma \right\}$ is the vector of normal stresses. The meanings of vectors $\left\{ \rho_z^f \right\}$, $\left\{ I^f \right\}$ and matrix $\left[ I^r \right]$ remain unaltered. In the case of an inflexible strip the beam displacement vector was equal

to the rigid body displacement vector (Eq. 4.15).

The total soil displacement vector, $\left\{ \rho_z^s \right\}$, is the difference of Eqs. 5.21 and 5.22 expressed as

$$\left\{ \rho_z^s \right\} = \left\{ \rho_z^f \right\} - \left\{ \rho_z^r \right\} \tag{5.23}$$

or

$$\left\{ \frac{\rho_z^s}{B_f} \right\} = \frac{q}{E_s} \left\{ I^f \right\} - \frac{1}{E_s} \left[ I^r \right] \left\{ \sigma \right\} \tag{5.24}$$

For calculating the strip displacement, the beam equation is used. The loading on the beam is the normal stresses mobilised at the soil-strip interface. The beam equation is

$$E_r I_r \frac{d^2 w}{dx^2} = M \tag{5.25}$$

where w is the beam deflection in the z direction, M is the moment and $E_r I_r$ is the flexural rigidity of the beam. The moment, M, is produced due to the stresses acting over the length, of the beam away from the point. The moment of the normal stresses about node i (Fig. 5.6) is

$$M_i = \sigma_i \frac{dA}{2} \frac{dl}{4} + \sum_{k=i+1}^{N} \sigma_k \, dA \, x \tag{5.26}$$

where x is the distance between node i and the centre of the area over which the normal stress, $\sigma_k$ is acting and $dA=2B_r dl$ is the area of the element.

The vertical displacement of any node i, from Eq. 5.25, expressed in the finite difference form is

$$E_r I_r \left( \frac{w_{i-1} - 2w_i + w_{i+1}}{dl^2} \right) = M_i \qquad (5.27)$$

Substituting Eq. 5.26 in 5.27 one obtains

$$E_r I_r \left( \frac{w_{i-1} - 2w_i + w_{i+1}}{dl^2} \right) = \sigma_N \frac{dl}{2} 2B_r \left( (N-i)dl - \frac{dl}{4} \right) + \sum_{k=i+1}^{N-1} \sigma_k dl \; 2B_r \left( (k-i)dl \right) + \sigma_i \frac{dl}{2} 2B_r \frac{dl}{4} \qquad (5.28)$$

Eq. 5.28 is written in matrix form as

$$\frac{E_r I_r}{dl^2} \left[ I_b \right] \left\{ w \right\} = \left[ I_\sigma \right] \left\{ \sigma \right\} \qquad (5.29)$$

where $\left[ I_b \right]$ is the finite difference coefficient matrix and $\left[ I_\sigma \right]$ is moment coefficient matrix.

The boundary conditions for Eq. 5.25 are as follows.

At x = 0, slope, $\frac{dw}{dx} = 0$ (5.30)

and

at $x = L_r$, moment, $\frac{d^2w}{dx^2} = 0$ (5.31)

The displacement of node 1 expressed in the finite difference form is

$$E_r I_r \left( \frac{w_2^* - 2w_1 + w_2}{dl^2} \right) = M_1 \qquad (5.32)$$

where $w_2^*$ (Fig. 5.7) is the displacement of the node $2^*$ at a distance dl to the left of node 1. From the boundary condition at node 1 (Eq. 5.30), one obtains

$$w_2^* = w_2 \qquad (5.33)$$

Substituting Eq. 5.33 in Eq. 5.32 the equation for displacement of node 1 is

$$E_r I_r \left( \frac{-2w_1 + 2w_2}{dl^2} \right) = M_1 \qquad (5.34)$$

The second boundary condition will be applied later in terms of the normal stresses mobilised. Hence the matrices $\left[ I_b \right]$ and $\left[ I_\sigma \right]$ are of size N-1×N while vectors $\left\{ \sigma \right\}$ and $\left\{ w \right\}$ are of size N where

$$\left[ I_b \right] = \begin{bmatrix} -2 & 2 & 0 & 0 & & & 0 \\ 1 & -2 & 1 & 0 & & & 0 \\ 0 & 1 & -2 & 1 & & & 0 \\ & & & & & & \\ 0 & & & & 0 & 1 & -2 & 1 \end{bmatrix}$$

Non-dimensionalising the length parameters with the half-width of the loaded area, $B_f$, Eq. 5.29 is written as

$$K_r \left[ I_b \right] \left\{ \frac{w}{B_f} \right\} = \left[ I_\sigma \right] \left\{ \sigma \right\} \qquad (5.35)$$

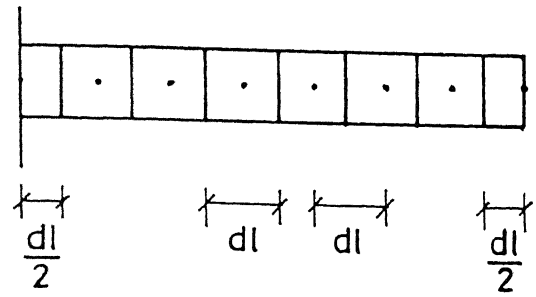


Fig. 5.5 Discretization of the Strip

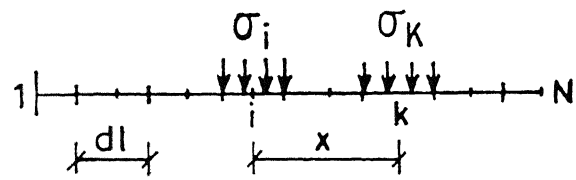


Fig. 5.6 Normal Stresses

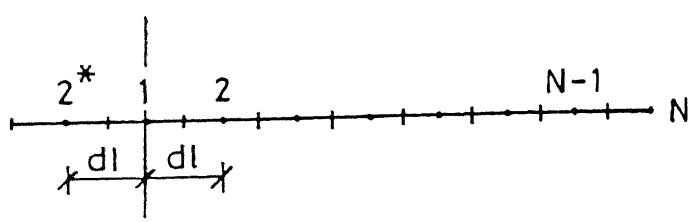


Fig. 5.7 Node 2* for Calculation of Moment at Node 1

where $K_r = \dfrac{E_r I_r}{\left(\frac{dl}{B_f}\right)^2 B_f^4}$

Eq. 5.35 gives the vertical displacement vector $\left\{ w/B_f \right\}$ of the points along the beam. Satisfying the compatibility of displacements at the nodes by equating the net soil displacements and the strip displacements the following equation is obtained

$$\left[\left[ I_b \right]\left[ I^r \right] + \frac{1}{E_r/E_s} \frac{(L_r/B_f)^2}{I_r/B_f^4\ (N-1)^2} \left[ I_\sigma \right]\right]\left\{ \sigma/q \right\} = \left[ I_b \right]\left\{ I^f \right\} \tag{5.36}$$

At this juncture, a dimensionless parameter, $K_B = \dfrac{E_r}{E_s} \dfrac{I_r}{B_f^4}$ is defined as the flexibility ratio which takes into account the flexural rigidity of the strip. Eq. 5.36 is rewritten as

$$\left[ A \right]\left\{ \sigma/q \right\} = \left[ I_b \right]\left\{ I^f \right\} \tag{5.37}$$

where $\left[ A \right] = \left[\left[ I_b \right]\left[ I^r \right] + \dfrac{(L_r/B_f)^2}{K_B (N-1)^2} \left[ I_\sigma \right]\right]$ is of size N-1xN and $\left\{ \sigma/q \right\}$ and $\left\{ I^f \right\}$ are vectors of size N.

The second boundary condition defined by Eq. 5.31 is now applied in terms of the stresses, $\left\{ \sigma \right\}$. In calculating the moment at node N, stresses mobilised along the whole length of the strip, i.e., $2L_r$ are to be considered. For every element i, there is an image element i′ over which the stresses are the same. The moment

at the $N^{th}$ node is written as

$$M_N = \sigma_1 \frac{dl}{2} 2B_r \left[ \left( (N-1)dl - \frac{dl}{4} \right) + \left( 2L_r - \{ (N-1)dl - \frac{dl}{4} \} \right) \right] + \sum_{i=2}^{N-1} \sigma_i dl \; 2B_r \left[ (N-i)dl + \left( 2L_r - (N-i)dl \right) \right] + \sigma_N \frac{dl}{2} 2B_r \left[ \frac{dl}{4} + \left( 2L_r - \frac{dl}{4} \right) \right] \quad (5.38)$$

Boundary condition 2 (Eq. 5.31) requires M to be zero at $x=L_r$. Hence equating Eq. 5.36 to zero one obtains

$$\sum_{i=2}^{N-1} \sigma_i + \frac{\sigma_1}{2} + \frac{\sigma_N}{2} = 0 \quad (5.39)$$

Eq. 5.39 is expressed in dimensionless form as

$$\sum_{i=2}^{N-1} \frac{\sigma_i}{q} + 0.5\left(\frac{\sigma_1}{q} + \frac{\sigma_N}{q}\right) = 0 \quad (5.40)$$

Eq. 5.40 implies that the force equilibrium for the strip is also satisfied. Substituting Eq. 5.40 in Eq. 5.37, N equations for the normalised normal stresses, $\{ \sigma/q \}$ are obtained. Once the stresses are obtained, the displacements are calculated using either Eq. 5.22 or Eq. 5.35. The settlement reduction coefficients (SRC) of the points along the surface are calculated in the same manner as explained for rigid inflexible strips in chapter 4.

## 5.5 Coupled Effect (Horizontal and Vertical Rigidity)

### Rigid Single Strip

Thus far, the rigidity of the strip in the horizontal and

vertical directions were considered separately. The horizontal and vertical displacements of the nodes along the strip, independently due to the shear and normal stresses apart from those due to the surface load were considered. In this section the influence of the shear stresses in causing vertical displacements and normal stresses in causing horizontal displacements are also coupled. The reinforcing strip now acts as an inextensible and inflexible one.

### 5.5.1 Problem Definition

The definition of the problem is the same as that for a single strip, i.e., a strip of size, $2L_r \times 2B_r$ is placed centrally below a rectangular area transmitting an uniform load of intensity q, at a depth $U_o$. The strip being rigid does not experience any elongation while it undergoes a uniform vertical translation due to the soil displacements.

### 5.5.2 Analysis

The discretizations of the loaded area and the reinforcing strip are the same as explained in chapter 3 or 4. The vectors of the horizontal and vertical displacements of the N nodes along the half-length of the strip due to the surface load, computed from Boussinesq's equations are

$$\left\{ \rho_x^f \right\} = \frac{B_f}{E_s} \left\{ I_x^f \right\} q \qquad (5.41)$$

and

$$\left\{ \rho_z^f \right\} = \frac{B_f}{E_s} \left\{ I_z^f \right\} q \qquad (5.42)$$

The horizontal displacements of the N nodes due to the mobilised shear stresses $\left\{ \sigma \right\}$ and the normal stresses $\left\{ \sigma \right\}$ computed from Mindlin's equations are

$$\left\{ \rho^{r}_{x\tau} \right\} = \frac{B_f}{E_s} \left[ I^{r}_{x\tau} \right] \left\{ \tau \right\} \qquad (5.43)$$

and

$$\left\{ \rho^{r}_{x\sigma} \right\} = \frac{B_f}{E_s} \left[ I^{r}_{x\sigma} \right] \left\{ \sigma \right\} \qquad (5.44)$$

Similarly, the vertical displacements of the N nodes due to the mobilised shear stresses and normal stresses obtained from Mindlin's equations are

$$\left\{ \rho^{r}_{z\tau} \right\} = \frac{B_f}{E_s} \left[ I^{r}_{z\tau} \right] \left\{ \tau \right\} \qquad (5.45)$$

and

$$\left\{ \rho^{r}_{z\sigma} \right\} = \frac{B_f}{E_s} \left[ I^{r}_{z\sigma} \right] \left\{ \sigma \right\} \qquad (5.46)$$

It is to be remembered that, as explained in section 4.2.1 the noraml stresses considered are the difference of the stresses acting on the top and bottom faces of the strip.

Combining Eqs. 5.43 and 5.44, the vector of horizontal displacements of the N nodes due to the shear and normal stresses are

$$\left\{ \rho^{r}_{x} \right\} = \frac{B_f}{E_s} \left[ I^{r}_{x} \right] \left\{ p \right\} \qquad (5.47)$$

where $\left\{ \rho_x^r \right\}$ is a vector of size N, $\left\{ P \right\}$ is a stress vector of size 2N and $\left[ I^r \right]$ is a matrix of size N x 2N. Further

$$\left\{ \rho_x^r \right\} = \left\{ \rho_{x\tau}^r \right\} + \left\{ \rho_{x\sigma}^r \right\} \tag{5.48}$$

$$\left\{ P \right\}^T = \left[ \left[ \tau \right] \left[ \sigma \right] \right] \tag{5.49}$$

$$\left[ I_x^r \right] = \left[ I_{x\tau}^r \; ; \; I_{x\sigma}^r \right] \tag{5.50}$$

Combining Eqs. 5.45 and 5.46, the vector of vertical displacements of the N nodes due to the stresses is

$$\left\{ \rho_z^r \right\} = \frac{B_f}{E_s} \left[ I_z^r \right] \left\{ P \right\} \tag{5.51}$$

where $\left\{ \rho_z^r \right\} = \left\{ \rho_{z\tau}^r \right\} + \left\{ \rho_{z\sigma}^r \right\}$ (5.52)

and

$$\left[ I_z^r \right] = \left[ I_{z\tau}^r \; ; \; I_{z\sigma}^r \right] \tag{5.53}$$

Satisfying the compatibility of displacements for the nodes as (i) the net horizontal displacements equal zero, and (ii) the net vertical displacements are equal to the rigid body displacement, $\delta_o$, one obtains

$$\left\{ \rho_x^f \right\} - \left\{ \rho_x^r \right\} = \left\{ 0 \right\} \tag{5.54}$$

and

$$\left\{ \rho_z^f \right\} - \left\{ \rho_z^r \right\} = \delta_o \left\{ 1 \right\} \tag{5.55}$$

Hence

$$\left[ I_x^r \right] \left\{ \frac{p}{q} \right\} = \left\{ I_x^f \right\} \tag{5.56}$$

and

$$\left[ I_z^r \right] \left\{ \frac{p}{q} \right\} = \left\{ I_z^f \right\} \tag{5.57}$$

Eq. 5.56 gives N equations for 2N stresses (N values of $\left\{ \tau/q \right\}$ and $\left\{ \sigma/q \right\}$ each) and Eq. 5.57 gives N equations in 2N stresses and a rigid body displacement. Combining Eq. 5.56 and 5.57 and satisfying the force equilibrium relation as in section 4.2.2, one obtains 2N+1 equations in N values of shear stresses, $\left\{ \tau/q \right\}$, and normal stresses, $\left\{ \sigma/q \right\}$ each, and a rigid body displacement, $\delta_o$, as

$$\left[ I^r \right] \left\{ \begin{matrix} \tau/q \\ \sigma/q \end{matrix} \right\} + \frac{\delta_o E_s}{B_f q} \left\{ \begin{matrix} 0 \\ 1 \end{matrix} \right\} = \left\{ I^f \right\} \tag{5.58}$$

where

$$\left[ I^r \right] = \left[ \begin{matrix} I_x^r \\ \hline I_z^r \end{matrix} \right] = \left[ \begin{matrix} I_{x\tau}^r & I_{x\sigma}^r \\ \hline I_{z\tau}^r & I_{z\sigma}^r \end{matrix} \right] \tag{5.59}$$

and

$$\left\{ I^f \right\}^T = \left\lfloor \left\lfloor I_x^f \right\rfloor \left\lfloor I_z^f \right\rfloor \right\rfloor \tag{5.60}$$

These equations are solved for the stresses on and the uniform displacement of the strip. Once the stresses are obtained the settlement reduction coefficients of points along the surface are calculated as explained in sections 3.2.2 for shear stresses and 4.2.2 for normal stresses.

### 5.5.3 Slip at the Interface

It is essential that the shear stresses moblised at the strip-soil interface do not exceed the frictional resistance available at the interface due to the normal stresses and overburden stresses at that depth so that slip is prevented. This condition may be expressed as

$$\mu \left( \frac{\sigma}{q} + \frac{\gamma B_f}{q} \frac{U_o}{B_f} \right) \geq \frac{\tau}{q} \qquad (5.61)$$

where $\mu$ is the coefficient of friction at the strip-soil interface, $\frac{\gamma B_f}{q} \frac{U_o}{B_f}$ is the normalised overburden stress, and $\sigma/q$ and $\tau/q$ are the normalised normal and shear stresses mobilised at the interface.

If this condition is not satisfied, the shear stresses are limited to the frictional resistance as

$$\frac{\tau}{q} = \mu \left( \frac{\sigma}{q} + \frac{\gamma B_f}{q} \frac{U_o}{B_f} \right) \qquad (5.62)$$

Eq. 5.61 is checked for stresses at all the elements. Wherever the condition is violated, Eq. 5.62 is applied. The shear stresses on elements where slip occurs are now known and these values are substituted in Eq. 5.58 which is solved for the stresses on the remaining elements.

## 5.6 Results and Discussion

The effects of the extensibility and flexural rigidity of the reinforcing strip on the stresses mobilised and settlement reduction of the points on the surface, are studied herein. As discussed in the section on analysis, the net displacement of the soil at the soil-strip interface is equated to the elongation or the flexural deformation of the strip, as the case may be. The discretizations of the loaded area, and of the reinforcing strip for shear interaction are the same as in section 3.6. The strip is discretized for flexure differently as discussed in section 5.4.2.

### 5.6.1 Extensible Strip

As in the case of a rigid strip (Chapter 3), the stresses mobilised at the interface are evaluated at the centre of each element. Apart from the parameters studied in section 3.6, the elongation ratio, $K_\tau$, defined as $K_\tau = E_r t_r / E_s B_f$ is also considered, where $E_r$ and $t_r$ are the elasticity modulus and the thickness of the strip respectively. $K_\tau = 0$ indicates absence of reinforcement (unreinforced soil) implying zero stress mobilisation, while $K_\tau = \infty$ implies presence of a rigid strip. The range of the ratio, $K_\tau$, in the parametric study is 5 to 5000. The upper limit of $K_\tau$ is restricted to 5000 because the results obtained for this value agree well with those for a rigid strip considered in chapter 3. Further, for this value of $K_\tau$, the elongations are negligibly small. The Poisson's ratio, $\nu_s$, is maintained at 0.3.

Fig. 5.8 presents the variation of the normalised shear stress, $\tau/q$, with the distance, $x/B_f$, along the half-length of the

strip for different $K_\tau$ values and for a strip of length, $L_r/B_f=2$, placed below a square loaded area with an aspect ratio, $L_f/B_f=1$ at a depth, $U_o/B_f=1$. For all values of the elongation ratio, $K_\tau$, the shear stresses are a maximum at a distance, $x/B_f=1$, i.e. below the edge of the loaded area. For a highly extensible strip with $K_\tau=5$, the stresses mobilised are the least, with the edge of the strip showing negative stresses. With an increase in the $K_\tau$ value, the stresses increase and are positive throughout the length. For strips with $K_\tau=5000$, the shear stresses are the same as those for a rigid strip considered in chapter 3. The maximum shear stress, $\tau/q$, is 0.8 in this case, and is observed at a distance, $x/B_f=1$. For strips with $K_\tau=5$, a small negative stress is observed near the centre. This negative stress is possibly mobilised due to two conflicting criteria. Due to symmetry of the problem, the displacements at and near the centre have to be zero or extremely small. However, since the tensile force at the centre is maximum and the strip is highly extensible, the displacement of node 1 could be significant. Thus the negative stress is a consequence of the need to satisfy these two mechanisms. The net lateral displacements for an extensible strip are high owing to the high elongations experienced by the strip. Hence, the displacements which the shear stresses have to counteract are less resulting in low shear stress values. As $K_\tau$ increases, the elongations in the strip decrease, consequently the displacements to be resisted by the interacting or mobilised shear stresses increase significantly.

The effect of the depth of placement, $U_o/B_f$, of a strip with $K_\tau=50$, and length, $L_r/B_f=2$, placed below a square area with,

$L_f/B_f=1$, on the normalised shear stresses, $\tau/q$, is depicted in Fig. 5.9. This figure shows a trend similar to the one seen in Fig. 3.14 for a rigid strip. A maxmimum stress of $\tau=0.672q$ is observed for strips placed at depth, $U_o/B_f=1$ at a distance, $x/B_f=1$ along the length of the strip. In contrast, rigid strips show a maximum stress of 0.8q at the same depth (Fig. 3.14). Because of the extensibility of the strip, the net displacements are relatively large resulting in smaller shear stress mobilisation at the soil-strip interface.

The variation of the tensile forces, $T/qB_f^2$, induced in the strip of length, $L_r/B_f=2$, placed under a square area with $L_f/B_f=1$, at a depth, $U_o/B_f=1$, for various $K_\tau$ values is presented in Fig. 5.10. The tension for the strip with, $K_\tau=5$ is the least owing to low shear stress mobilisation. Strips with $K_\tau=5000$ exhibit a tension of $0.105qB_f^2$ at the centre which compares very well with that for a rigid strip (Fig. 3.18). For highly extensible strips with $K_\tau=5$, the tension at the centre is $0.038qB_f^2$. Near the edge, these strips experience a small compression due to the mobilisation of negative stresses there at (Fig. 5.8)

Fig. 5.11 depicts the effect of the elongation ratio, $K_\tau$ on the elongation, $\delta E_s/B_f q$, of the strips of length, $L_r/B_f=2$, placed below square area ($L_f/B_f=1$) at a depth, $U_o=B_f$. As expected, strips with an elongation ratio, $K_\tau=5$ show maximum extension. The total elongation, $\delta E_s/B_f q$, of these strips is of the order of 0.067. The elongation is maximum for these strips at a distance, $x/B_f=1.5$ along the length of the strip. Beyond this distance, it decreases marginally as the strip is subjected to a small amount of compression in this zone. Elongations of the strips decrease with

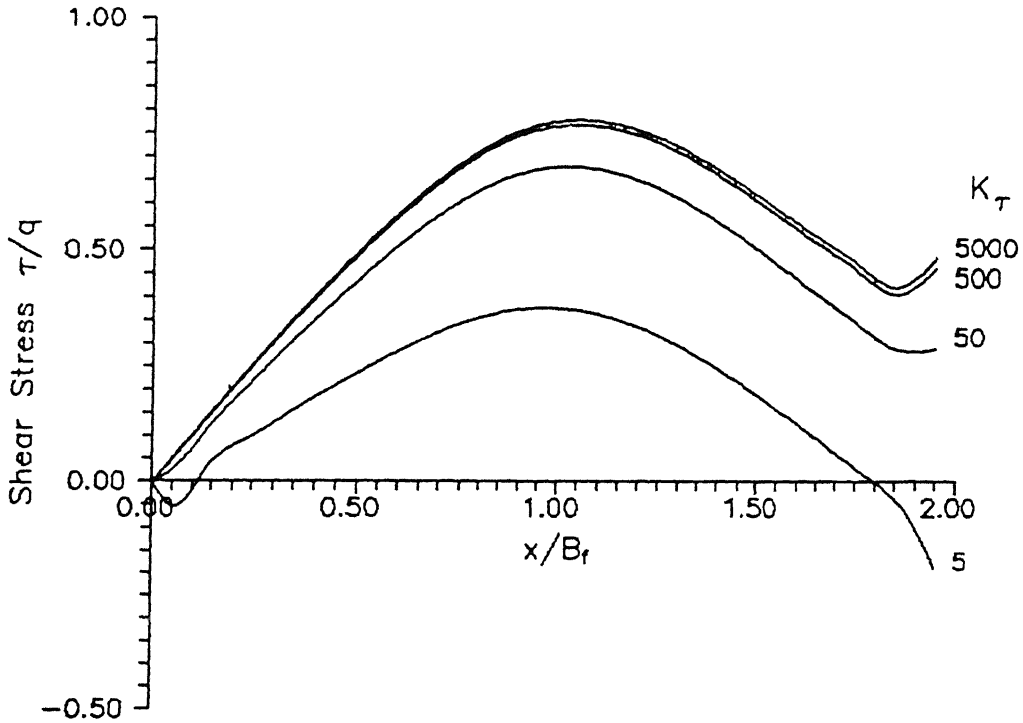


Fig. 5.8 Variation of Shear Stress with Distance for Different Elongation Ratios ($L_r/B_f$=2, $L_f/B_f$=1, $U_0/B_f$=1, $\nu_s$=0.3)

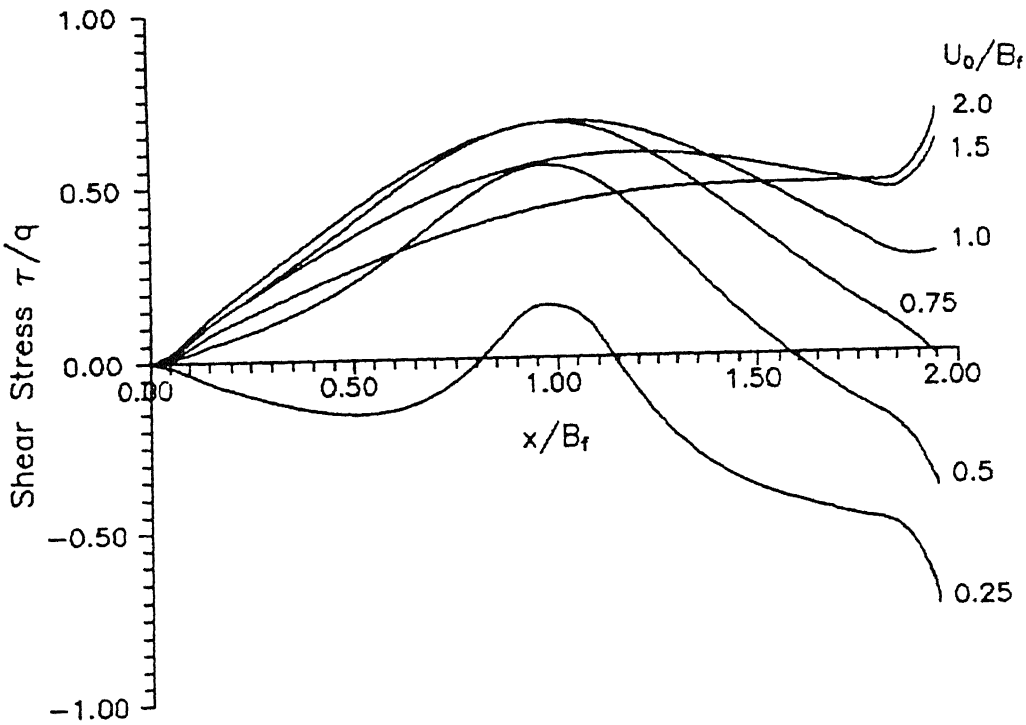


Fig. 5.9 Variation of Shear Stress with Distance for Different Depths of Placement of Strip ($L_r/B_f$=2, $L_f/B_f$=1, $K_\tau$=50, $\nu_s$=0.3)

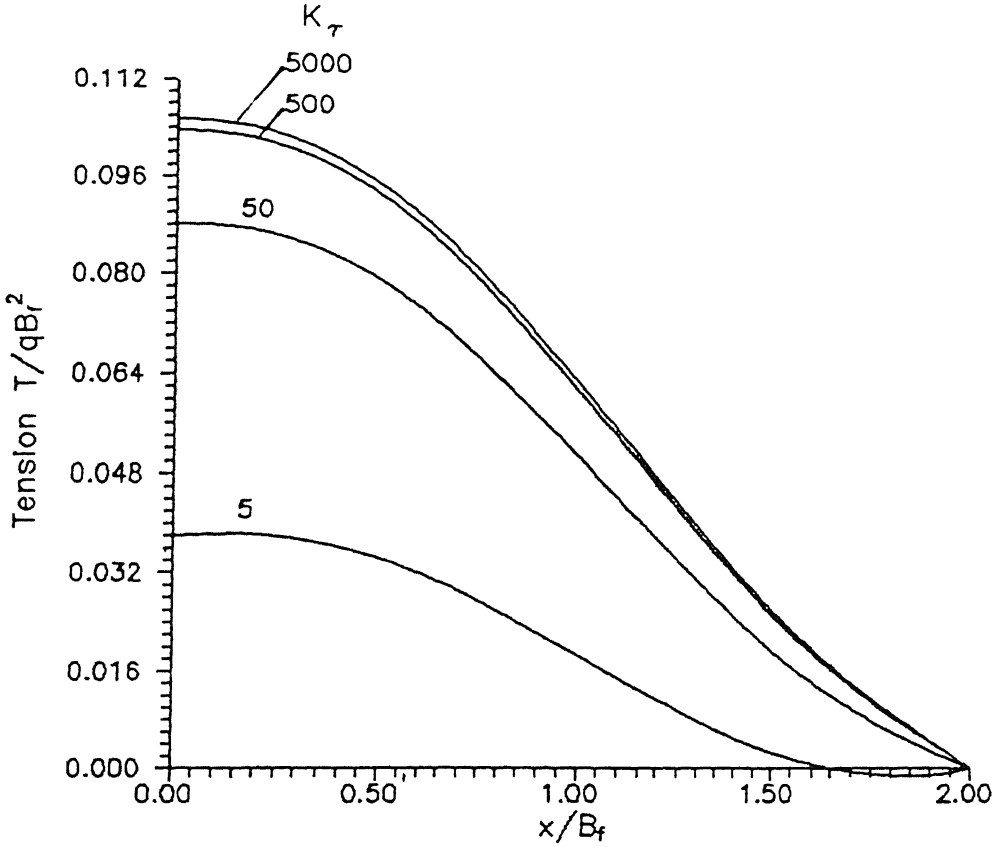


Fig. 5.10 Variation of Tension with Distance for Different Elongation Ratios ($L_r/B_f=2$, $L_f/B_f=1$, $U_o/B_f=1$, $\nu_s=0.3$)

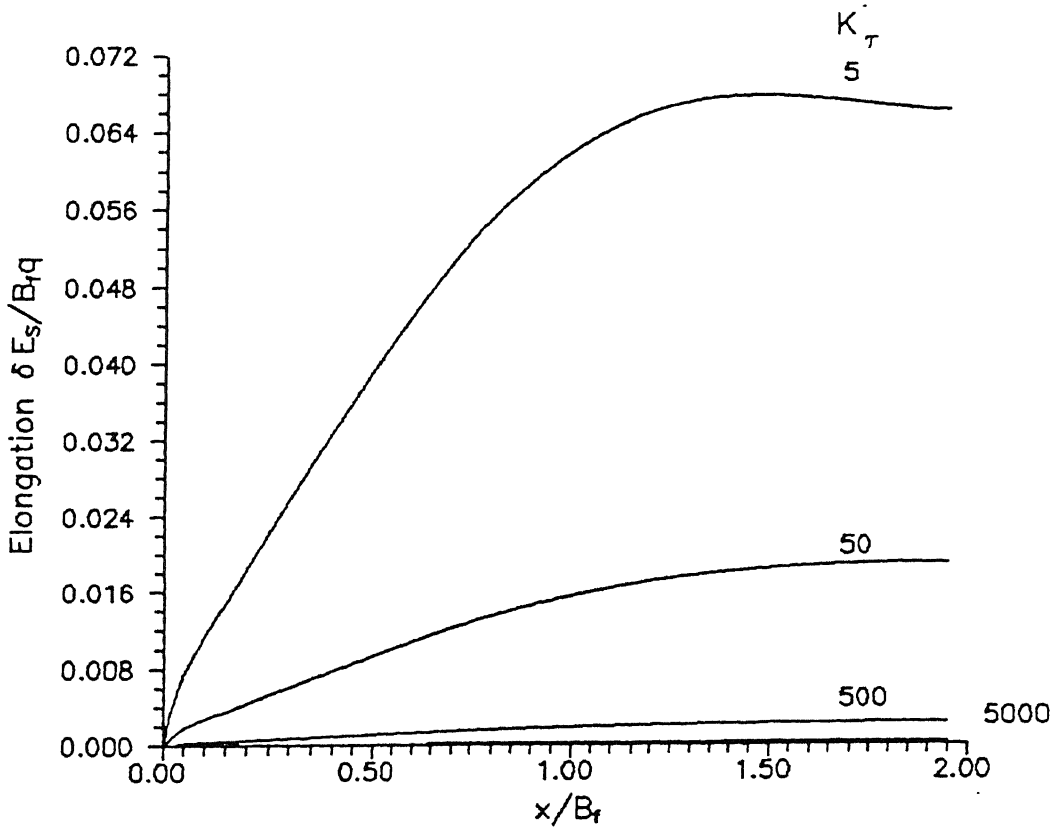


Fig. 5.11 Variation of Elongation with Distance for Different Elongation Ratios ($L_r/B_f=2$, $L_f/B_f=1$, $U_o/B_f=1$, $\nu_s=0.3$)

increasing values of $K_\tau$, as can be anticipated.

The variation of SRC with distance, $x_f/B_f$, along the surface for various $K_\tau$ values for strips of length, $L_r/B_f=2$, placed below a square area at a depth, $U_o=B_f$ is presented in Fig. 5.12. The trend for all the curves in this figure are similar to that for rigid strips placed at the same depth (Fig. 3.20). The SRC at the centre ($x_f/B_f=0$) and at the edge of the loaded area ($x_f/B_f=1$) for a highly extensible strip with $K_\tau=5$ are 0.0014 and 0.0001 respectively while those for a strip with $K_\tau=50$ are 0.00285 and 0.0007 respectively. As $K_\tau$ increases, the SRC values tend to those (0.00335 and 0.0009) of a rigid inextensible strip. The increase in SRC values with $K_\tau$ is a consequence of the increase in the shear stresses with $K_\tau$.

The effect of the elongation ratio, $K_\tau$, on the settlement reduction coefficient at the centre, $I_{sc}$, for various depths of placement, $U_o/B_f$, and for strips with length, $L_r/B_f=2$, placed below a square area is presented in Fig. 5.13. $I_{sc}$ is a maximum in the depth range, $U_o/B_f$ of 0.75 to 1 depending on the values of $K_\tau$. For low values of $K_\tau$ ($K_\tau=5$) a maximum $I_{sc}$ value of 0.0015 is observed at a depth $U_o/B_f=0.75$. At very shallow depths, $U_o/B_f=0.25$, the $I_{sc}$ values are practically zero. As $K_\tau$ increases, the $I_{sc}$ values at all depths tend to those of a rigid strip. The maximum $I_{sc}$ value for strips with $K_\tau=5$ are around 0.45 times that for a rigid strip.

Fig. 5.14 shows the plot of the settlement reduction

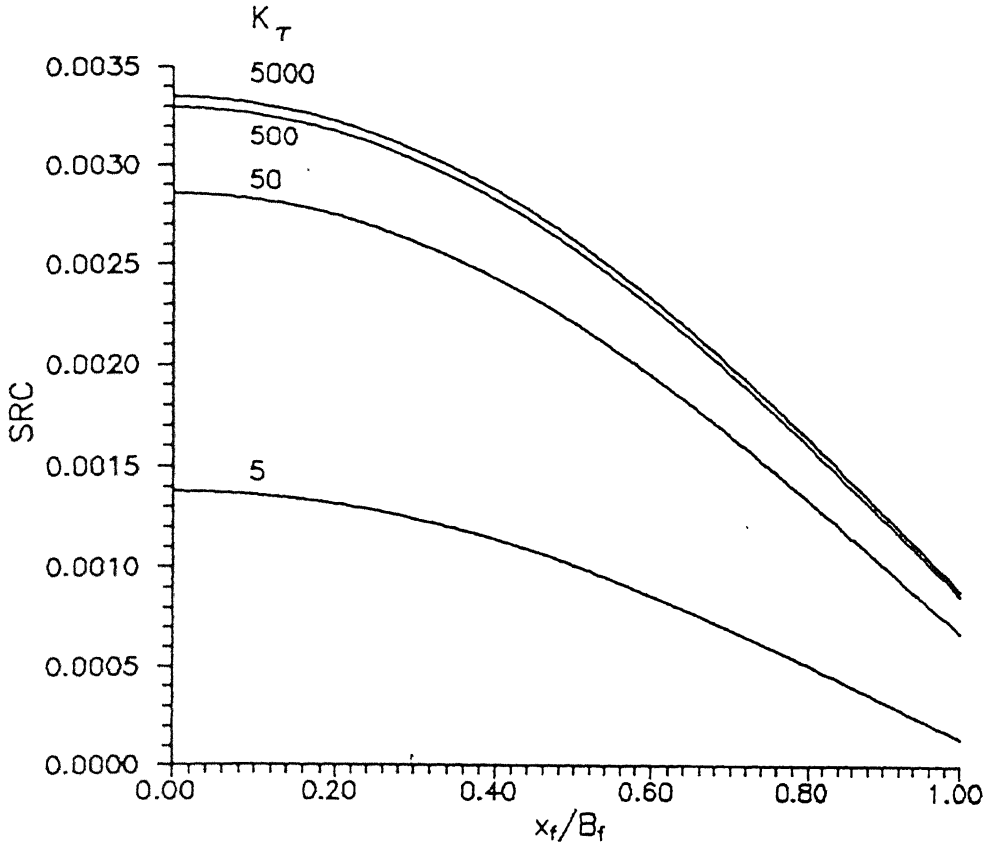


Fig. 5.12 Variation of SRC with Distance along Surface for Different Elongation Ratios ($L_r/B_f$=2, $L_f/B_f$=1, $U_o/B_f$=1, $\nu_s$=0.3)

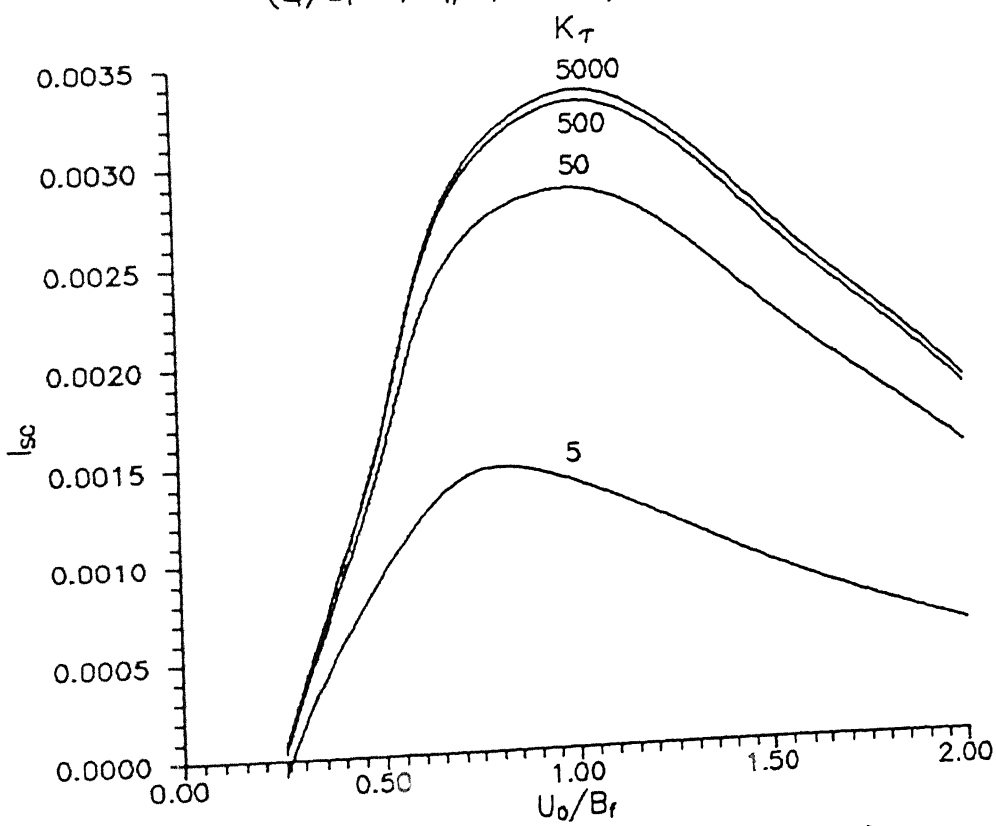


Fig. 5.13 Effect of Depth of Placement of Strip on $I_{sc}$ for Different Elongation Ratios ($L_r/B_f$=2, $L_f/B_f$=1, $\nu_s$=0.3)

coefficient, $I_{sc}$, at the centre of the loaded area versus the length, $L_r/B_f$, of the strip for various aspect ratios, $L_f/B_f$ of the loaded area and for a depth ratio, $U_o/B_f=1$ and elongation ratio, $K_\tau=50$. It is evident from the figure that the length of the strip, $L_r/B_f$, and aspect ratio, $L_f/B_f$, of the loaded area affect the $I_{sc}$ values considerably. The trends in this plot are similar to the ones observed for rigid strips. The $I_{sc}$ values, in this case have a smaller magnitude as compared to rigid strips. This is because, the stresses mobilised at the interface are smaller. The explanations for the trends observed, given for a rigid strip hold good in this case also.

The effect of the elongation ratio, $K_\tau$, on the $I_{sc}$ for strips located at various distances from x-axis, $S_y/B_f$, and for strips of length, $L_r/B_f=2$, placed below a square area at a depth $U_o/B_f=1$ is studied in Fig. 5.15. Here it is to be remembered that since two strips are placed off-centre, the half-width of the strips considered are $0.025B_f$ and the $I_{sc}$ values presented are for one strip only. The trends in the curves are very similar to those observed for rigid strips (Fig. 3.34). The distance, $S_y/B_f$, where the maximum $I_{sc}$ occurs is a function of $K_\tau$. For strips with small $K_\tau$ values, this distance is 0.15 whereas for rigid strips it is 0.25. At large $S_y/B_f$ values ($S_y/B_f>1.5$) the $I_{sc}$ values are negligibly small. The maximum value of $I_{sc}$ for strips with $K_\tau=5$ is 0.00075 which is around 0.33 times that for a rigid strip.

The effect of the length of the strip, $L_r/B_f$, on the ratio of the $I_{sc}$ for an extensible strip to that of a rigid one,

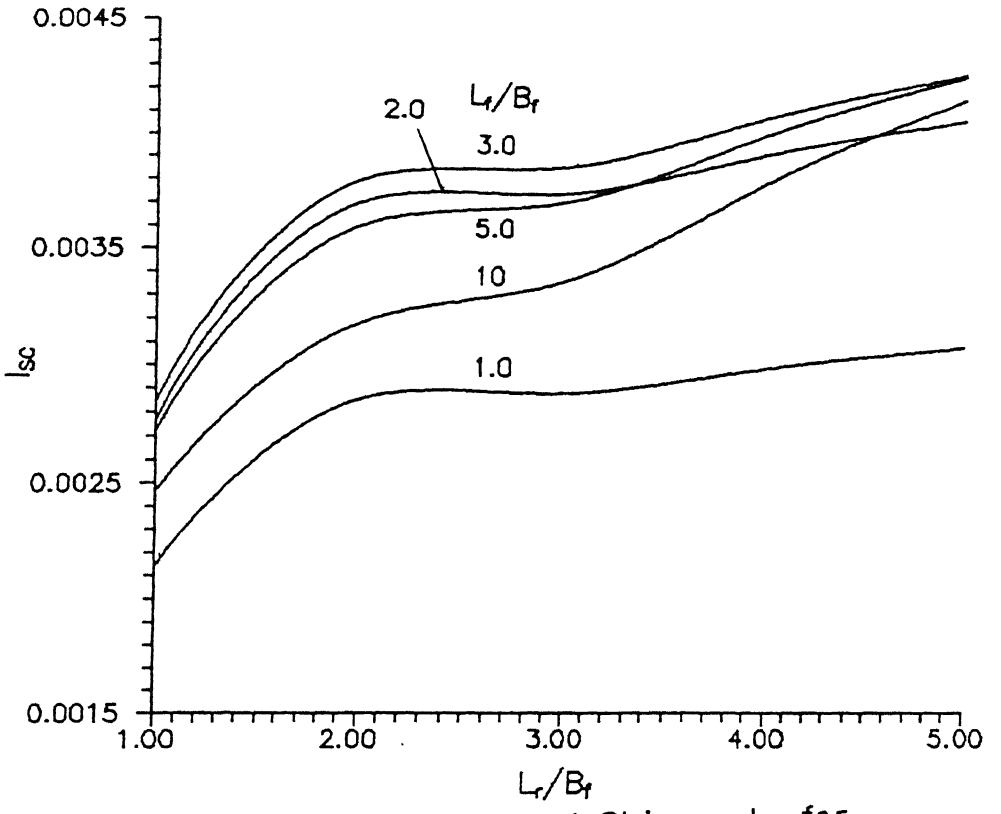


Fig. 5.14 Effect of Length of Strip on $I_{sc}$ for Different Aspect Ratios of Loaded Area ($U_0/B_f=1$, $K_T=50$, $\nu_s=0.3$)

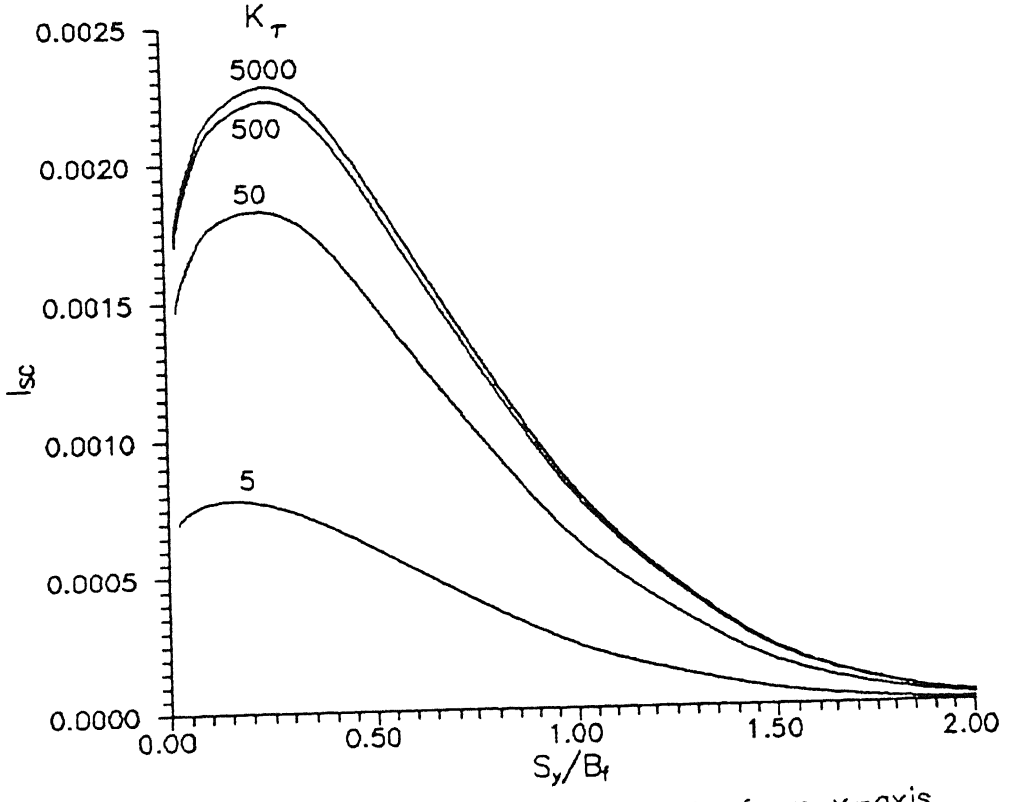


Fig. 5.15 Effect of Distance of Strip from x-axis on $I_{sc}$ for Different Elongation Ratios ($L_r/B_f=2$, $L_f/B_f=1$, $U_0/B_f=1$, $\nu_s=0.3$)

$I_{sc(e)}/I_{sc(r)}$, for various $K_\tau$ values and for strips placed below square areas at a depth, $U_o/B_f$=1, is depicted in Fig. 5.16. The ratio, $I_{sc(e)}/I_{sc(r)}$, increases with $K_\tau$ and tends to a value of 1 indicating that the strips behave as rigid ones. At low $K_\tau$ values ($K_\tau$=5), the values of the ratio are 0.56 and 0.4 for strips of length, $L_r/B_f$ equal to 1 and 2 respectively. Based on this plot, $I_{sc}$ values for extensible strips can be calculated from those for rigid strips by choosing the appropriate correction factor.

Based on the plots discussed so far it is clear that the variation of tension in the strip or the settlement reduction coefficient for an extensible strip follow the same trends as those for a rigid inextensible one. It is only the magnitude of these values that differ depending on the values of the elongation ratio, $K_\tau$, and the length, $L_r$. From Figs. 5.8 and 5.9 it is evident that the stresses mobilised are small for extensible strips resulting in low values of SRC and tensions in the strip. For design purposes, the SRC values for extensible strips may be obtained by multiplying the corresponding values for a rigid inextensible strip by an appropriate correction factor based on the value of the elongation ratio, $K_\tau$, and the length of the reinforcement. This factor is low for very low values of $K_\tau$. For strips with the ratio, $500>K_\tau>100$, a correction factor of 0.9 may be used for any length of the strip. For strips with $K_\tau \geq 500$ the correction factor can be taken as 1.0.

### 5.6.2 Flexible Strip

The strip, as mentioned in section 5.4 is modelled to behave

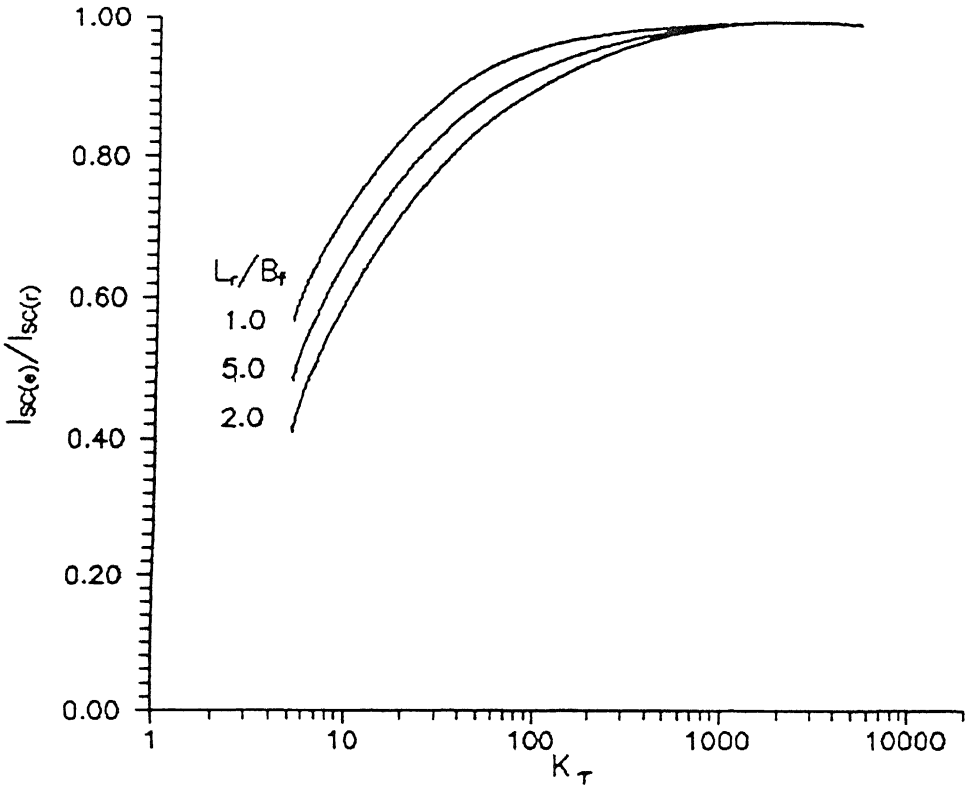


Fig. 5.16 Effect of Elongation Ratio on Ratio of $I_{sc}$ for Extensible and Rigid Strip, for Different Strip Lengths ($U_0/B_f=1$, $L_f/B_f=1$, $\nu_s=0.3$)

as a beam. The second order differential equation given in Eq. 5.25 is solved using the finite-difference technique. The stresses and SRC obtained with $dl=0.1B_f$ were compared with those obtained with a finer discretization of $0.05B_f$. There wasn't any significant improvement in the values as a consequence of this finer element size. The nodes were selected in such a manner that the boundary conditions for the beam may be satisfied without any difficulty. It is to be noted at this juncture that due to edge effect, the stresses of a point at the edge of the strip tend to infinity. Hence, if the node is considered to be exactly at the edge of the strip, i.e, at $x=L_r$, then the stresses resulting from the solution of the simultaneous equations given by Eq. 5.37 are highly sensitive to the value of the stress at the edge of the strip which is very high. As a result, the variation of stresses along the strip is erratic. In order to eliminate or minimise this inconsistency, the last node i.e, the $N^{th}$ node is considered to be not at the edge but at a distance of dl/4 from the edge (Fig. 5.17). The stress at this point is definitely a finite quantity and hence the solution obtained for normal stresses is stable. For the beam equations the boundary conditions for $x=L_r$ are applied at node N which is just at a distance of dl/4, i.e, $0.025B_f$ ($0.1B_f/4$) from the edge.

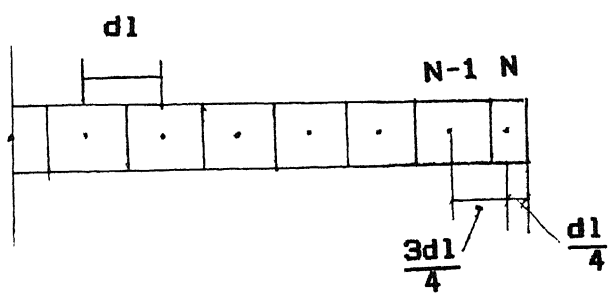


Fig. 5.17 Discretization for Beam

The effects of the various parameters mentioned in chapter 4, are studied on the normal stresses mobilised and the SRC at the surface. The main parameter considered in addition to these, is the flexibility ratio of the strip, $K_B$, defined as $E_r I_r / E_s B_f^4$. $K_B=0$ indicates no (or infinitely flexible) reinforcement while $K_B=\infty$ represents a rigid strip. The range of $K_B$ considered in this analysis is $10^{-2}$ to $10^2$. The upper limit of $K_B$ is limited to $10^2$ since for this value the strip behaves as a rigid one. All parameters are studied for a Poisson`s ratio, $\nu_s=0.3$

Fig. 5.18 presents the variation of the normalised normal stress, $\sigma/q$, with the distance, $x/B_f$, along the strip for various values of the flexibility ratio, $K_B$, and for strips of length, $L_r/B_f=2$ placed below a square area at a depth $U_o/B_f=1$. The stresses for strips with low $K_B$ values ($K_B=10^{-2}$) are practically zero. As $K_B$ increases, the stresses increase and tend close to those observed for rigid strips. For intermediate values ($K_B=1$), the stresses, as expected are maximum at the centre ($x/B_f=0$) and decrease with distance, $x/B_f$. The stresses change sign close to a point at a distance, $x/B_f=1$, i.e near the edge of the loaded area and tend to very large negative values at the edge of the strip. The peaking of stress is due to the edge effect. For strips with $K_B<10^2$, the stresses are less compared to those for a rigid strip and consequently the edge stresses are also smaller. For strips with low $K_B$ values the flexural deflections are high. These deflections tend to the vertical displacements of the soil due to the surface loading alone (as $K_B$ decreases). The difference between the soil displacements and the strip deflections being

small, the normal stresses mobilised in order to counteract this difference in displacements is small. As $K_B$ increases, the flexural deflections decrease and for $K_B>10^2$, the deflections are uniform as for a rigid strip. The difference between the soil displacements due to applied surface loading alone and the actual strip deflections are high, and hence, the stresses mobilised also are high.

The effect of the depth of strip, $U_o/B_f$, on the normalised normal stresses, $\sigma/q$, for strips with $K_B=1$ and length $L_r/B_f=2$, placed below a square area ($L_f/B_f=1$), is depicted in Fig. 5.19. The variation of the stresses with distance, $x/B_f$, along the strip is similar to those for a rigid strip (Fig. 4.11). Maximum stresses are observed for strips at shallow depths. At a depth $U_o/B_f=0.25$ the stress, $\sigma/q$, at $x/B_f=0$ is 3.1 while for a rigid strip it is of the order of 4.25. With increasing depth of the strip the stresses decrease and consequently the peak negative stresses at the strip edge also decrease.

Fig. 5.20 presents the variation of the strip deflections, $wE_s/B_fq$, with the distance, $x/B_f$, along the strip for various $K_B$ values, and for strips of length, $L_r/B_f=2$, placed at a depth, $U_o/B_f=1$, below a square area. It is seen that for strips with low $K_B$ values ($K_B=10^{-2}$) the deflections tend to the displacements of the soil due to surface loading. At the centre, the deflection, $wE_s/B_fq$, is 1.34 while at the edge it is 0.6. For strips with $K_B=1$, the corresponding displacements are 1.12 and 0.82 respectively. With $K_B$ increasing to $10^2$, the deflections equal

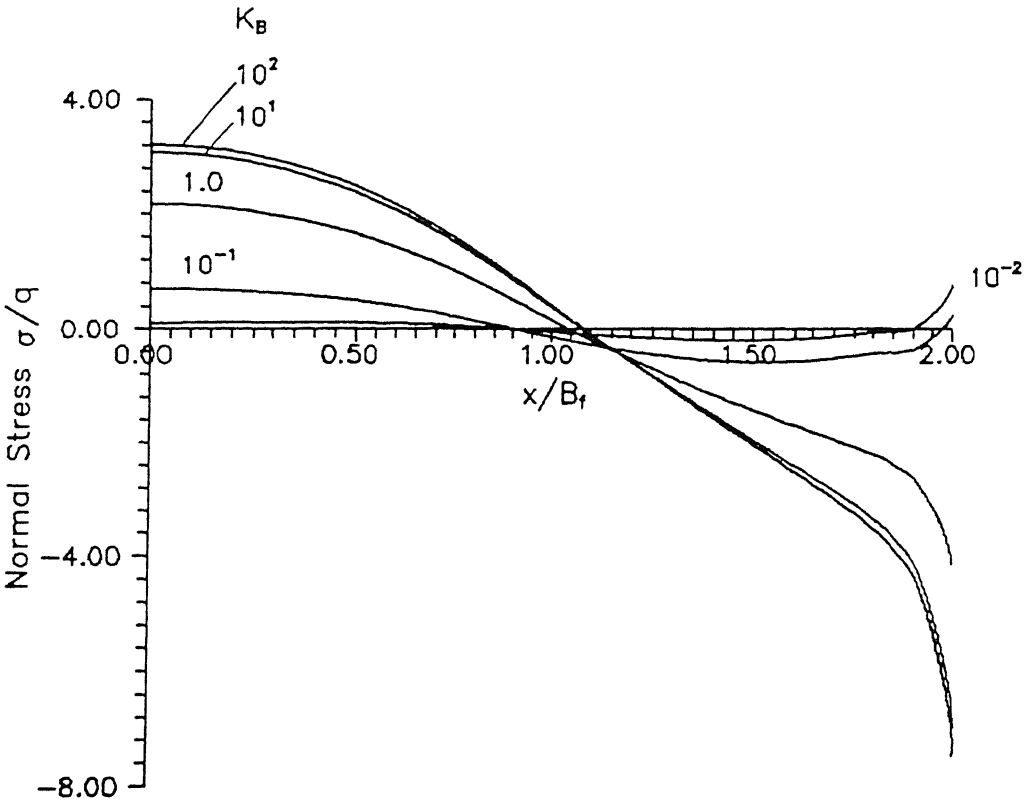


Fig. 5.18 Variation of Normal Stress with Distance for Different Flexibility Ratios ($L_r/B_f$=2, $L_f/B_f$=1, $U_0/B_f$=1, $\nu_s$=0.3)

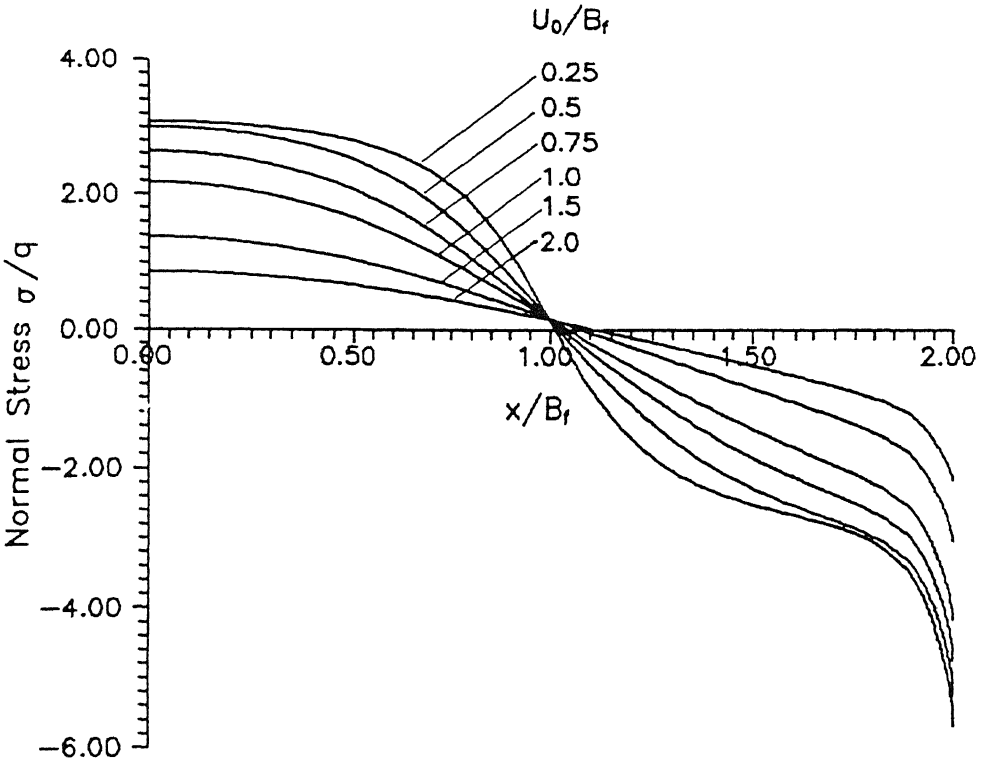


Fig. 5.19 Variation of Normal Stress with Distance for Different Depths of Placement of Strip ($L_r/B_f$=2, $L_f/B_f$=1, $K_B$=1, $\nu_s$=0.3)

those for a rigid strip and are equal to the rigid body displacement, $\delta_o E_s/B_f q$, of 0.99.

The effect of flexibility ratio, $K_B$ on the settlement reduction coefficient, SRC, on the surface for strips of length, $L_r/B_f=2$, placed below a square area at a depth, $U_o/B_f=1$, is shown in Fig. 5.21. The SRC is maximum at the centre and decreases with the distance, $x_f/B_f$, along the surface for all $K_B$ values. For strips with very low values of the flexibility ratio ($K_B=10^{-2}$), the SRC is negligibly small. This is obvious because the stresses are very small (Fig. 5.18) for the highly flexible strips. As $K_B$ increases, the flexural rigidity of the strips become prominent, the stresses mobilised increase and consequently the SRC values increase. For strips with $K_B=10^2$, the SRC values coincide with those for a rigid strip (Fig. 4.16) with the centre and edge exhibiting SRC values of 0.048 and 0.013 respectively. The corresponding values of SRC for strips with an intermediate value of the flexibility ratio ($K_B=1$) are 0.29 and 0.008. The SRC at the centre for strips with $K_B=1$ is about 0.6 times that of a rigid inflexible one.

Fig. 5.22 presents the effect of $K_B$ on the SRC at the centre of the loaded area, $I_{sc}$, for different depths, $U_o/B_f$, of the strip of length, $L_r/B_f=2$ placed below a square area. The trends of the curves are again similar to those of a rigid strip (Fig. 4.20) with maximum $I_{sc}$ being observed at shallow depths. The $I_{sc}$ value decreases rapidly with depth of placement of strip, since the stresses mobilised decrease and the influence of the strips in

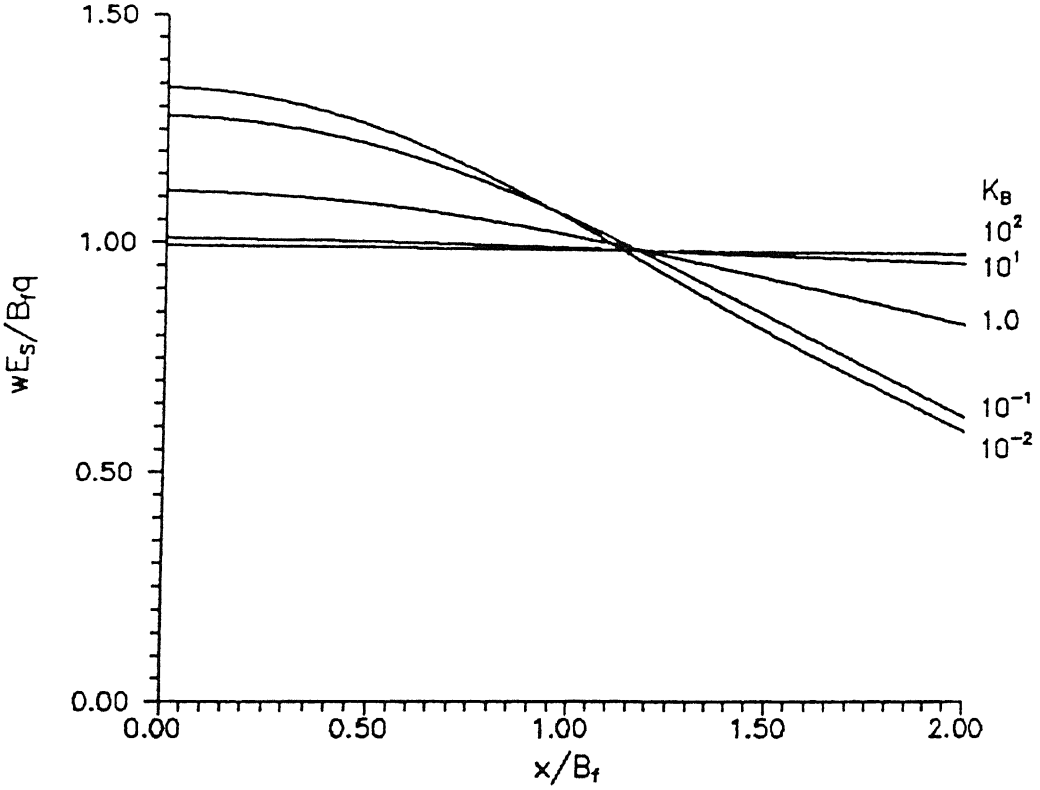


Fig. 5.20 Variation of Strip Deflection with Distance for Different Flexibility Ratios ($L_r/B_f$=2, $L_f/B_f$=1, $U_0/B_f$=1, $\nu_s$=0.3)

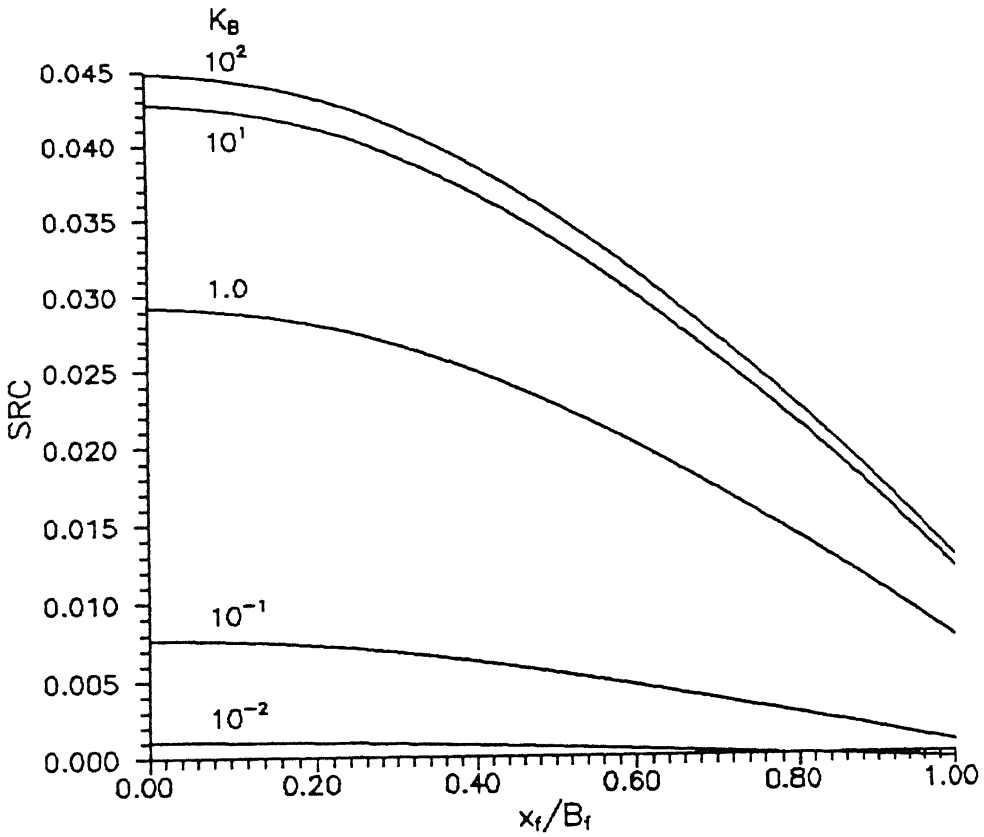


Fig. 5.21 Variation of SRC with Distance along Surface for Different Flexibility Ratios ($L_r/B_f$=2, $L_f/B_f$=1, $U_0/B_f$=1, $\nu_s$=0.3)

causing settlement reduction reduces. Highly flexible strips show negligibly small $I_{sc}$ values. Strips with $K_B=10^2$ show an $I_{sc}$ value of 0.19 at a depth, $U_o/B_f=0.25$, which is equal to the value for a rigid strip. As the depth increases, the effect of $K_B$ on $I_{sc}$ decreases. At great depths, ($U_o/B_f \geq 1.5$), $I_{sc}$ values are very small. The $I_{sc}$ value for strips with $K_B=1$ is 0.135 at a depth, $U_o/B_f=0.25$, which is about 0.7 times the value for a rigid strip.

The effect of the aspect ratio, $L_f/B_f$, of the loaded area on $I_{sc}$ values, for different lengths of the strip, $L_r/B_f$, and for strips with $K_B=1$, and placed at a depth, $U_o/B_f=1$ is depicted in Fig. 5.23. It is clear from the figure that $I_{sc}$ values increase with the length of the strip, $L_r/B_f$, and the aspect ratio, $L_f/B_f$ of the loaded area. As observed in Fig. 4.21 longer rectangles show higher $I_{sc}$ values for all lengths of the strip. The increase in the $I_{sc}$ values from $L_f/B_f=1$ to 2 is significant while the increase is less for further increase in the aspect ratio from 2 to 10. For rigid strips (Fig. 4.21) it is seen that $I_{sc}$ values increase monotonically with the length of the strips, $L_r/B_f$, while for strips with $K_B=1$ the increase in $I_{sc}$ is gradual beyond a length, $L_r/B_f$ of 2. The reason for this may be attributed to the low normal stress mobilisation for flexible strips. The $I_{sc}$ values are less compared to those for rigid strips. For the length of strips, $L_r/B_f=5$, the $I_{sc}$ values for aspect ratio, $L_f/B_f=1$ and 10 are 0.035 and 0.053 respectively, while the corresponding values for a rigid strip are 0.125 and 0.245 respectively. Thus for strips with $K_B=1$ the $I_{sc}$ values for $L_r/B_f=1$ and 5 are about 0.28 times and 0.22 times the values for a rigid strip.

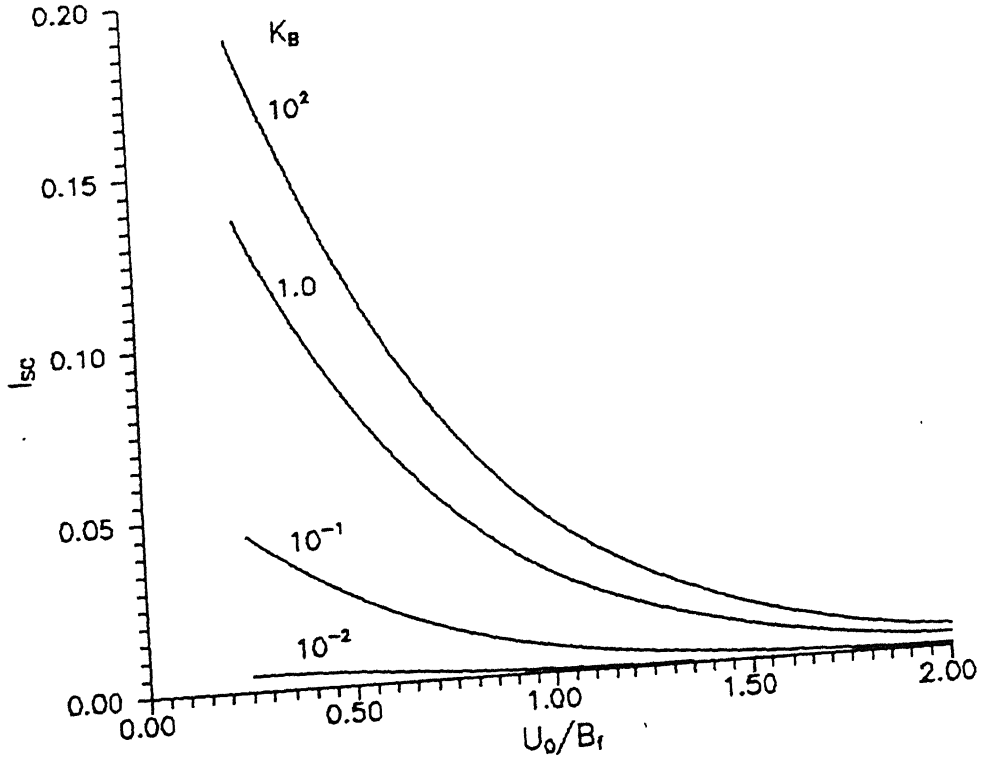


Fig. 5.22 Effect of Depth of Strip Placement on $I_{sc}$ for Different Flexibility Ratios ($L_r/B_f$=2, $L_f/B_f$=1, $\nu_s$=0.3)

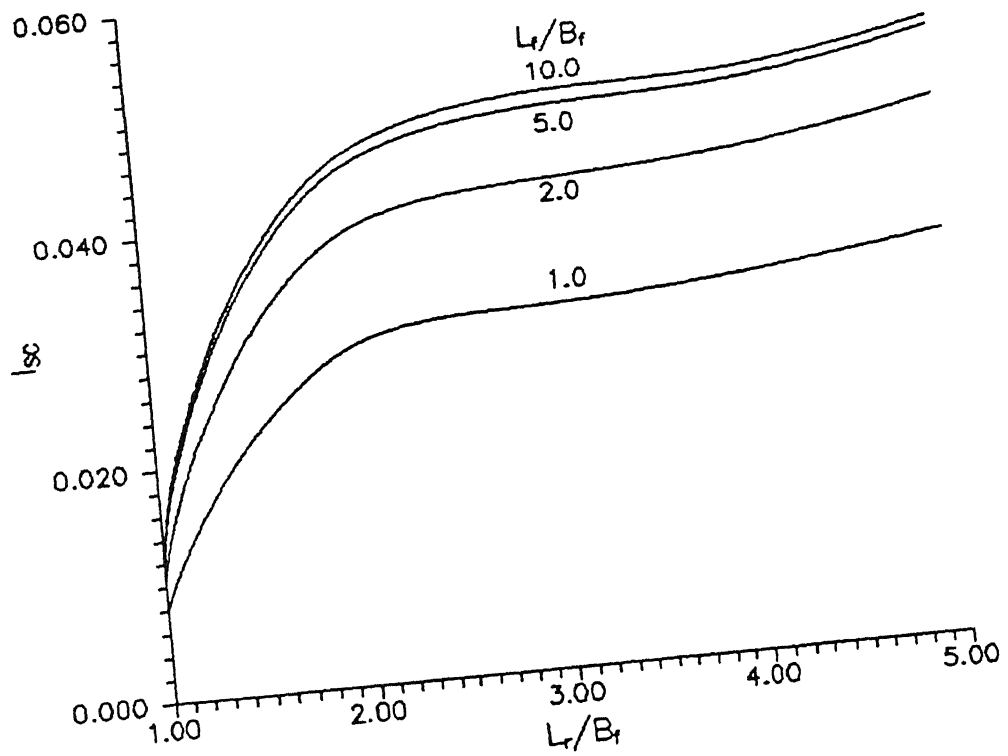


Fig. 5.23 Effect of Length of Strip on $I_{sc}$ for Different Aspect Ratios of Loaded Area ($U_o/B_f$=1, $K_B$=1, $\nu_s$=0.3)

The variation of $I_{sc}$ with the distance of the strip, $S_y/B_f$, from the x-axis for various $K_B$ values and for strips with length, $L_r/B_f=2$ placed below a square area at a depth, $U_o/B_f=1$, is presented in Fig. 5.24. It is to be remembered here that, for strips placed off-centrally the half-width of the strips, $B_r$ is $0.025B_f$. Further, the settlement reduction is calculated for one strip only. For the estimation of the effect of both the strips on the settlement reduction, these values are to be doubled. In the figure, the trends are similar to those observed for rigid strips (Fig. 4.27). Maximum $I_{sc}$ values occur for strips at a distance, $S_y/B_f=0.25$, from the x-axis. As $S_y/B_f$ increases beyond 0.25, $I_{sc}$ drops rapidly. The reason for this trend is as discussed for rigid strips in Fig. 4.27. Strips with very small $K_B$ values show negligible $I_{sc}$ values. $I_{sc}$ for strips with intermediate $K_B$ values ($K_B=1$), placed at a distance $S_y/B_f=0.25$ is 0.021 while for strips with $K_B=10^2$ it is 0.0295 which coincides with that of a rigid strip.

The effect of the length, $L_r/B_f$, of the strips on the ratio of $I_{sc}$ for a flexible strip to that of a rigid one, $I_{sc(f)}/I_{sc(r)}$ for various flexibility ratios, is presented in Fig. 5.25. It is evident that the length of the strip affects this ratio considerably. For shorter strips with $L_r/B_f=1$, the ratio, $I_{sc(f)}/I_{sc(r)}>0.9$ for $K_B>0.5$ while for strips with $L_r/B_f=5$ it is equal to 0.9 for $K_B=100$. For $K_B=1$, strips of length, $L_r/B_f=1$ are rigid while the ratio is around 0.2 for strips of length $L_r/B_f=5$. The reason for this is that for shorter strips the difference in vertical displacement at the centre and edge of the strip due to

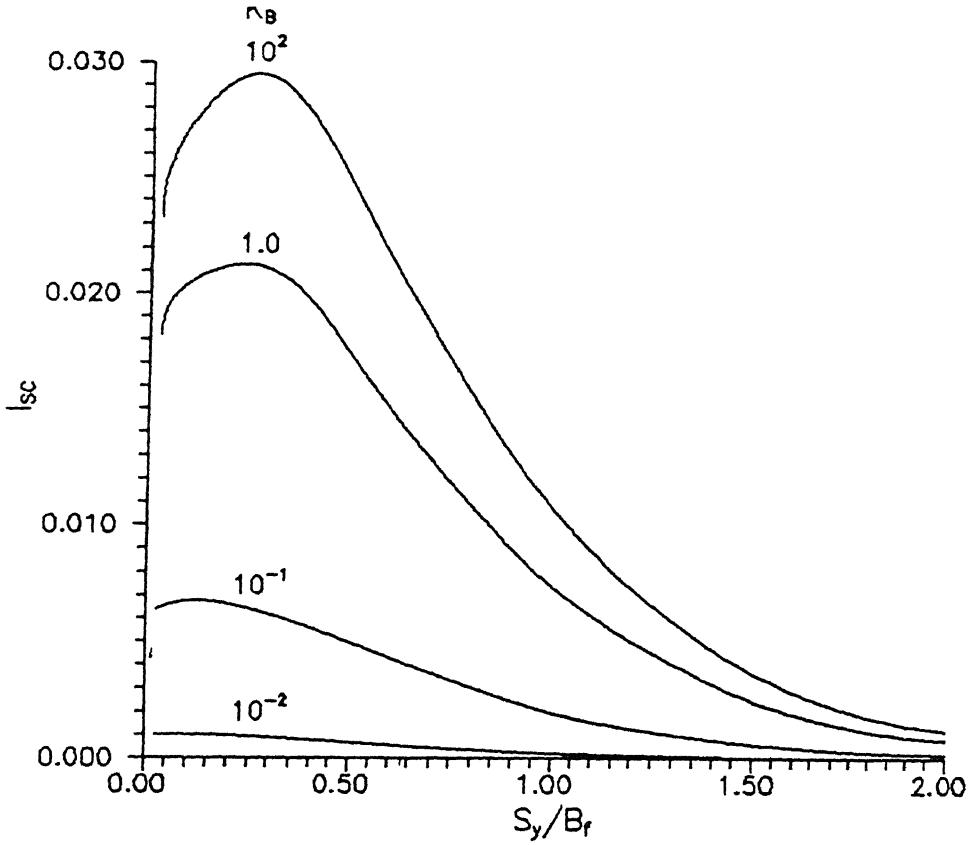


Fig. 5.24 Effect of Distance of Strip from x-axis on $I_{sc}$ for Different Flexibility Ratios ($L_f/B_f=2$, $U_o/B_f=1$, $L_f/B_f=1$, $\nu_s=0.3$)

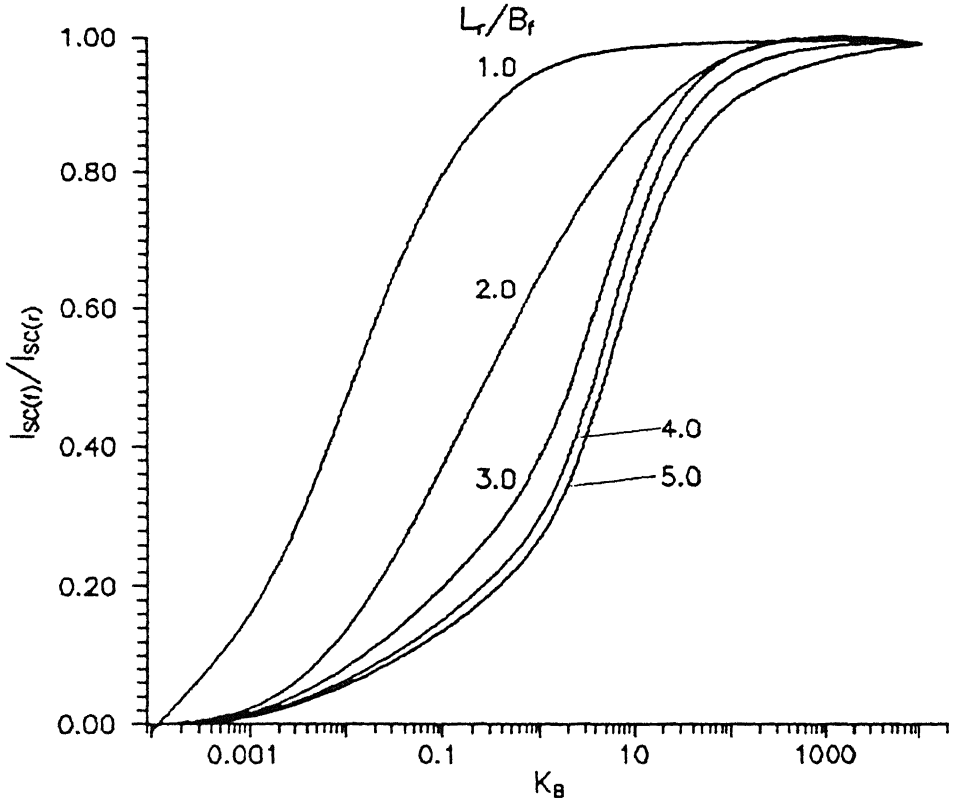


Fig. 5.25 Effcet of Flexibility Ratio on Ratio of $I_{sc}$ for Flexible and Rigid Strips, for Different Strip Lengths ($L_f/B_f=1$, $U_o/B_f=1$, $\nu_s=0.3$)

surface loading is small and hence the flexural rigidity required to deform the strip uniformly is small. On the other hand, this difference in displacements for longer strips is high and hence a higher flexural rigidity is required to cause the strips to displace uniformly. This figure can be used as a design chart. Knowing the flexibility ratio of a strip, the settlement reduction at the centre can be evaluated by multiplying those values for a rigid strip by a suitable correction factor obtained from this figure.

From the illustrations seen thus far, it is clear that for very flexible strips the stresses mobilised are very small. The normal stresses tend to those for a rigid strip with increase in the flexibility ratio. Consequently, as $K_B$ increases the displacements at the soil-strip interface also change from those of soil displacements due to the applied loading alone to a uniform rigid body translation. The variations in the calculated quantities, viz., stresses and settlement reduction coefficients for the flexibility ratio ranging from $10^{-2}$ (for a highly flexible case) to $10^{2}$ (a rigid strip) are similar to those considered in chapter 4. It is also perceived that the relative rigidity of the strip does not only depend on the flexibility ($E_r I_r$) but also on the length of the strip, $L_r$. $K_B$=1 is sufficient to make a strip of length, $L_r/B_f$=1 behave as a rigid one while a value of $K_B$=500 is necessary to make a strip of length, $L_r/B_f$=5 behave as a sufficiently rigid one. Fig. 5.25 can be conveniently used for strips below square areas at a depth, $U_o/B_f$=1, to predict the $I_{sc}$ values for flexible strips from those of a rigid one.

### 5.6.3 Coupled Shear and Normal Stress Interactions

The coupled effect of the shear and normal stresses for a rigid strip are considered. This implies that the effect of the shear stresses on vertical displacements and vice-versa are also accounted for. The shear and normal stresses mobilised at the interface are evaluated.

The variation of the normalised shear stress, $\tau/q$, with distance, $x/B_f$ along the length of the strip of length, $L_r/B_f=2$, placed at various depths, $U_o/B_f$, below a square area ($L_f/B_f=1$) is presented in Fig. 5.26. It is evident that the shear stresses follow exactly the same trend as for the case where the shear interactions alone were considered (Fig. 3.14). The magnitude of the stresses are marginally smaller as compared to Fig. 3.14 but for all practical purposes it may be stated that there is no difference in the magnitudes of the shear stresses.

Fig. 5.27 depicts the variation of the normalised normal stresses, $\sigma/q$, along the length of the strip described in the previous paragraph. Here again, it can be seen that the stresses follow the same trend as for the case where the normal stress interactions alone were considered (Fig. 4.11). The difference in the magnitudes of the stresses, too is marginal. From Figs. 5.26 and 5.27 it is clear that the effect of shear stresses in causing vertical displacements and normal stresses in producing horizontal displacements is negligible. It, hence follows that mechanisms considered individually result in accurate values of shear and normal stresses.

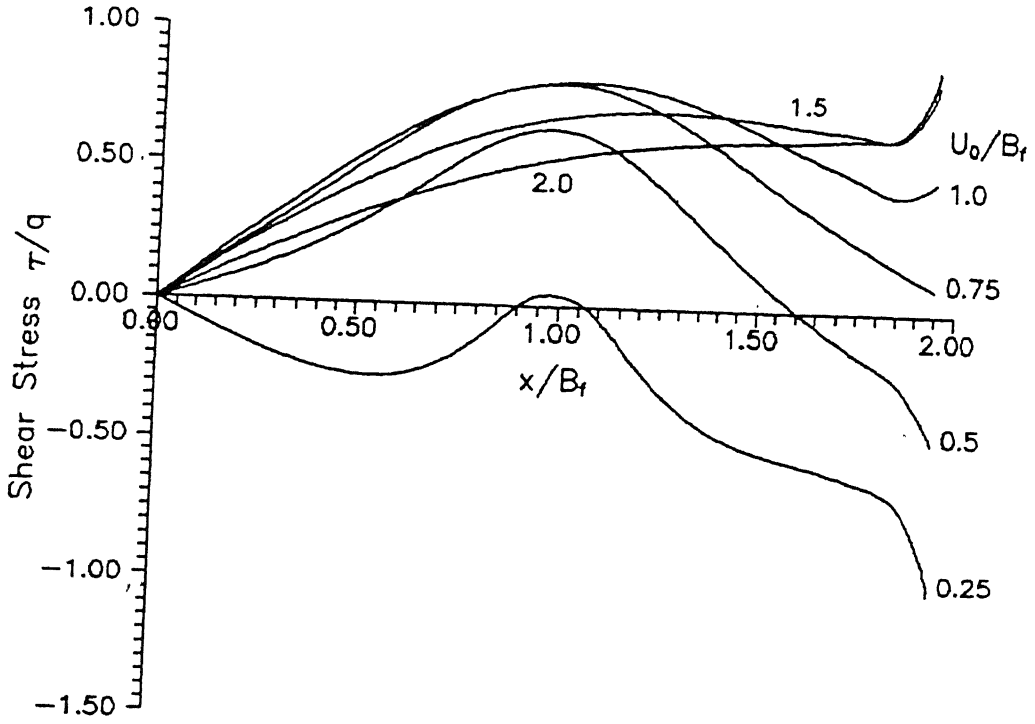


Fig. 5.26 Variation of Shear Stress with Distance for Different Depths of Strip (Coupled Effect) ($L_r/B_f$=2, $L_f/B_f$=1, $\nu_s$=0.3)

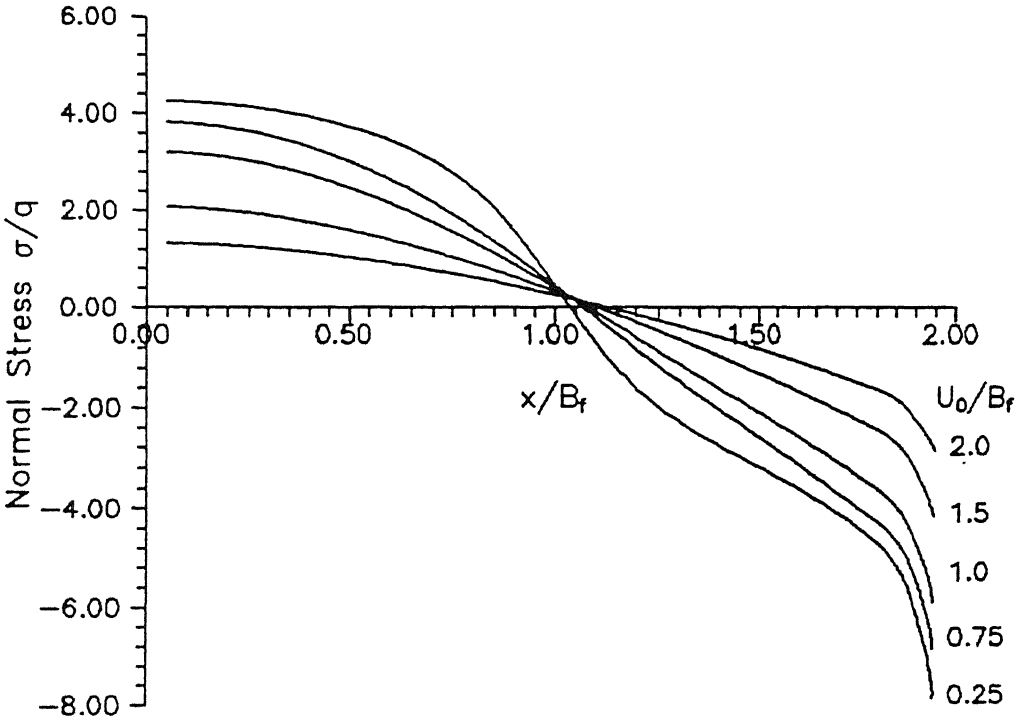


Fig. 5.27. Variation of Normal Stress with Distance for Different Depths of Strip (Coupled Effect) ($L_r/B_f$=2, $L_f/B_f$=1, $\nu_s$=0.3)

The effect of both the stresses in causing reduction of settlements of points along the surface is depicted in Fig. 5.28. This figure presents the variation of SRC with distance, $x_f/B_f$, for strips of various lengths, $L_r/B_f$, placed below a square area at a depth, $U_o/B_f=1$. The curves follow the same trend as those for a rigid strip undergoing uniform vertical displacement (Fig. 4.16). The magnitudes of the SRC values are also the same as those observed in Fig. 4.16. In fact, the magnitudes are equal to the summation of the SRC values for a rigid strip where shear (Fig. 3.20) and normal (Fig. 4.16) stresses are taken into account separately. It so turns out that the SRC values due to shear stresses are much smaller than those due to normal stresses and hence the SRC values for the coupled case are very close to those due to normal stresses alone.

It can hence be concluded that settlement reduction of points on the surface for a rigid strip result predominantly due to the normal stress mobilisation. For design purposes it is sufficient if SRC values due to normal stresses alone are considered. Further, these values will be on the conservative side.

### 5.6.4 Slip at the interface

Fig. 5.29 shows the variation of the normalised shear stress, $\tau/q$, with the distance, $x/B_f$, for different coefficient of friction values, $\mu$, for an overburden stress ratio, $\gamma B_f/q=0.5$. The results are for strips of length, $L_r/B_f=2$, placed at a depth, $U_o/B_f=1$, below a square loaded area. The dotted line depicts the shear stress variation for the coupled case without slip. It is

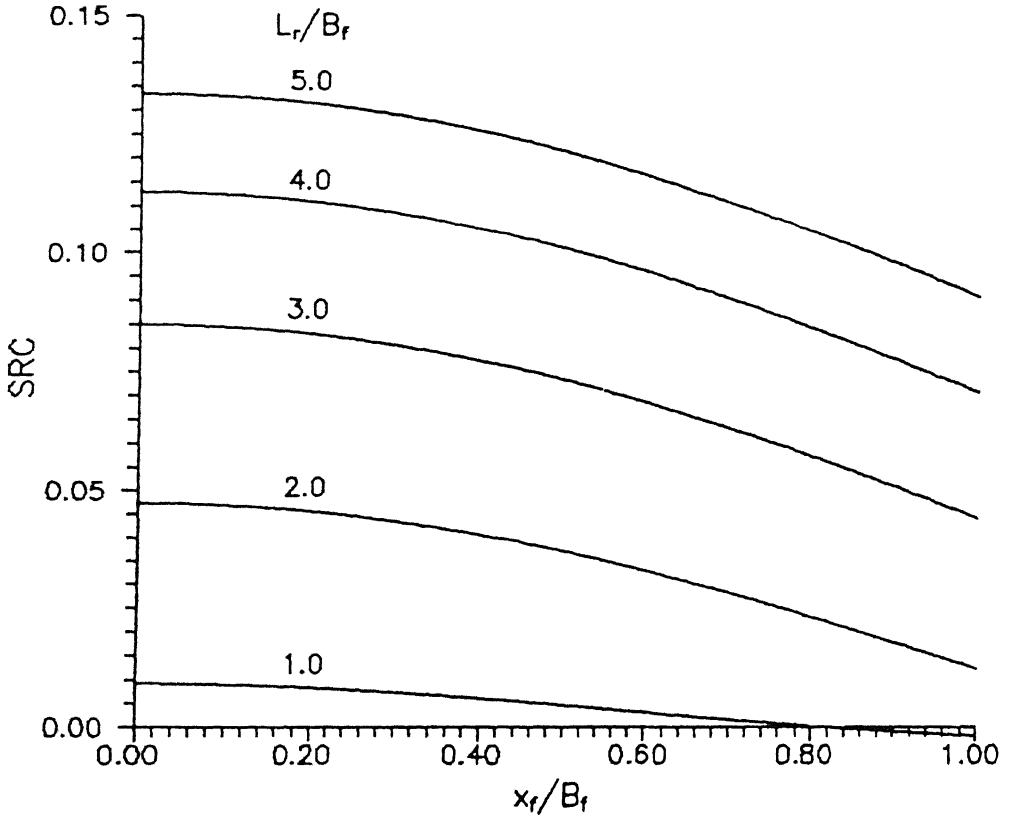


Fig. 5.28 Variation of SRC with Distance along Surface for Different Strip Lengths (Coupled Effect) ($U_0/B_f=1$, $L_f/B_f=1$, $\nu_s=0.3$)

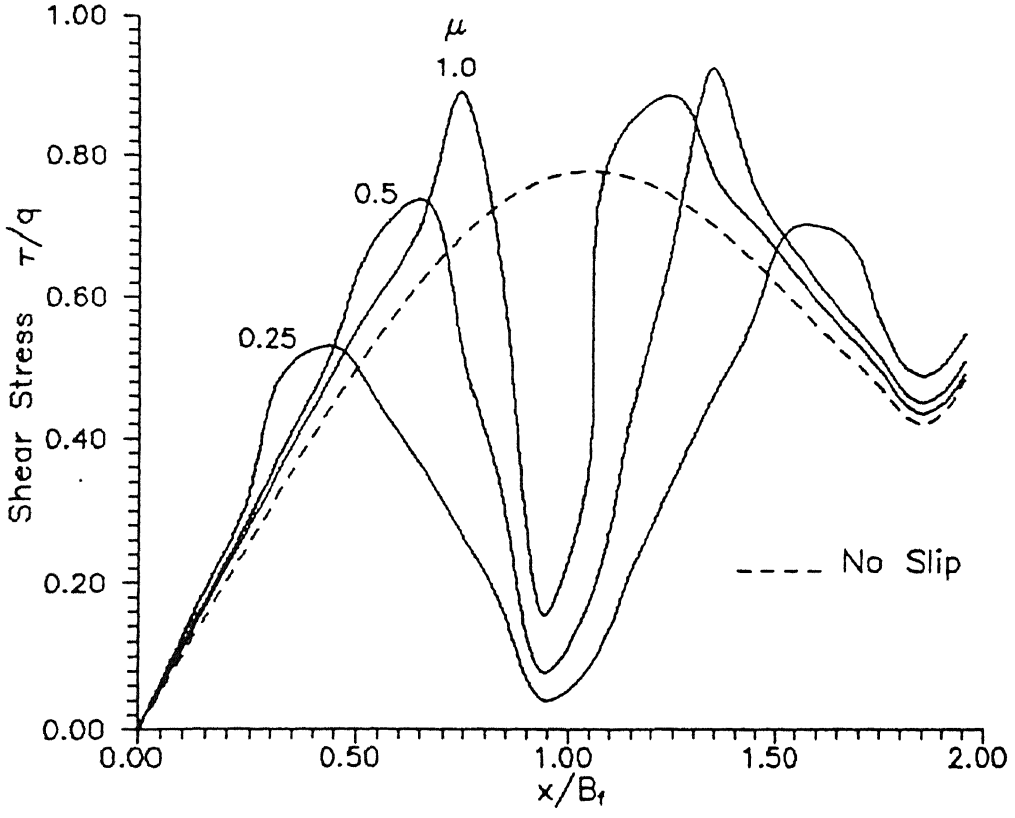


Fig. 5.29 Variation of Shear Stress with Distance for Different Coefficient of Friction Values ($L_r/B_f=2$, $L_f/B_f=1$, $U_0/B_f=1$, $\gamma B_f/q=0.5$, $\nu_s=0.3$)

seen that a portion of the strip beneath the edge of the loaded area , i.e., at $x/B_f = 1$, predominantly experiences slip. Shear stresses at these points reduce to low values because the normal stresses in this region are very small and the condition that shear stresses cannot exceed $\mu$ times normal stresses (given by Eq. 5.61) is to be satisfied. For a low coefficient of friction value ($\mu$=0.25), the strength available is small and slip occurs over a large distance ($0.4 \leq x/B_f \leq 1.5$). Further, the stresses on elements which do not fail are higher than those observed for the no slip case. The stresses on the elements along which slip occurs are forced to the limiting values resulting in a redistribution of stresses on the adjacent elements. As a result the stresses on the adjacent elements increase. As expected, the shear stresses are higher for higher coefficient of friction values.

Fig. 5.30 shows the normalised shear stress variation for different overburden ratios, $\gamma B_f/q$, for strips of length, $L_r/B_f$=2, placed at a depth, $U_o/B_f$=1, below a square surface loaded area. The results are for a coefficient of friction, $\mu$, of 0.5. The elements within the region, $0.6 \leq x/B_f \leq 1.5$, depending on the overburden stress ratio, experience slip. The region shifts to the left with an increase in the value of $\gamma B_f/q$. The stresses along elements which do not undergo slip are once again higher than those for the no slip case.

The variation of the normalised shear stress, $\tau/q$, with distance for various depths of placement of the strip is presented in Fig. 5.31. The results presented are for a coefficient of

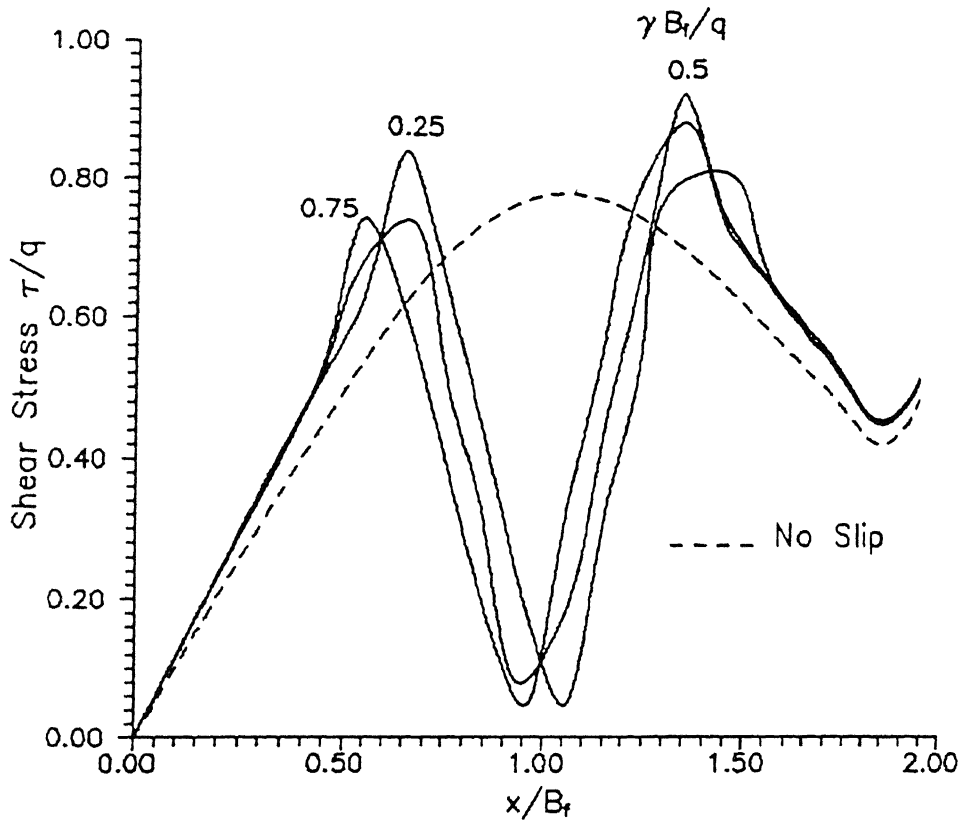


Fig. 5.30 Variation of Shear Stress with Distance for Different Overburden Ratios ($L_r/B_f=2$, $L_f/B_f=1$, $U_0/B_f=1$, $\mu=0.5$, $\nu_s=0.3$)

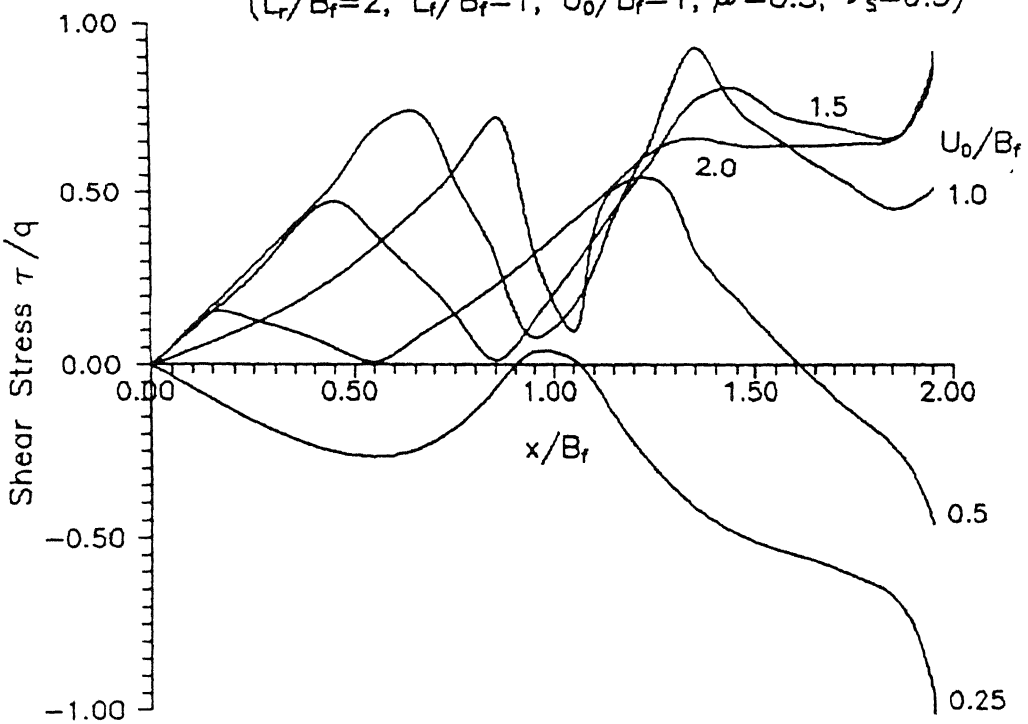


Fig. 5.31 Variation of Shear Stress with Distance for Different Depths of Strip Placement ($L_r/B_f=2$, $L_f/B_f=1$, $\mu=0.5$, $\gamma B_f/q=0.5$, $\nu_s=0.3$)

friction, $\mu$=0.5, and overburden ratio of 0.5. At a depth, $U_o/B_f$=0.25, no element along the length of the strip experiences slip. For a strip at depth, $U_o/B_f$=0.25, the value of shear stress beneath the edge of the loaded area is very small unlike the values of shear stresses for strips at depths greater than 0.25. Also, the normal stresses for strips closer to the surface are higher. Hence, none of the elements of the strip at $U_o/B_f$=0.25 experience slip. With increasing depths of the strips the normal stresses tend to become somewhat uniform and the points where the shear resistance is least move closer to the centre of the strip. Therefore, slip occurs along more number of elements and on elements relatively closer to the centre.

Fig. 5.31 shows the variation of SRC with distance, $x_f/B_f$, along the surface for various values of the coefficient of friction, $\mu$, for an overburden stress ratio, $\gamma B_f/q$=0.5. The results are for strips of length, $L_r/B_f$=2, placed below a square area at a depth, $U_o$=$B_f$. It is seen that there is a marginal decrease in SRC values with decreasing values of the friction coefficient, $\mu$. SRC at the centre of the loaded area ($x_f/B_f$=0) for $\mu$=0.25 is 0.046 which is 0.97 times that for the no slip case (0.0473). This shows that the slip at the interface does not affect the settlement reduction of points along the surface. It was seen earlier that the settlement reduction due to shear stresses is much less than that due to normal stresses. Hence, slip failure along few elements below the edge of the loaded area and the consequent redistribution in stresses does not affect the settlement reduction. It is thus evident that the failure of the

reinforcement in not mobilising the elastic shear stresses, does not lead to any significant decrease in the reduction of surface settlements.

The shape of the $\tau/q$ versus distance curves reflect the influence of slip along the reinforcement. Where slip occurs, the shear stress is limited to $\mu$ times the total normal stress. The difference between the elastic shear stress and the limiting value is redistributed to the adjacent elements. The redistribution effect does not appear in the shear stresses on elements farther away from the elements along which slip has occured. From these results it is clear that the elements on which the normal stresses are small, fail in shear. The reduction in shear stresses along these elements results in an increase in the shear stresses along the adjacent ones. The number and the distance from the centre, of the elements which fail by slip depend on the coefficient of friction, $\mu$, the overburden stress ratio, $\gamma B_f/q$ and the depth of placement, $U_o/B_f$, of the strip. It is also noted that at greater depths, relatively a larger number of elements fail by slip, because the normal stresses are uniformly distributed and thus smaller in magnitude.

## 5.7 Comparison with available literature

Brown and Poulos (1981) have presented a finite element analysis of foundations on reinforced soil. The problem consists of a strip footing on the surface of a soil layer reinforced with strip reinforcements. Four layers of reinforcements have been considered with zero flexural stiffness and transmitting axial

forces only. The parameters of their analysis expressed in terms of the parameters selected in this present analysis are as follows: aspect ratio of the loaded area, $L_f/B_f=10$ (strip footing), length of the reinforcement, $L_r/B_f=5$, depth of the first layer, $U_o/B_f=0.33$. For the soil, $E'/c'=1000$ and $\nu_s=0.3$. The authors have conducted the analysis for a linear density ratio (LDR) of 0.5. This corresponds to strips of width ratio, $B_r/B_f=0.025$ at a spacing of $0.105B_f$ throughout the length of footing.

For the parameters mentioned above, the settlement reduction coefficients at the centre of the loaded area ($I_{sc}$) are calculated for each strip considered independently. For the configuration, $I_{sc}$, computed as the sum of the values obtained individually is 0.4272. Choosing a correction factor for interference effect (Fig. 3.23) as 0.5, the net $I_{sc}=0.2136$. The reduction in settlement at the centre of the footing is calculated from Eq. 3.35 as

$$\frac{\rho_z}{B_f} = \frac{I_{sc}}{G_s} q$$

This is valid for loading levels within the elastic range. At a loading level of $q=16c'$ the reduction is

$$\frac{\rho_z}{B_f} = \frac{0.2136 \times 16c' \times 2(1+0.3)}{1000c'} = 0.0089$$

From Fig. 5.30 the corresponding settlement for the unreinforced case is about $0.075B_f$. This implies a reduction in settlement of 11.9%. At a loading level of $q=20c'$, the reduction is 13%. These reductions are for a single layer of reinforcement.

For the second layer of reinforcements at a depth, $U_o/B_f$=0.66, the $I_{sc}$ computed as the sum of the values due to single strips is 0.166. Considering both layers and choosing a correction factor of 0.4 for horizontal and vertical interference the net $I_{sc}$ is 0.237. The settlement reduction for the stress levels of 16c′ and 20c′ are 13% and 14.5% respectively. The reductions obtained are for rigid strips as the elongation stiffnesses are not known. The actual settlement reductions for elastic strips will be smaller than those obtained. The results compare reasonably well with those reported (Table 5.1a).

Shankariah and Narahari (1988) conducted model tests on a sand bed reinforced with G.I.strips. The test details are shown in Table 5.1b. Reinforcements were placed in both directions, occupying an area of 43 cm. square. The parameters of the tests in non-dimensional form are: aspect ratio of the footing, $L_f/B_f$=1, length of the strips, $L_r/B_f$=5, depth, $U_o/B_f$=0.47, width of each strip $B_r/B_f$=0.058. Spacing between each strip = $0.82B_f$.

The settlement reduction coefficient at the centre of the footing, $I_{sc}$, due to shear stresses and normal stresses mobilised along the strips are calculated for single strips independently. $I_{sc}$ due to shear stresses for strips in a single direction is calculated as 0.0069. Considering both directions, the $I_{sc}$ is 0.0138. Since the spacing between the strips is of the order of $0.82B_f$, a correction factor due to interference of 0.9 is taken. Hence, the net $I_{sc}$ due to shear stresses is 0.0124. $I_{sc}$ due to normal stresses for strips in both directions is calculated as

0.905. Choosing an interference correction of 0.8, the $I_{sc}$ is 0.724. Based on the flexural ratio of the strips, a correction factor of 0.3 is taken which gives a net $I_{sc}$ value of 0.217 due to normal stresses. The total $I_{sc}$ due to horizontal and vertical rigidity is 0.2294. The reduction in settlements due to reinforcements is calculated from Eq. 3.35. The elasticity modulus $E_s$ of the soil is calculated as the slope of the load settlement curve given for the unreinforced case within elastic range as 2000 $t/m^2$. The computed reduction in settlement is 0.51 mm at a loading of 40 $t/m^2$ and 0.26 mm at a loading of 20 $t/m^2$. These values correspond to an improvement of 10% and 9.6% respectively whereas the observed improvements at these loading levels are (Table 5.1b) around 20%. The reasons for the difference in the predicted and observed values are possibly due to the following reason; (i) assumed value of $E_s$; (ii) for strips with low flexural rigidity the membrane effect is also important at large vertical deformations; and (iii) the depth of the sand bed is finite and hence the solution based on a semi-infinite layer will be approximate.

Fragaszy and Lawton (1984) conducted laboratory model tests to study the load-settlement behaviour of reinforced sand. The test set up details are given in Table 5.1c. In the dimensionless form, the parameters of the model tests are; footing aspect ratio, $L_f/B_f=2$, length of strips, $L_r/B_f=2.675$, width of strips $B_r/B_f=0.11$, interval between strips = $0.45B_f$. The depths are $0.22B_f$, $0.45B_f$ and $0.67B_f$. The $I_{sc}$ value due to shear stresses for the strips in three layers considered as single strips is

Table 5.1 Reduction in Surface Settlements; Comparison with Selected Results

(a) Brown, B.S. and Poulos, H.G., (1981)

| No. of layers | q=16c | | q=20c | |
|---|---|---|---|---|
| | Predicted | Actual | Predicted | Actual |
| 1 | 11.9% | ≅13% | 13% | ≅14% |
| 2 | 13% | ≅14% | 14.5% | ≅16% |

(b) Shankariah, B., and Narahari, R., (1988)

| Footing Dimensions | | Reinforcement Details | | | Depth of first layer | E of Soil | Settlement Reduction $q=20t/m^2$ | | $q=40t/m^2$ | |
|---|---|---|---|---|---|---|---|---|---|---|
| L cm | B cm | L cm | B cm | Spacing cm | cm | $t/m^2$ | Pred. | Act. | Pred. | Act. |
| 8.5 | 8.5 | 43 | 0.5 | 3.5 | 2 | 2000 | 9.6% | 20% | 10% | 20% |

(c) Fragaszy, R.J., and Lawton, E., (1984)

| Footing Dimensions | | Reinforcement Details | | | No.of strips in a layer | Spacing | Depth of layers | | |
|---|---|---|---|---|---|---|---|---|---|
| L cm | B cm | L cm | B cm | Thickness cm | cm | cm | $u_1$ cm | $u_2$ cm | $u_3$ cm |
| 45.6 | 22.8 | 61 | 2.54 | 0.0254 | 9 | 5.08 | 2.54 | 5.08 | 7.62 |

| E of Soil KPa | | Settlement Reduction | | | |
|---|---|---|---|---|---|
| | | q=20KPa | $D_r$=61% | q=20KPa | $D_r$=70% |
| $D_r$=61% | $D_r$=70% | Predicted | Actual | Predicted | Actual |
| 1260 | 1850 | 31% | 35% | 32% | 41% |

L = Length, B = Width, Pred. = Predicted, Act. = Actual

0.0303. Multiplying this value by a factor of 0.6 to account for the extensibility, the net $I_{sc}$ is 0.0182. The $I_{sc}$ value due to normal stresses for all the strips is 4.1226. Choosing a correction factor of 0.2 for flexural deformations, the net $I_{sc}$ is 0.825. Summing up the two $I_{sc}$ values and using an interference correction factor of 0.45 the total $I_{sc}$ is 0.379. At a loading of 20 KPa and for 61% relative density the predicted reduction in settlements is 0.178 cm (31%) whereas the observed reduction is around 0.2 cm (≅35%) (Fig. 5.33). Under the same loading and for a relative density of 70% the predicted reduction in settlements is 0.125 cm (≅32%) as against the observed value of 0.16 cm (≅41%). Thus there appears to be a reasonable agreement between the results of Fragaszy and Lawton and the reduction predicted from the present analysis. At larger relative densities the discrepency increases. This is probably due to increased confinement action at greater relative densities which are not considered in the analysis.

## 5.8 Conclusions

The analysis developed in chapters 3 and 4 respectively for the interaction of embedded rigid (inextensible and inflexible) strips are extended for extensible and flexible ones. In the former case, i.e. extensible strip the strip is treated as a uniaxial member while in the latter case it is idealised as a beam. The effects of the elongation ratio, $K_\tau$, for extensible strips and flexibility ratio, $K_B$, for flexible strips on the stresses mobilised at the strip-soil interface and the consequent reduction in surface settlements have been studied. The combined

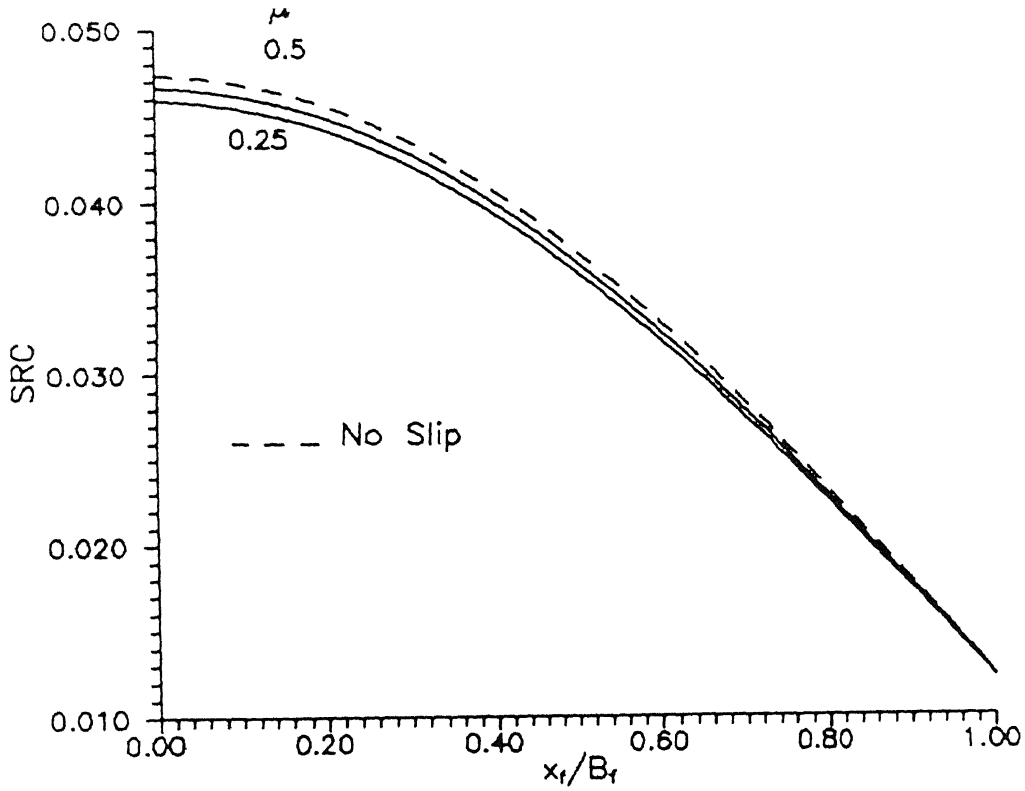


Fig. 5.32 Variation of SRC with Distance along Surface for Different Coefficient of Friction Values ($L_r/B_f=2$, $L_f/B_f=1$, $U_0/B_f=1$, $\gamma B_f/q=0.5$, $\nu_s=0,3$)

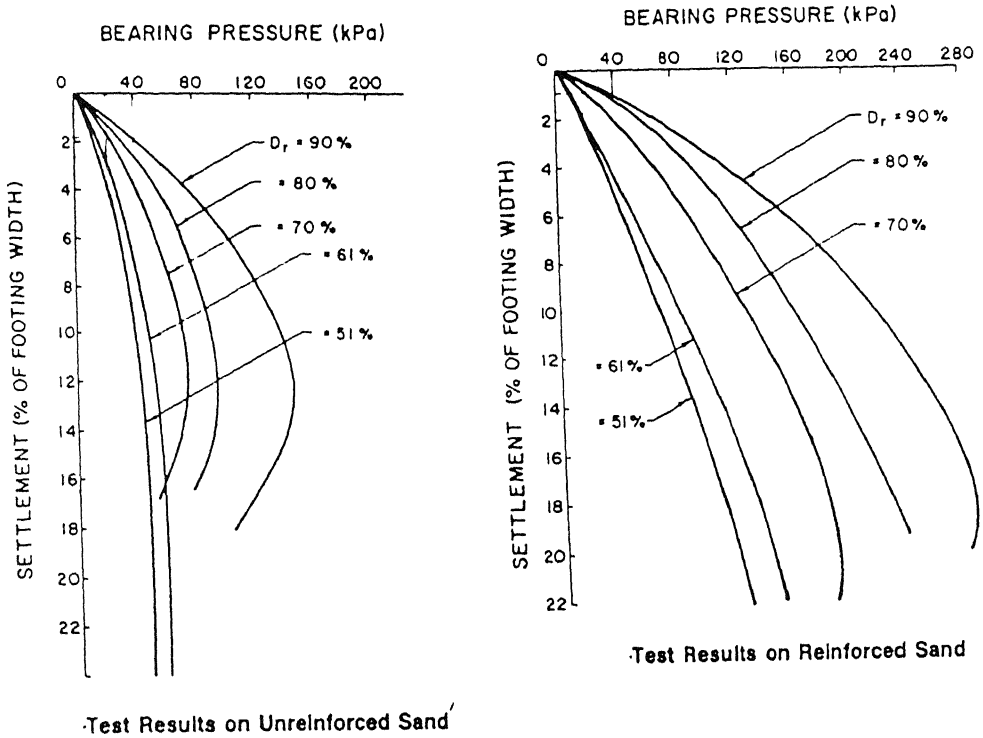


Fig. 5.33 Comparison with Fragaszy and Lawton 's (1984) Experimental Results

effect of considering simultaneously the rigidity of the strip in the horizontal and vertical directions has also been accounted for and provision made for possible slip at the interface. The settlement reduction of the points along the surface are computed considering the combined effect and for cases where slip is accounted for. Conclusions drawn from the results obtained from the parametric study are listed below.

1. The variations in the SRC for an extensible strip follow the same trend as those for a rigid one (chapter 3) and range from negligible values to those of a rigid one depending on the value of the elongation ratio, $K_\tau$.
2. The depth at which the SRC at the centre of the loaded area is a maximum, ranges from $0.75B_f$ to $1B_f$ for $K_\tau$ ranging from very low values to that of a rigid strip.
3. For a pair of strips placed symmetrically about the x-axis, the distance of the centre of each strip from the x-axis for which the settlement reduction is maximum lies in the range of $0.1B_f$ to $0.25B_f$ for the ratio $K_\tau$, varying from very low values to that of a rigid strip. This is applicable for both extensible and flexible strips.
4. A suitable correction factor is obtained for the SRC at the centre of the loaded area for an extensible strip from the corresponding value for a rigid one depending on its length and the value of its ratios $K_\tau$ (extensible) or $K_B$ (flexible).
5. For a flexible strip the variations in SRC follow the same trends as those for a rigid one (chapter 4).
6. For the case where the coupled effect of rigidity of the strip in the longitudinal and normal directions is considered, the

shear stresses reduce marginally whereas the normal stresses remain unaltered as compared to the case where the rigidity of the strip in both the directions are considered independently. Consequently the resulting values of SRC are the sums of the values observed for shear and normal stresses considered separately.

7. The region along the strip where normal stresses mobilised are small, fail due to slip. The settlement reduction coefficients are not significantly affected due to slip as the stresses get redistributed over the adjacent elements.
8. The model is able to predict the settlement reductions due to strip reinforcements quite satisfactorily.

# CHAPTER 6

# SOIL-REINFORCEMENT SHEET INTERACTION : AXI-SYMMETRIC CASE

## 6.1 Introduction

The previous chapters dealt with the analysis of interaction between soil and long, narrow strip reinforcements beneath rectangular loaded areas. Another form of reinforcement commonly used in practice is reinforcement in the form of sheets. Sheet reinforcement is often used to design embankments over soft soils and to reinforce highway subgrades. In the latter case, the contact area between the wheel and the subgrade can be approximated by a circle. Thus, a simple approach to evaluate the influence of sheet reinforcement is to consider an axi-symmetric problem in which the applied surface load and the reinforcement are circular areas. Thus, in this chapter, the influence of a single circular sheet placed at some depth, on settlement reduction at the surface is evaluated. The sheet firstly is treated as rigid, transversely (inextensible) and normally (inflexible). Subsequently, analyses of extensible and multiple layers of reinforcement beneath a uniformly loaded circular area, are presented.

The Boussinesq's equation for radial displacements due to point load on the surface is integrated over the circular loaded area to obtain the radial displacements for points along the sheet. Mindlin's equation is used to calculate the radial displacements at various points of the sheet due to the radial

shear stresses mobilised. Satisfying the compatibility of radial displacements, and solving the resulting equations, yield the shear stresses mobilised at the soil-reinforcement interface. For an inextensible sheet, the net displacements are zero while for an extensible one they equal the radial elongations of the points along the sheet. In order to compute these elongations, the governing differential equation for a circular membrane subjected to tension is used. Following this analysis, rigidity of the sheet in the vertical direction, i.e. a rigid disc is considered. Normal stresses mobilised at the soil-sheet interface, as in the case for strips, are computed. The disc being rigid, experiences a uniform vertical displacement. Consequently the stresses act upward over the central portion and downward over the latter portion. The settlement reduction of points along the surface due to the stresses mobilised are then calculated.

## 6.2 Horizontal Rigidity (Sheet Reinforcement)

### 6.2.1 Problem Definition

In this section, the rigidity of the sheet i.e. its inextensibility alone is considered. The problem consists of a circular sheet of reinforcement of radius, R, placed symmetrically below a circular loaded area of radius 'a' transmitting a uniform load of intensity, q (Fig. 6.1). The surface load causes the soil to move downward and radially outward. The outward radial displacements of the points at the soil-sheet interface are resisted by the shear stresses mobilised. These stresses, in turn push the soil above upward, thereby causing the surface to heave,

resulting in settlement reduction of points along the surface.

### 6.2.2 Rigid (Inextensible) Sheet

The radial displacement of a point within the elastic continuum with co-ordinates, (r,z) due to a point force on the surface is given by Eq. 3.1. In order to obtain the displacements of points along the soil-sheet interface at depth, $U_o$, Eq. 3.1 is integrated numerically over the loaded area. For this purpose the loaded area is divided into $n_f$ elements of length, $\Delta r$, along its radius and $n_\theta$ elements of $\Delta\theta$ radians along the tangential direction. Since the loading is symmetric, integration is performed over half the loaded area only, i.e., over 180 degrees. The sheet is divided into N elements, each of length dr, along its radius and the shear stresses mobilised are assumed to be constant over each element.

The global radial diplacement of the centre of any element, i on the sheet, due to the surface load is given by

$$\rho^f_{ri} = \sum_{i_f=1}^{n_f} \sum_{j_f=1}^{n_\theta} \frac{q(1+\nu_s)}{2\pi E_s R} \left( \frac{rU_o}{R^2} - \frac{(1-2\nu_s)r}{(R+U_o)} \right) \Delta A_j \, \mathrm{Cos}\alpha_{ij} \qquad (6.1)$$

where $\Delta A_j$ is the area of element, j over the loaded area, $\alpha_{ij}$ is the angle between radial line joining element j and node i, and the axis along which the displacements are desired. The meanings of all other parameters are the same as in Eq. 3.1. Nondimensionalising all length parameters with the radius of the loaded area 'a' and calculating the radial displacements at all N

nodes along the sheet, Eq. 6.1 is expressed in vector form as

$$\left\{ \rho^f \right\} = \frac{a}{E_s} \left\{ I^f \right\} q \qquad (6.2)$$

where $\left\{ I^f \right\}$ is a coefficient vector for the influence of the surface load on the displacements of the nodes along the radius of the sheet. $\left\{ \rho^f \right\}$ and $\left\{ I^f \right\}$ are vectors of size N.

The radial displacements of the N nodes due to the shear stresses mobilised along the radius, R, are computed using Mindlin's equation for horizontal displacements due to a horizontal force within the elastic continuum. This equation is integrated numerically over the radial and circumferential directions to obtain the displacements of all nodes due to shear stresses along the sheet. For this purpose, the area of the sheet is further divided along the circumferential directions into $N'_\theta$ elements of $d\theta$ radians each. The area of each element is then equal to $r_j d\theta dr$ where $r_j$ is the distance to the centre of each element from the centre of the sheet and dr is the length of each element. Fig. 6.2a shows the shear stresses over the sheet. Due to symmetry of the problem, the shear stresses are independent of $\theta$, the tangential direction, i.e. for $0^\circ \leq \theta \leq 360^\circ$, but vary with the radial distance, r.

It is to be noted here that the Mindlin's solution for a horizontal force beneath the surface is in terms of the cartesian co-ordinates. In order to calculate the radial displacements of the N nodes along the radius of the sheet, the components of the

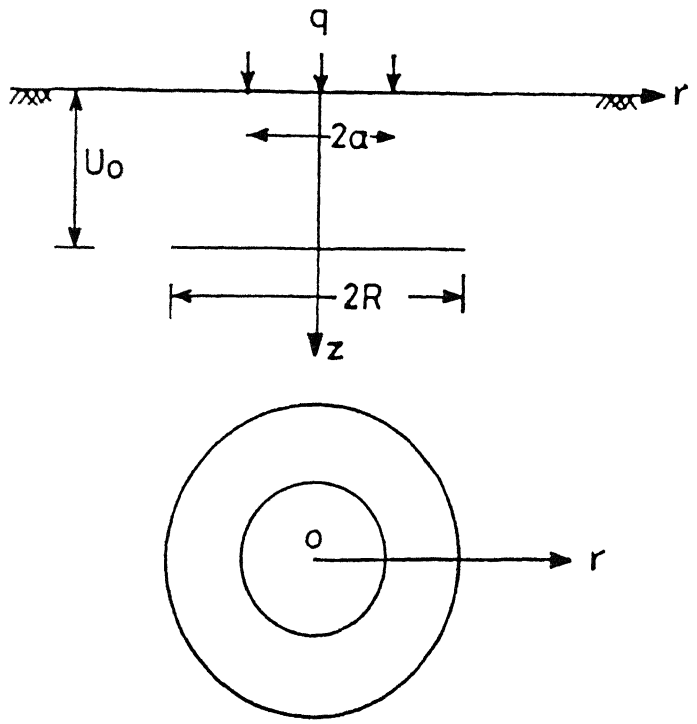


Fig. 6.1 Definition Sketch

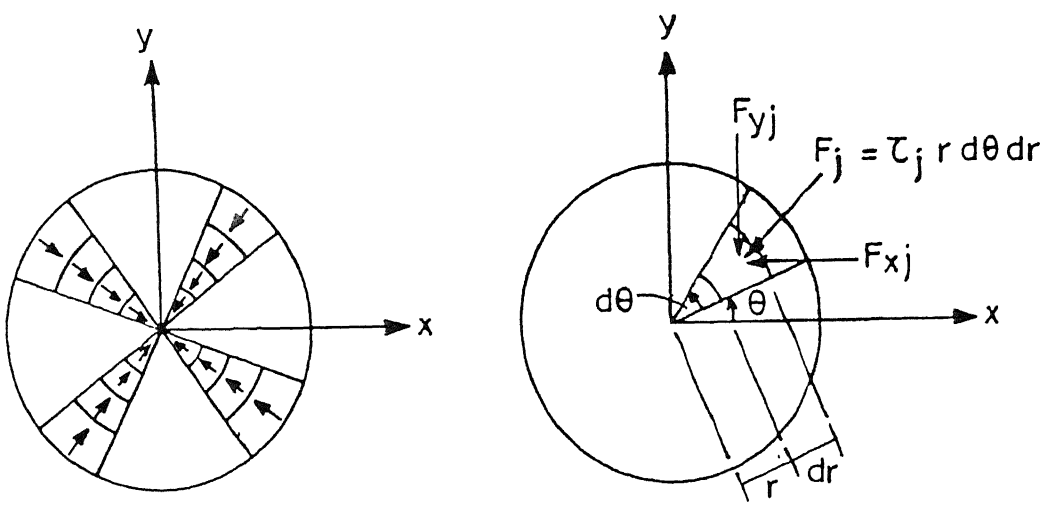


Fig. 6.2 a) Stresses on the Sheet
b) Force Components on an Element

forces over each element are to be taken. The force on element j (Fig. 6.2b), is given by

$$F_j = \tau_j \, r_j \, d\theta \, dr \qquad (6.3)$$

The components in the x and y directions are

$$F_{xj} = F_j \, Cos\theta \qquad (6.4)$$

and

$$F_{yj} = F_j \, Sin\theta \qquad (6.5)$$

where $\theta$ is the angle made by the radial line joining the centre of the sheet and node j, with the x-axis.

The radial displacements of the nodes are now calculated for the forces defined by Eqs. 6.4 and 6.5. The nodes are considered along the x-axis and the radial displacements of these points with respect to the global x-axis may as well be termed as horizontal displacements. The displacements are calculated at the points along the x-axis as shown in Fig. 6.2b.

The horizontal displacements of the nodes due to the force, $F_{xj}$, acting on any element j, is calculated from the Mindlin's equation (Eq. 3.10). The displacement of node i due to $F_{xj}$ is written as

$$\rho^{r}_{xij} = \frac{F_{xj}(1+\nu_s)x}{8\pi E_s(1-\nu_s)} \left[ F \right] \qquad (6.6)$$

where x is the distance along the x-axis between nodes i and j while all other parameters are as defined in Eq. 3.10.

Substituting Eqs. 6.3 and 6.4 in Eq. 6.6 one obtains

$$\rho^{r}_{xij} = \frac{\tau_j(1+\nu_s)x}{8\pi E_s(1-\nu_s)} \left[ F \right] r_j \, Cos\theta \, d\theta \, dr \qquad (6.7)$$

In order to obtain the horizontal displacement of node i due to force, $F_{yj}$, Mindlin's equation for displacements along x-axis due to a force, Q, parallel to y-axis is used, and given as

$$\rho_x = \frac{Q(1+\nu_s)}{8\pi E_s(1-\nu_s)} x \; y \left[ H \right] \qquad (6.8)$$

where

$$H = \frac{1}{R_1^3} + \frac{(3-4\nu_s)}{R_2^3} - \frac{6cz}{R_2^5} + \frac{4(1-\nu_s)(1-2\nu_s)}{R_2(R_2+z+c)^2}$$

$$R_1 = \sqrt{x^2 + y^2 + (z-c)^2}$$

$$R_2 = \sqrt{x^2 + y^2 + (z+c)^2}$$

and x, y and z are the co-ordinates of the point where the displacement is to be calculated due to the horizontal force. Substituting for the force, $F_{yj}$, in Eq. 6.8, the horizontal displacement of node i is

$$\rho^{r}_{xij} = \frac{F_{yj}(1+\nu_s)}{8\pi E_s(1-\nu_s)} x \; y \left[ H \right] \qquad (6.9)$$

Substituting for $F_{yj}$ in terms of the stress, $\tau_j$, one obtains

$$\rho^{r_y}_{xij} = \frac{\tau_j (1+\nu_s) xy}{8\pi E_s (1-\nu_s)} \left[ H \right] r_j \, Sin\theta \, d\theta \, dr \qquad (6.10)$$

Eq. 6.6, in dimensionless form is

$$\rho^{r_x}_{xij} = \frac{a}{E_s} I^{r_x}_{ij} \tau_j \, d\theta \, dr \qquad (6.11)$$

where $I^{r_x}_{ij}$ is a dimensionless coefficient for the influence of the force component, $F_{xj}$ along x-axis due to the stress, $\tau_j$, on the displacement of node i and 'a' is the radius of the loaded area on the surface. Eq. 6.10, expressed in the dimensionless form is

$$\rho^{r_y}_{xij} = \frac{a}{E_s} I^{r_y}_{ij} \tau_j \, d\theta \, dr \qquad (6.12)$$

where $I^{r_y}_{ij}$ is a dimensionless coefficient for the influence of the force component, $F_{yj}$ along y-axis due to the stress, $\tau_j$, on the displacement of node i. The net horizontal displacement of node i due to the stress $\tau_j$ on element j is obtained by summing up Eqs. 6.11 and 6.12 as

$$\rho^{r}_{xij} = \frac{a}{E_s} \left[ I^{r_x}_{ij} + I^{r_y}_{ij} \right] \tau_j \, d\theta \, dr \qquad (6.13)$$

The displacement of node i due to stresses on all the elements along the radius and along the circumference of the sheet is obtained by integrating Eq. 6.13 over the area of the sheet as

$$\rho^{r}_{xi} = \int_{0}^{R}\int_{0}^{2\pi} \frac{a}{E_s}\left( I^{r_x}_{ij} + I^{r_y}_{ij} \right) \tau_j \, d\theta \, dr \qquad (6.14)$$

Due to symmetry the integration is carried out only over half the area of the sheet, as

$$\rho^{r}_{xi} = 2\int_{0}^{R}\int_{0}^{\pi} \frac{a}{E_s}\left( I^{r_x}_{ij} + I^{r_y}_{ij} \right) \tau_j \, d\theta \, dr \qquad (6.15)$$

Integrating numerically, Eq. 6.15 is expressed as

$$\rho^{r}_{xi} = 2\,\frac{a}{E_s} \sum_{j=1}^{N} \sum_{k=1}^{N_\theta} \left( I^{r_x}_{ij} + I^{r_y}_{ij} \right) \tau_j \, d\theta \, dr \qquad (6.16)$$

where $N_\theta = N'_\theta/2$, is the number of elements along half the circumference of the sheet. The horizontal displacements of all the N nodes in vector form is

$$\left\{ \rho^{r} \right\} = \frac{a}{E_s} \left[ I^{r} \right] \left\{ \tau \right\} \qquad (6.17)$$

where $\left[ I^{r} \right]$ is a dimensionless coefficient matrix for the influence of the stresses on the displacements of the nodes and is a function of the depth ratio, $U_o/a$ , radius of the sheet, R/a and Poisson's ratio $\nu_s$.

For a rigid sheet, the net radial displacements equal zero, i.e.

$$\left\{ \rho^{f} \right\} - \left\{ \rho^{r} \right\} = \left\{ 0 \right\} \qquad (6.18)$$

Substituting for $\{\rho^f\}$ and $\{\rho^r\}$ one obtains

$$[I^r]\{\tau/q\} = \{I^f\} \tag{6.19}$$

Eq. 6.21 gives N equations, the solution of which gives the shear stresses mobilised along the reinforcement.

The settlement reduction of points on the surface are evaluated using Mindlin's equation for vertical displacement of a point within the elastic half-space due to a horizontal force within the continuum given by Eq. 3.26. In order to apply the equation, the force component of the stresses have to be resolved parallel to the axes corresponding to the cartesian co-ordinates (Fig. 6.2b). The points on the surface where the settlement reductions are calculated are points with co-ordinates (x,0,0), i.e., they lie along along the global x-axis on the surface. The settlement reductions of these points alone are calculated.

Substituting z=0 in Eq. 3.26 one obtains

$$\rho_z = \frac{Q(1+\nu_s)x}{2\pi E_s}\left[-\frac{c}{R^3} + \frac{(1-2\nu_s)}{R(R+c)}\right] \tag{6.20}$$

where $R = \sqrt{x^2 + y^2 + c^2}$

Eq. 6.20 gives the vertical displacement of the point on the surface due to a horizontal force, Q, at a depth, c. The vertical displacement of node k along the surface due to the force, $F_{xj}$, acting on element j (Fig. 6.2b) at a depth $U_o$ is given by

$$\rho^{x}_{zkj} = \frac{F_{xj}(1+\nu_s)x_{kj}}{2\pi E_s}\left[-\frac{U_o}{R^3} + \frac{(1-2\nu_s)}{R(R+U_o)}\right] \qquad (6.21)$$

where $R=\sqrt{x^2_{kj}+y^2_{kj}+U^2_o}$, $x_{kj}$ and $y_{kj}$ are the distances between the centre of element j and node k along the x and y axis respectively. Substituting Eq. 6.3 and Eq. 6.4 in Eq. 6.21 one obtains

$$\rho^{x}_{zkj} = \frac{\tau_j(1+\nu_s)x_{kj}}{2\pi E_s}\left[-\frac{U_o}{R^3} + \frac{(1-2\nu_s)}{R(R+U_o)}\right] r_j \,\mathrm{Cos}\theta \, d\theta \, dr \qquad (6.22)$$

Eq. 6.22 is expressed in dimensionless form as

$$\rho^{x}_{zkj} = \frac{a}{G_s} I^{x}_{kj} \tau_j \, d\theta \, dr \qquad (6.23)$$

where $G_s = E_s/2(1+\nu_s)$.

The vertical displacement of node k due to the force $F_{yj}$ acting on element j at a depth $U_o$ is given by

$$\rho^{y}_{zkj} = \frac{F_{yj}(1+\nu_s)y_{kj}}{2\pi E_s}\left[-\frac{U_o}{R^3} + \frac{(1-2\nu_s)}{R(R+U_o)}\right] \qquad (6.24)$$

where $R=\sqrt{x^2_{kj}+y^2_{kj}+U^2_o}$. The terms, $x_{kj}$ and $y_{kj}$ in Eq. 6.21 are interchanged in Eq. 6.24 since the force, $F_{yj}$ is parallel to the y-axis. Substituting Eqs. 6.3 and 6.5 in Eq. 6.24., one obtains

$$\rho^{y}_{zkj} = \frac{\tau_j(1+\nu_s)y_{kj}}{2\pi E_s}\left[-\frac{U_o}{R^3} + \frac{(1-2\nu_s)}{R(R+U_o)}\right] r_j \,\mathrm{Sin}\theta \, d\theta \, dr \qquad (6.25)$$

Eq. 6.25 is expressed in dimensionless form as

$$\rho^{y}_{zkj} = \frac{a}{G_s} I^{y}_{kj} \tau_j \, d\theta \, dr \qquad (6.26)$$

The net vertical displacement of node k due to shear stress $\tau_j$, is obtained by summing up Eqs. 6.23 and 6.26 as

$$\rho_{zkj} = \frac{a}{G_s} \left( I^{x}_{kj} + I^{y}_{kj} \right) \tau_j \, d\theta \, dr \qquad (6.27)$$

The vertical displacement of node k, due to shear stresses on all the elements on the sheet, is obtained by integrating Eq. 6.27 numerically over the area of the reinforcement as

$$\rho_{zk} = 2 \frac{a}{G_s} \sum_{j=1}^{N} \sum_{i=1}^{N_\theta} \left( I^{x}_{kj} + I^{y}_{kj} \right) \tau_j \, d\theta \, dr \qquad (6.28)$$

The integration is performed over half the area only because of symmetry. The vertical displacements of all the nodes along the surface in vector form is

$$\left\{ \rho_z \right\} = \frac{a}{G_s} \left[ I^{r}_{s} \right] \left\{ \tau \right\} \qquad (6.29)$$

The settlement reduction is desired at points along the radius of the loaded area, which is divided into $N_f$ points. Hence $\left\{ \rho_z \right\}$ is a vector of size $N_f$ and $\left[ I^{r}_{s} \right]$ is a matrix of size ($N_f$xN).

Eq. 6.29 is rewritten as

$$\left\{ \rho_z \right\} = \frac{a}{G_s} \left\{ I_s \right\} q \qquad (6.30)$$

$\{ I_s \}$ is a Settlement Reduction Coefficient vector of size $N_f$ which is obtained as

$$\{ I_s \} = [ I_s^r ] \{ \tau \} \qquad (6.31)$$

The vector of SRC along the surface is

$$\{ I_s \} = \frac{1}{a} \frac{G_s}{q} \{ \rho_z \} \qquad (6.32)$$

From Eq. 6.30, the reduction of settlements of points along the surface due to a circular reinforcement sheet at depth, $U_o$, is obtained.

### 6.2.3 Extensible Sheet

The net radial displacements of the nodes for the rigid (inextensible) sheet, as seen in section 6.2.2 were equal to zero. For an extensible sheet the net radial displacements due to the surface load and the shear stresses are equal to the elongations of the points on the circular sheet in the radial direction. In order to compute the elongation of the sheet, the same is considered to be a thin circular membrane. The thickness of the sheet is negligibly small in comparison to its radius.

Fig. 6.3 shows the forces on an element of the circular membrane in polar co-ordinates. Satisfying the force equilibrium of an element, two equations of equilibrium in the radial and tangential directions are arrived at, as

$$\frac{\partial \sigma_r}{\partial r} + \frac{1}{r}\frac{\partial \tau_{r\theta}}{\partial \theta} + \frac{\sigma_r - \sigma_\theta}{r} + F_N = 0 \qquad (6.33)$$

and

$$\frac{1}{r}\frac{\partial \sigma_\theta}{\partial \theta} + \frac{\partial \tau_{r\theta}}{\partial r} + \frac{2\tau_{r\theta}}{r} + F_T = 0 \qquad (6.34)$$

where $F_N$ and $F_T$ are the body forces in the radial and tangential directions respectively.

In the case of circular reinforcement, i.e. in an axi-symmetric case, $\sigma_\theta$ and $\tau_{r\theta}$ vanish and $\sigma_r$ is independent of $\theta$, due to symmetry. The term $F_N$ can be substituted by the force per unit volume on the element due to the mobilised shear stress, $\tau$. The body force, $F_T$ in the tangential direction is zero. Eq. 6.34 is identically satisfied. Eq. 6.33 reduces to

$$\frac{d\sigma_r}{dr} + \frac{\sigma_r - \sigma_\theta}{r} + \frac{\tau}{t_m} = 0 \qquad (6.35)$$

where $t_m$ is the thickness of the sheet.

The strain components in the radial and tangential directions in terms of the displacement or the elongation, u, are

$$\varepsilon_r = \frac{du}{dr} \qquad \text{and} \qquad \varepsilon_\theta = \frac{u}{r} \qquad (6.36)$$

Stress components expressed in terms of the strain components are

$$\sigma_r = \frac{E_m}{(1-\nu_m^2)}\left[\varepsilon_r + \nu_m \varepsilon_\theta\right] \quad \text{and} \quad \sigma_\theta = \frac{E_m}{(1-\nu_m^2)}\left[\varepsilon_\theta + \nu_m \varepsilon_r\right] \qquad (6.37)$$

where $\nu_m$ is the Poisson's ratio of the reinforcing sheet, and $E_m$,

its the elastic modulus. Substituting Eqs. 6.36 and 6.37 in Eq. 6.35 the governing differential equation is obtained as

$$r^2\frac{d^2u}{dr^2} + r\frac{du}{dr} - u = \frac{r^2(\nu_m^2-1)\tau}{E_m t_m} \qquad (6.38)$$

Eq. 6.38 is expressed in finite difference form for the N nodes along the radius of the sheet. The equation for node i written in finite difference form (Fig. 6.4) is

$$r_i^2\frac{u_{i+1}-2u_i+u_{i-1}}{dr^2} + r_i\frac{u_{i+1}-u_{i-1}}{2dr} - u_i = \frac{r_i^2(\nu_m^2-1)\tau_i}{E_m t_m} \qquad (6.39)$$

Eq. 6.39 written in matrix form is

$$\frac{E_m t_m}{(\nu_m^2-1)}\left[ I_E \right]\left\{ u \right\} = \left\{ \tau \right\} \qquad (6.40)$$

where $\left[ I_E \right]$ is the finite difference coefficient matrix for the extensible sheet.

The boundary conditions are

At r = 0, elongation, u = 0 (6.41)

At r = R, the radial stress is zero, i.e., $\sigma_r = 0$ (6.42)

r=0 and r=R correspond to the nodes, 0 and N+1 (Fig. 6.4). These nodes are at a distance of dr/2 from their adjacent nodes while all the other N nodes are equidistantly spaced at a distance, dr. Hence, second degree polynomials in u are fitted through the first

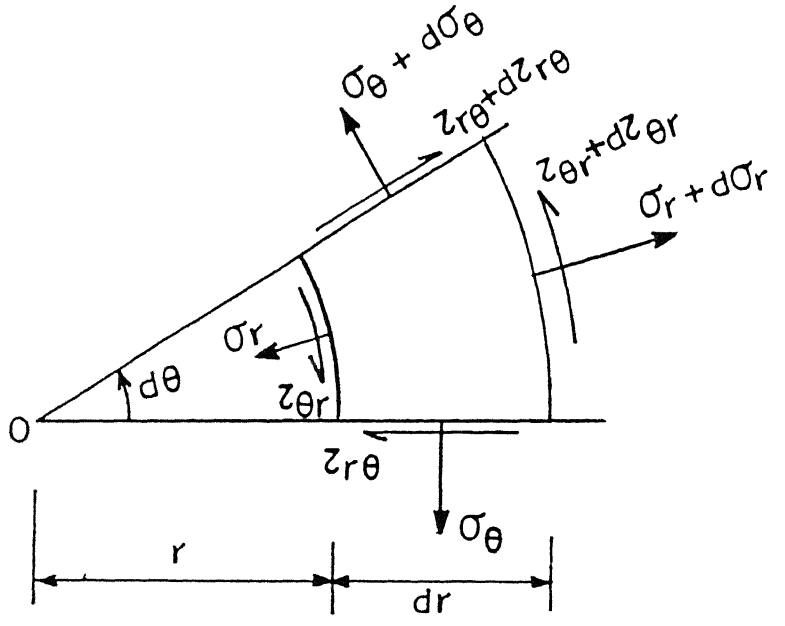


Fig. 6.3 Stresses on a Typical Element

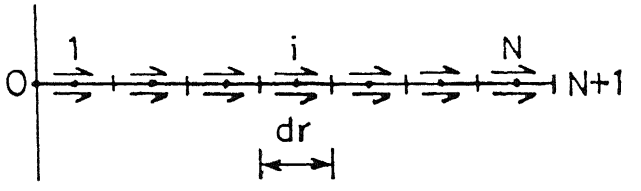


Fig. 6.4 Discretization for Extensible Sheet

and last three nodes such that they satisfy the boundary conditions. The constants of the polynomials are obtained in terms of elongations of the three nodes. The first and last rows of the coefficient matrix, $\left[ I_E \right]$ are thus obtained.

The net soil displacements from section 6.2.2 are

$$\left\{ u_s \right\} = \frac{a}{E_s} \left\{ I^f \right\} q - \frac{a}{E_s} \left[ I^r \right] \left\{ \tau \right\} \qquad (6.43)$$

The sheet displacements as expressed by Eq. 6.40 are

$$\left[ I_E \right] \left\{ u \right\} = \frac{a(\nu_m^2 - 1)}{E_m t_m} \qquad (6.44)$$

The compatibility of displacements of all nodes is satisfied by equating the net soil and sheet displacements. Substituting Eq. 6.43 in Eq. 6.44, one obtains

$$\left[ \left[ I_E \right] \left[ I^r \right] + \frac{(\nu_m^2 - 1)}{K_\tau} \left[ I \right] \right] \left\{ \tau/q \right\} = \left[ I_E \right] \left\{ I^f \right\} \qquad (6.45)$$

where $\left[ I \right]$ is an identity matrix and $K_\tau = \frac{E_m}{E_s} \frac{t_m}{a}$ is the relative elongation ratio of the reinforcement sheet. Eq. 6.45 gives N equations for the shear stresses, $\left\{ \tau/q \right\}$ mobilised at the soil-sheet interface which are solved for the same.

The SRC of points along the surface are calculated as described in section 6.2.2.

## 6.3 Vertical Rigidity (Rigid Inflexible Disc)

The problem definition is the same as in section 6.2.1 with the difference that the rigidity of the sheet in the vertical direction alone is considered. The disc is assumed to undergo uniform vertical translation due to the loading on the surface and as a result normal stresses are mobilised at soil-sheet interface. The discretisation of the loaded area and the reinforcing sheet are the same as explained in section 6.2.2.

The vertical displacements of the nodes along the sheet are calculated using Boussinesq's equation defined by Eq. 4.1. The displacement of node i at a radial distance, $r_i$ on the sheet due to the surface load is obtained by integrating Eq. 4.1 over the loaded area as

$$\rho^{f}_{zi} = \sum_{i_f=1}^{n_f} \sum_{j_f=1}^{n_\theta} \frac{q(1+\nu_s)}{2\pi E_s R} \left[ 2(1-\nu_s) + \frac{U_o}{R^2} \right] \Delta A_j \qquad (6.46)$$

where the terms $n_f$, $n_\theta$, and $\Delta A_j$ are as defined in section 6.2.2 and other parameters are as defined in section 4.2.2. Eq. 6.46 expressed in vector form is

$$\left\{ \rho^{f}_{z} \right\} = \frac{a}{E_s} \left\{ I^{f} \right\} q \qquad (6.47)$$

where $\left\{ I^{f} \right\}$ is a coefficient vector for the influence of the surface load on the vertical displacements of the nodes along the radius.

The displacements of the N nodes due to the normal stresses mobilised at the interface are computed using Eq. 4.6. The diaplacement of node i due to the stresses over all the elements is calculated by integrating Eq. 4.6 along the radial and tangential directions of the sheet as

$$\rho^{r}_{zi} = \int_{0}^{R}\int_{0}^{2\pi} \frac{\sigma_j (1+\nu_s)}{8\pi E_s (1-\nu_s)} \left[ G \right] r_j \, d\theta \, dr \qquad (6.48)$$

Performing the integration numerically and over half the area because of symmetry, Eq. 6.48 is written as

$$\rho^{r}_{zi} = 2\sum_{j=1}^{N}\sum_{k=1}^{N_\theta} \frac{\sigma_j (1+\nu_s)}{8\pi E_s (1-\nu_s)} \left[ G \right] r_j \, d\theta \, dr \qquad (6.49)$$

where $N_\theta$ is the number of elements along half the circumference of the sheet. The vertical displacements of all the N nodes in vector form are

$$\left\{ \rho^{r}_{z} \right\} = \frac{a}{E_s} \left[ I^{r} \right] \left\{ \sigma \right\} \qquad (6.50)$$

where $\left[ I^{r} \right]$ is a dimensionless coefficient matrix for the influence of the stresses on the vertical displacements of the nodes and is a function of the depth, $U_o/a$, radius of the sheet, R/a, and Poisson's ratio of the soil, $\nu_s$.

For a rigid sheet, the net vertical displacements equal the rigid body translation, $\delta_o$ of the sheet, which is written as

$$\{\rho_z\} - \{\rho_z\} = \delta_o\{1\} \tag{6.51}$$

Substituting Eqs. 6.47 and 6.50 in Eq. 6.51, one obtains

$$\frac{a}{E_s}\{I^f\}q - \frac{a}{E_s}[I^r]\{\sigma\} = \delta_o\{1\} \tag{6.52}$$

Eq. 6.52 gives N equations, while there are N unknowns in $\{\sigma\}$ and a rigid body translation. The additional equation is obtained by satisfying the force equilibrium along the radius of the sheet which is

$$\sum_{i=1}^{N}\sigma_i dA = 0 \tag{6.53}$$

Eqs 6.52 and 6.53 are rewritten as

$$[I^r]\{\sigma/q\} + \frac{\delta_o E_s}{aq} = \{I^f\} \tag{6.54}$$

and

$$\sum^{N}\sigma_i/q dA = 0 \tag{6.55}$$

$$\sum_{i=1}^{N}(\sigma_i/q)dA = 0 \tag{6.55}$$

Eqs. 6.54 and 6.55 are solved for the normal stresses, $\sigma/q$ and the rigid body translation, $\delta_o$.

These normal stresses push the soil upward, thus bringing about a reduction in settlements of points along the surface. In order to compute these reductions in settlements Eq. 4.20 is integrated over the area of the circular disc. The vertical

displacement of node k, on the surface due to the mobilised normal stresses on the sheet is given by

$$\rho_{zk} = 2\,\frac{1}{16\pi G_s(1-\nu_s)}\sum_{j=1}^{N}\sum_{i=1}^{N_\theta}\sigma_j\left[\frac{8(1-\nu_s)^2}{R}+\frac{(3-4\nu_s)U_o^2+U_o}{R^3}\right]\times r_j\,d\theta\,dr \qquad (6.56)$$

The vertical displacements of all the $N_f$ nodes on the surface in the vector form is

$$\left\{\rho_z\right\} = \frac{a}{G_s}\left[I_n^r\right]\left\{\sigma\right\} \qquad (6.57)$$

$\left\{\rho_z\right\}$ is a vector of size $N_f$ and $\left[I_n^r\right]$ is a matrix of size ($N_f$xN). Eq. 6.56 is rewritten as

$$\left\{\rho_z\right\} = \frac{a}{G_s}\left\{I_n\right\}q \qquad (6.58)$$

$\left\{I_n\right\}$ is the SRC vector of size $N_f$. From Eq. 6.58, the reduction of settlements of points along the surface due to a circular reinforcement disc at depth $U_o$ experiencing vertical displacement alone, is obtained.

## 6.4 Results and Discussion

### 6.4.1 Rigid Sheet and Disc

It is intended to evaluate the shear and normal stresses mobilised at the soil-reinforcement interface along the radius of the circular reinforcement. The Boussinesq's equation is integrated numerically over the cicular loaded area to obtain the radial displacements in the case of shear stresses and vertical displacements in the case of normal stresses. The area is discretized into $n_f$ subelements of length, 0.02a, each along the radius and $n_\theta$ subelements of 0.4 degrees each along the tangential direction. Further discretization did not improve the solution. Due to symmetry, the integration is performed over half the loaded area. The displacements are obtained at the centre of the N elements along the radius of the reinforcement.

In order to compute the influence coefficients for the displacements of points along the radius of the reinforcement due to the stresses mobilised at the interface, the reinforcement is divided in the tangential direction into elements of 2 degrees each ($\Delta\theta$=0.0349$^c$). The radius is divided in such a way that the area of each element remains the same. In doing so, the length of each element j, ($\Delta r_j$) decreases with increase in the distance from the centre. If the number of elements along the radius are large, the centre of the last element gets located very close to the edge. For eg., if a sheet of radius, R/a=1 is divided into 10 elements, the centre of the $10^{th}$ element lies at a distance of 0.973a from the centre of the sheet. For a rigid reinforcement

the edge stresses increase rapidly (as is evident in the strip case) and hence care is taken to position the centre of the last element sufficiently away from the edge to prevent the stress there from being infinitely large. It was seen that for $R/a \leq 4$, 5 elements over a distance of $r/a=1$ were sufficient and for $R/a=5$, 6 elements over the same distance were required. Hence, the number of elements equal $5 \times R/a$ for sheets upto radius, $R/a=4$ and 30 for sheets with $R/a=5$. The discretization is carried out such that no further improvement in the influence coefficient due to stress on element j, on the displacement of any node i, is observed. The stress over each element is assumed to be constant. For the aforementioned discretization the length of the first element is comparatively large and the centroid of the element lies at a considerable distance from the centre. It hence becomes imperative to extrapolate the stresses over a distance from the centre to the centroid of the first element. The variation in normal stresses over this region may not be significant (as seen for the strip case) and the assumption that stress over the element is constant stands valid. On the other hand, shear stresses increase from zero at the centre to the calculated value at the centroid of the element. The assumption, hence does not stand to reason atleast for the first element. To solve for the stresses within this region, element 1 is discretized further into subelements and the displacements of these subelements due to the surface load, due to the stresses over these subelements and those computed for the other elements, are calculated. The stresses are evaluated by solving the equations resulting from the displacement compatibility.

A parametric study enumerates the effects of the depth, $U_o/a$, and the radius, R/a, of the reinforcement on the stresses mobilised and the settlement reduction resulting thereof. The first few figures illustrate the effects of the parameters on the shear stresses mobilised at the interface and the resulting settlement reductions for a rigid sheet. All results are obtained for a Poisson's ratio of the soil, $\nu_s$=0.3.

Fig. 6.5 illustrates the numerical instability with elements of equal lengths. The figure plots the variation of the normalised shear stress, $\tau/q$, with distance, r/a, for different radii of the sheet placed at a depth, $U_o/a$. The instability is reflected on the stresses mobilised along the elements close to the centre of the sheet. Elements of equal lengths imply that the area of elements increase with distance along the radius of the sheet. As a result, the influences of shear stresses on elements farther away from the centre, on the displacements of nodes close to the centre are very high. Moreover, these influences are much higher than the influence of the stresses on the first few elements, on the displacements at these nodes. The stresses mobilised along the first few elements, hence show an erratic behaviour. With increase in the distance from the centre, this instability reduces.

Fig. 6.6 shows the variation of the normalised shear stress, $\tau/q$, with distance, r/a, along the radius of the sheet for various depths of placement, $U_o/a$, and for a sheet of radius, R/a=2. The trends are similar to those of the strip reinforcement

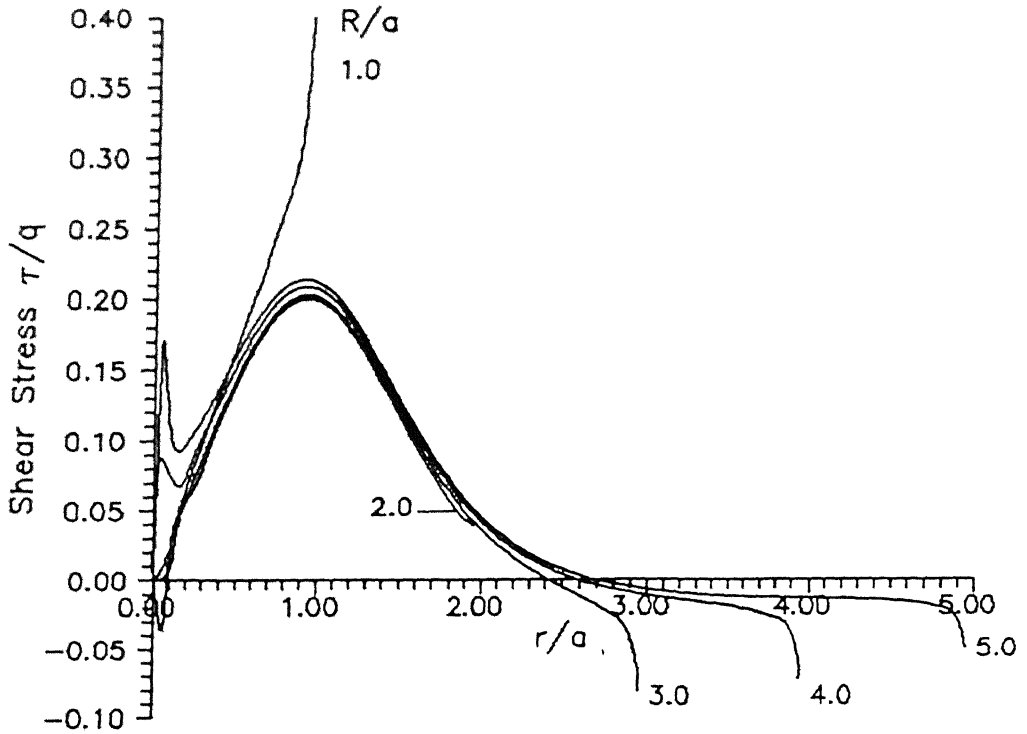


Fig. 6.5 Variation of Shear Stress with Distance for Various Radii of Sheet ($U_o/a=1$, $\nu_s=0.3$)

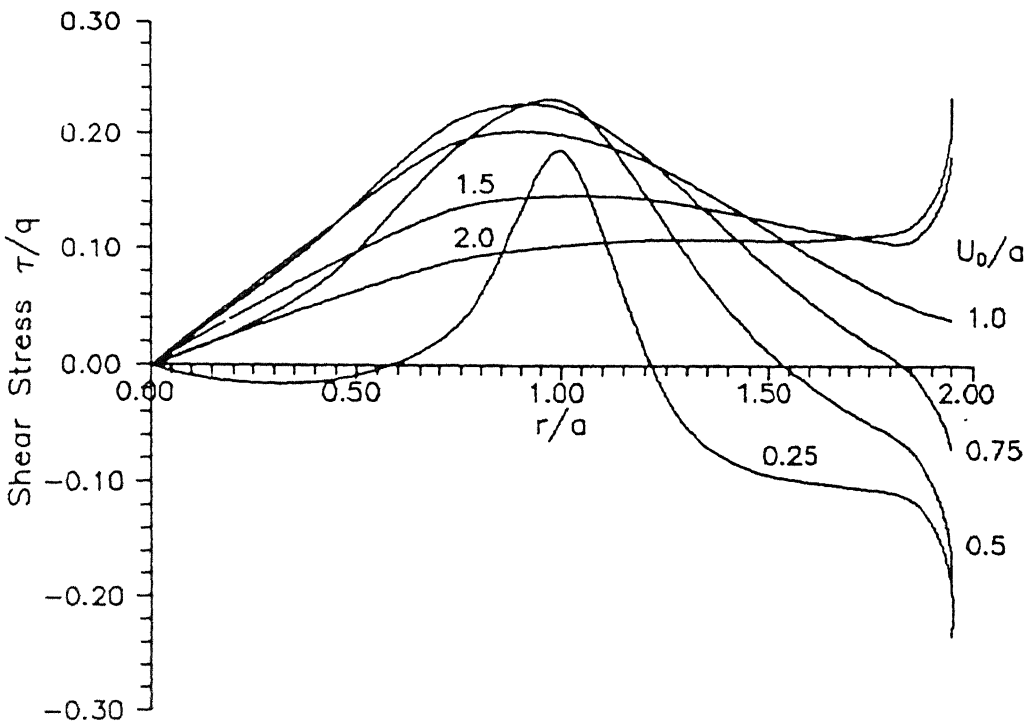


Fig. 6.6 Variation of Shear Stress with Distance for Various Depths of Placement of Sheet ($R/a=2$, $\nu_s=0.3$)

case. Shear stresses increase from zero at the centre (r/a=0) and reach a maximum value at a distance of around 0.8a to 'a' (i.e., below the edge of the loaded area). At shallow depths, $U_o/a=0.25$, the stresses are positive only over distances in the range, r/a=0.6 to 1.2. A maximum stress of 0.22q is observed at a distance of r/a=1 for the sheet placed at a depth of 0.5a. As the depth increases the stresses decrease and become uniform over the radius of the sheet. The maximum stresses occuring below the edge of the loaded area for the sheet at shallow to intermediate depths ($0.25 \leq U_o/a \leq 1$) is due to the fact that maximum radial displacements occur at this distance.

The variation of the normalised shear stress, $\tau/q$, with the distance along the radius, r/a, for various radii, R/a, of the sheet and placed at a depth, $U_o/a=1$, is depicted in Fig. 6.7. It is evident that for sheets of radius equal to that of the loaded area the stress increases monotonically and at the edge it reaches a high value ($\tau/q=0.58$). As the radii of the sheets increase, the positive shear stresses remain unaltered with a maximum stress of around 0.2q occuring below the edge of the loaded area (r/a=1). For greater radii of the sheets (R/a>2) the stresses change sign beyond a distance of around 2.5a to 2.7a. This is because the radial displacements beyond this distance are negative and as such the shear stresses are directed outward. The stresses at the edge for sheets of radii, R/a>2, drop down sharply to about -0.08q for R/a=3 and about -0.06q for R/a=5.

The effect of the shear stresses in reducing surface

settlements is studied in the subsequent figures. Fig. 6.8 shows the variation of SRC with distance along the radius of the loaded area on the surface for various radii of the reinforcement placed at a depth of 1a. The maximum SRC is observed at the centre of the loaded area which decreases with the distance, $r_f/a$. The increase in SRC with increase in the radius, R/a, of the sheet from 1 to 2 is significant. There is a marginal decrease in the SRC with increase in the radius, R upto 4a. This decrease is due to the negative stresses mobilised at the interface beyond a distance of around 2.6a along the radius of the sheet. The SRC at the centre of the loaded area for sheets with R/a=1 is 0.033 while for sheets with R/a=2 it is about 0.05.

The variation of SRC with distance for various depths of placement of the sheet of radius, R/a=2, is presented in Fig. 6.9. Similar to the results for the strip case, sheets placed at very shallow depths ($U_o/a=0.25$) show negative SRC, i.e. the points on the surface undergo additional settlement. This result indicates that sheets of intermediate radii ($R/a\leq2$) placed at shallow depths are detrimental to the foundation. The maximum SRC is observed for sheets placed at a depth of 0.75a to 1.0a. As the depth increases, the SRC decrease and become uniform over the distance along the surface. The maximum SRC at the centre is of the order of 0.05 for sheets placed at a depth of 0.75a to 1.0a.

Fig. 6.10 shows the variation of the SRC at the centre, $I_{sc}$, with the depth, $U_o/a$, for various radii of the reinforcement. For all radii the $I_{sc}$ is a maximum at a depth of about

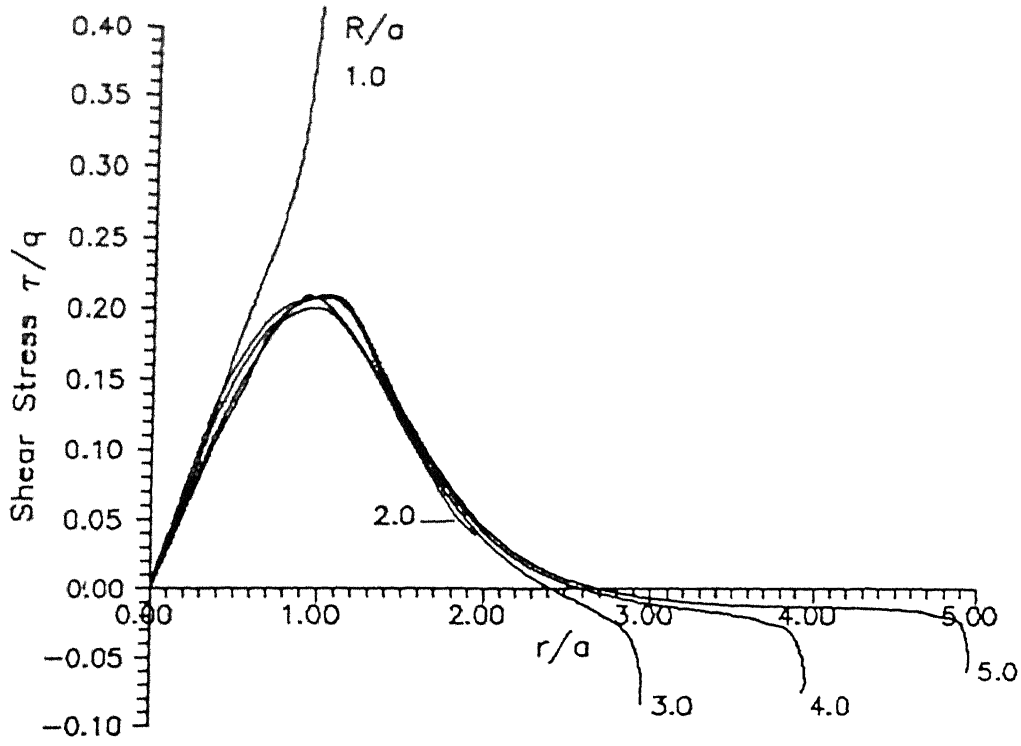


Fig. 6.7 Variation of Shear Stress with Distance for Various Radii of Sheet ($U_0/a=1$, $\nu_s=0.3$)

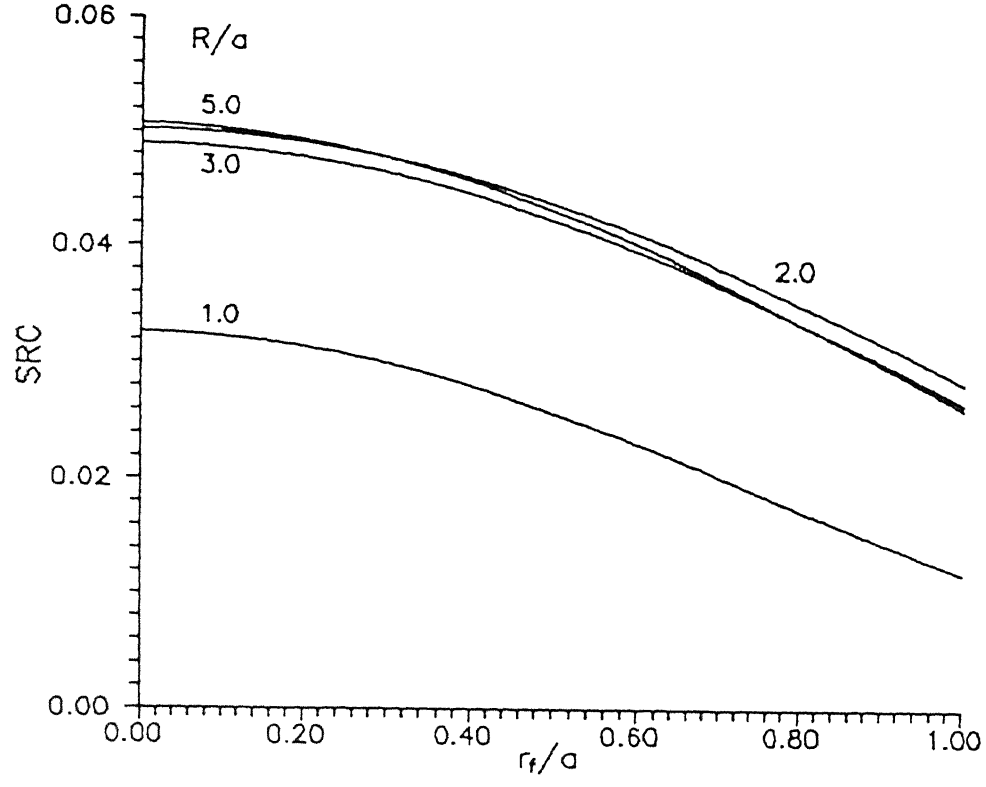


Fig. 6.8 Variation of SRC with Distance along Surface for Various Radii of Sheet ($U_0/a=1$, $\nu_s=0.3$)

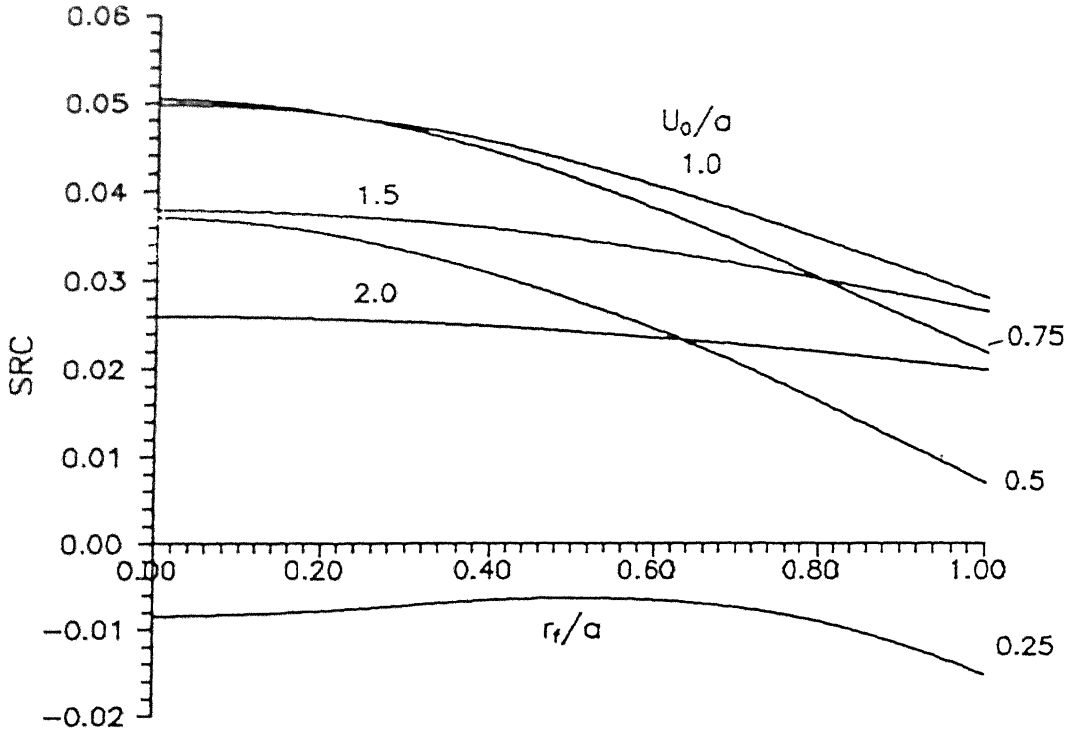


Fig. 6.9 Variation of SRC with Distance along Surface for Various Depths of Placement of Sheet ($R/a=2$, $\nu_s=0.3$)

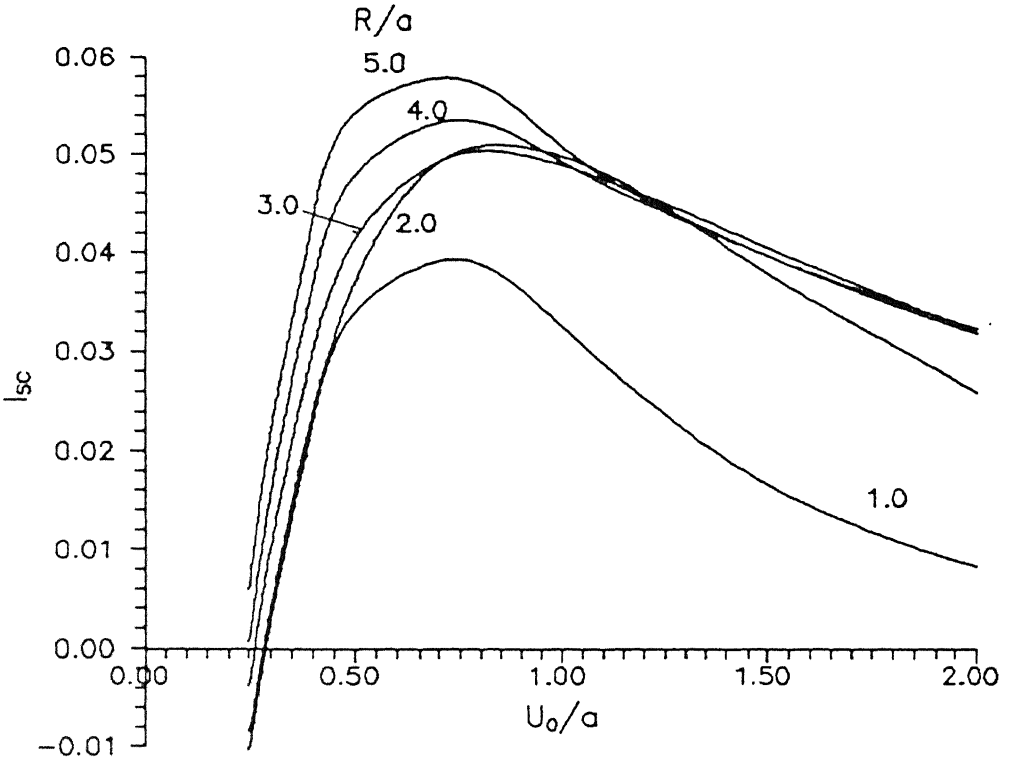


Fig. 6.10 Effect of Depth of Placement on $I_{sc}$ for Different Radii of Sheet ($\nu_s=0.3$)

0.75a. The $I_{sc}$, at a shallow depth, $U_o/a=0.25$, is negative. It increases rapidly with increase in depth and reaches a maximum value at about $U_o=0.75a$. Beyond depths of 0.75a, $I_{sc}$ reduces gradually with $U_o$. The rapid increase in $I_{sc}$ from shallow to intermediate depths ($0.25 \leq U_o/a \leq 0.75$) can be attributed to the change of stresses from negative to positive in this depth range and the mobilisation of maximum positive stresses at a depth, $U_o \cong 0.75a$. A maximum $I_{sc}$ of about 0.057 is observed at a depth of 0.75a for a sheet of radius 5a. For sheets with radius equal to that of the loaded area, i.e., R/a=1, the maximum $I_{sc}$ is 0.038 and is observed at a depth, $U_o=0.75$. At greater depths ($U_o/a=2$) the increase in $I_{sc}$ with increase in radius of the reinforcement is not appreciable for sheets with radius, R>2a.

On having looked into the variation of shear stresses along the radius of the sheet and its effect on the settlement reduction of points on the surface, the rigidity of the reinforcement in the vertical direction is considered in the subsequent figures. The effect of the parameters mentioned earlier on the normal stresses mobilised at the interface of the reinforcement disc and the soil are studied. The reduction of settlements of points along the surface as a consequence of the mobilised normal stresses are also evaluated.

Fig. 6.11 presents the variation of the normalised normal stress, $\sigma/q$, with the distance, r/a, along the radius of the disc for various depths of placement of the disc of radius, R/a=2. The variation is similar to the trend observed for strip form of

reinforcement. The normal stress decreases from a maximum at the centre, changes sign and approaches a large negative value at the edge of the disc. Discs placed at shallow depths show maximum normal stresses due to high vertical displacements due to the loading. As the depth increases, stresses decrease and tend to become uniform. This is due to decrease in vertical displacements of points at depth resulting from the surface load.

The effect of the radius of the reinforcement disc, R/a, on the normalised normal stresses, $\sigma/q$, for the disc placed at a depth, $U_o/a=1$, is presented in Fig. 6.12. For a disc of radius equal to that of the loaded area the normal stress near the centre of the disc is of the order of 0.52q. The stress decreases and becomes negative at a distance of 0.8a. Due to the edge effect, the stress near the edge is around -0.92q. As the radius of the disc increases, the positive stresses do not show an appreciable change. For any radius greater than 2a, the stresses become negative beyond a distance, $r/a=1.8$. The maximum negative stress at the edge decreases with increase in the radius of the disc. The maximum stress near the centre of the disc is of the order of 0.68q for $R/a \geq 1$.

Fig. 6.13 shows the variation of SRC with the distance along the surface for various radii, R/a, of the disc placed at a depth, $U_o/a=1$. The SRC at the centre of the loaded area is a maximum for all radii of the disc. The SRC increases with increase in the radius of the disc. The positive stresses increase with increase in the radius from R/a=1 to 2. As a

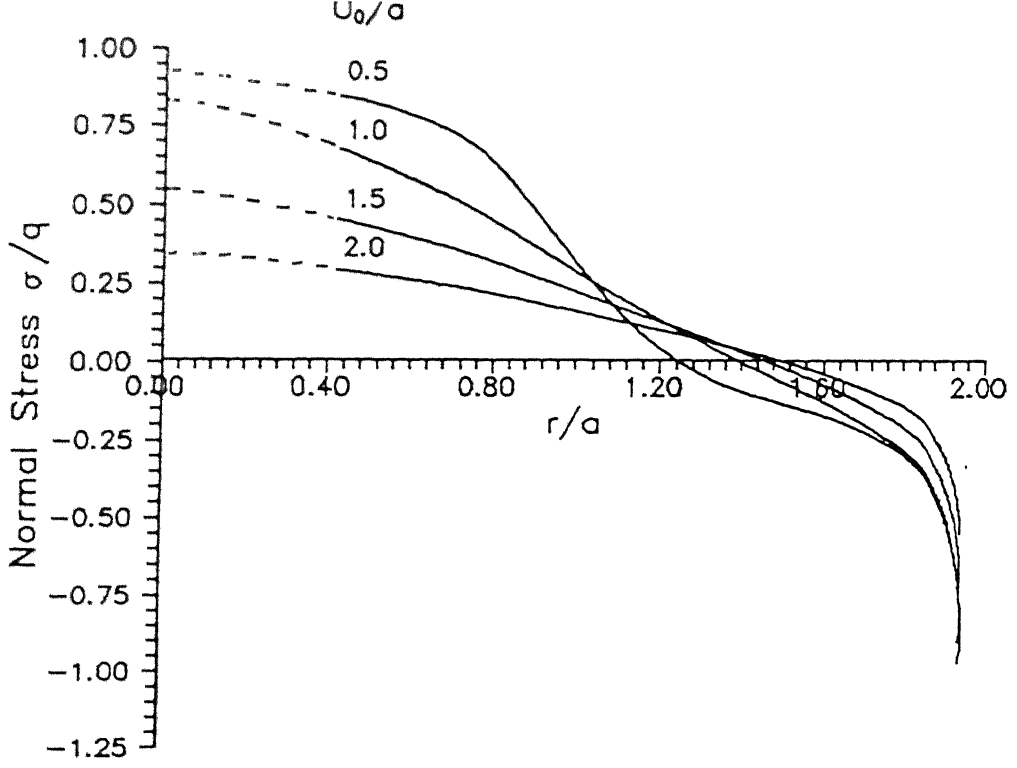


Fig. 6.11 Variation of Normal Stress with Distance for Various Depths of Placement of Disc ($R/a=2$, $\nu_s=0.3$)

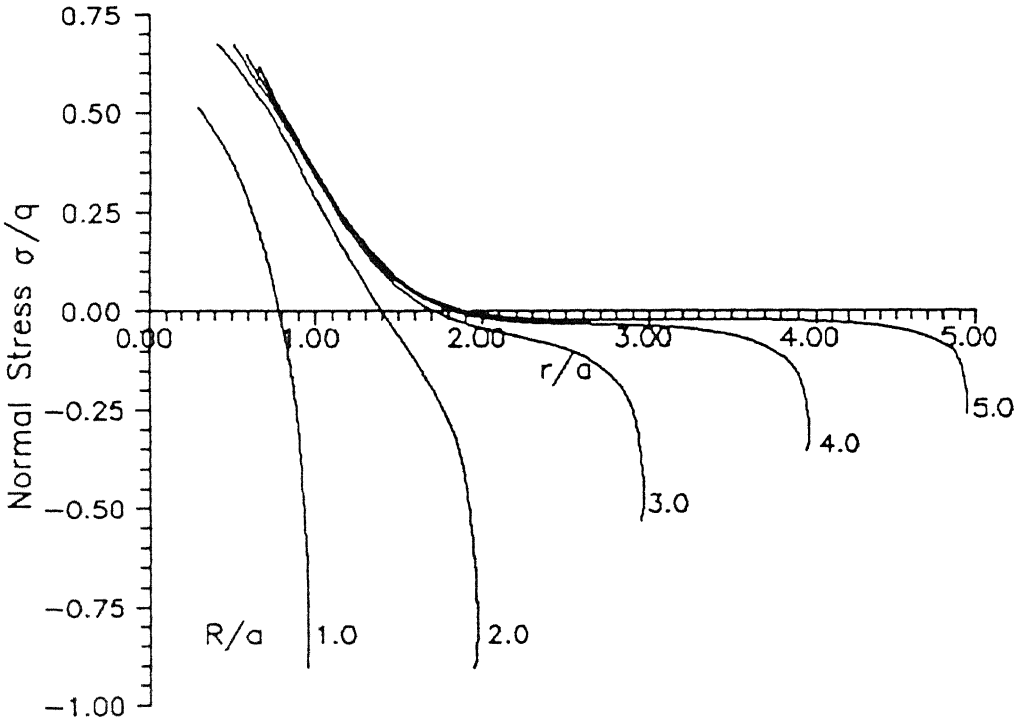


Fig. 6.12 Variation of Normal Stress with Distance for Various Radii of Disc ($U_0/a=1$, $\nu_s=0.3$)

result the increase in SRC is significant with the radius, R/a, increasing from 1 to 2. With further increase in the radius the rate of increase in SRC decreases. This is because the increase in stresses with increase in the radius is marginal.

The effect of the depth of placement of the disc, $U_o/a$, on the SRC of points on the surface for a disc with a radius, R/a=2 is presented in Fig. 6.14. The SRC at the centre of the loaded area, again is a maximum for all depths. The stresses being high for the disc placed at a shallow depth ($U_o/a$=0.25), the SRC at that depth is high. The variation in SRC with the distance along the surface, $r_f/a$, is high for shallow depths. As the depth increases the SRC tend to become uniform. This is because the stresses at greater depths tend to become uniform. The SRC at the centre is about 0.385 for a disc placed at a depth, $U_o/a$=0.25, while that for a disc at a greater depth ($U_o/a$=2), is 0.02. The decrease in SRC with depth is due to the decrease in stresses with depth.

Fig. 6.15 depicts the variation of the settlement reduction coefficient at the centre, $I_{sc}$, of the loaded area with depth, $U_o/a$, for various radii of the disc. As expected, the $I_{sc}$ decreases with depth, the disc with larger radii showing higher $I_{sc}$ values. A maximum $I_{sc}$ of 0.58 is witnessed for a disc of radius, R/a=5 at a depth, $U_o/a$=0.25. The rate of increase in $I_{sc}$ decreases with an increase in R/a. This, again is due to the fact that the increase in stresses with increase in R/a from 1 to 2 is significant while the rate of increase in stresses beyond

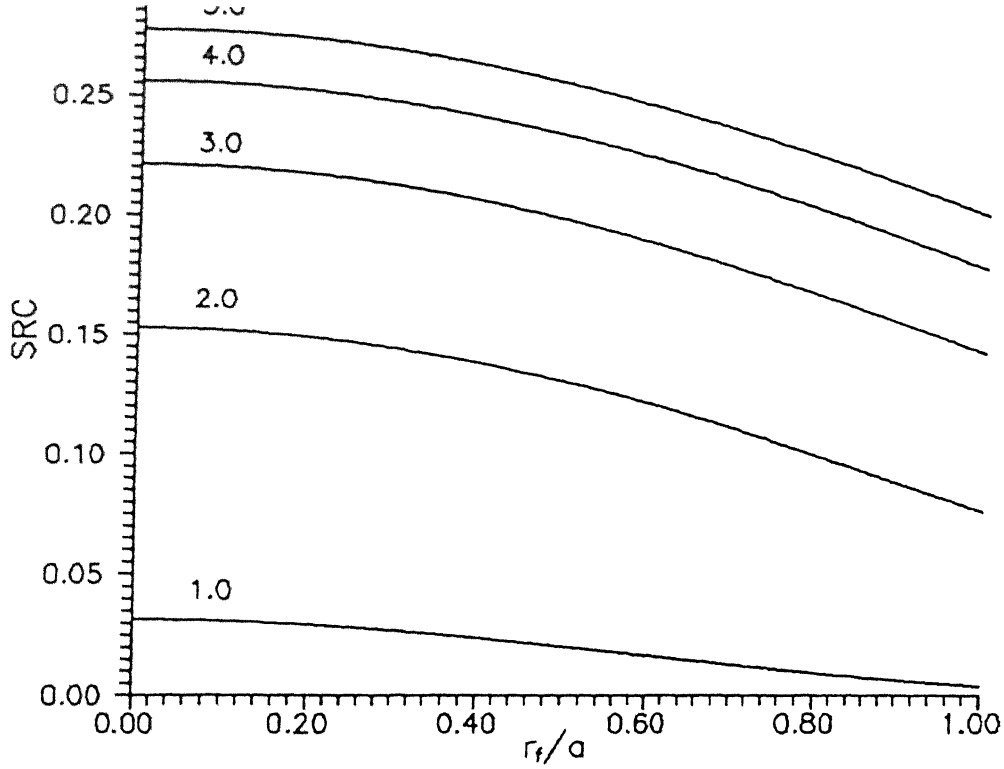


Fig. 6.13 Variation of SRC with Distance along Surface for Various Radii of Disc ($U_0/a=1$, $\nu_s=0.3$)

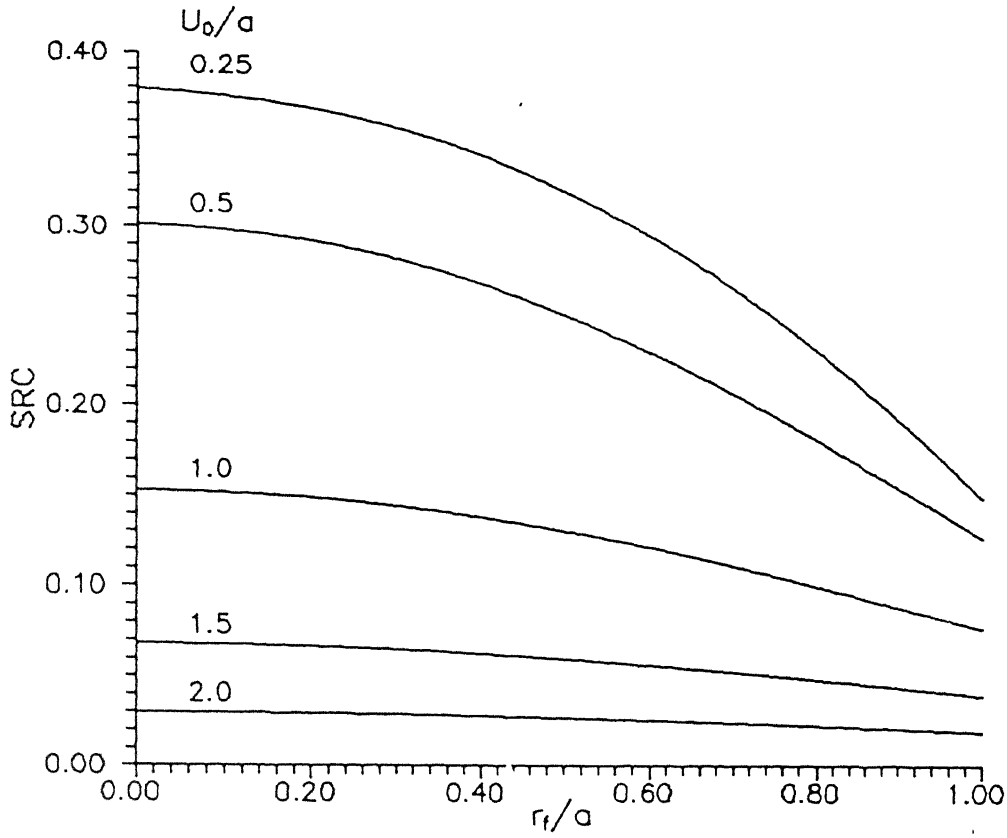


Fig. 6 14 Variation of SRC with Distance along Surface for Various Depths of Placement ($R/a=2$, $\nu_s=0.3$)

this radius decreases with R/a.

In Fig. 6.16 the effect of the depth of placement of the reinforcement disc, $U_o/a$, on the uniform translation, $\delta_o E_s/aq$, of the disc for various radii of the disc is presented. The uniform vertical translation decreases with increase in depth and radius of the disc. When the radius of the disc is small, the difference between the vertical displacements at the centre and the edge of the disc due to loading is small while for a larger radius this difference is large. In order to maintain a uniform displacement the disc with a smaller radius undergoes a larger uniform translation as compared to the one with a larger radius. As the radius increases, the rate of decrease in the uniform translation, $\delta_o E_s/aq$, with depth also decreases. At a depth, $U_o/a=0.25$, the uniform vertical displacement of the disc with radius, $R/a=1$, is 1.38 while for a larger radius, $R/a=5$, it is 0.28. At a depth, $U_o/a=2$, the corresponding values are 0.8 and 0.27 respectively.

From these figures it is clear that the settlement reductions due to shear stresses are much smaller than those resulting from normal stress mobilisation. It is advantageous to place a circular reinforcement rigid in the vertical direction at shallow depths while a reinforcement highly flexible in the vertical direction but rigid axially is best utilised if placed at a depth, $U_o=0.75a$ to 1a, where 'a' is the radius of the loaded area.

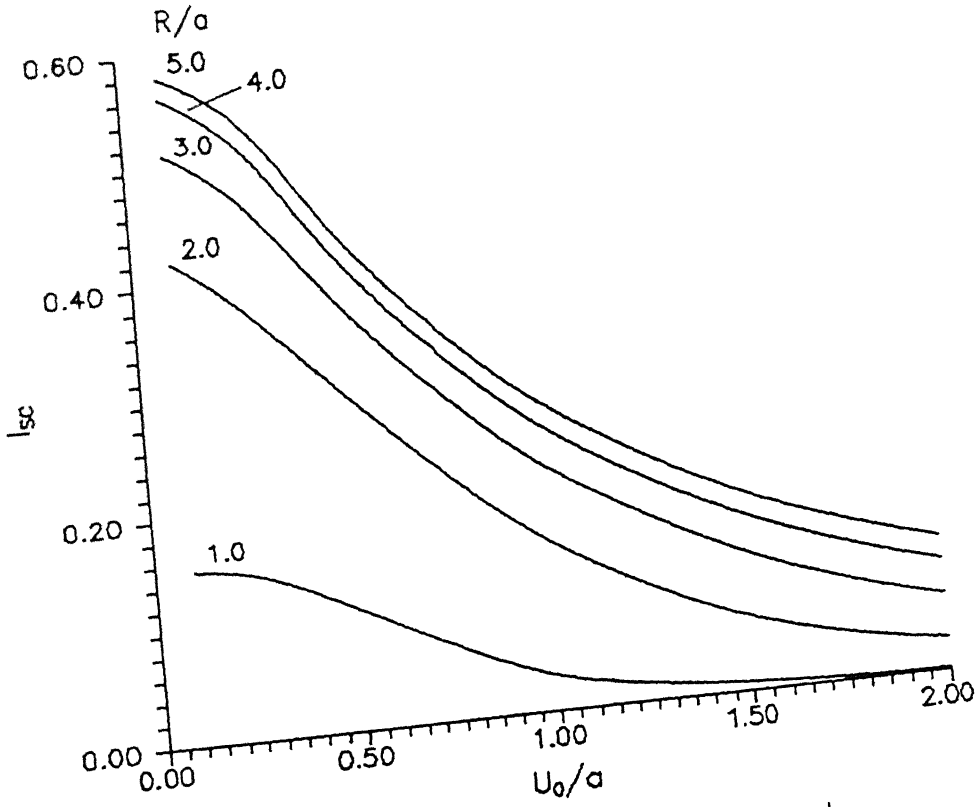


Fig. 6.15 Effect of Depth of Placement on $I_{sc}$ for Various Radii of Disc ($\nu_s$=0.3)

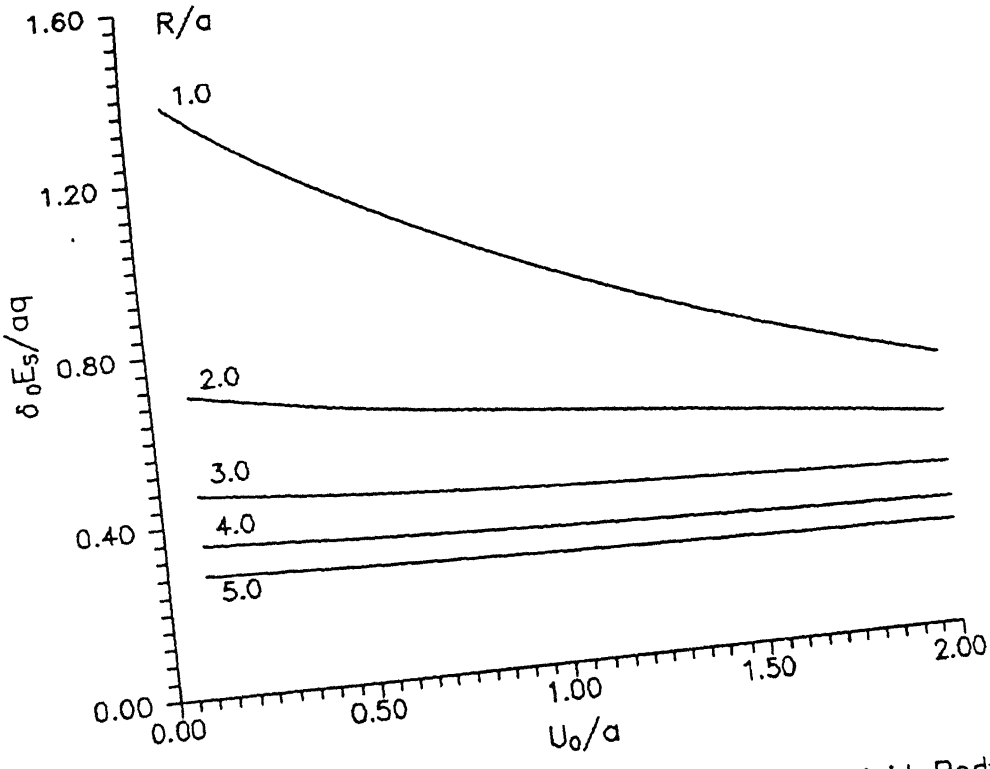


Fig. 6.16 Effect of Depth of Placement on Rigid Body Displacement for Various Radii of Disc ($\nu_s$=0.3)

### 6.4.2 Extensible Sheet

As seen in Fig. 6.5, equal lengths of elements result in erratic values of shear stresses along the first three elements. This was the reason why elements of equal areas were selected for rigid (inextensible) sheets and inflexible discs. For an extensible sheet, the elongations are expressed as a differential equation which are solved using the finite difference technique. The formulation for the finite difference calculations are based on equal lengths of the elements. Hence, shear stresses are computed using elements of equal lengths. It is known that the shear stresses should vary smoothly starting from zero at the centre of the sheet. To smoothen the stresses along the first three elements, a quadratic curve for shear stresses is fitted between the centre of the sheet, and elements 4 and 5.

The elongation ratio, $K_\tau$, is varied from $10^{-1}$ to $10^4$. For $K_\tau > 10^4$ there was no difference in the values of shear stresses and the settlement reduction coefficients as compared to those obtained for $K_\tau = 10^4$. Hence, the upper limit of $K_\tau$ was restricted to $10^4$.

Fig. 6.17 depicts the variation of the normalised shear stress, $\tau/q$, along the radius of the sheet for different values of the elongation ratio, $K_\tau$, and for a sheet of radius, $R/a=2$, placed at depth $U_o/a=1$. It is evident that as the value of $K_\tau$ increases, the stresses also increase and tend to those of a rigid sheet for $K_\tau = 10^4$. Stresses, for a highly extensible sheet ($K_\tau = 10^{-1}$) are very small owing to large elongations of the sheet.

For sheets with $K_\tau \leq 1$ the stresses at the edges are negative. The stresses are maximum at a distance equal to the radius of the loaded area, and a maximum stress, $\tau/q$, of around 0.2 is observed for sheets with $K_\tau = 10^4$ which equals that of a rigid sheet ($\tau/q = 0.2$).

The variation of the normalised shear stresses, $\tau/q$, with distance, $r/a$, for different depths of placement, $U_o/a$, and for a sheet of radius, $R/a = 2$ and $K_\tau = 1$ is shown in Fig. 6.18. The variations in shear stresses follow the same trend as those for a rigid sheet. The maximum shear stress is observed below the edge of the loaded area for sheets at a depth, $U_o/a = 0.5$ which equals 0.165. For sheets at shallow depths ($U_o/a = 0.25$) stresses over a distance, $r/a$, of 0.75 to 1.25 are positive with a maximum positive stress, $\tau/q$, of 0.15 occuring below the edge of the loaded area.

Fig. 6.19 shows the effect of depth, $U_o/a$, on the settlement reduction coefficient, $I_{sc}$, at the centre of the loaded area for different values of the elongation ratio, $K_\tau$, and for sheets of radius, $R/a = 2$. It is seen that for all $K_\tau$ values a maximum $I_{sc}$ occurs in the depth range of $U_o/a = 0.65$ to 0.8. $I_{sc}$ values increase with increase in $K_\tau$ values owing to the increase in shear stresses with $K_\tau$. Isc values for sheets with $K_\tau = 10^4$ tend to those of a rigid sheet (Fig. 6.9). At shallow depths ($U_o/a = 0.25$), $I_{sc}$ values are negative since the stresses are predominantly negative.

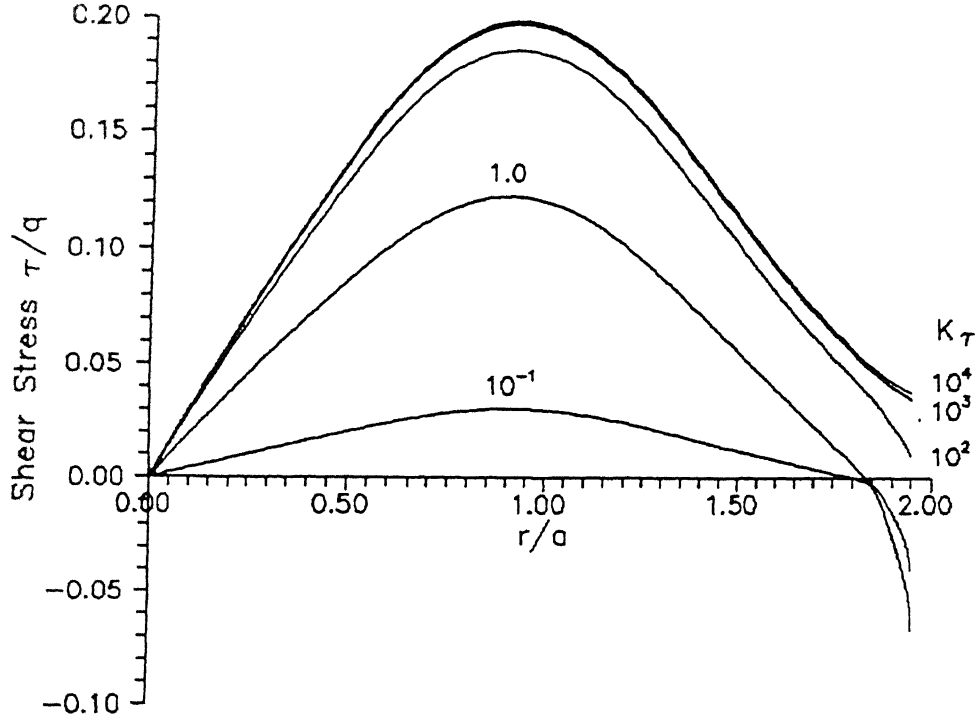


Fig. 6.17 Variation of Shear Stress with Distance for Various Elongation Ratios ($R/a=2$, $U_0/a=1$, $\nu_s=0.3$)

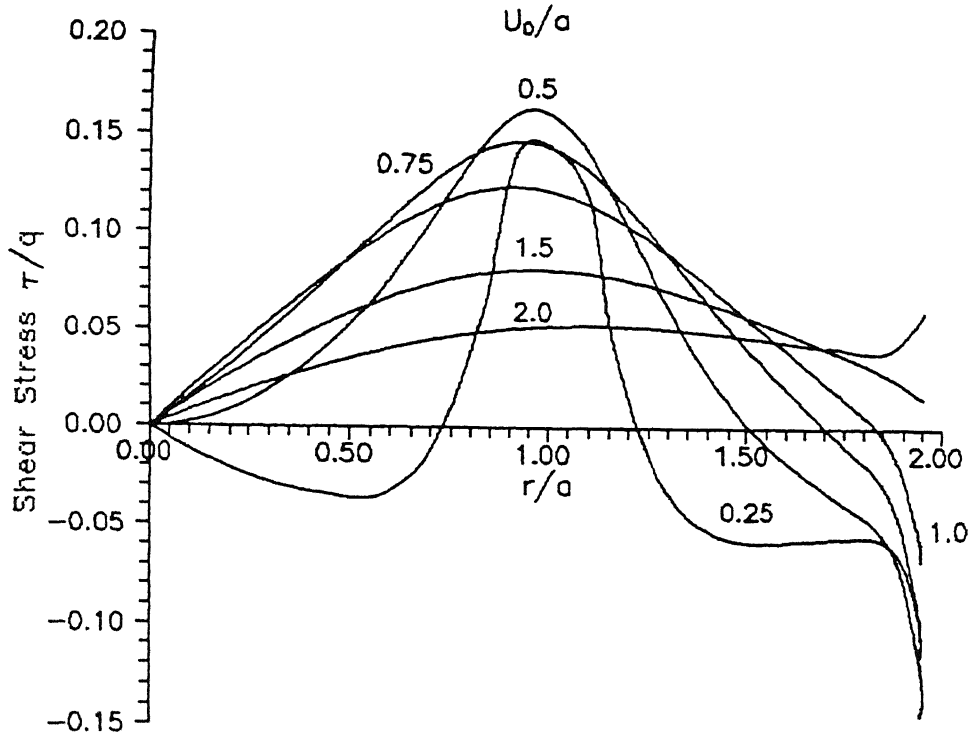


Fig. 6.18 Variation of Shear Stress with Distance for Various Depths of Placement of Sheet ($R/a=2$, $K_T=1$, $\nu_s=0.3$)

The variation of $I_{sc}$ with radius, R/a, of the sheet for different $K_\tau$ values and for the sheet at a depth, $U_o/a=1$ is presented in Fig. 6.20. For $K_\tau \leq 1$, $I_{sc}$ values gradually increase with R/a increasing upto 2 and with further increase in the radius of the sheet the $I_{sc}$ values are almost constant. For $K_\tau > 1$ there is a small decrease in the $I_{sc}$ values with R/a increasing from 2 to 3. With further increase in R/a, $I_{sc}$ increases gradually. This trend is prominent for sufficiently rigid to inextensible sheets and can be explained in conjunction with the results presented in Figs. 6.7, 6.8 and 6.10. In addition to the comments made with reference to Fig. 6.8, it may be noted from 6.10 that $I_{sc}$ values attain their maximum values at different depths for sheets of different radii. For a sheet with R/a=2, the maximum $I_{sc}$ is for a depth, $U_o/a$ of 0.85 while for other combinations, $I_{sc}$ is maximum at $U_o/a=0.75$. The slight reduction in $I_{sc}$ with increasing values of R/a beyond R/a=2 is due to the increasing stretch of negative stresses (Fig. 6.7) over the sheet for r/a>2.0.

The varation of the ratio of the $I_{sc}$ for an extensible sheet, $I_{sc(E)}$, to that for a rigid (inextensible) one, $I_{sc(r)}$, with the elongation ratio, $K_\tau$, for various radii, R/a, of the sheet placed at a depth, $U_o/a=1$ is depicted in Fig. 6.21. The ratio, $I_{sc(E)}/I_{sc(r)}$, increases with $K_\tau$ for all radii of the sheet and approaches 1 for $K_\tau=10^4$. Sheets with R/a=5 show marginally higher values of the ratio, $I_{sc(E)}/I_{sc(r)}$, as compared to sheets with R/a=1, while sheets with R/a=2 show the least values of the ratio. The reason for this behaviour is due to the

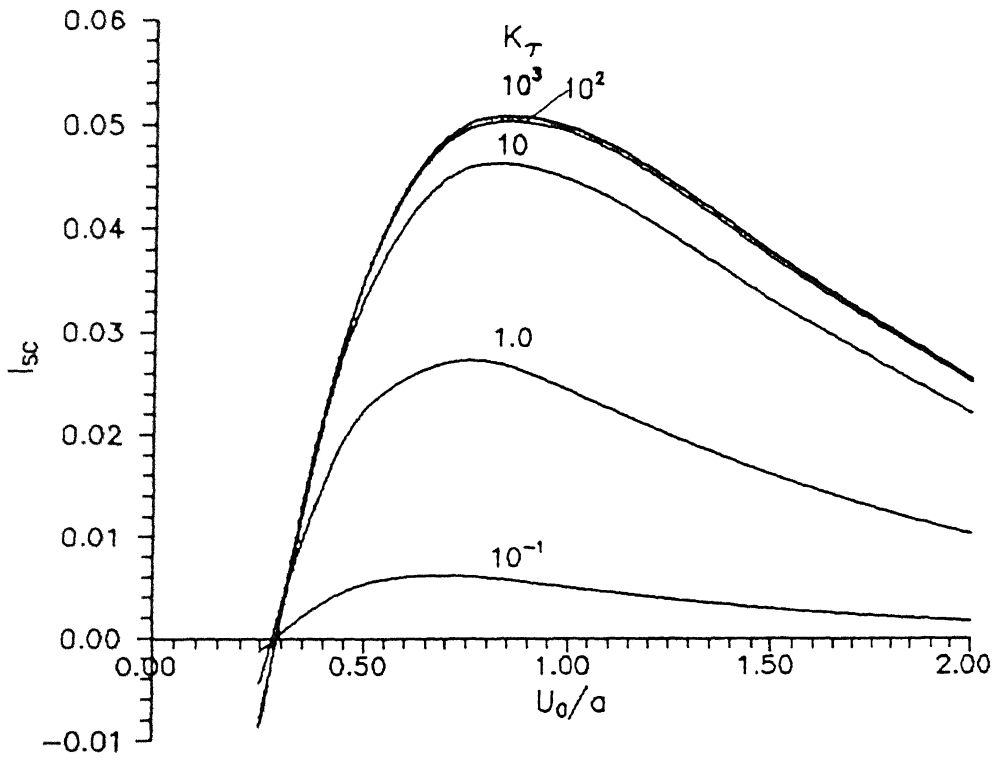


Fig. 6.19 Effect of Depth of Placement of Sheet on $I_{sc}$ for Various Elongation Ratios ($R/a=2$, $\nu_s=0.3$)

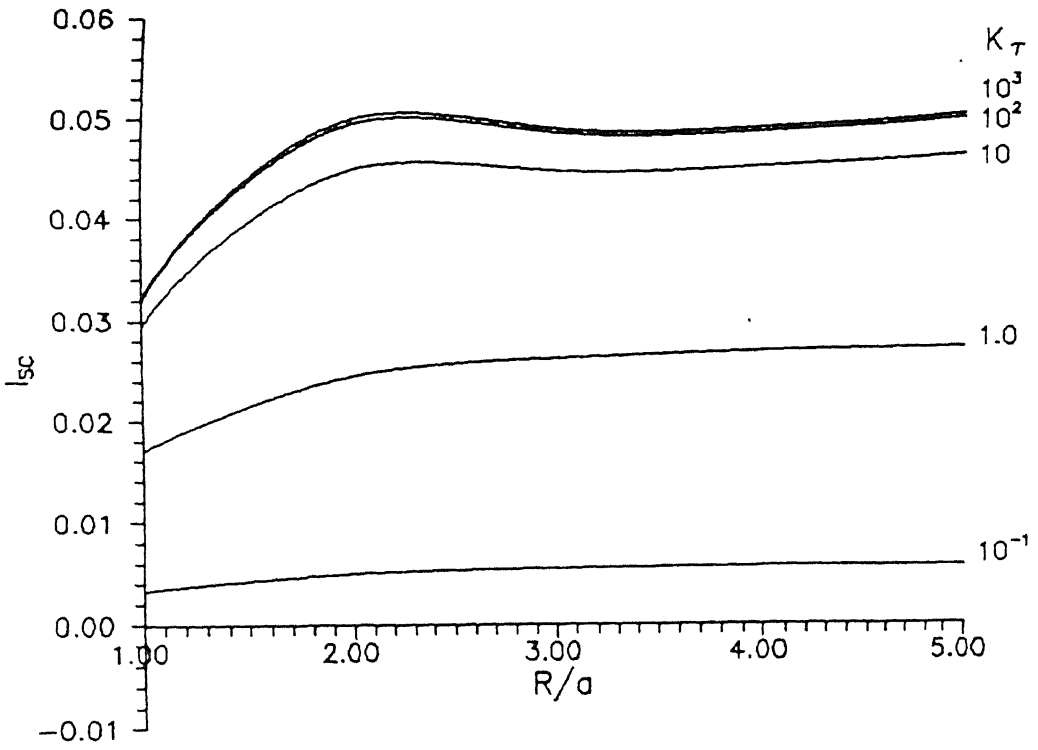


Fig. 6.20 Effect of Radius of Sheet on $I_{sc}$ for Various Elongation Ratios ($U_0/a=1$, $\nu_s=0.3$)

decrease in $I_{sc}$ values with increase in the radius, R/a, of the rigid sheet from 2 to 3 (Fig. 6.20) and follows from the above discussion. For $K_\tau \geq 10$ the value of the ratio, $I_{sc(E)}/I_{sc(r)}$, for sheets of all radii is greater than 0.9 which means that the sheets become almost rigid. This figure can be used to calculate the settlement reduction coefficients due to an extensible sheet placed at a depth, $U_o/a=1$, from those of a rigid one.

The variation of the ratio, $I_{sc(E)}/I_{sc(r)}$, with $K_\tau$ for different depths of placement, $U_o/a$, of the sheet of radius, R/a=2 is presented in Fig. 6.22. With increase in the value of the elongation ratio, $K_\tau$, the ratio, $I_{sc(E)}/I_{sc(r)}$, increases and approaches 1 for large values of $K_\tau$. It is seen that for the sheet placed at a depth, $U_o/a=0.5$, the values of the ratio, $I_{sc(E)}/I_{sc(r)}$, are the maximum while they decrease with increasing values of $U_o/a$ and are the least for the sheet at a depth, $U_o/a=2$. Results depicted in this figure are the same data shown in Fig. 6.19 but with $I_{sc}$ values normalised with respect to the $I_{sc}$ values for an inextensible sheet ($K_\tau=1000$). The ratio $I_{sc(E)}/I_{sc(r)}$ reflects the relative variations of the coefficient $I_{sc}$ with the parameters, $U_o/a$ and $K_\tau$. It may be noted that the rate of change of $I_{sc}$ with depth, for rigid sheets is high as compared to extensible ones. The increase in $I_{sc}$ for a rigid sheet from $U_o/a=0.5$ to 1.0 is sharp as compared to that for a sheet with $K_\tau=1$ in the same depth range. As a result the ratio, $I_{sc(E)}/I_{sc(r)}$, is high for $U_o/a=0.5$ and decreases with depth. From this figure the settlement reduction coefficients for extensible sheets of radius, R/a=2, placed at different depths

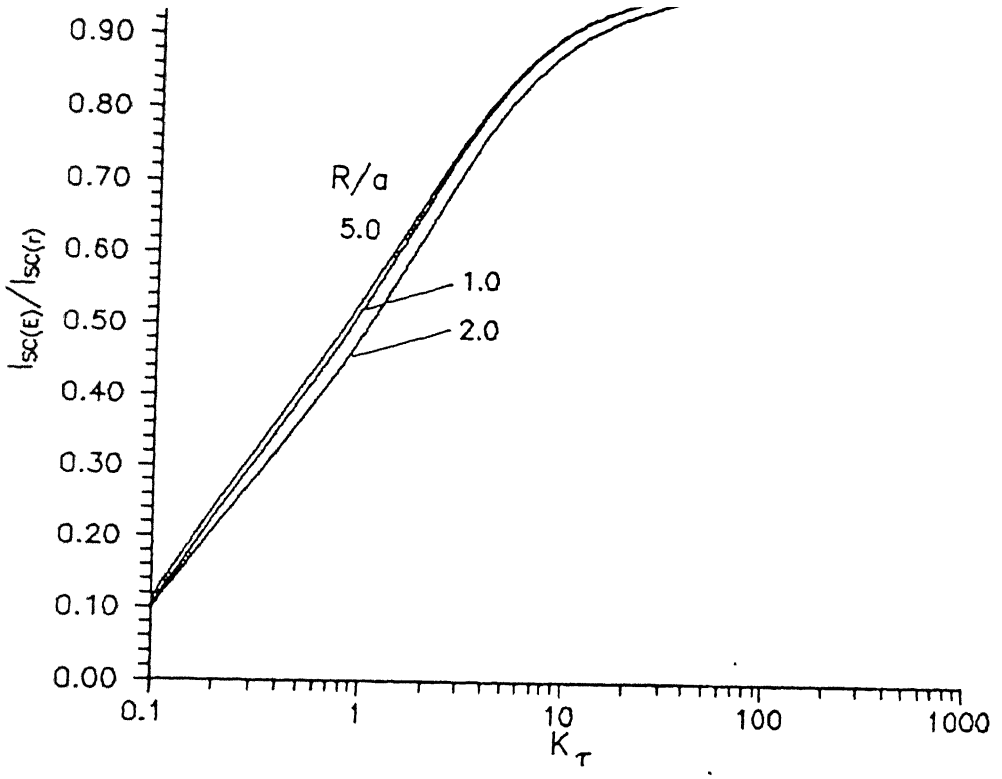


Fig. 6.21 Effect of Elongation Ratio on ratio of $I_{sc}$ for Extensible and Rigid Sheets, for Various Radii of Sheet ($U_0/a=1$, $\nu_s=0.3$)

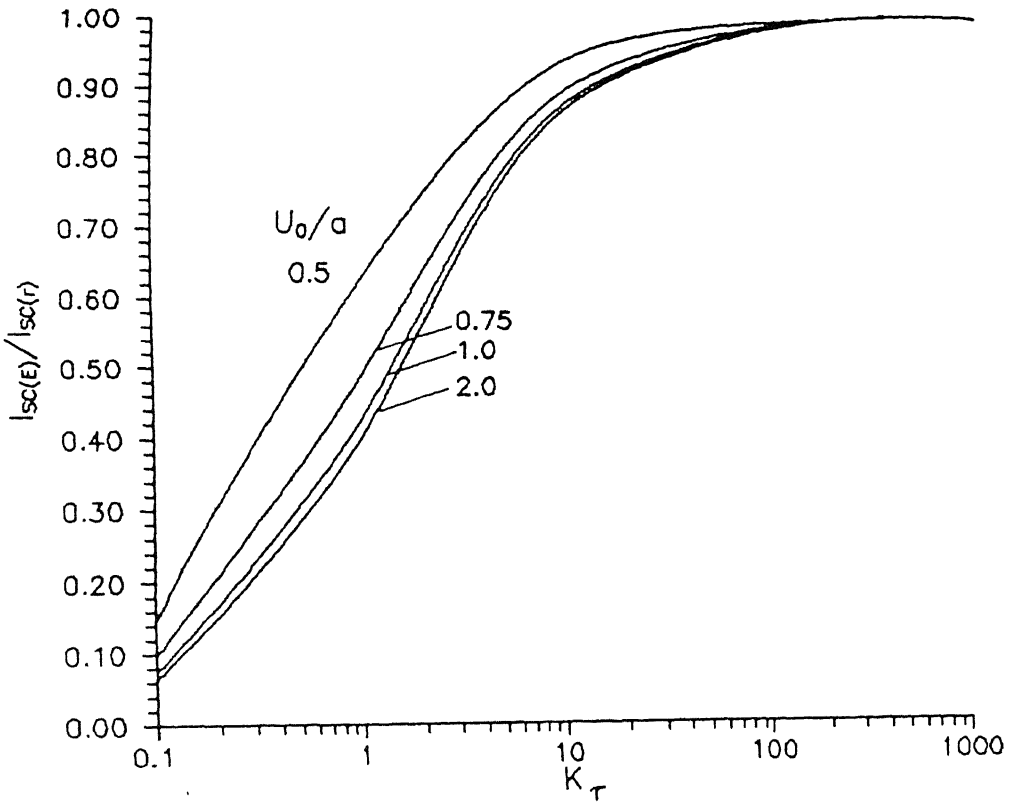


Fig. 6.22 Effect of Elongation Ratio on ratio of $I_{sc}$ for Extensible and Rigid Sheets, for different Depths of Placement ($R/a=2$, $\nu_s=0.3$)

can be calculated from those values of a rigid sheet.

## 6.5 Conclusions

Based on the elastic continuum approach a model has been proposed to predict the reduction in settlements of points along the surface due to the presence of a circular reinforcement at depth. The problem considered is axi-symmetric in nature. The effects of the radius of the reinforcement, and depth of its placement on the shear and normal stresses mobilised along the reinforcement-soil interface and the subsequent reduction in surface settlements are studied. The horizontal and vertical rigidity of the reinforcement are considered separately. Subsequently, the extensibility of the sheet is also accounted for. The results of the parametric study are listed below:

1. Rigid (inextensible) reinforcement sheets of large size show maximum settlement reduction in the depth range 0.6 to 0.8 times the radius of the loaded area.
2. In the case of rigid (inflexible) reinforcement discs, maximum benefit is accrued when the discs of large radii are placed close to the ground surface.
3. Extensible sheets exhibit trends similar to those of an inextensible one. Based on the radius, depth of placement and elongation ratio of extensible sheets the settlement reduction coefficients can be obtained from those of a rigid (inextensible) one.

# CHAPTER 7

# SUMMARY AND CONCLUSIONS

Using the elastic continuum approach an analytical model to study the interactions between reinforcements and soil, and to predict the reduction in surface settlements due to reinforcements below a loaded area, at depth is presented. Two forms of reinforcements are considered, viz., strip and sheet or disc reinforcements. The mechanisms considered are the shear and normal stress interactions. Initially, each of the two mechanisms are considered independently. In the case of strip reinforcements, rigid strips of sufficiently small widths are considered so that the stresses vary along the length of the strip alone. The compatibility of horizontal and vertical displacements at the interface of the strips, considered separately gives rise to equations which on solving yield the shear and normal stresses mobilised at the interface of the strips. The reductions in surface settlements, as a consequence of these stresses are evaluated. The analyses consider a single strip, a pair of strips at the same depth, two strips one below the other and multiple strips at the same depth. In the case of strips one below the other and multiple strips the validity of the principle of superposition is examined.

Following the analysis for rigid strips, the same is extended for extensible and flexible ones. In these cases the elongations and flexural deformations of the strips are considered

separately. The equations resulting from the displacement compatibility and force equilibrium relationships are solved to obtain the shear and normal stresses mobilised at the interface. The reductions in surface settlements due to these stresses are computed. The coupled effect of the horizontal and vertical interactions of rigid strips is examined subsequently. In this analysis the influence of horizontal stresses on vertical displacements and vice-versa are considered. Slip at the interface for rigid strips resulting due to the mobilisation of shear stresses greater than the available strength is accounted for.

The analyses for strips is extended for sheet reinforcements beneath circular loaded areas (axi-symmetric case). Rigid (in-extensible) and extensible sheets are considered. The shear stresses mobilised at the interface and consequently, the reduction in surface settlements are evaluated. Rigid discs experiencing uniform vertical displacements are also considered.

Based on the results of the analyses for all these cases the following general or broad conclusions are drawn:

1. The normal stresses resulting from vertical stress interactions for the strips as well as the sheets (axi-symmetric case) are much higher than the shear stresses resulting from the horizontal stress interactions. As a result, the Settlement Reduction Coefficients (SRC) due to normal stress interactions are much higher than those due to shear stress interactions.
2. Rigid (inflexible) strips of lengths ($2B_f$ to $5B_f$) placed at

shallow depths reduce settlements significantly.

3. The optimum location for placing a pair of strips is to place them at a distance, $S_y/B_f=0.25$ from the centre of the loaded area.

4. Slip along the rigid strip occurs at points where the normal stresses mobilised are low. Relatively more number of points fail on strips at greater depths due to slip, since normal stresses are uniformly distributed over it.

5. Highly flexible but inextensibile strips or sheets if placed in the depth range of 0.5 to 1 times the half-width of the loaded area provide maximum settlement reduction. The optimum length of the strips is 2 to 2.5 times the width of the loaded area.

6. The same conclusions apply for circular reinforcements also.

The above study can be extended by considering

(i) the elasto-plastic response of the soil;

(ii) the membrane effect at relatively large displacements;

(iii) grid type reinforcement;

(iv) the elasto-plastic type deformation of the interface and of the strips or sheets;

(v) the soil encapsulated by reinforcement as a relatively stiff or rigid inclusion, etc.

## REFERENCES


Akinmusuru, J.O., and Akinbolade, J.A., (1981), "Stability of Loaded Areas on Reinforced Soil", *Jl. of the Geotechnical Engg. Div.*, ASCE, Vol. 107, No. GT6, June, pp. 819-827.

Akinmusuru, J.O., Akinbolade, J.A., and Odigie, D.O., (1982), "Bearing Capacity Tests on Fiber-Reinforced Soil", *Second Int. Conf. on Geotextiles*, Vol. 3., Las Vegas, Aug., pp. 599-603.

Andrawes, K.Z., McGown, A., Wilson-Fahmy, R.F., and Mashhour, M.M. (1982), "Finite Element Method of Analysis applied to Soil-Geotextile System", *Second Int. Conf. on Geotextiles*, Vol. 3., Las Vegas, Aug., pp. 695-699.

Andrawes, K.Z., McGown, A., and Wilson-Fahmy, R.F., (1983), "Behaviour of a Geotextile Reinforced Sand Loaded by a Strip Footing", *Proc. of the Eighth European Conf. on Soil Mechanics, and Foundation Engg.*, Helsinki, May, pp. 329-334.

Basset, R.H., and Last, N.C., (1978), "Reinforcing Earth Below Footings and Embankments", *Proc. of the Symposium on Earth Reinforcement*, ASCE Annual Convention, Pittsburgh, pp. 202-231.

Binquet, J., and Lee, K.L., (1975a), " Bearing Capacity Tests on Reinforced Earth Slabs", *Jl. of the Geotechnical Engg. Div.*, ASCE, Vol. 101, No. GT12, Dec, pp. 1241-1255.

Binquet, J., and Lee, K.L., (1975b), " Bearing Capacity Analysis of Reinforced Earth Slabs", *Jl. of the Geotechnical Engg. Div.*, ASCE, Vol. 101, No. GT12, Dec, pp. 1257-1276.

Bowles, J.E., (1968), *Foundation Analysis and Design*, McGraw-Hill & Co., Inc.

Broms, B.B., and Massarch, K.R., (1977), "Grid Mats - A New Foundation Method", *Proc. of the Ninth Int. Conf. in Soil Mechanics*, Tokyo, Vol. 2, pp. 433-438

Brown, B.S., and Poulos, H.G., (1981), "Analysis of Foundations on Reinforced Soil", *Proc. of the Tenth Int. Conf. on Soil Mechanics and Foundation Engg.*, Stockholm, Vol. 3, June, pp. 595-598.

Burd, H.J., and Houlsby, G.T., (1989), "Numerical Modelling of Reinforced Unpaved roads", *Numerical Models in Geomechanics*, NUMOG III, pp. 699-706.

Burd, H.J., and Brocklehurst, C.J. (1990), "Finite Element Studies on the Mechanics of Reinforced Unpaved Roads", *Fourth Int. Conf. on Geotextiles and Geomembranes*, The Hague, Vol. 1, pp. 217-221.

Das, B.M., (1988), "Shallow Foundation on Sand Underlain by Soft Clay with Geotextlie Interface", *Geosynthetics*, Ed. Holtz, R.D., ASCE Geotechnical Special Publication No. 18, pp. 112-126.

Das, B.M., (1989), "Foundations on Sand Underlain by Soft Clay with Geotextile at Sand-Clay Interface", *Geosynthetics '89 Conf. Proceedings*, California, Vol. 1, Feb., pp. 203-214.

Dembicki, E., and Alenowicz, J.M., (1988), "Influence of Geotextiles on Bearing Capacity of Two-Layer Subsoil", *Proc. of the First Indian Geotextiles Conf.*, Bombay, Vol. 1, Dec., A.61-A.66.

Floss, R., and Gold, G., (1990), "Use of FEM for Single Reinforced Two-Layered Systems", *Fourth Int. Conf. on Geotextiles and Geomembranes*, The Hague, Vol. 1, pp. 248.

Fowler, J., and Koerner, R.M., (1987), "Stabilisation of very Soft Soils using Geosynthetics", *Proc. of the Geosynthetics Conf.*, Los Angeles, Vol. 1, pp. 289-300.

Fragaszy, R.J., and Lawton, E., (1984), "Bearing Capacity of Reinforced Sand Subgrades", *Jl. of the Geotechnical Engg. Div.*, ASCE, Vol. 110, No. GT10, Oct., pp. 1500-1507.

Giroud, J.P., and Noiray, L., (1981), "Geotextile-Reinforced Unpaved Road Design", *Jl. of the Geotechnical Engg. Div.*, ASCE, Vol. 107, GT9, Sept., pp. 1233-1254.

Guido, V.A., Biesiadecki, G.L., and Sullivan, M.J., (1985), "Bearing Capacity of a Geotextile-Reinforced Foundation", *Proc. of the XI Int. Conf. in Soil Mechanics and Foundation Engg.*, San Francisco, Vol. 3, Aug., pp. 1777-1780.

Guido, V.A., Chang, D.K., and Sweeney, M.A., (1986), "Comparison of Geogrid and Geotextile Reinforced Earth Slabs", *Canadian Geotechnical Journal*, Vol. 23, No. 4, Nov., pp. 435-440.

Hird, C.C., and Kwok, C.M., (1990), "Parametric Studies of the Behaviour of a Reinforced Embankment", *Fourth Int. Conf. on Geotextiles and Geomembranes*, The Hague, Vol. 1, pp. 137-142.

Houlsby, G.T., and Jewell, (1990), " Design of Reinforced Unpaved Roads for Small Rut Depths", *Fourth Int. Conf. on Geotextiles and Geomembranes*, The Hague, Vol. 1, pp. 171-176.

Huang, C-C., and Tatsuoka, F., (1988), "Prediction of Bearing Capacity in Level Sandy Ground Reinforced with Strip Reinforcement", *Proc. of the Int. Geotechnical Symposium on Theory and Practice of Earth Reinforcement*, Fukuoka, Oct., pp. 191-196.

Ingold, T.S., and Miller, K.S., (1982), "Analytical and Laboratory Investigation of Reinforced Clay", *Second Int. Conf. on Geotextiles*, Las Vegas, Vol. 3, Aug., pp. 587-592.

Ingold, T.S., and Miller, K.S., (1982), "The Behaviour of Geotextile Reinforced Clay Subject to Undrained Loading", *Second Int. Conf. on Geotextiles*, Las Vegas, Vol. 3, Aug., pp. 593-597.

Jones, C.J.F.P., (1985), *Earth Reinforcement and Soil Structures*, Butterworth and Co. Ltd.

Jones, R.H., and Dawson, A.R., (1990), "Reinforced Soil Foundations for Buildings", *Proc. of the Int. Reinforced Soil Conf.*, British Geotechnical Soc., Glasgow, Sept. pp. 477-478.

Koerner, R.M., (1990), *Designing with Geosynthetics*, Prentice Hall and Co., Inc.

Lindh, E., and Erikkson, L., (1990), "Sand Reinforced with Plastic Fibres. A Field Experiment", *Proc. of the Int. Reinforced Soil Conf.*, British Geotechnical Soc., Glasgow, Sept. pp. 471-474.

Love, J.P., Burd, H.J., Milligan, G.W.E., & Houslby, G.T., (1987), "Analytical and Model Studies on Reinforcement of a layer of Granular Fill on Soft Clay Subgrades", *Canadian Geotechnical Journal*, Vol. 24, pp. 611-622.

Madhav, M.R., and Ghosh, C., (1988), "Modelling for Settlement Analysis of Reinforced Soils", *Proc. of the First Indian Geotextiles Conf.*, Bombay, Vol. 1, Dec., pp. C.33-C40.

Madhav, M.R., and Poorooshasb, H.B., (1988), "A New Model for Geosynthetic Reinforced Soils", *Computers and Geotechnics.*

Madhav, M.R., and Poorooshasb, H.B., (1989), "Modelling of Embankment on Near Surface Reinforced Soils", *Numerical Models in Geomechanics*, NUMOG III, pp. 657-666.

Mitchell, J.K., and Schlosser, F., (1979), General Report, *Int. Conf. on Soil Reinforcement*, Paris, Vol. 3, March, pp. 25-62.

Miura, N., Sakai, A., Taesiri, Y., Mouri, K., and Ohtsubo, M., (1988), "Model and Field Tests of Reinforced Pavement on Soft Clay Ground", *Proc. of the Int. Geotechnical Symposium on Theory and Practice of Earth Reinforcement*, Fukuoka, Oct., pp. 227-232.

Poulos, H.G., and Davis, E.H., (1975), *Elastic Solutions for Soil and Rock Mechanics*, John Wiley & Sons, New York.

Saragunan, A., and Hussain, A.S.J., (1988), "Stability of Loaded Footings in Reinforced Soils", *Proc. of the First Indian Geotextiles Conf.*, Bombay, Vol. 1, Dec., pp. C.27-C.32.

Schlosser, F., Jacobsen, H.M., and Juran, L., (1983), "Soil Reinforcement", General Report, *Proc. of the Eighth European Conf. on Soil Mechanics and Foundation Engg.*, Helsinki, Vol. 3, pp. 1159-1180.

Sellmeijer, J.B., (1990), "Design of Geotextile Reinforced Paved Roads and Parking Areas", *Fourth Int. Conf. on Geotextiles and Geomembranes*, The Hague, Vol. 1, pp. 177-182.

Setty, N.S.K.R., and Rao, G.S.V., (1987), "Charecterisation of Fibre Reinforced Lateritic Soil", *Indian Geotechnical Conf.*, Dec., pp. 329-333.

Shankariah, B., and Narahari, R., (1988), " Bearing Capacity of Reinforced Sand Beds", *Proc. of the First Indian Geotextiles Conf.*, Bombay, Vol. 1, Dec., pp. C.9-C.14.

Shimuzu, M. and Inui, T., (1990), "Increase in Bearing Capacity of Ground with Geotextile Wall Frame", *Fourth Int. Conf. on Geotextiles and Geomembranes*, The Hague, Vol. 1, pp. 254.

Sreekantiah, H.R., (1988), "Stability of Loaded Footings on Reinforced Sand", *Proc. of the First Indian Geotextiles Conf.*, Bombay, Vol. 1, Dec., pp. C.3-C.8.

Sridharan, A., Murthy, B.R.S., Bindumadhava, and Vasudevan, A.K., (1988), "Reinforced Soil Foundation on Soft Soil", *Proc. of the First Indian Geotextiles Conf.*, Bombay, Vol. 1, Dec., pp. C.53-C.60.

Sridharan, A., Murthy, B.R.S., Bindumadhava, and Vasudevan, A.K., (1989), "Model Tests on Reinforced Soil Mattress on Soft Soil", *Proc. of the XII Int. Conf. in Soil Mechanics and Foundation Engg.*, Rio de Janeiro, Vol. 3, Aug., pp. 1765-1768.

Sridharan, A., Murthy, B.R.S., and Singh, H.R., (1989), *Indian Contributions to Reinforced Soil*, Central Board of Irrigation & Power, New Delhi.

Sridharan, A., Murthy, B.R.S., and Singh, H.R., (1991), "Bearing Capacity Tests on Reinforced Sand Beds", *Proc. of the Ninth Regional Conf. on Soil Mechanics and Foundation Engg.*, Vol. 1, Dec.

Teferra, A., and Schultze, E., (1988), *Formulae, Charts & Tables in the Area of Soil Mechanics and Foundation Engineering:Stresses*, Balkema A.A. Publishers, Netherlands.

Vaziri, H., Simpson, B., Pappin, J.W., and Simpson, L., (1982), "Integrated form of Mindlin's Equations", *Geotechnique*, Vol. 32, No. 3, Sept., pp. 275-278.

Veldhuijzen, R.V.Z., (1986), *Geotextiles and Geomembranes in Civil Engineering*, Balkema, A.A. Publishers, Netherlands.

Verma, B.P., and Char, A.N.R., (1986), "Bearing Capacity Tests on Reinforced Sand Subgrades", *Jl. of the Geotechnical Engg. Div.*, ASCE, Vol. 112, No. GT7, July, pp. 701-706.

Winterkorn, H.F., and Fang, H.Y., (1975), *Foundation Engineering Handbook*, Van Nostrand Reinhold Co., Inc.